



LUND UNIVERSITY

Coarse-Grained Modelling of Protein Adsorption

Hyltegren, Kristin

2020

Document Version:

Publisher's PDF, also known as Version of record

[Link to publication](#)

Citation for published version (APA):

Hyltegren, K. (2020). *Coarse-Grained Modelling of Protein Adsorption*. [Doctoral Thesis (compilation), Lund University]. Lund University (Media-Tryck).

Total number of authors:

1

General rights

Unless other specific re-use rights are stated the following general rights apply:

Copyright and moral rights for the publications made accessible in the public portal are retained by the authors and/or other copyright owners and it is a condition of accessing publications that users recognise and abide by the legal requirements associated with these rights.

- Users may download and print one copy of any publication from the public portal for the purpose of private study or research.
- You may not further distribute the material or use it for any profit-making activity or commercial gain
- You may freely distribute the URL identifying the publication in the public portal

Read more about Creative commons licenses: <https://creativecommons.org/licenses/>

Take down policy

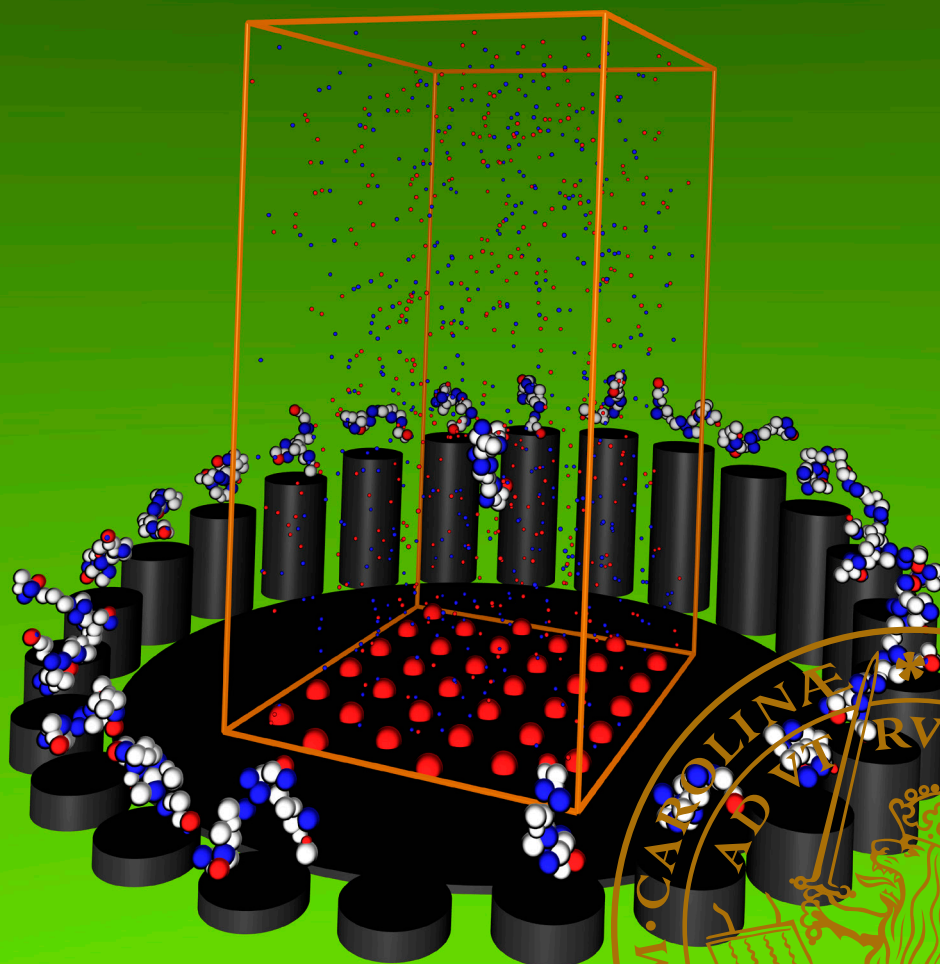
If you believe that this document breaches copyright please contact us providing details, and we will remove access to the work immediately and investigate your claim.

LUND UNIVERSITY

PO Box 117
221 00 Lund
+46 46-222 00 00

Coarse-Grained Modelling of Protein Adsorption

KRISTIN HYLTEGREN | DIVISION OF THEORETICAL CHEMISTRY | LUND UNIVERSITY



COARSE-GRAINED MODELLING OF PROTEIN ADSORPTION

Kristin Hyltegren



LUND UNIVERSITY

DOCTORAL DISSERTATION

To be presented, with the permission of the Faculty of Science of Lund University, for public criticism in lecture hall B, Centre for Chemistry and Chemical Engineering, Naturvetarvägen 14, Lund, Friday 24 April 2020, 9.15.

Faculty opponent

Johan Bergenholtz

Department of Chemistry and Molecular Biology
University of Gothenburg, Gothenburg, Sweden

| | | |
|---|--|--|
| Organization LUND UNIVERSITY | Document name DOCTORAL DISSERTATION | |
| | Date of issue 31 March 2020 | |
| | | |
| Author(s) Kristin Hyltegren | Sponsoring organizations Organizing Molecular Matter (OMM); The Craaford Foundation | |
| Title and subtitle Coarse-Grained Modelling of Protein Adsorption | | |
| <p>Abstract</p> <p>The adsorption of proteins is a very common phenomenon, happening almost always when a protein solution comes into contact with a solid. However, it is far from always clear what the results of adsorption will be in terms of adsorbed amount, protein orientation, and protein conformation. In this work, the adsorption of two proteins – histatin 5 and fibrinogen – has been studied using coarse-grained Monte Carlo simulations and, in case of histatin 5, ellipsometry. Histatin 5 is a short (24 residues long), cationic protein present in the saliva of higher primates. Its main function is that it kills the fungus <i>Candida albicans</i>. Fibrinogen is a 340 kDa rod-like protein that is abundant in the blood of vertebrates. It has an important role in blood clotting. While histatin 5 is an intrinsically disordered protein, fibrinogen is mainly ordered with two ~400 amino acid residues long disordered appendages. This difference made us use two different models for the proteins– one for histatin 5 and the disordered fibrinogen fragments, and another for the main body of fibrinogen. Whereas the disordered proteins were modelled as beads on a necklace, the fibrinogen main body was modelled as a completely rigid body based on the crystal structure. The surface that the proteins were adsorbed on was a hydrophilic silica surface – modelled in the simulations as completely flat with (most of the time) a uniform, smeared charge.</p> <p>The main results for histatin 5 are the following: (i) the adsorbed amount of histatin 5 changes with ionic strength – but the trends are different depending on pH, (ii) the electrostatic interactions between charged groups are not enough to account for the experimentally observed adsorption of histatin 5 to silica surfaces, (iii) the coarse-grained model used in these studies cannot explain the experimentally observed pH-dependence of the adsorbed amount as a function of ionic strength, (iv) a library of only a few structures (with different weights) represent well the conformational ensemble of histatin 5, and (v) simulations suggest that the amount of secondary structure motifs of histatin 5 increases somewhat upon adsorption.</p> <p>The main results for fibrinogen are the following: (i) the disordered appendages make an important contribution to the adsorption free energy, (ii) the side of the end of the fibrinogen rod adsorbs in a similar manner regardless of surface curvature, meaning that the protein protrudes further into solution the higher the surface curvature, and (iii) we hypothesise that this difference in protrusion can account for the fact that adsorbed fibrinogen increases adhesion of the bacterium <i>S. epidermidis</i> on smooth surfaces while decreasing it on nanostructured surfaces.</p> | | |
| Key words Intrinsically disordered proteins, histatin 5, fibrinogen, protein adsorption, nanotopography, ellipsometry, Monte Carlo simulations, coarse-grained modelling, charge regulation | | |
| Classification system and/or index terms (if any) | | |
| Supplementary bibliographical information | | Language English |
| ISSN and key title | | ISBN 978-91-7422-734-5 (print) 978-91-7422-735-2 (pdf) |
| Recipient's notes | Number of pages 176 | Price |
| | Security classification | |

I, the undersigned, being the copyright owner of the abstract of the above-mentioned dissertation, hereby grant to all reference sources permission to publish and disseminate the abstract of the above-mentioned dissertation.

Signature 

Date 11 March 2020

COARSE-GRAINED MODELLING OF PROTEIN ADSORPTION

Kristin Hyltegren



LUND UNIVERSITY

Doctoral dissertation
2020

COARSE-GRAINED MODELLING OF PROTEIN ADSORPTION

Front cover:

Conformational swap model, courtesy of Mikael Lund

Parts of this thesis have been published before in:

Hyltegren, Kristin *Making sense of adsorption: Attempting to explain the adsorption of histatin 5 with models, metaphors, and machines* (2016).


© 2020 Kristin Hyltegren

All rights reserved

Printed in Sweden by Media-Tryck, Lund, 2020



Media-Tryck is a Nordic Swan Ecolabel
certified provider of printed material.
Read more about our environmental
work at www.mediatryck.lu.se

MADE IN SWEDEN 

Theoretical Chemistry
Department of Chemistry
Lund University
P.O. Box 124
SE-221 00 Lund
Sweden

<http://www.teokem.lu.se>

ISBN 978-91-7422-734-5 (print), 978-91-7422-735-2 (pdf)

Dedicated to my parents

Till mina föräldrar

Mamma och pappa. Jag har ofta tänkt på hur jag yrkesmässigt har hamnat någonstans mittemellan er två. Med en mamma som är programmerare och en pappa som är gymnasielärare i bland annat kemi så känns det inte särskilt oväntat att jag fastnade för teoretisk kemi.

När jag var barn var jag medveten om att jag hade privilegiet att kunna få hjälp med i princip alla naturvetenskapliga ämnen hemma – något som jag upplevde att jag väldigt sällan utnyttjade. Men såhär i efterhand kan jag tänka att det nog inte går att underskatta betydelsen av att ha någon att diskutera nya läroämnen med. Någon som förstod och som uppmuntrade. Tack!

Mamma, vad hade jag gjort utan ditt stöd genom alla upp- och nedgångar? Tack för att du år efter år lyssnat på mitt gnäll och tjuvat på mig om det som är viktigt. Och tack för alla gånger du fått mig att skratta när jag varit arg eller grinig.

Pappa, det har betytt enormt mycket för mig att få dela så många intressen med dig. Jag tror inte ens att jag ska försöka räkna upp alla – det tar för mycket plats.

Jag minns i högstadiet när jag skulle prata om USA i skolan. Jag bad dig lyssna på min presentation, inte för att jag egentligen ville ha några råd, utan för att jag ville att du skulle säga att det var bra så att jag kunde göra något annat sedan. Där misstog jag mig! Du talade om för mig att min inledning inte väckte något intresse och att jag måste sätta siffrorna jag presenterade i relation till något annat. Det var där och då mitt intresse för undervisning vaknade! Paradoxalt nog gjorde mina ökade krav på presentationen att nervositeten minskade. Nu kunde jag rikta fokus mot det jag hade att säga istället för mot det faktum att jag hade trettio personers blickar riktade mot mig.

ABSTRACT

The adsorption of proteins is a very common phenomenon, happening almost always when a protein solution comes into contact with a solid. However, it is far from always clear what the results of adsorption will be in terms of adsorbed amount, protein orientation, and protein conformation. In this work, the adsorption of two proteins – histatin 5 and fibrinogen – has been studied using coarse-grained Monte Carlo simulations and, in case of histatin 5, ellipsometry. Histatin 5 is a short (24 residues long), cationic protein present in the saliva of higher primates. Its main function is that it kills the fungus *Candida albicans*. Fibrinogen is a 340 kDa rod-like protein that is abundant in the blood of vertebrates. It has an important role in blood clotting. While histatin 5 is an intrinsically disordered protein, fibrinogen is mainly ordered with two ~ 400 amino acid residues long disordered appendages. This difference made us use two different models for the proteins – one for histatin 5 and the disordered fibrinogen fragments, and another for the main body of fibrinogen. Whereas the disordered proteins were modelled as beads on a necklace, the fibrinogen main body was modelled as a completely rigid body based on the crystal structure. The surface that the proteins were adsorbed on was a hydrophilic silica surface – modelled in the simulations as completely flat with (most of the time) a uniform, smeared charge.

The main results for histatin 5 are the following: (i) the adsorbed amount of histatin 5 changes with ionic strength – but the trends are different depending on pH, (ii) the electrostatic interactions between charged groups are not enough to account for the experimentally observed adsorption of histatin 5 to silica surfaces, (iii) the coarse-grained model used in these studies cannot explain the experimentally observed pH-dependence of the adsorbed amount as a function of ionic strength, (iv) a library of only a few structures (with different weights) represent well the conformational ensemble of histatin 5, and (v) simulations suggest that the amount of secondary structure motifs of histatin 5 increases somewhat upon adsorption.

The main results for fibrinogen are the following: (i) the disordered appendages make an important contribution to the adsorption free energy, (ii) the side of the end of the fibrinogen rod adsorbs in a similar manner regardless of surface curvature, meaning that the protein protrudes further into solution the higher the surface curvature, and (iii) we hypothesise that this difference in protrusion can account for the fact that adsorbed fibrinogen increases adhesion of the bacterium *S. epidermidis* on smooth surfaces while decreasing it on nanostructured surfaces.

CONTENTS

| | |
|---|--------------|
| Abstract | vii |
| Preface | xiii |
| Populärvetenskaplig sammanfattning | xv |
| List of Publications | xxv |
| Contribution Report | xxvii |
| 1 Introduction | 1 |
| 1.1 Initial reflections | 1 |
| 1.2 The ‘I’ in (this) science | 2 |
| 1.2.1 My journey as a researcher | 2 |
| 1.2.2 What constitutes a good model? | 4 |
| 1.2.3 What is the ultimate goal of the research project? | 4 |
| 2 The Studied Proteins | 5 |
| 2.1 Proteins and polypeptides | 5 |
| 2.1.1 Protein structure | 6 |
| 2.1.2 Does structure determine function? | 9 |
| 2.1.3 Intrinsically disordered proteins | 9 |
| 2.2 Histatin 5 | 10 |
| 2.2.1 The structure of histatin 5 | 10 |
| 2.2.2 The protein content and functions of saliva | 10 |
| 2.2.3 The antifungal effect of histatin 5 | 11 |
| 2.3 Fibrinogen | 12 |
| 2.3.1 The structure of fibrinogen | 12 |
| 2.3.2 Fibrinogen’s role in blood clotting | 13 |
| 2.3.3 Fibrinogen adsorption on implants | 13 |
| 3 The Studied Surfaces | 15 |
| 3.1 Silica | 15 |
| 3.1.1 The silica surface and its silanol groups | 15 |
| 3.1.2 The surface charge density of silica | 16 |
| 3.1.3 Silica as a model surface | 17 |
| 3.2 Tooth enamel and hydroxyapatite | 17 |
| 3.2.1 Tooth enamel | 17 |
| 3.2.2 Hydroxyapatite | 17 |
| 3.2.3 The surface charge density of enamel and hydroxyapatite | 18 |
| 3.3 Surface roughness or nanostructure | 18 |

| | | |
|----------|---|-----------|
| 4 | The Problem of Protein Adsorption | 19 |
| 4.1 | Where does protein adsorption happen and why do we study it? | 19 |
| 4.2 | Is adsorption related to protein function? | 20 |
| 4.3 | Why is protein adsorption a difficult research problem? | 20 |
| 5 | Interactions in the Molecular World | 23 |
| 5.1 | Coulomb interactions | 23 |
| 5.1.1 | Screened Coulomb interactions | 24 |
| 5.1.2 | Charge regulation and protein charge capacitance | 24 |
| 5.2 | Interactions involving permanent dipoles | 25 |
| 5.2.1 | Ion–dipole interactions | 25 |
| 5.2.2 | Dipole–dipole interactions | 26 |
| 5.2.3 | Hydrogen bonding | 26 |
| 5.2.4 | Dipole–induced dipole interactions | 27 |
| 5.3 | London dispersion forces (induced dipole–induced dipole) | 27 |
| 5.4 | Excluded volume/Pauli repulsion | 27 |
| 5.5 | Pauli repulsion + dispersion \approx the Lennard-Jones potential | 27 |
| 5.6 | Hydrophobic interactions | 28 |
| 5.7 | Adsorption and forces between macromolecules and charged surfaces | 28 |
| 5.7.1 | The electrical double layer | 28 |
| 5.7.2 | Entropic repulsion/attraction | 29 |
| 6 | Thermodynamics and Statistical Mechanics | 31 |
| 6.1 | What are thermodynamics and statistical mechanics? | 31 |
| 6.2 | The laws of thermodynamics | 32 |
| 6.2.1 | The laws of classical thermodynamics | 32 |
| 6.2.2 | The postulates of statistical mechanics | 33 |
| 6.3 | Thermodynamic ensembles | 34 |
| 6.3.1 | The microcanonical ensemble | 34 |
| 6.3.2 | The canonical ensemble | 34 |
| 6.3.3 | The isobaric–isothermal ensemble | 34 |
| 6.3.4 | The grand canonical ensemble | 34 |
| 6.4 | Free energy | 34 |
| 7 | Molecular Simulations and the Coarse-Grained Model | 37 |
| 7.1 | Molecular simulations | 37 |
| 7.2 | Molecular dynamics simulations | 38 |
| 7.2.1 | All-atom molecular dynamics simulations of proteins | 38 |
| 7.2.2 | Force fields and water models for IDP simulations | 38 |
| 7.3 | Molecular Monte Carlo simulations | 39 |
| 7.3.1 | The problem with naive Monte Carlo simulations | 39 |
| 7.3.2 | Importance sampling – the solution provided by Metropolis <i>et al.</i> | 39 |
| 7.3.3 | Monte Carlo moves | 40 |
| 7.4 | The coarse-grained protein models | 40 |
| 7.4.1 | The flexible bead model | 40 |
| 7.4.2 | The conformational swap model | 42 |
| 7.4.3 | The rigid body model | 43 |
| 7.5 | The modelling of the surface | 43 |
| 7.5.1 | The Gouy–Chapman surface | 43 |
| 7.5.2 | The nanostructured surface | 44 |
| 7.5.3 | The surface with explicit charges | 44 |
| 7.5.4 | The short-ranged attraction | 44 |
| 7.6 | The modelling of the salt ions | 45 |
| 7.6.1 | Implicit salt | 45 |
| 7.6.2 | Explicit grand canonical salt | 45 |
| 7.7 | Implicit water | 45 |
| 7.8 | The simulation box | 45 |

| | | |
|-----------|--|-----------|
| 7.8.1 | Periodic boundary conditions | 45 |
| 7.8.2 | The minimum image convention | 46 |
| 8 | Experimental Methods | 49 |
| 8.1 | Purification and cleaning of protein and surface | 49 |
| 8.1.1 | Size exclusion chromatography | 49 |
| 8.1.2 | Surface cleaning procedure | 50 |
| 8.2 | Null ellipsometry | 50 |
| 8.2.1 | The polarisation of light | 50 |
| 8.2.2 | The principle behind null ellipsometry | 51 |
| 8.2.3 | Null ellipsometry setup | 52 |
| 8.2.4 | Models and calculations behind ellipsometry | 53 |
| 9 | Results | 59 |
| 9.1 | Histatin 5 | 59 |
| 9.1.1 | Ellipsometry | 59 |
| 9.1.2 | Single-protein coarse-grained Monte Carlo | 59 |
| 9.1.3 | Multi-protein coarse-grained Monte Carlo | 60 |
| 9.1.4 | Conformational swap Monte Carlo | 62 |
| 9.1.5 | The effect of urea on adsorption – an unsolved question | 63 |
| 9.2 | Fibrinogen | 64 |
| 9.2.1 | Experimental background | 64 |
| 9.2.2 | Simulations of the main body of fibrinogen | 65 |
| 9.2.3 | Simulations of the disordered part of fibrinogen | 65 |
| 10 | Discussion | 67 |
| 10.1 | Too little adsorption of histatin 5 – what are we missing? | 67 |
| 10.2 | The histatin 5 chain entropy and the conformational swap model | 69 |
| 10.3 | Opposite change in salt-dependence with pH – why? | 69 |
| 10.4 | The effect of urea on adsorption – an unsolved question | 69 |
| 10.5 | Fibrinogen and <i>S. epidermidis</i> adhesion | 70 |
| 11 | Outlook | 71 |
| | References | 73 |
| | Acknowledgements | 79 |

Papers

| | | |
|-----|--|-----|
| I | Adsorption of the intrinsically disordered saliva protein histatin 5 to silica surfaces. A Monte Carlo simulation and ellipsometry study | 83 |
| II | Adsorption of polyelectrolyte-like proteins to silica surfaces and the impact of pH on the response to ionic strength. A Monte Carlo simulation and ellipsometry study | 101 |
| III | Integrating All-Atom and Coarse-Grained Simulations—Toward Understanding of IDPs at Surfaces | 111 |
| IV | Adsorption of Fibrinogen on Silica Surfaces—The Effect of Attached Nanoparticles | 125 |

PREFACE

“ I fell in love, simultaneously and inextricably, with my professors, with a discipline of pure, precise, definitive thought, and with what I conceived of as its ambitions. I fell in love with the life of the mind. I also fell in love, I might add, with the image of myself striving and succeeding in an area where women had rarely ventured. ”

Evelyn Fox Keller, The Anomaly of a Woman in Physics, in S. Rudnick and P. Daniels (eds) Working It Out: Twenty-Three Writers, Scientists and Scholars Talk about Their Lives (1977)

My love affair with theoretical physical chemistry began in 2008 in a lecture hall at the University of Gothenburg. We were having our first lecture in thermodynamics and professor Roland Kjellander was teaching. I remember how he wrote 0's all over the board because he did not think we would understand the magnitude of 10^{23} otherwise. If it is even possible to understand it... Roland's enthusiasm was contagious and I was fascinated by how one can calculate whether it is possible for a chemical reaction to occur or not. This really appealed to a theoretically oriented person like me.

In my second year at university, Magnus Gustafson was the one who made me fall in love with physics. His demonstrations of simple experiments and his questions that we discussed and answered with clickers made both classical mechanics and quantum mechanics enjoyable. I proceeded to do a small project under Magnus' guidance. He showed me how to work at the computer terminal and lent me a book about programming. Unfortunately, we did not get much further.

I was studying with passion, I was learning, I was making new friends. However, as the course in physical chemistry progressed, I started sleeping less and, when I did not manage to concentrate on the subject anymore, I started

analysing the lecturers' ways of teaching instead. I did not have time to finish the small project or the course before the crash came.

With this shaky beginning of my love affair with theoretical physical chemistry, one might have thought I would give up. I did not. I started taking courses in physics and did my bachelor project in physical chemistry. However, I cannot say that I was happy when I was working on my thesis. Once, my supervisor asked me how I had been doing during the project and after hearing my answer he said: "If you do this well when you are not feeling well, imagine what you could do if you *were* feeling well!" The thought almost made me dizzy. Back then, I really believed in my own capacity.

After finishing my master's studies in Gothenburg, I moved to Lund to start my graduate studies with the supervisor I had found to be worthy of me. I was confident that I would contribute significantly to her scientific career achievements and I was motivated to do so. However, it was almost immediately apparent that I was not able to live up to my own (admittedly, very high) expectations.

I had chosen theoretical chemistry because it dealt with what I perceived as the big questions about the nature of matter and its interactions, but every day I was faced with small and uninteresting questions. At least they felt small compared to the effort it took trying to answer them... I felt like a failure as a PhD student, not even able to understand such a tiny process as the adsorption of histatin 5.

The turning point came when I decided to quit and finish with a licentiate degree instead. I let go of the pressure I had put on myself and focused on what I enjoy – writing, reflecting and creating a product out of that. And then I discovered that the big questions had been there waiting for me all the time – I had just been too afraid to attack them. Finally, I had gotten so far that I could experience what I had dreamt of – intellectual freedom, stimulating discussions and the possibility to write a thesis on my own terms, reflecting my own interests and concerns. For that, I am immensely grateful.

With this new energy and a gentle push from Roland, I decided to continue towards the doctoral degree. I also decided that it was time to have a baby. The last two years of my doctoral studies have thus revolved a lot around becoming a parent. This has taught me not to let my research define me as a person. However, I still struggle with forming a new identity. I may not continue in science, but who am I if I am not a researcher or a scientist?

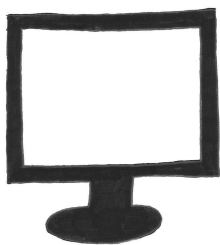
Whatever the answer may be, I will always be someone who once fell in love with theoretical physical chemistry. This book is the child of that love affair.

With love,

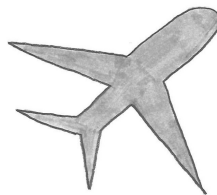
Kristin Hyltegren, September 2019–March 2020

POPULÄRVETENSKAPLIG SAMMANFATTNING

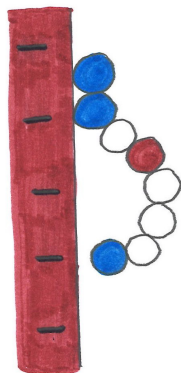
När någon frågar mig vad jag jobbar med brukar jag svara att jag studerar hur proteiner fäster på negativt laddade ytor. Om samtalet fortsätter kommer vi in på datorsimuleringar och tillämpningar av forskningen. Det är sällan lätt att svara på frågor om min forskning och samtidigt hålla det på en lagom nivå. Därför har jag valt att ta hjälp av bilder för att försöka berätta vad den här avhandlingen egentligen handlar om. Välkommen in i världen av teoretisk kemi och statistisk mekanik!



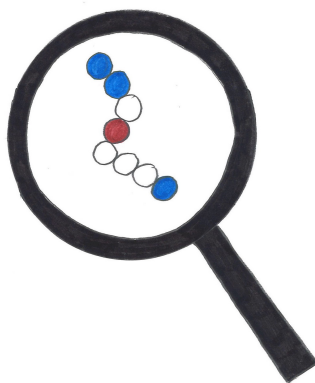
Som teoretiska kemister försöker vi att förstå molekylers egenskaper och beteenden genom modeller och beräkningar. Till vår hjälp har vi ofta datorer.



I en datorsimulering kan man på ett kontrollerat sätt studera eller uppleva en imitation av verkligheten. Ett exempel är en flygsimulator.



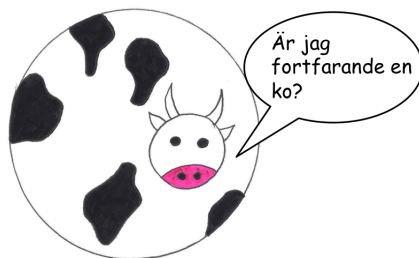
I mina datorsimuleringar studerar jag hur molekyler, närmare bestämt proteiner, fastnar (adsorberas) på negativt laddade ytor.



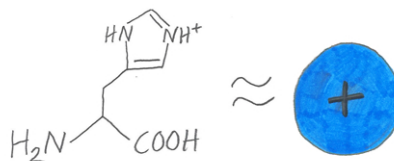
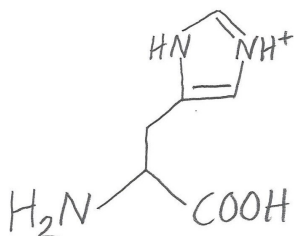
Från simuleringarna kan vi få detaljerad information om enskilda proteiner som inte går att få från experiment.



Samtidigt är det viktigt att komplettera med experiment för att, om möjligt, testa att våra modeller faktiskt representerar verkligheten.

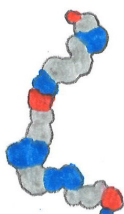


I modellerna görs nämligen förenklingar – dels för att beräkningarna inte ska kräva för mycket datorkraft och dels för att vi inte vet exakt hur molekylerna interagerar.

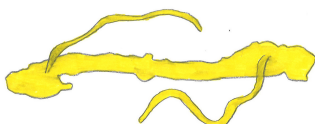


Ett protein består av olika aminosyror som är hopkopplade med varandra genom kemiska bindningar.

Istället för att ha med varje atom i proteinet har vi använt så kallade grovkorniga modeller. Varje aminosyra representeras av en sfär. Eventuella laddningar placeras i mitten av sfären.



Histatin 5



Fibrinogen

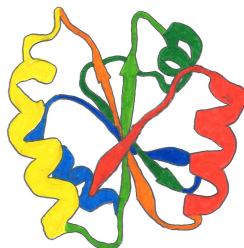
Vi har tittat på två olika proteiner: histatin 5 och fibrinogen.



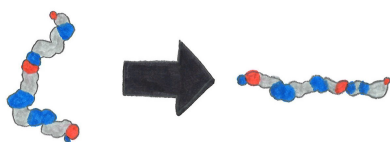
Histatin 5 finns i mänsklig saliv och kan förhindra svampinfektioner i munnen.



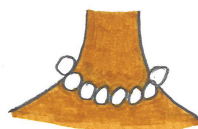
Fibrinogen finns i blod och hjälper till att få det att koagulera.



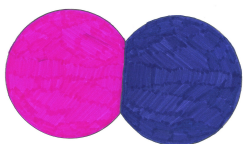
De flesta proteiner veckar sig till en väldefinierad struktur.



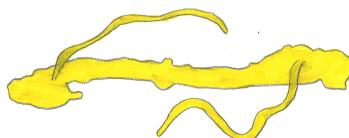
Histatin 5, däremot, är ett exempel på ett oordnat protein, vilket innebär att det inte veckar sig till en särskild struktur utan kan se ut på många olika sätt.



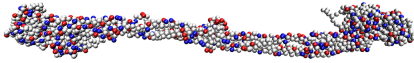
Vi har modellerat histatin 5 ungefär som ett pärlhalsband med mjuka pärlor. Att pärlorna är mjuka innebär att de kan tryckas ihop/överlappa, men bara lite eftersom energin som krävs för att trycka ihop pärlorna annars blir för stor.



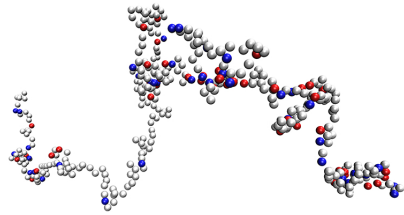
Jämför med vad som händer om du försöker pressa ihop två pumpade bollar.



Modellen för fibrinogen ser annorlunda ut. Det är nämligen till största delen ett ordnat protein, men med två oordnade svansar.



Den ordnade delen av fibrinogen är modellerad som en helt rigid struktur med sfäriska aminosyror vars positioner har bestämts av var de befinner sig när proteinet är i kristallform.



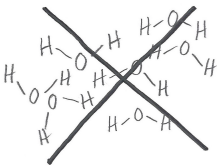
De oordnade svansarna är modellerade på i princip samma sätt som histatin 5.



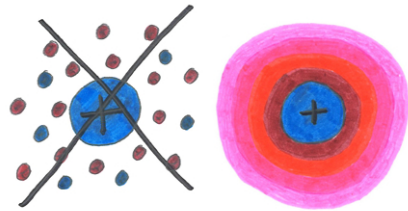
Men vi har mer än proteiner i systemet! Vi har en yta, vatten och salt, som alla består av atomer/joner. De måste också modelleras på något vis!



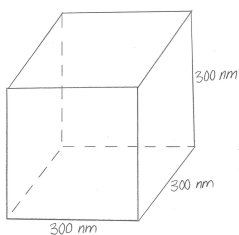
Ytan modelleras som helt slät och oftast med laddningen utsmetad jämnt över hela ytan, fastän laddningen i verkligheten är utspridd på ett visst antal laddade grupper.



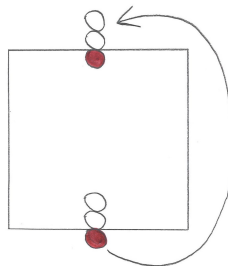
Själva vattenmolekylerna finns inte med utan beskrivs som ett enhetligt medium.



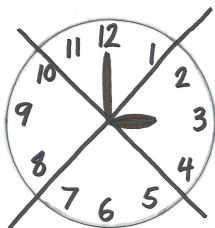
Saltjonerna finns i de flesta av mina simuleringar inte heller med utan effekten av dem beskrivs på ett förenklat sätt.



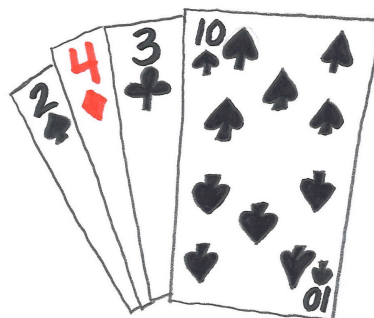
Vi måste också begränsa storleken på vårt system betydligt mer än när man gör experiment. Det kan till exempel vara rimligt att ha en låda på $300 \text{ nm} \times 300 \text{ nm} \times 300 \text{ nm}$ ($1 \text{ nm} = 0.000000001 \text{ m}$).



För att inte lådans kanter ska påverka resultaten används så kallade periodiska randvillkor. Det innebär att om molekyler rör sig ut ur lådan från en sida kommer de in i lådan från motsatt sida.



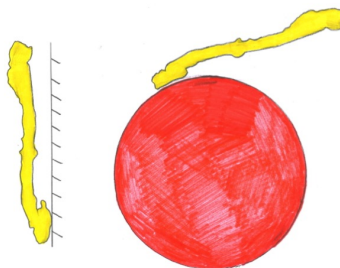
Istället för att förflytta våra molekyler som i verkligheten genom tid och rum gör vi Monte Carlo-simuleringar. Där finns ingen tid och molekylerna förflyttas slumpvis enligt vissa regler som ger korrekta medelvärden.



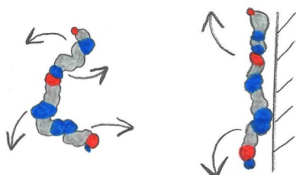
Det är lite som att dra kort ur en kortlek – alla kort representerar leken oavsett i vilken ordning vi tittar på dem.



Genom att observera var molekylerna befinner sig under simuleringarna och vilka strukturer de har kan vi, om modellen stämmer tillräckligt väl, få information om hur det förhåller sig i verkligheten.



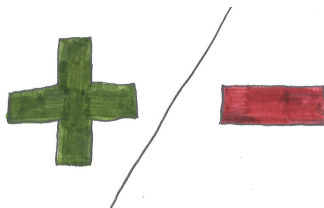
Vi har sett att fibrinogen sticker ut mer i lösningen när det adsorberar till en böjd yta än till en platt.



Adsorberat histatin 5 har en något lite mer ordnad struktur än i lösning.

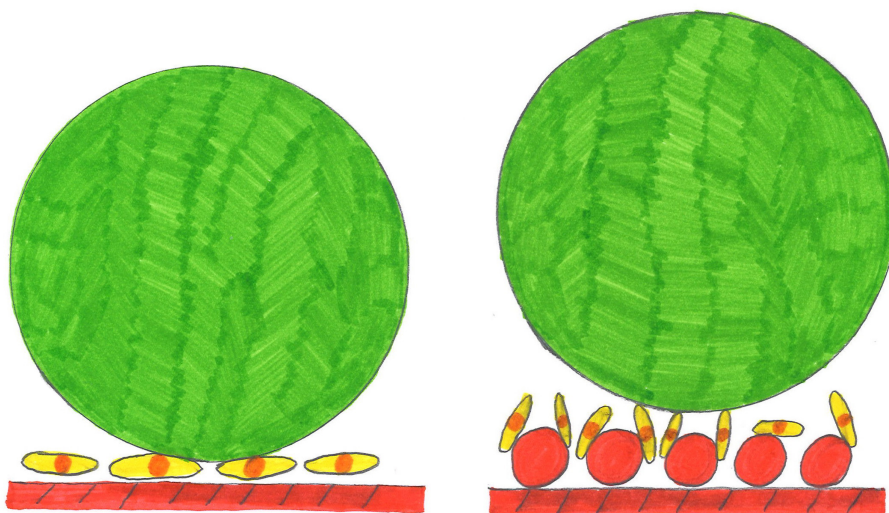
Modell
≠
experiment

Jämförelse mellan simuleringar och experiment har visat att något i modellen saknades för att ge lika mycket adsorption av histatin 5 som i experimenten. Det kan till exempel vara att ytladdningen i verkligheten är större än det uppmätta värde vi har använt i simuleringarna, att saltjonerna behöver vara med och/eller att vattnets struktur behöver finnas med i modellen.



Vad kan då resultaten användas till?

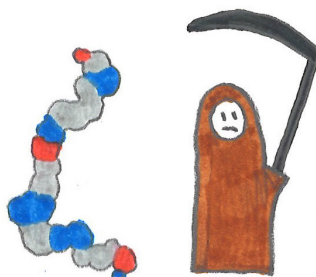
Jo, hur fibrinogen adsorberar på platta ytor respektive på små, sfäriska partiklar är relevant för design av material som används för olika sorters implantat. Fibrinogen adsorberar på implantat och kan både öka och minska hur mycket bakterier som fäster på ytan beroende på om ytan är slät eller försedd med sfäriska partiklar.



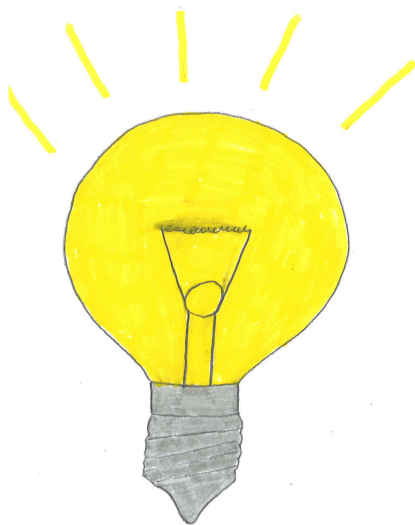
De olika orienteringarna hos adsorberat fibrinogen kan vara en förklaring till att bakterierna binder olika väl till proteinet. När proteinerna ligger platt på ytan är stället bakterierna helst binder till (orange) tillgängligt. När proteinet står ut i lösning, däremot, kommer bakterierna inte åt stället de helst binder till.



En ökad förståelse för hur oordnade salivproteiner, bland annat histatin 5, adsorberar skulle kunna leda till att bättre saliversättningsmedel utvecklades.



Hur histatin 5 adsorberar till cellmembran och om det förändrar sin struktur vid adsorption är relevant för att förstå dess svampdödande funktion.



Genom att teorin tar hjälp av experiment, och tvärtom, får man draghjälp på resan mot förståelse.

LIST OF PUBLICATIONS

This thesis is based on the following papers, which will be referred to by their Roman numerals in the text.

- I Adsorption of the intrinsically disordered saliva protein histatin 5 to silica surfaces. A Monte Carlo simulation and ellipsometry study**
K. Hyltegren, T. Nylander, M. Lund, M. Skepö.
Journal of Colloid and Interface Science, 467, **2016**, pp. 280–290.
- II Adsorption of polyelectrolyte-like proteins to silica surfaces and the impact of pH on the response to ionic strength. A Monte Carlo simulation and ellipsometry study**
K. Hyltegren, M. Skepö.
Journal of Colloid and Interface Science, 494, **2017**, pp. 266–273.
- III Integrating All-Atom and Coarse-Grained Simulations—Toward Understanding of IDPs at Surfaces**
K. Hyltegren, M. Polimeni, M. Skepö, M. Lund.
Journal of Chemical Theory and Computation, 16, **2020**, pp. 1843–1853.
- IV Adsorption of Fibrinogen on Silica Surfaces—The Effect of Attached Nanoparticles**
K. Hyltegren, M. Hulander, M. Andersson, M. Skepö.
Biomolecules, 10, **2020**, 413.

CONTRIBUTION REPORT

I Adsorption of the intrinsically disordered saliva protein histatin 5 to silica surfaces. A Monte Carlo simulation and ellipsometry study

I performed the experiments and the simulations, analysed the data, and wrote the manuscript with support from the co-authors.

II Adsorption of polyelectrolyte-like proteins to silica surfaces and the impact of pH on the response to ionic strength. A Monte Carlo simulation and ellipsometry study

I took part in designing the study, performed the simulations, analysed the data, and wrote the manuscript with support from M.S.

III Integrating All-Atom and Coarse-Grained Simulations—Toward Understanding of IDPs at Surfaces

I performed the conformational swap simulations, analysed the data, and wrote the manuscript with support from the co-authors.

IV Adsorption of Fibrinogen on Silica Surfaces—The Effect of Attached Nanoparticles

I was main responsible for designing the study, and setting up the model of the protein. I performed all the simulations and analysed the data. I wrote the manuscript with support from the co-authors.

INTRODUCTION

“Representation of the world, like the world itself, is the work of men; they describe it from their own point of view, which they confuse with the absolute truth.”

Simone de Beauvoir, The Second Sex (1949)

1.1 Initial reflections

While Simone de Beauvoir wrote about men, I believe that the quote above is also relevant for a tendency among us natural scientists. We are often interested in finding some kind of truth about the world, while forgetting our own role in the “production” of knowledge. In a chemistry textbook, the pages are often full of conclusions about the world presented as truths. In general, we get to know very little about how people came to those conclusions and what kind of support they have. This leaves little room for discussion and does not prepare students for doing research.

As science students, we are taught to always erase ourselves from our work when we write reports. It is not *we* who mix two solutions with each other, the solutions *are mixed*. It is of course an important principle when doing experimental work that the work should be possible to reproduce by others and therefore, ideally, the identity of the experimenter is irrelevant. However,

in reality reproducibility is not easy to achieve [1].* I believe that the identity of the researchers and the environment they are working in are relevant since that determines the parameters that are not described in *e.g.* a “Materials and methods” section, and thus are difficult to reproduce by others.

What is also important here is that science is not only about performing experiments or simulations. It is maybe even more about interpreting your data, designing studies, making up hypotheses etc. Here, I would say, the identities and beliefs of the researchers are even more important. In the debated book *The Golem: What Everyone Should Know About Science*, Collins and Pinch describe an experiment by Eddington that was claimed to have proved Einstein’s theory of relativity [2]. However, Eddington’s measurements were not very exact, and when he chose which to keep and which to discard, he had the theory of relativity in mind, meaning that he used the theory he had set out to prove.

It is not nature that tells us how to interpret an experiment. We interpret and explain results of experiments. I am happy that it is accepted to explicitly write for example “we believe” when discussing your results in a paper. This makes the paper easier to read and also makes it more clear where the interpretation comes from. It is simply more honest.

In some science disciplines it is common for the researcher to write something about who they are and their pre-understanding of their research area, in order to increase transparency towards the reader. Often, this is made with a reference to Haraway, who writes about “situated knowledges” [3].

Here, I would like to make it somewhat more clear where my interpretations come from.

1.2 The ‘I’ in (this) science

Here, I describe my research journey, my view on a good scientific model, and the ultimate goals of the research projects in the thesis.

1.2.1 My journey as a researcher

My background

I come mainly from a chemistry background. I took my master’s degree in chemistry at The University of Gothenburg in 2013. However, I also took some courses in physics, programming, and mathematics. I did my master’s project in statistical mechanics at the Division of Physical Chemistry. In the autumn of 2013 I started my doctoral studies at Lund University.

*Actually, chemistry did the worst among the science disciplines studied in the cited survey, with almost 90 % having failed to reproduce results of others and more than 60 % having failed to reproduce their own results.

My beliefs and their effect on the science

In the beginning of my doctoral studies, I viewed experiments as the truth that all simulations should approach. For example, I started performing simulations with a titrating surface (a surface that may change its charge due to uptake or release of protons). I used four different sets of parameters and none of them were close to the experimental results for surface charge density. I felt discouraged by this and moved on to another project. If I would go back, with the knowledge I have today, I would have more faith in my model since the exact value of the charge density at a surface is not easy to measure experimentally.

Most experimental techniques rely on models and assumptions in order to interpret the raw data. Thus, it is important to know something about the assumptions made in the experiments before comparing experimental and theoretical data.

I had the unrealistic hope for quantitative agreement between experiment and simulations, but even if the simulations were perfect representations of reality, they would not agree with experimental data due to the approximations made *e.g.* in ellipsometry.

Ellipsometry, reproducibility, and discarding data

In the beginning of my doctoral studies, I encountered the experimental technique of ellipsometry, which was completely new to me. The ellipsometry journey has not been straightforward. Sometimes there was a drift in the instrument, and I also realised that I had used two different procedures for cleaning the surface, giving different results. Therefore, I had to discard a lot of data.

The measurements at pH 6 and 10 mM salt were especially challenging. That is visible in the standard deviation in Figure 9.1. One of the five measurements I conducted gave a much higher adsorbed amount than the others. I do not trust that result but I looked through my lab journal and could find no reason to discard it. Therefore, I included it in order not to make the same mistake as Eddington.

I once heard a man joke about physical chemists, saying that they only make a single measurement for each condition they study, while in other areas of chemistry one always repeats measurements. If I would go back, and if I had more time, I would have made several measurements for *every* condition that I used, since apparently the reproducibility depended on the system.

My understanding of the surface

I performed experiments with the protein histatin 5 in solution and a smooth silica surface, and in the beginning I viewed the surface as a constant while the protein was able to undergo changes in conformation, net charge etc. However, I learned gradually that things were not that simple. The surface had different charges depending on the pH of the surrounding solution, and it also gained different charges depending on the pretreatment.

I would say that the understanding of the surface chemistry, and what affects it, constitutes one of the main learning achievements of my doctoral studies. Now, I believe that the surface chemistry could be even more important for the adsorption (when a molecule adheres to a surface without any surface penetration) of histatin 5 than the chemistry of the histatin.

My role in the modelling

When I started doing simulations, which was also new to me, I inherited a model from another PhD student. After a while, I made small changes to the model (such as changing the pK_a values of the amino acids), but on the whole I have not developed the model that I have been using. This means that while many researchers start by exploring models or methods, and choose what they can defend best, I started with the model and the method and then gradually learned to defend it. In Paper IV, however, I took more responsibility for the modelling, and added analysis routines that I needed to the program I used. While I am still not completely content with my work, I have learned to accept the limitations of our models and instead appreciate the beauty of what they *can* do.

1.2.2 What constitutes a good model?

Here, I would like to quote Albert Einstein: “Everything should be made as simple as possible but not simpler.” To me, this is an accurate description of a good model. Maybe that is why I have continued to use the coarse-grained models of proteins that I was introduced to in the beginning of my doctoral studies, with only minor changes. However, I believe that there is not a single type of model that can be used for every chemical problem. Of course, the model must fit the purpose. Here, the purpose of the research project is important.

1.2.3 What is the ultimate goal of the research project?

The ultimate goal of this research project has been to understand how proteins adsorb: Which conformations do they have? How strongly do they attach? What is the influence of pH, ionic strength, and surface nanostructure? These questions have implications for the creation of antifungal peptides and implants to better resist bacterial adhesion leading to infections.

Now that you now something about my personal research journey, I hope that you would like to follow me on the scientific journey through this thesis.

THE STUDIED PROTEINS

“Proteins are the machinery of living tissue that builds the structures and carries out the chemical reactions necessary for life.”

Michael Behe

The goal of this chapter is to introduce the proteins that I have studied throughout this research project, namely histatin 5 and fibrinogen. I will also discuss proteins in general.

2.1 Proteins and polypeptides

A protein is a large molecule made from amino acids which are bound to each other through a peptide bond, see Figure 2.1. Since the amino acids lose a few of their original atoms (a water molecule) upon forming a peptide bond, the residual parts that make up the proteins are called amino acid *residues*. A molecule where several amino acid residues are connected by peptide bonds is called a polypeptide.

Proteins are a type of polypeptides. The building blocks are 20 different amino acids, see Figure 2.2. The word protein is generally reserved only for longer polypeptides. There is no absolute requirement for how long a polypeptide has to be to be called a protein, but most proteins contain between 50 and 2000 residues [4]. Interestingly, histatin 5 is referred to as a protein in the literature even though it is only 24 amino acid residues long [5]. In earlier literature, it was named HRP-5 (histidine-rich polypeptide 5) [6, 7] but it seems that as its antifungal function was discovered, it started to be referred to as a protein [5].

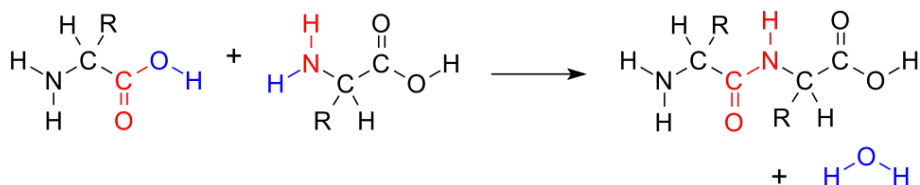


Figure 2.1: The formation of a peptide bond between two amino acids. R denotes the side chains of the amino acids and the other atoms form the *backbone* of the peptide. (Public domain, <https://commons.wikimedia.org/wiki/File:AminoacidCondensation.svg>)

2.1.1 Protein structure

The structure of a protein is generally described as divided into four different layers: primary, secondary, tertiary, and quaternary structure. The definitions are given below and illustrated in Figure 2.3.

Primary structure

The primary structure of a protein is defined as the sequence of amino acid residues from the N- to the C-terminal. The N-terminal is the end of the protein that contains the amino group (NH_2) and the C-terminal contains the carboxylic acid group (COOH) of the backbone, see Figure 2.1.

Secondary structure

The secondary structure are common structural elements of proteins, for example α -helices and β -sheets. Such regular patterns are made possible by specific hydrogen-bonding patterns of the protein backbone (see Figure 2.1 for a definition of the backbone). The oxygen atoms of the $\text{C}=\text{O}$ -groups bind to the hydrogens of the $\text{N}-\text{H}$ -groups. Several of these bonds in a row connect two different parts of the backbone with each other and a secondary structure is formed.

Tertiary structure

The tertiary structure is the three-dimensional structure of the protein as a whole. Hydrophobic interactions are the main driving force for the process where a protein folds into its tertiary structure [8]. However, covalent bonds (sulfur bridges), electrostatic interactions (such as salt bridges), and hydrogen bonds are also important. Most of these interactions are described in more detail in chapter 5.

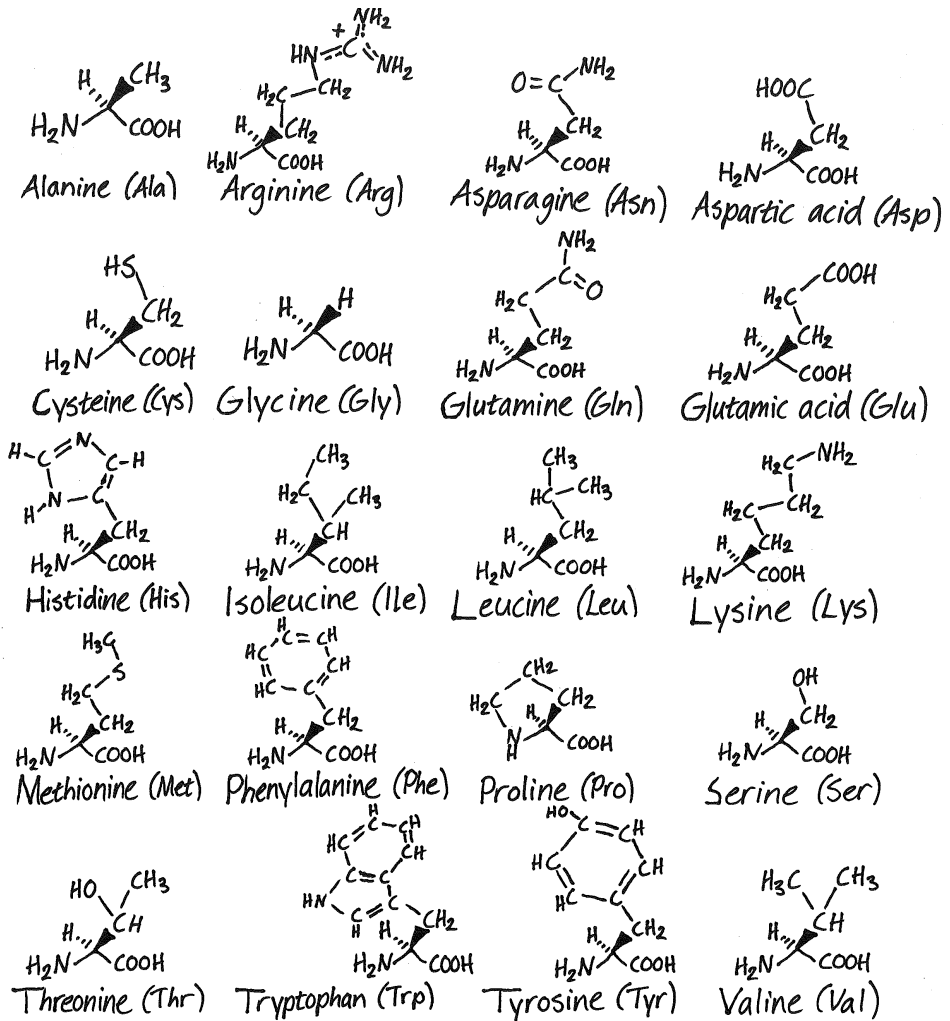


Figure 2.2: The structures of the 20 different amino acids that are the building blocks for proteins.

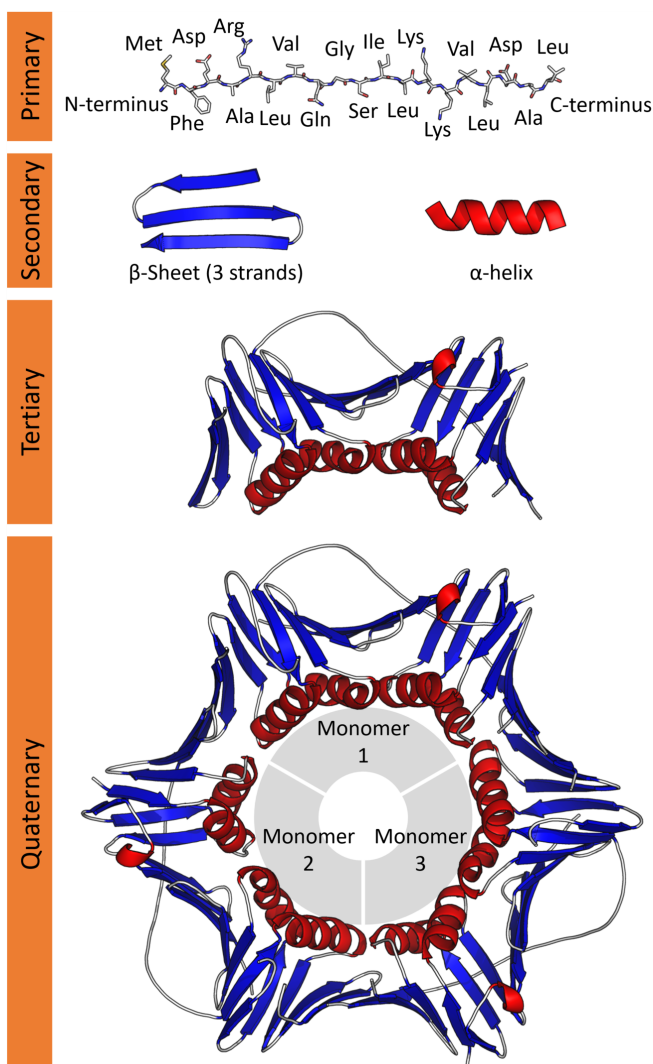


Figure 2.3: An illustration of primary, secondary, tertiary, and quaternary structures of the protein PCNA (proliferating cell nuclear antigen). (By Thomas Shafee – Own work, CC BY 4.0, <https://commons.wikimedia.org/w/index.php?curid=52821068>.)

Quaternary structure

Quaternary structure is the three-dimensional structure of two or more proteins forming a larger functional unit. A well-known example of such a unit is haemoglobin, which consists of four protein subunits in most vertebrates.

2.1.2 Does structure determine function?

Many proteins are like molecular machines performing different tasks in the body, for example catalysing chemical reactions (these proteins are called enzymes), transporting molecules and replicating DNA. Some proteins are also essential for providing structure for various tissues etc. For example, collagen – the most common protein in mammals – is an extracellular protein that is an important constituent of skin, bone, teeth, cartilage, and tendon [4].

For a long time, it was assumed that proteins needed a well-defined 3D-structure in order to be functional. For example, an enzyme is often thought to be like a lock, which can only perform its function (open) when the right substrate (key) enters the active site (keyhole). In addition, proteins that are important for building structures also depend on having a specific structure themselves.

However, there are many proteins that do not adopt a well-defined 3D-structure under physiological conditions, and they are still functional – a discovery that ended the so-called “structure–function paradigm” within protein science [9–13].

2.1.3 Intrinsically disordered proteins

Intrinsically disordered proteins are proteins that do not adopt a well-defined secondary or tertiary structure under physiological conditions ($\text{pH} \approx 7$, ionic strength $\approx 150 \text{ mM}$). Instead, they behave essentially as random coils in solution. A random coil is like a chain – the different parts are bonded to each other but apart from that condition, the chain/molecule can adopt essentially any conformation. The probability that a part of the chain has a specific conformation is unaffected by the conformation of the rest of the chain.

Approximately 30 % of the proteins present in eukaryotes have disordered regions with a length of ≥ 50 residues [10]. Counting also shorter proteins, the number would increase since short proteins are less likely to fold into well-defined tertiary structures.

Examples of intrinsically disordered proteins are the milk protein β -casein (209 residues) [14] and the saliva protein histatin 5 (24 residues) [15, 16]. Both of them have important functions – β -casein transports calcium to the suckling infant [17] and histatin 5 has antimicrobial effects [5, 18].

2.2 Histatin 5

Histatin 5 is a saliva protein produced in humans and higher primates. It is a short, disordered protein of 24 amino acid residues. Its main function is that it is antifungal.

2.2.1 The structure of histatin 5

The amino acid sequence of histatin 5 is Asp-Ser-His-Ala-Lys-Arg-His-His-Gly-Tyr-Lys-Arg-Lys-Phe-His-Glu-Lys-His-His-Ser-His-Arg-Gly-Tyr [5]. Notably, one third (7 out of 24) of the amino acid residues are histidines.

Histidine is an unusual amino acid since it is mainly uncharged above pH 6 and mainly positively charged below pH 6. The other amino acids that can be positively charged (lysine and arginine) are so below pH 11 and 12, respectively. The amino acids that can be negatively charged (aspartic and glutamic acid) are so above a pH of 4. This means that histidine is the only amino acid that can change its charge at physiological pH ($\text{pH} \approx 7$). This so-called “charge regulation” mechanism of histatin 5 will be described in more detail in chapter 5.

2.2.2 The protein content and functions of saliva

Saliva consists to approximately 99.5 % of water. The rest can be divided into inorganic constituents – for example sodium, potassium, chloride, and iodide – and organic constituents such as proteins, carbohydrates, and amino acids [19]. Proteins make up between 1.0 and 6.4 g/l of saliva. Several of the proteins are intrinsically disordered (proline-rich proteins, statherin, histatins, mucins [20]). There are conflicting reports about the concentration of histatin 5 in human saliva – according to Castagnola *et al.* the mean concentration is 47 $\mu\text{g}/\text{ml}$ [21] and according to Campese *et al.* it is 8 $\mu\text{g}/\text{ml}$ [22].

Even though proteins constitute only a tiny fraction of saliva, they are important for almost all of its functions, see Figure 2.4, and thus of major importance for our oral health.

Proteins adsorb to the tooth enamel, creating a layer that protects the teeth against acid degradation and affects the attachment of bacteria to the tooth surface [24]. This layer is called the acquired enamel pellicle.

Histatin 5 selectively adsorbs to hydroxyapatite (the main constituent of the tooth enamel) [25], making it a so-called pellicle precursor. It has been shown that intact histatin 5 is present in the *in vivo* acquired enamel pellicle to some degree and that it can protect the enamel from acid injury [26]. However, histatin 5 has another function which is even more important.

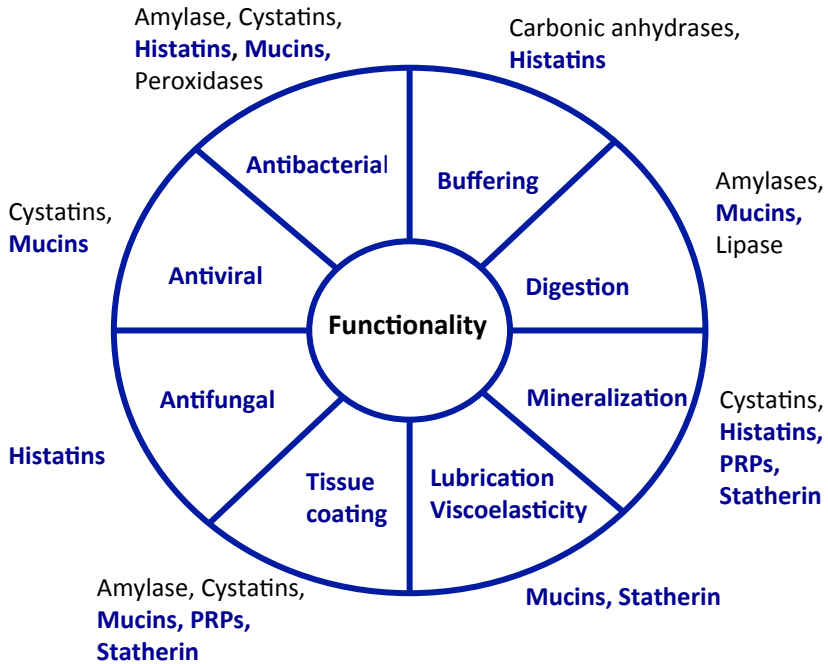


Figure 2.4: The functions of saliva and the proteins responsible for each function, adapted from Levine [23]. The intrinsically disordered proteins are marked in blue. (PRPs = proline-rich proteins)

2.2.3 The antifungal effect of histatin 5

Histatin 5 kills the fungus *Candida albicans* [5], which is commonly present in the mouths of humans.* A healthy person who carries *Candida albicans* in the mouth generally experiences no problems. However, if the fungus grows too much it causes an infection called oral candidiasis (or oral thrush). It shows up as white patches in some parts of the mouth, often on the tongue, see Figure 2.5. The infection can cause discomfort or bad taste. In extreme cases it can spread through the bloodstream or the upper gastrointestinal tract and even become fatal [28].

People with HIV, people with very dry mouths, smokers and people with diabetes are examples of people who are extra susceptible to oral candidiasis [28].

It has been suggested that histatin 5 could work as a drug against oral candidiasis [29]. There are already antifungal drugs that work but as the fungi

*More exact estimates of the prevalence of *Candida albicans* in human mouths have varied greatly and depend on the method of measurement [27].



Figure 2.5: Human tongue infected by oral candidiasis (thrush). (Photo by James Heilman, MD, distributed under a CC BY-SA 3.0 license. https://commons.wikimedia.org/wiki/File:Human_tongue_infected_with_oral_candidiasis.jpg)

become resistant, new drugs are needed. The problem with histatin 5 is that it is quickly degraded in the oral environment, which means that it is impractical and uneconomical to use the protein as it is. An interesting possibility is to connect an active fragment of histatin 5 with a molecule called spermidine. This histatin–spermidine-conjugate has shown promising results as an anticandidal drug in mice [29].

Adsorption might reduce the proteolytic degradation of histatin 5 just as for histatin 1 [30]. Thus, designing an antifungal peptide that adsorbs more strongly to the tooth enamel could be another way of limiting the problem of proteolytic degradation [31]. This means that by enhancing the understanding of the mechanisms behind the adsorption of histatin 5 to negatively charged surfaces, we could gain insights relevant for the design of new peptide-based antifungal drugs. This is one of the motivations behind the studies we have performed on histatin 5.

2.3 Fibrinogen

Fibrinogen is a blood protein that exists in vertebrates. It has a molecular weight of approximately 340 kDa and is involved in blood clotting.

2.3.1 The structure of fibrinogen

Fibrinogen consists of six polypeptide chains: two $A\alpha$ -chains, two $B\beta$ -chains, and two γ -chains. Most of the chains fold into a 45 nm long rod, while the C-terminal ~ 400 amino acid residues of the two $A\alpha$ -chains form two mostly unstructured appendages, extending out from positions close to the ends of the rod. Figure 2.6(a) shows an atomistic representation of the human fibrinogen rod as determined from the crystal structure [32]. Figure 2.6(b) shows the locations of the $A\alpha$, $B\beta$, and γ -chains in the folded fibrinogen. The unstructured appendages are not visible in the crystal structure.

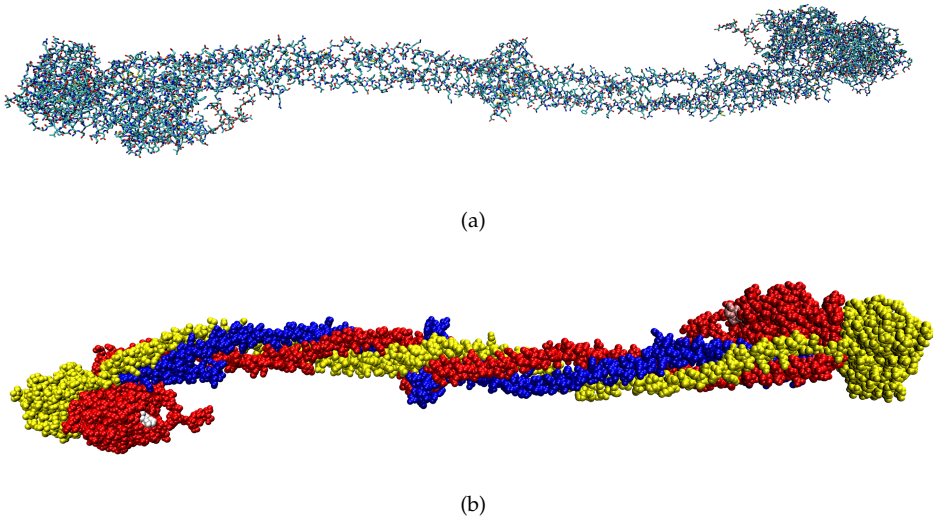


Figure 2.6: The crystal structure of human fibrinogen [32] coloured after (a) atoms, and (b) chains (blue = A α -chains, red = B β -chains, yellow = γ -chains).

2.3.2 Fibrinogen's role in blood clotting

Fibrinogen has an important role in blood clotting. When there is a wound, the enzyme thrombin attacks fibrinogen, causing it to polymerise into a fibrous protein called fibrin. Together with platelets, fibrin forms a clot over the wound site.

2.3.3 Fibrinogen adsorption on implants

When an implant is inserted into the body, its surface is quickly covered with adsorbing proteins. This protein film affects the attachment of bacteria to the implant surface. Bacteria adhering to an implant surface may find shelter from the host's immune response and colonise the surface, leading to biomaterials-associated infections. Biomaterials-associated infections are one of the most common causes of implant failure.

Since fibrinogen is an abundant blood protein, its adsorption onto biomaterials, and bacterial adhesion to adsorbed fibrinogen, are of great importance for the functionality of the biomaterials. It has been shown that while adsorbed fibrinogen increases adhesion of the bacterium *Staphylococcus epidermidis* on a smooth surface, the opposite is true for a nanostructured surface (with attached nanospheres) [33]. We investigated these systems with simulations in order to try to explain these findings.

THE STUDIED SURFACES

“ You look at the floor and see the floor. I look at the floor and see molecules. ”

Dan Aykroyd

In this chapter, I am “scratching the surface” of the complex surface chemistry of silica and tooth enamel/hydroxyapatite – the types of surfaces that are most important for my work.

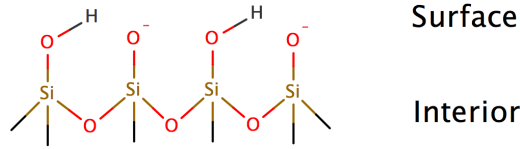
Silica is a convenient model surface to use for ellipsometry measurements, which is why I have used it for the experiments on histatin 5 adsorption in this thesis. However, tooth enamel, which consists mainly of hydroxyapatite, is the surface that is relevant in the biological system where histatin 5 is present naturally. The adsorption experiments that we compare with in Paper IV (on fibrinogen) were also made using silica surfaces.

3.1 Silica

Silica is another name for silicon dioxide (SiO_2). It is by far the most common material of the earth’s crust. It is most commonly found in the form of the mineral quartz.

3.1.1 The silica surface and its silanol groups

A silica surface that is exposed to air at ordinary temperatures reacts with water so that the surface becomes covered with silanol groups (SiOH) [34]. Immersed

Figure 3.1: The SiO_2 surface.

in an aqueous solution, these silanol groups can lose a proton (H^+), yielding charged SiO^- -groups, see Figure 3.1. This is the main mechanism by which silica surfaces acquire a negative charge. In an aqueous solution, the extent to which this happens is determined by the pH and the ionic strength of the solution.

3.1.2 The surface charge density of silica

The surface charge densities of silica particles at different pH and salt concentrations have been measured by Bolt [35] and by Samoshina *et al.* [36]. The values are given in Table 3.1.

Table 3.1: Surface charge densities of silica particles at different pH-values and concentrations of monovalent salt (c_s) in $\mu\text{C}/\text{cm}^2$. The surface charge densities determined by Samoshina *et al.* have been reproduced by measuring from a graph, and the numbers in this table are therefore approximate.

| pH | $c_s = 10 \text{ mM}$ | | $c_s = 100 \text{ mM}$ | |
|----|-----------------------|------------------------------|------------------------|------------------------------|
| | Bolt [35] | Samoshina <i>et al.</i> [36] | Bolt [35] | Samoshina <i>et al.</i> [36] |
| 6 | -0.9 | -0.25 | -1.5 | -0.50 |
| 7 | -1.8 | -1.00 | -3.2 | -2.00 |
| 8 | -3.8 | -2.75 | -6.2 | -5.75 |
| 9 | -6.9 | -7.00 | -11.6 | -12.75 |

Even though the numerical values differ between the two studies, the trends are the same. The surface charge of silica increases approximately by a factor of two when the salt concentration is increased from 10 mM to 100 mM. We have used the surface charge densities determined by Samoshina *et al.* [36] for most simulations included in this thesis.

The negative charge of the hydroxylated silica surface keeps increasing with pH until about pH 10.7. The maximum charge is limited by the density of silanol groups on the surface, which is 4–5 per nm^2 [34]. However, above a pH of 8–9, silica starts to dissolve forming silicate ions (HSiO_3^-). Complete ionisation of the surface can be achieved just below the pH where silica dissolves completely, in the presence of a concentrated salt solution.

3.1.3 Silica as a model surface

Silica has been used as a model surface both for the ellipsometry measurements made in this work, and for the measurements of fibrinogen adsorption with which we have compared our simulation results [33]. One reason for this choice is that the silica surfaces are relatively flat (according to AFM measurements the roughness is less than 0.5 nm [37]), which is a requirement for ellipsometry. In addition, these surfaces have good optical properties. When performing simulations of the same system, it is also an advantage that the surface may be modelled as completely flat. However, a real surface such as tooth enamel has significant roughness, and with flat silica surfaces as model surfaces we miss some effects of roughness.

Another disadvantage of using silica as a model surface is that the surface charge density changes so dramatically with pH. The more factors that change between different measurements, the more parameters need to be controlled and varied to simulate the systems.

3.2 Tooth enamel and hydroxyapatite

3.2.1 Tooth enamel

The tooth enamel surface consists of a mineral component – impure hydroxyapatite – and organic material forming a matrix. The organic matrix holds the mineral crystals together and regulates their formation [19]. When a newly formed tooth has appeared in the mouth, the tissue-forming cells are worn off, and the fate of the enamel is no longer determined by cellular processes but by the interactions with the fluids in the mouth [19].

The surface roughness of tooth enamel has been measured as ranging between 1.72 and 9.15 μm [38]. These values are centre-line averages, meaning that it is the average height/depth measured from a mean line of all points of the surface.

Hydroxyapatite occupies approximately 86 % of the volume of enamel and makes up 96–97 % of its weight [39].

3.2.2 Hydroxyapatite

The chemical formula of hydroxyapatite is $\text{Ca}_{10}(\text{PO}_4)_6(\text{OH})_2$. In addition to being the main component of tooth enamel, it also constitutes up to 50 % of human bone by volume.

The surface of hydroxyapatite contains approximately 80 % phosphate. In aqueous solutions at pH 7, the surface is likely to be dominated by HPO_4^{2-} and H_2PO_4^- [20].

3.2.3 The surface charge density of enamel and hydroxyapatite

The surface charge densities of enamel and hydroxyapatite vary significantly depending on the pH of the solution, the solid-to-liquid ratio, the pretreatment of the surface and, in case of hydroxyapatite, its purity [40].

According to Arends [40], enamel surfaces and hydroxyapatite surfaces of various purities are positively charged in doubly distilled water at high solid-to-liquid ratio (similar to the conditions in the mouth). However, after pretreatment with saliva from the submandibular glands, the surfaces became negatively charged, indicating that the acquired pellicle (film of proteins from the saliva) would make the enamel surfaces negatively charged *in vivo*.

At low solid-to-liquid ratios, Arends found that the enamel and hydroxyapatite surfaces were negatively charged above $\text{pH} \approx 5.5\text{--}6$ [40]. However, not as negatively charged as a silica surface would be under similar conditions.

3.3 Surface roughness or nanostructure

In my simulations, I have mainly considered the ideal case of a completely smooth surface. However, most surfaces have significant roughness, which affects how proteins adsorb. While Cai *et al.* saw little effect of surface roughness on the adsorption of fibrinogen and albumin [41], Rechendorff *et al.* used QCM-D and ellipsometry and observed a significant increase in the adsorbed amount of fibrinogen the larger the root-mean-square random roughness of the surface [42]. In fact, the adsorption increased more than the increase in available surface area. Monte Carlo simulations supported the conclusion that for the rough surfaces, the fibrinogen adsorbed to a higher degree with an end-on orientation. However, there are also cases when less protein adsorb onto a rough surface than a smooth one. For example, Deligianni *et al.* observed this for albumin [43]. The explanation here was that roughening of the Ti surface makes it more hydrophilic, thus diminishing the adsorption of albumin.

In the study of fibrinogen, we have investigated the effect of surface nanostructure on adsorption. The surface used was not rough in a normal sense but consisted of a completely flat surface covered with nanospheres. The spheres had different sizes and were placed with different spacings to test the effects of those parameters on fibrinogen adsorption. The study was initiated in order to try to explain some experimental findings where fibrinogen was adsorbed on the same kind of nanostructured surfaces. It was observed that adhesion of the bacterium *Staphylococcus epidermidis* was increased when nanoparticles were added. However, after preadsorption with fibrinogen, the opposite was found [33].

The studies with nanoparticles are designed to systematically investigate different well-defined geometries. However, they also represent a step towards understanding naturally occurring surface roughness.

THE PROBLEM OF PROTEIN ADSORPTION

“ The most complicated language we can ever attempt to learn is the one spelled by the proteins within us and rapidly written by them on any blank surface they face. Each of the “words” is long enough to fill an entire page if printed legibly, and as they are being “written” on the blank surface, they may rapidly change their meaning or, in the presence of more protein species, be displaced by a succession of these others. How then can we ever hope to read the significance of such a briefly present and changing text and context? ”

Leo Vroman, Prologue to Proteins at Interfaces II [44, p. xiii]

This work focuses on two problems of protein adsorption: The adsorption of the saliva protein histatin 5 and of the blood protein fibrinogen to silica surfaces. The purpose of this chapter is to give a brief overview of the field of protein adsorption research in order to put this work into context.

4.1 Where does protein adsorption happen and why do we study it?

Brash and Horbett write “A good perspective for adoption by the novice approaching this field is that all proteins adsorb to all surfaces.” [44]. Thus, it is not

particularly easy to design protein-repellent surfaces, which would be of use for medical devices etc. – since the adsorbed proteins can attract *e.g.* bacteria and lead to biomaterials-associated infections. Finding protein-repellent biomaterials is an active area of research.

Protein adsorption to solid surfaces is also common in nature – an example is the formation of the acquired enamel pellicle (see section 2.2.2). Other areas where protein adsorption is important involve adsorption chromatography, membrane separation, food manufacturing processes, biosensors, and drug delivery systems [45]. Thus, an understanding of protein adsorption can have many different applications.

In this work, the adsorption that happens on the tooth enamel and adsorption on implants in the body are the most relevant. For the case of histatin 5, adsorption on the *C. albicans** cell surface is also interesting, but this has not been explored in the present study.

4.2 Is adsorption related to protein function?

When a protein adsorbs on a surface it may change its conformation. For example, an intrinsically disordered protein may gain secondary structure. This conformational change may be necessary for the function of the protein. A hypothesis is that such a conformational change is what happens when histatin 5 adsorbs to the *C. albicans* cell surface.

4.3 Why is protein adsorption a difficult research problem?

Ideally, there would be a unified theory for protein adsorption that worked for every protein and every surface. We are far from being there. One of the reasons that makes this a difficult research problem is the flexibility, the large volume, and the heterogeneous surfaces of proteins [46]. Also, force fields and water models that are developed for bulk simulations are often not directly transferable to surface simulations and vice versa [47], making it difficult to simulate the process of adsorption since the protein needs to be correctly described both in the bulk state and the adsorbed state.

Another challenge is the timescale – a normal molecular dynamics simulation[†] simulates events happening on the order of nanoseconds, while an adsorption process may take hours or even days before equilibrium is reached in experiments (if slow conformational changes take place) [48].

Vroman also writes “Even single purified proteins must be suspected of not behaving as they would normally in the environment where they evolved their specific and often unknown functions.” [44, p. xiv]. Thus, even if we understand the adsorption of a single protein on a specific surface, we are far from understanding how the protein behaves in its natural, crowded environment

*The fungus that histatin 5 kills.

[†]Molecular dynamics simulations are introduced in section 7.2.

inside the body. However, we need to start somewhere, and a good place to start is to review the non-covalent interactions that are present between atoms and ions.

INTERACTIONS IN THE MOLECULAR WORLD

“ No lens is quick enough to track the movement of the human body. The molecules are always moving. ”

Roger Rees

In order to understand how and why proteins form structures, interact with each other and adsorb on surfaces (the theme of this work), we must understand what kinds of interactions that are present between molecules and atoms in general. In this chapter, I will describe the different interactions that are important in the world that molecules experience.

Most of the information in this chapter is taken from Israelachvili [49] and for more in-depth information, I refer the reader to this book.

5.1 Coulomb interactions

The electrostatic interaction between two charged atoms (ions) is described by Coulomb's law:

$$F = \frac{|Q_1 Q_2|}{4\pi\epsilon_0\epsilon_r r^2} \quad (5.1)$$

where F is the magnitude of the electrostatic force between the atoms, Q_1 and Q_2 are the charges of atoms 1 and 2, ϵ_0 is the vacuum permittivity, ϵ_r is the relative

permittivity of the medium surrounding the atoms, and r is the distance between the atoms.

The potential energy between two charges is given by

$$V = \frac{Q_1 Q_2}{4\pi\epsilon_0\epsilon_r r} \quad (5.2)$$

which means that the distance dependence is $1/r$.

5.1.1 Screened Coulomb interactions

In a solution containing ions, the ionic atmosphere causes the net pair interaction to decay more rapidly with distance than the individual contributions of Equation (5.2). This *electrostatic screening* effect is taken into account by the screened Coulomb potential:

$$V = \frac{Q_1 Q_2}{4\pi\epsilon_0\epsilon_r r} e^{-\kappa r} \quad (5.3)$$

where κ^{-1} is the *Debye length*.

$$\frac{1}{\kappa} = \sqrt{\frac{\epsilon_0\epsilon_r k_B T}{2N_A e^2 I}} \quad (5.4)$$

where k_B is the Boltzmann constant, T is the temperature, N_A is Avogadro's constant, e is the elementary charge, and I is the *ionic strength* defined by

$$I = \frac{1}{2} \sum_{i=1}^n z_i^2 c_i \quad (5.5)$$

where n is the number of different ionic species, z_i is the charge number of an ion of type i and c_i is the concentration of ions of type i .

5.1.2 Charge regulation and protein charge capacitance

Acids and bases are molecules that can exchange protons with the surrounding solution, meaning that their charges change. That makes it possible for acids and bases to respond to an electric field. This phenomenon is called *charge regulation*, since the molecule regulates its charge depending on the environment. In case it is close to a positively charged object, it is more favourable for it to become more negatively charged and, conversely, if it is close to a negatively charged object it is favourable for it to become more positively charged.

At a certain pH (equal to the pK_a), an isolated (non-interacting) acid or base has an equal probability of being charged or neutral. Around this pH, it is particularly easy to perturb the degree of ionisation because there is a large natural fluctuation, which can be expressed as a high *charge capacitance* [50].

The pK_a of the amino acid histidine is approximately 6, which is close to physiological pH. The high content of histidines in histatin 5 means that it has an unusually high charge capacitance compared to other proteins under physiological conditions. Thus, charge regulation can sometimes contribute significantly to the driving forces behind the adsorption of histatin 5 [51].

5.2 Interactions involving permanent dipoles

Most molecules have no net charge, but many molecules are polar. This means that the equal number of positive and negative charges are not evenly distributed, but the electrons are shifted towards one end of the molecule. This leads to an excess (partial) negative charge at one end and an excess (partial) positive charge at the other end. Polar molecules/objects can be characterised by a vector quantity called the dipole moment. For the case of two point charges separated by a distance l , the dipole moment is:

$$\mu = ql, \quad (5.6)$$

where q is the absolute value of the charges ($+q$ and $-q$), and l is the distance vector from the negative charge to the positive charge.

5.2.1 Ion–dipole interactions

When an ion interacts with a polar molecule and the dipole moment can be described as a point in space, the potential energy becomes:

$$V = -\frac{Q\mu \cos \theta}{4\pi\epsilon_0\epsilon_r r^2} \quad (5.7)$$

where Q is the charge of the ion, μ is the magnitude of the dipole moment, and θ is the angle between \mathbf{r} (the vector from the ion to the centre of the dipole) and \mathbf{l} . Note that the distance dependence is $1/r^2$.

In case the factor determining the magnitude of the angular dependence in Equation (5.7) $\left(\frac{Q\mu}{4\pi\epsilon_0\epsilon_r r^2}\right)$ falls below $k_B T$, the dipole can rotate more or less freely. However, since the attractive interactions are more favourable, the angularly averaged potential will not be zero. By averaging in a way that takes into account that some orientations are more favourable than others (more specifically, by using Boltzmann averaging) one gets the following expression for the interactions between ions and rotating dipoles [49]:

$$V \approx -\frac{Q^2\mu^2}{6(4\pi\epsilon_0\epsilon_r)^2 k_B T r^4} \text{ for } k_B T > \frac{Q\mu}{4\pi\epsilon_0\epsilon_r r^2} \quad (5.8)$$

Note that this potential decays more rapidly with distance than the one described by Equation (5.7).

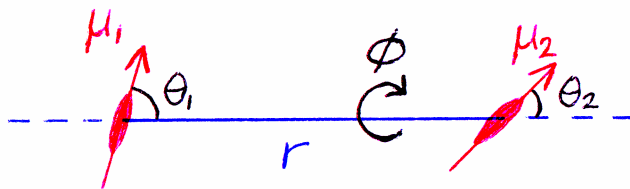


Figure 5.1: The angles θ_1 , θ_2 , and ϕ between two stationary dipoles separated by a distance r .

5.2.2 Dipole–dipole interactions

The potential energy between two stationary dipoles is given by:

$$V = -\frac{\mu_1\mu_2}{4\pi\epsilon_0\epsilon_r r^3} (2\cos\theta_1\cos\theta_2 - \sin\theta_1\sin\theta_2\cos\phi), \quad (5.9)$$

where ϕ is the azimuthal angle, see Fig. 5.1. However, in solution the dipoles rotate. Thus, the angle-averaged potential found by using the Boltzmann weight is more relevant for this type of system [49]:

$$V \approx -\frac{\mu_1^2\mu_2^2}{3(4\pi\epsilon_0\epsilon_r)^2 k_B T r^6} \text{ for } k_B T > \frac{\mu_1\mu_2}{4\pi\epsilon_0\epsilon_r r^3} \quad (5.10)$$

Note that the distance dependence is now $1/r^6$ instead of $1/r^3$ as in Equation (5.9).

The Boltzmann-averaged interaction described by Equation (5.10) is called the *Keesom* interaction and it is one of three $1/r^6$ -dependent interactions which are included in the so-called *van der Waals* interactions.

5.2.3 Hydrogen bonding

The hydrogen bond is mainly an unusually strong electrostatic interaction which can orient neighbouring molecules in both liquids and gases [49]. A hydrogen bond can form between an electronegative atom with a free electron pair, such as O, N or F, and a hydrogen atom bound to such an electronegative atom. The reasons for the strength of this type of electrostatic interactions are the small size of the H-atom, allowing for smaller separations, and the high electronegativity of O-, N- and F-atoms leading to a relatively large positive charge on the H-atom.

5.2.4 Dipole–induced dipole interactions

A polar molecule can induce a dipole in a nonpolar molecule since its electric field makes it more favourable for the electrons of the nonpolar molecule to reside on a specific side of the molecule. This process is called *polarisation* and gives rise to another $1/r^6$ -dependent potential which is the second component belonging to the van der Waals interactions. It is often called the *Debye interaction*.*

5.3 London dispersion forces (induced dipole–induced dipole)

London dispersion forces are interactions occurring between all molecules – both polar and nonpolar. Dispersion forces are of quantum mechanical origin [49], but they can be understood without diving deeply into quantum mechanics.

A nonpolar molecule has zero dipole moment averaged over time. However, at a specific moment in time, it has a dipole moment due to the specific positions of the electrons around the nuclei. This dipole generates an electric field, which polarises nearby atoms. Therefore, there is an instantaneous attractive force between nearby molecules – the dispersion attraction. Dispersion forces are stronger between larger molecules since, in general, large molecules have more electrons and valence electrons are farther from the nuclei, and thus the molecules are more easily polarised.

The London dispersion interaction energy has a distance dependence of $1/r^6$ and it is the third component belonging to the van der Waals interactions. Often, the term “van der Waals interactions” is used to describe only dispersion interactions.

5.4 Excluded volume/Pauli repulsion

According to the Pauli exclusion principle, two electrons cannot occupy the same space/state. This means that when two atoms come close to each other they will feel a Pauli repulsion, which is of quantum mechanical origin. This gives rise to excluded volume – a volume that is impossible for an atom or molecule to enter since it is already occupied.

5.5 Pauli repulsion + dispersion \approx the Lennard-Jones potential

A common way of describing Pauli repulsion and dispersion attraction between two particles mathematically is by using the Lennard-Jones potential:

$$V = 4\epsilon_{\text{LJ}} \left[\left(\frac{\sigma}{r} \right)^{12} - \left(\frac{\sigma}{r} \right)^6 \right], \quad (5.11)$$

*Note that ions can also induce dipoles, but a description of this type of interactions has been omitted since the mechanism is the same as for the Debye interaction.

where ϵ_{LJ} is the depth of the potential well between the interacting particles, σ is the distance where the potential is zero (equal to the sum of the Lennard-Jones radii of the two interacting particles), and r is the distance between the particles.

As stated before, the dispersion interaction has a distance dependence of $1/r^6$. The repulsion should be steep and the specific choice of a $1/r^{12}$ -dependence is only motivated by computational convenience ($1/r^{12} = (1/r^6)^2$).

5.6 Hydrophobic interactions

Water is a polar solvent. This means that it is unfavourable to dissolve nonpolar molecules in water. The low solubility of nonpolar molecules/fragments in water gives rise to a “hydrophobic attraction” between such molecules/fragments in water.

5.7 Adsorption and forces between macromolecules and charged surfaces

The forces between surfaces and molecules are similar to the ones described above – after all, a surface also consists of atoms, and/or ions. However, there are some interactions that become more important when we look at molecules in relation to surfaces.

5.7.1 The electrical double layer

Since there are equal amounts of positive and negative charges in nature, a charged surface must have counterions that together have a charge that is of equal magnitude, but with the opposite sign. When the surface is immersed in solution, the counterions are present in a layer extending out from the surface. The surface and the layer containing the counterions make up the so-called electrical double layer, see Figure 5.2. The double layer has been treated mathematically in several different ways. In most simulations included in this work, Gouy–Chapman theory has been used.

Gouy–Chapman theory

A charged surface is characterised by its surface charge density ρ and its electrostatic potential Φ_0 . Gouy–Chapman theory describes the relationship between these two quantities and also how the potential and the distribution of ions in solution vary with the distance from the surface.

Gouy–Chapman theory is derived from a model where the charged surface is infinite in the x - and y -directions and has a smeared charge, and the ions in solution are point charges. According to Gouy–Chapman theory, the electrostatic potential decreases exponentially with distance from the surface. For a more

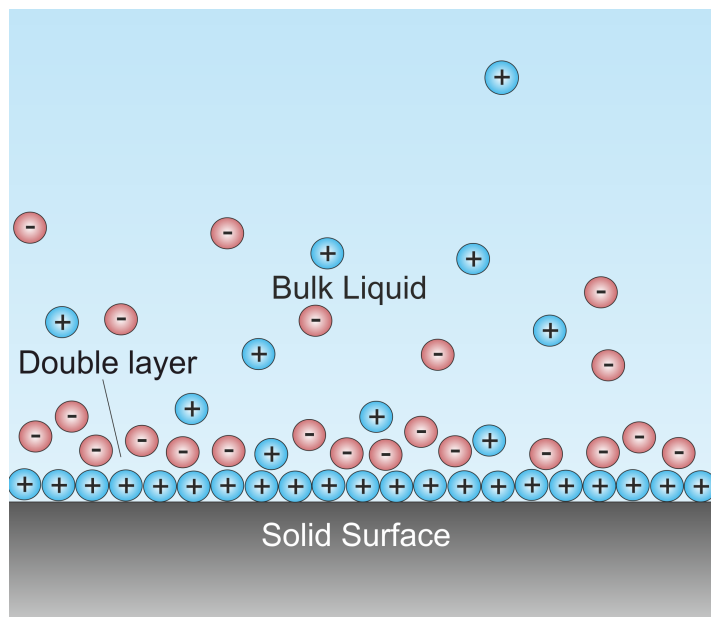


Figure 5.2: An illustration of the electrical double layer with a negatively charged surface. (Creative Commons Attribution-Share Alike 3.0 Unported license, https://commons.wikimedia.org/wiki/File:Double_Layer.png.)

in-depth discussion and treatment, the reader is referred to, for example, Evans and Wennerström [52].

5.7.2 Entropic repulsion/attraction

When a large, flexible molecule approaches a surface, its available conformations will be severely restricted by the presence of the surface. This leads to an effective repulsion of entropic origin.

However, if the molecule is oppositely charged compared to the surface it may, in addition to being electrostatically attracted to the surface, be *entropically attracted* to the surface. Let's say that we have a negatively charged surface, a flexible macromolecule with a charge of $+5$ and counterions to the surface that each have a charge of $+1$. Then it will be entropically favourable for the macromolecule to replace the counterions in the electrical double layer since five counterions have more available configurations in solution than a macromolecule, which is restricted by the fact that its different parts are chemically bonded to each other. Thus, the loss in entropy is less for the adsorption of one macromolecule with a charge of $+5$ than for the adsorption of five counterions that each have a charge of $+1$.

Entropy will be discussed more in chapter 6.

THERMODYNAMICS AND STATISTICAL MECHANICS

“ Nothing in life is certain except death, taxes and the second law of thermodynamics. ”

Seth Lloyd

In this chapter, I will begin by introducing the fundamental laws of thermodynamics and statistical mechanics. Then I will introduce the concept of thermodynamic ensembles and present some of them, and finally introduce the adsorption free energy.

6.1 What are thermodynamics and statistical mechanics?

Thermodynamics concerns the relation between macroscopic properties of matter and the ability of a system to do work or produce heat. Using classical thermodynamics, it is possible to understand how a refrigerator works or to determine whether a chemical reaction can occur spontaneously under certain conditions or not.

Statistical mechanics is the theoretical framework that connects the *microscopic world* that molecules experience with the *macroscopic world* that we ourselves can experience. The objective of statistical mechanics is to provide the tools to calculate properties of macroscopic systems from a molecular perspective by averaging over properties of individual molecules and their interactions [53].

6.2 The laws of thermodynamics

6.2.1 The laws of classical thermodynamics

The theoretical basis for thermodynamics is generally formulated as four laws:

The zeroth law

The zeroth law of thermodynamics states that if two systems are each in thermal equilibrium with a third system, they are also in thermal equilibrium with each other. This means that there exists a property which is the same in all of these three systems, and this property is called temperature.

This law is a basic requirement for thermodynamics to make sense, and since it was formulated after the other three it was named the zeroth law.

The first law

The first law of thermodynamics states that the energy change in a system is a sum of the energy that passes its boundaries as heat, work, or via particles. This means that for an isolated system (a system that cannot exchange energy or particles with its surroundings), the energy is constant.

The first law is often expressed in the form of the energy principle: Energy cannot be destroyed or created, it can only change form.

The second law

The second law of thermodynamics states that heat cannot spontaneously flow from a colder location to a hotter location. Here, the word *spontaneously* is important. As we all know, there are inventions such as fridges, where heat is somehow transferred from inside the fridge to its surroundings even though the inside of the fridge is cooler than the outside. However, this heat transfer is not a spontaneous flow of energy – it requires the input of energy to occur. A spontaneous process happens by itself and does not require that another process occurs at the same time to provide a driving force.

The second law of thermodynamics states which kind of processes that can occur spontaneously and can also be formulated in terms of entropy, S : For all spontaneous processes that occur in an isolated system, $\Delta S \geq 0$. Thus, by calculating the total change in entropy due to a process, we can determine whether it can occur spontaneously or not. This is an extremely powerful tool *e.g.* for theoretical chemists.

The third law

The third law of thermodynamics states that as a system approaches a temperature of absolute zero (meaning 0 K), the entropy of the system approaches zero, and becomes so in the case of perfect crystalline substances [54].

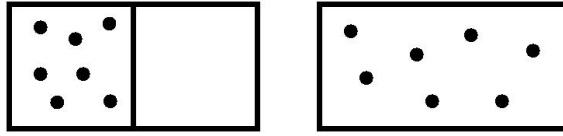


Figure 6.1: The gas in the left box expands to fill the whole volume when the middle wall is removed. (Courtesy of Magnus Ullner.)

6.2.2 The postulates of statistical mechanics

Statistical mechanics has two important postulates:

Postulate one: Equal *a priori* probabilities

This postulate states that, in an isolated system, all states consistent with the number of particles,* the volume and the internal energy of the system are equally probable [53].

The connection to entropy. This means that if we have a system, it is more likely to be in a macroscopic state corresponding to many different microscopic states than in a macroscopic state corresponding to a smaller number of microscopic states. For example, the gas depicted in Figure 6.1 expands to fill the volume of the entire box when the wall in the middle is removed, because the movement is no longer restricted. Configurations where all gas molecules are gathered in the initial volume are still possible, but since there are many more configurations where the gas molecules explore the whole box this is the state that we will observe.

This is intimately coupled to the concept of entropy. For an isolated system

$$S = k_B \ln \Omega, \quad (6.1)$$

where Ω is the number of available microscopic states [54].

Postulate two: Time average equals ensemble average

Within the context of statistical mechanics, an ensemble is a large (mental) collection of systems that have the same values of the macroscopic properties that define them (for example the number of particles, the volume, and the internal energy as in the microcanonical ensemble introduced in section 6.3.1). Postulate two states that a long *time average* of a mechanical property in a thermodynamic system is equal to the *ensemble average* of the same property [53].

*Note, however, that if we have chemical reactions in the system, the number of particles may change. Perhaps it is better to say that the available states should be consistent with the *possible* numbers of particles.

6.3 Thermodynamic ensembles

Here, I will introduce some different types of thermodynamic ensembles that can be used for molecular computer simulations or theoretical discussions. For more detailed information, see for example Frenkel and Smit [55].

6.3.1 The microcanonical ensemble

In the microcanonical ensemble, the number of particles (N), the volume (V), and the internal energy (U) are constant. The microcanonical ensemble thus describes an isolated system.

6.3.2 The canonical ensemble

In the canonical ensemble, the number of particles (N), the volume (V), and the temperature (T) are constant. This is the ensemble that has been used for most simulations performed in this study.

6.3.3 The isobaric–isothermal ensemble

In case we want to describe a system with specific values for the temperature and pressure, the isobaric–isothermal ensemble is a good choice. In this ensemble, the number of particles (N), the pressure (p), and the temperature (T) are constant. The pressure can be kept constant by fluctuations in volume.

6.3.4 The grand canonical ensemble

In the grand canonical ensemble, the number of particles is allowed to fluctuate, while the chemical potential (μ), the volume (V), and the temperature (T) are constant. This ensemble describes a system of constant volume that is free to exchange energy and particles with its surroundings. This ensemble has been used for the explicit salt ions introduced in some of the simulations in this work.

6.4 Free energy

Later, adsorption free energies will be used and therefore I will introduce them here.

The change in free energy for a process equals the maximum work that the process can do.[†] If the change in free energy is negative, the process is spontaneous. If it is zero, the system is at equilibrium. For constant pressure, the Gibbs free energy is used. For constant volume, as in this work, we look at the Helmholtz free energy.

The free energy of adsorption (the potential of mean force) is defined by the following expression:

[†]Note, however, that for Gibbs free energy, expansion work is not included.

$$f(r_{s,\text{cm}}) = -k_{\text{B}} T \ln[g(r_{s,\text{cm}})], \quad (6.2)$$

where $r_{s,\text{cm}}$ is the distance between the mass centre of the molecule and the surface, and $g(r_{s,\text{cm}})$ is:

$$g(r_{s,\text{cm}}) = \frac{C(r_{s,\text{cm}})}{C_{\text{bulk}}}, \quad (6.3)$$

where $C(r_{s,\text{cm}})$ is the concentration of the molecule at a distance $r_{s,\text{cm}}$ from the surface and C_{bulk} is the bulk concentration (in principle the concentration at an infinite distance from the surface).

MOLECULAR SIMULATIONS AND THE COARSE-GRAINED MODEL

“ The simplification of life is one of the steps to inner peace. A persistent simplification will create an inner and outer well-being that places harmony in one’s life. ”

Peace Pilgrim

In this chapter, I introduce the concept of molecular simulations and then I continue by describing the coarse-grained models that we have used for our simulations of the adsorption of histatin 5 and fibrinogen.

7.1 Molecular simulations

There are two main ways of conducting molecular simulations – molecular dynamics simulations and Monte Carlo simulations.

In molecular dynamics simulations, one follows the movements of molecules with time using Newtonian mechanics. The velocities and positions of the molecules change with time depending on the forces that the molecules experience due to for example mutual interactions. The time that is simulated is usually on the order of nanoseconds, but the time it takes for the computer to perform the calculations is usually on the order of a few days or even months. Of course, the exact times vary greatly depending on the studied system and the level of complexity of the model.

In Monte Carlo simulations, a different technique is used. Instead of calculating a time average, an ensemble average is determined, meaning that the purpose of a simulation is to generate many configurations to achieve good statistics of the average. An efficient method for doing so is the Metropolis scheme, described in section 7.3.2.

According to one of the postulates of statistical mechanics (section 6.2.2), also called *the ergodic hypothesis*, the results from molecular dynamics simulations and Monte Carlo simulations will be the same if the model and the conditions are the same.

7.2 Molecular dynamics simulations

In this work, results from all-atom molecular dynamics simulations of histatin 5 in bulk solution [56] have been used in Monte Carlo simulations of surface adsorption. Therefore, a short introduction to molecular dynamics simulations is given here.

7.2.1 All-atom molecular dynamics simulations of proteins

In all-atom molecular dynamics simulations, a molecule is described as points (atoms) connected by springs (bonds). The molecule experiences a force field, which is a collection of mathematical expressions with parameters that are designed to reproduce molecular geometry and selected properties. There are a lot of different available force fields, and they are usually specialised for some specific system. Apart from the force field used for the protein, the choice of water model is also important. The water is treated explicitly, and different water models differ for example in number of interaction sites and non-bonded interaction strength.

7.2.2 Force fields and water models for IDP simulations

Traditional protein force fields tend to yield too compact structures when used for modelling IDPs. This can be remedied for example by using a different force field with increased protein–water interactions [57]. Another strategy has been to develop a new water model with increased dispersion interactions [58]. This water model was used for the all-atom simulations that gave the trajectory used for this work. Since IDPs tend to adopt extended structures, they are in contact with water to a higher degree than globular proteins, and thus the choice of water model is especially important.

7.3 Molecular Monte Carlo simulations

7.3.1 The problem with naive Monte Carlo simulations

The most naive way of carrying out Monte Carlo simulations would be to generate lots of configurations where the molecules are placed randomly, and then calculate, for example, the potential energy of the system by averaging the potential energies of the different configurations. Each contribution to the average must be weighted by the Boltzmann factor for the configuration ($e^{-U/k_B T}$, where U is the internal energy), since the more likely types of configurations contribute more to the average than the unlikely ones.

The problem is that, for somewhat concentrated systems, this method is extremely computationally inefficient. Over and over again, systems would be generated in which molecules overlap, and where $e^{-U/k_B T}$ is too low for the configuration to give any significant contribution to the average. Thus, another method of generating configurations is needed.

7.3.2 Importance sampling – the solution provided by Metropolis *et al.*

The Metropolis scheme [59] solves the problem. The procedure goes like this:

- (i) Generate a start configuration.
- (ii) Pick a molecule and try to move it to a new coordinate: $X \rightarrow X + \alpha \zeta$, where α is the maximum allowed displacement and ζ is a random number between -1 and 1 .
- (iii) Compare the energy of the configuration before the trial move with that of the configuration after the trial move. If the new energy is lower ($\Delta U < 0$), accept the trial move. If the new energy is higher, accept the trial move with the probability $e^{-\Delta U/k_B T}$.
- (iv) Repeat from step (ii).

The averaging is performed over all accepted configurations. An old configuration counts as an accepted one in case the trial move was rejected, meaning that some configurations will contribute several times to the average. All accepted configurations now contribute equally to the average, since the configurations are generated according to their Boltzmann weight.

By using this scheme, we will find the most important configurations with their correct weight, hence we will not need to explore unlikely configurations, which means fewer configurations and, thus, less time to obtain a good estimate of the ensemble average. Therefore, the computational resources are used more efficiently than with the naive method.

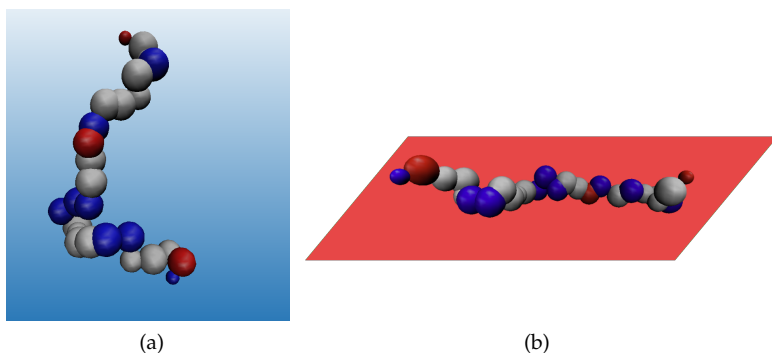


Figure 7.1: Snapshots from coarse-grained simulations showing histatin 5 (a) in bulk solution and (b) adsorbed to a negatively charged surface. The blue beads are positively charged, the red ones are negatively charged, and the grey ones are neutral.

7.3.3 Monte Carlo moves

Within the Metropolis scheme, Monte Carlo simulations involve the movement of molecules. However, many of the moves are not physical, as they are in molecular dynamics simulations, but generated randomly from predetermined types of possible moves. It is important to choose these moves in such a way that the generated configurations will sample the relevant parts of the configurational space in an unbiased way.

Since the types of moves that need to be used are dependent on the system and the model, the Monte Carlo moves used for our simulations of histatin 5 are described in section 7.4, after each coarse-grained model has been introduced.

7.4 The coarse-grained protein models

Simple models are powerful explanatory tools since it is possible to understand how they behave. However, if the model is too simple it gives qualitatively wrong results and may even be useless as an explanatory tool. Often, we end up somewhere in between, where some parts of the complex reality can be captured by the model and some parts not.

Here, I will introduce the coarse-grained models that I have used in my computer simulations.

7.4.1 The flexible bead model

The flexible bead model can be used for intrinsically disordered proteins. In this work, it has been used for histatin 5 and for the α C-chains of fibrinogen. Histatin 5 has been modelled as consisting of 26 differently sized beads on a necklace. The beads each represent one amino acid residue, except for the ones at

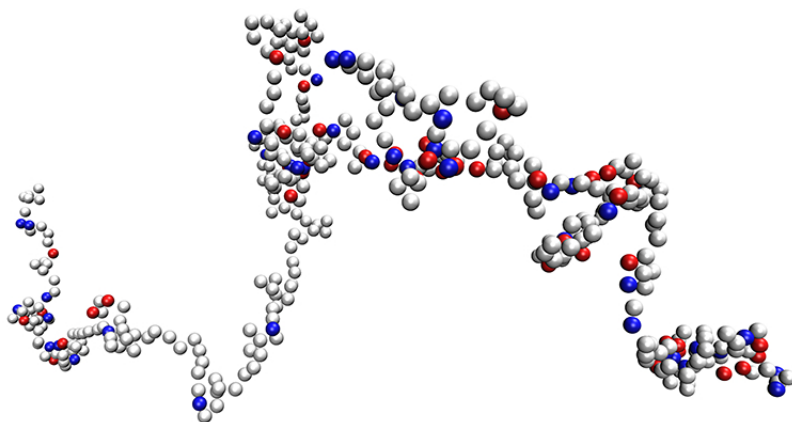


Figure 7.2: Snapshot from a coarse-grained simulation showing an α C-chain of fibrinogen in bulk solution. The blue beads are positively charged, the red ones are negatively charged, and the grey ones are neutral.

the ends which represent the N- and C-terminals, respectively. Figure 7.1 shows snapshots of histatin 5 from simulations using this model.

The model used for the fibrinogen α C-chains is somewhat different. There, all amino acid beads have equal size. A snapshot from a simulation of an α C-chain is shown in Figure 7.2.

The beads are connected by harmonic bonds (springs). In the model used for histatin 5, non-neighbouring beads experience a soft repulsion when they come close to each other (there is a Lennard-Jones potential with $\epsilon_{LJ} = 0.05 k_B T$ between non-neighbouring beads). In the model used for the fibrinogen α C-chains, however, the amino acid residues are represented as hard spheres.

The Monte Carlo moves

Protein translation/rotation: Translation or rotation of the whole protein molecule.

Single bead translation: Moves a single amino acid bead.

Crankshaft rotation: Defines a rotation axis between two randomly chosen beads and rotates the residues between the chosen beads around the axis, see Figure 7.3(a).

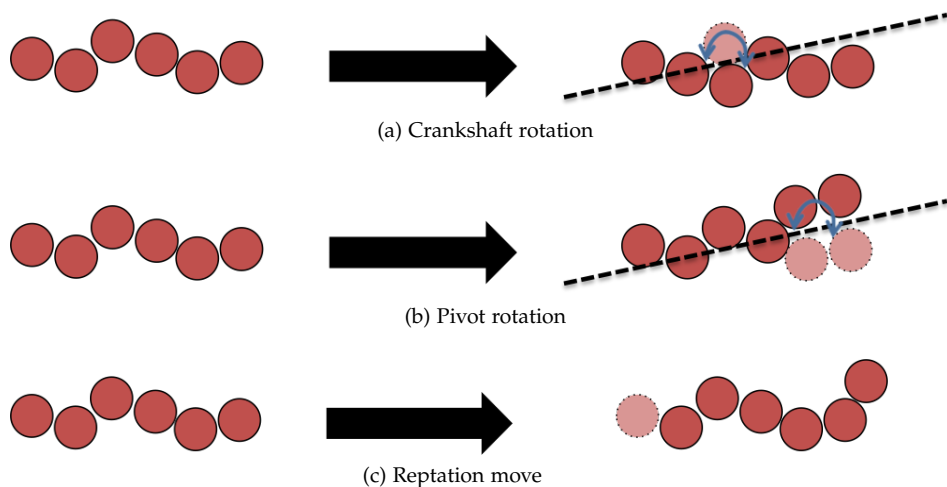


Figure 7.3: A schematic of three of the Monte Carlo moves used in simulations with the flexible bead model.

Pivot rotation: Defines a rotation axis in the same manner as for the crankshaft move and rotates the residues at one of the ends of the protein around the axis, see Figure 7.3(b).

Reptation move: Used in simulations with more than one protein molecule. Translates a bead at one of the ends of the protein chain to a random position a bond distance away from the original position, and then moves the neighbouring position to the former position of the bead that was translated first. The third bead is then moved to the former position of the second bead etc. through the whole protein chain, see Figure 7.3(c).

Titration move: Used in simulations with histatin 5. Protonates or deprotonates (changes the charge of) a bead.

7.4.2 The conformational swap model

In the conformational swap simulations, an all-atom trajectory of histatin 5 from molecular dynamics simulations in bulk [56] was used for simulations of surface adsorption of histatin 5. The all-atom trajectory was coarse-grained to amino acid level (Each amino acid and each terminal was represented as a sphere.), and reduced using *e.g.* RMSD clustering (based on the root-mean-square deviation of atomic positions). The coarse-grained, reduced trajectory formed a library of conformations that was used in the Monte Carlo simulations.

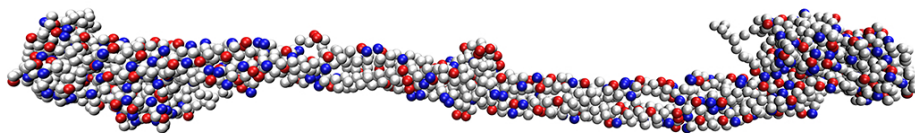


Figure 7.4: The completely rigid coarse-grained model used for the main body of fibrinogen. The blue beads are positively charged, the red ones are negatively charged, and the grey ones are neutral.

The Monte Carlo moves

Protein translation/rotation: Translation or rotation of the whole protein molecule.

Conformational swap move: Swaps one protein conformation for another one from the library.

Insertion/deletion of an ion pair: Used in simulations with explicit grand canonical salt. Inserts or deletes a salt ion pair (thus preserving electroneutrality of the system).

7.4.3 The rigid body model

The main body of fibrinogen was modelled as completely rigid. The conformation of the protein was taken from the crystal structure of human fibrinogen [32], which was coarse-grained to amino acid level. (Each amino acid and each terminal was represented as a sphere.) See Figure 7.4 for the coarse-grained representation of fibrinogen.

The Monte Carlo moves

Protein translation/rotation: Translation or rotation of the whole protein molecule.

7.5 The modelling of the surface

7.5.1 The Gouy–Chapman surface

Most surfaces were modelled as completely flat with an evenly smeared charge. The interactions between the charged amino acids and the surface decrease exponentially with distance from the surface according to Gouy–Chapman theory (section 5.7.1).

7.5.2 The nanostructured surface

For the simulations with fibrinogen, we used both flat and nanostructured surfaces. The nanostructured surfaces consisted of a flat Gouy–Chapman surface with nanospheres attached in a hexagonal pattern. The charges of the nanospheres were modelled as centred in the spheres, with a magnitude that gave a surface charge density equal to that of the flat surface.

7.5.3 The surface with explicit charges

For some simulations, a flat surface with explicit surface charges was used. The surface charges were then modelled as point charges placed on a hexagonal lattice at the interface.

7.5.4 The short-ranged attraction

In addition to the electrostatic interaction between the surface and the charged amino acid beads, we also had, in some simulations, a Lennard-Jones potential (Equation (5.11)) between each bead and the surface:

$$V = \sum_{i=1}^n \varepsilon \left[\left(\frac{\sigma_i}{r_i + \sigma_i} \right)^{12} - 2 \left(\frac{\sigma_i}{r_i + \sigma_i} \right)^6 \right], \quad (7.1)$$

where ε is the depth of the minimum of the potential, σ_i is the radius of bead i , and r_i is the distance between the mass centre of bead i and the surface.

Since a $1/r^3$ -dependence is more realistic for dispersion interactions with a surface than $1/r^6$, the following short-ranged attraction was instead used in Paper III:

$$V = \sum_{i=1}^n \frac{3\sqrt{3}}{2} \varepsilon \left[\left(\frac{\sigma_i}{r_i + \sigma_i} \right)^9 - \left(\frac{\sigma_i}{r_i + \sigma_i} \right)^3 \right]. \quad (7.2)$$

The potentials are shifted so that they are zero when the distance between the surface and the centre of the bead is zero. This is the closest possible distance in the model and if the normal form of the Lennard-Jones potential is kept, the repulsion may “win” over the attraction so that the adsorption decreases when the short-ranged attraction is turned on, thus counteracting the purpose.

The reason for including a short-ranged attractive interaction is that it is needed in order for our simulations to better match experiments. This potential may account for dispersion interactions, changes in water structure etc. We also hypothesised that it corrects for an overestimation of the entropy of the free histatin 5 chain in our model system. Since our model of histatin 5 does not include restrictions on dihedral angles, which are present in a real protein, our hypothesis was that the histatin 5 chain might be too flexible in our model (have

too high entropy in solution), giving rise to a too large entropic repulsion as the protein approaches a surface. However, this was contradicted by a later study of ours (see Paper III).

7.6 The modelling of the salt ions

7.6.1 Implicit salt

In most of our simulations, salt ions have not been included explicitly. Instead, the ionic strength has entered via the Debye length in the screened Coulomb potential (Equation (5.3)). When a large, multivalent ion of opposite charge adsorbs on a surface, several small counterions are released – increasing entropy. This effect is not accounted for by modelling the salt ions implicitly, and may lead to less adsorption than with explicit ions.

7.6.2 Explicit grand canonical salt

In some simulations, we have included salt ions explicitly using the grand canonical ensemble, see section 6.3.4.

7.7 Implicit water

The water molecules are not included explicitly in the simulations. Instead, water is represented as a dielectric continuum, affecting the electrostatics of the system through its relative permittivity ϵ_r . Since the most prevalent component of the experimental system is water, it might seem strange to describe water as crudely as we have done. This is indeed a weakness of the model because, since we are dealing with adsorption, confinement of water molecules may occur. Effects coming from the local water structure are not included by the implicit solvent model.

7.8 The simulation box

7.8.1 Periodic boundary conditions

Since it would be too time-consuming to simulate a system as large as the one used in the experiments, our digital protein molecules are placed in a small box. For example, for single-protein simulations of histatin 5, I have used a cubic box with a side length of 300 Å. In order to compensate for the fact that the box is so small, periodic boundaries are used. This means that whenever a molecule exits the box on one side, it reenters the box on the opposite side. Molecules also interact across the boundaries of the box. One can view the simulation box as being in contact with a replica of itself on each side where periodic boundary conditions are applied, see Figure 7.5(a). These replicas are also in contact with other replicas on all sides, forming an infinite periodic lattice. In principle, the

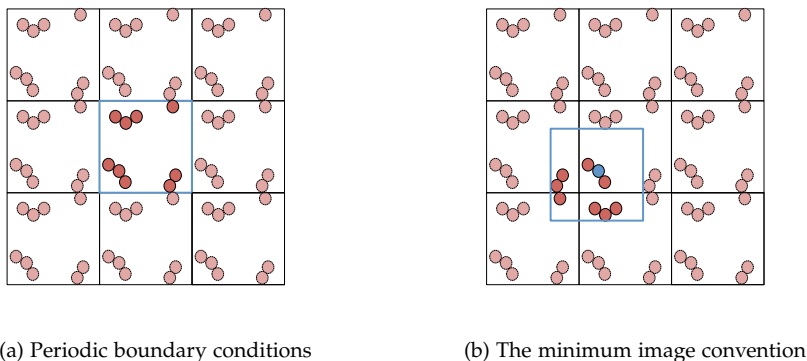


Figure 7.5: An illustration of periodic boundary conditions and the minimum image convention for a 2D-system. In (a), the blue box defines the system, and the other boxes are the replicas that it interacts with. In (b), the blue box defines the space holding the molecules/discs that the blue disc interacts with.

infinite number of molecules all interact with each other. However, in practice it is not feasible to calculate an infinite sum of interactions. Luckily, we are normally dealing with short-ranged interactions that are possible to truncate, for example using the minimum image convention described in the following section.

Even though periodic boundary conditions are effective for simulating homogeneous bulk systems, one should be aware that there might be correlations that are not present in a truly macroscopic system.

In simulations with a surface, periodic boundary conditions cannot be applied in the direction corresponding to the normal to the surface since molecules cannot be allowed to pass through the surface. Therefore, we applied hard boundaries in the z -direction for the simulations where a surface was included, meaning that there was an uncharged surface opposite the charged surface. In order for this neutral surface not to affect the results it is important that the simulation box is large enough.

7.8.2 The minimum image convention

In our simulations, the particles interact with each other via the minimum image convention. This means that out of the infinite number of images of the same particles that are present due to the periodic boundary conditions, a specific particle only interacts with one image of each particle – the one that is closest, see Figure 7.5(b). When using the minimum image convention it is important that the simulation box is large enough, and that long-ranged interactions are not important. In our systems, the electrostatic interactions are screened due to

the presence of the solvent and salt, and thus not as strong as they would be otherwise.

If the minimum image convention is used when long-ranged interactions are important, a large error is introduced in the potential energy of the system. Another aspect to consider is that an impulsive pressure correction needs to be included if one wishes to know the true pressure of a system with a truncated potential [55].

EXPERIMENTAL METHODS

“ Today’s scientists have substituted mathematics for experiments, and they wander off through equation after equation, and eventually build a structure which has no relation to reality. ”

Nikola Tesla

In this chapter, I will introduce the experimental technique of null ellipsometry, and describe the purification/cleaning procedures that were used before the ellipsometry measurements.

8.1 Purification and cleaning of protein and surface

Since even a 99 % pure protein sample may not be pure enough for controlled ellipsometry if the impurity is surface active [60], care was taken to ensure the use of pure protein and clean surfaces by using size exclusion chromatography and an established cleaning protocol, respectively.

8.1.1 Size exclusion chromatography

Size exclusion chromatography is a way of separating molecules according to size. The principle is that a concentrated solution of the compound to be purified is injected into a buffer which runs through a column packed with a material that separates molecules according to size (and, to some extent, shape). Small molecules are held up in the column longer than large molecules. The reason is that the small molecules are able to penetrate the pores in the material and thus

they experience something similar to a maze, while large molecules travel with the flow of the buffer and bypass the pores making up the labyrinth since they cannot enter due to their size. Molecules of intermediate size will be able to enter some of the pores and will thus have an intermediate retention time.

An important difference between size exclusion chromatography and other chromatographic procedures is that no chemical or physical interactions should occur between the analyte (the molecules to be separated) and the stationary phase (the column packing material) [61].

8.1.2 Surface cleaning procedure

The silica surfaces were cleaned by heating them in two different solutions – firstly in an alkaline solution containing ammonia, hydrogen peroxide and water, and secondly in an acidic solution containing hydrochloric acid, hydrogen peroxide and water, according to the procedure described by Landgren and Jönsson [37]. This type of cleaning procedure has been shown to effectively remove metal ions and organic contaminants [62].*

The surfaces were stored in ethanol and just before use they were cleaned in a plasma cleaner in order to remove any residual organic contaminants.

8.2 Null ellipsometry

Ellipsometry is named after the fact that it is based on the use of so-called elliptically polarised light. When the elliptically polarised light is reflected by a surface, the polarisation changes. The change is different depending on the characteristics of the surface and, if there is an adsorbed layer, on the thickness and refractive index of the adsorbed layer.

8.2.1 The polarisation of light

What is polarisation?

Light is an electromagnetic wave that propagates through space. The electric field and the magnetic field are perpendicular to each other and to the direction of travel.

For completely unpolarised light, the electric field oscillates in all possible directions. However, if the light is linearly polarised, it oscillates only in one direction and if it is circularly or elliptically polarised, the direction of polarisation rotates. Polarisation refers to the *behaviour in time* of the field vector *observed at a fixed point in space* [64].

*It is worth noting that the surface charge density of the silica surface depends on the cleaning procedure – if the surface is washed in an acidic solution last it gets a less negative surface charge than if finishing with the alkaline solution [63].

Linear polarisers

Linearly polarised light can be created using a linear polariser. An ideal linear polariser transmits light freely in one direction while it absorbs or deflects it completely in the perpendicular direction. Two ideal linear polarisers with the transmission axes perpendicular to each other extinguish light completely.

Waveplates and elliptically polarised light

In order to get elliptically polarised light, linearly polarised light can be passed through a waveplate (also called retarder). A waveplate has a different index of refraction depending on the orientation of the electric field.

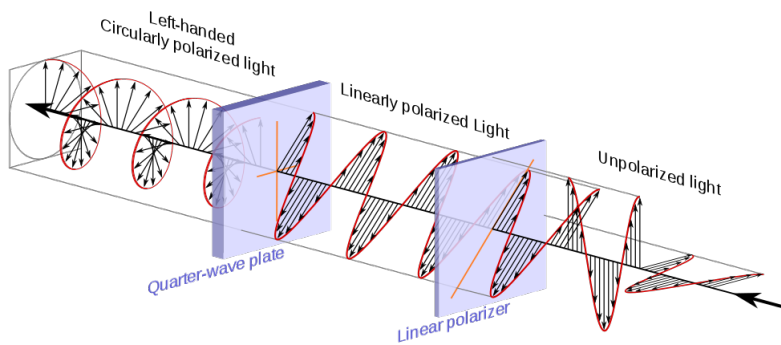


Figure 8.1: The creation of circularly polarised light. (Public domain, https://commons.wikimedia.org/wiki/File:Circular.Polarization.Circularly.Polarized.Light_Circular.Polarizer_Creating.Left.Handed.Helix.View.svg)

The creation of circularly polarised light is depicted in Figure 8.1. Polarised light can be described as composed of two perpendicular components. When linearly polarised light passes through a waveplate, one of the components (along one of the axes of the cross in the figure, for example) is retarded relative to the other (a phase shift is introduced between the components). This leads to elliptical or circular polarisation, since the sum of the two polarisation components will now vary in direction.

8.2.2 The principle behind null ellipsometry

For a given surface, it is possible to find an ellipticity of the incoming light that gives linearly polarised light after reflection. By letting the reflected linearly polarised light pass through a linear polariser, we can align the polariser in such a way that no light passes through. A light detector will then measure a null signal.[†] The angle at which this null signal is measured can then be related

[†]In practice you will not measure a null signal but rather a minimum in the signal strength.

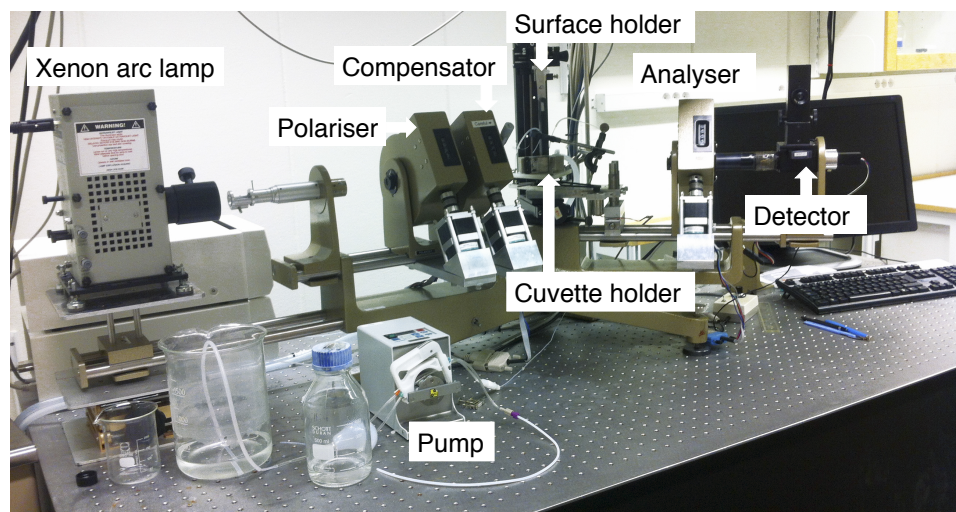


Figure 8.2: The Rudolph thin film ellipsometer used for the adsorption experiments at the Division of Physical Chemistry, Department of Chemistry, Lund University.

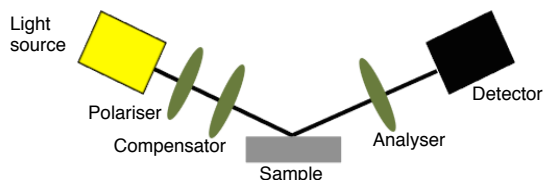


Figure 8.3: A schematic drawing of the ellipsometry setup in Figure 8.2

to the characteristics of the adsorbed layer. This is the principle behind null ellipsometry.

8.2.3 Null ellipsometry setup

I have used a Rudolph thin film ellipsometer (Figure 8.2) with the setup shown in Figure 8.3. Light from a xenon arc lamp (wavelength 401.5 nm) first passes through a linear polariser. The resulting linearly polarised light passes through the compensator, which creates elliptically polarised light. The light is reflected by the sample, and after that it travels through a second polariser (the analyser). The detector detects the intensity of the light that passes through the analyser.

By adjusting the angles of the polariser and the analyser while following the change in the detected light intensity, the angles that give the weakest light signal (corresponding to linear polarisation of the light that has been reflected by the sample) are found. From the angles of the polariser, the compensator, and the analyser, the so-called ellipsometric angles Ψ and Δ can be calculated.

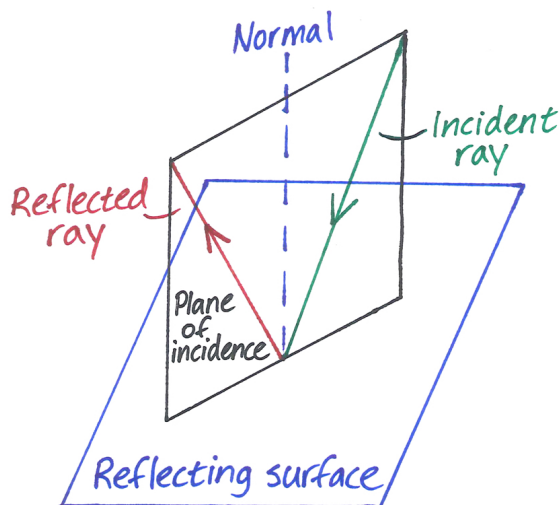


Figure 8.4: The plane of incidence is the plane that contains the incident ray and the normal to the surface at the point where the incident ray strikes the surface.

8.2.4 Models and calculations behind ellipsometry

Here, I will describe how the transformation from the ellipsometric angles to data about layer thickness, refractive index, and adsorbed amount takes place. Since our aim is to compare these experimental values to values from simulations, it is important to understand the assumptions involved in calculating the adsorbed amount.

s- and p-polarisation

As already mentioned, polarised light can be regarded as a superposition of two waves oscillating in perpendicular directions. In the case of light which is

reflected by a surface, the wave is often divided into a so-called p-component and an s-component. The p-component is parallel to the plane of incidence and the s-component is perpendicular to the plane of incidence, meaning that it is parallel to the surface. Figure 8.4 shows the location of the plane of incidence.

Upon reflection at the interface, the polarisation of light changes. This change is described by the reflection coefficient, which is the amplitude of the reflected wave divided by the amplitude of the incident wave, denoted R_p and R_s for the different components of the wave.

The ellipsometric angles (Ψ and Δ)

The ellipsometric angles, Ψ and Δ , are related to the reflection coefficients by the following relation [64]:

$$\frac{R_p}{R_s} = \frac{|R_p|}{|R_s|} e^{i(\delta_p - \delta_s)} = \tan \Psi e^{i\Delta}, \quad (8.1)$$

where

$$\tan \Psi = \frac{|R_p|}{|R_s|}, \quad (8.2)$$

and

$$\Delta = \delta_p - \delta_s, \quad (8.3)$$

where δ_p and δ_s are the phase shifts experienced by the p- and s-polarised light, respectively, upon reflection. From the ellipsometric measurements, the values of Ψ and Δ are found.

The optical model

The experimental system was described using a model where there were four different layers separated by completely flat interfaces, see Figure 8.5. The four layers are:

- The buffer (medium 0)
- The adsorbed protein film (medium f)
- The silica layer (medium 1)
- The silicon (medium 2)

The buffer, the protein film, and the silica layer were assumed to be transparent, meaning that their refractive indices are real numbers. However, the silicon is not transparent and thus its refractive index N_2 is a complex value [37].

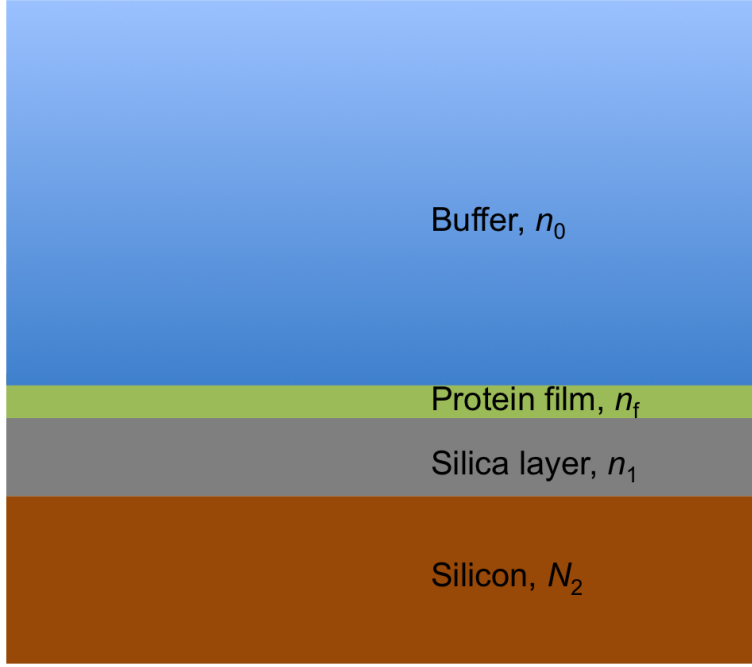


Figure 8.5: The optical model of the experimentally studied system.

Reflection coefficients in the optical model

The overall reflection coefficients R_p and R_s for a surface composed of several layers are functions of the reflection coefficients at each interface. In this system, there is one interface between the buffer and the film, one between the film and the silica, and one between the silica and the silicon. The reflection coefficients for the individual interfaces are denoted r_{ij} , where i and j refer to the media on each side of the interface.

$$R_x = \frac{r_{0f}^x + r_{f1}^x e^{-i2\beta_f} + (r_{0f}^x r_{f1}^x + e^{-i2\beta_f}) r_{12}^x e^{-i2\beta_1}}{1 + r_{0f}^x r_{f1}^x e^{-i2\beta_f} + (r_{f1}^x + r_{0f}^x e^{-i2\beta_f}) r_{12}^x e^{-i2\beta_1}}, \quad (8.4)$$

where x is either p or s,

$$\beta_1 = \frac{2\pi d_1 n_1 \cos \phi_1}{\lambda}, \quad (8.5)$$

$$\beta_f = \frac{2\pi d_f n_f \cos \phi_f}{\lambda}, \quad (8.6)$$

$$r_{ij}^p = \frac{N_j \cos \phi_i - N_i \cos \phi_j}{N_j \cos \phi_i + N_i \cos \phi_j}, \quad (8.7)$$

and

$$r_{ij}^s = \frac{N_i \cos \phi_i - N_j \cos \phi_j}{N_i \cos \phi_i + N_j \cos \phi_j}. \quad (8.8)$$

N_i and N_j are the complex refractive indices of layers i and j , ϕ_i and ϕ_j are the angles of incidence at layers i and j , and λ is the wavelength of the light [65].[‡]

In order to use the optical model described above to determine the properties of the adsorbed layer, we first need to know the thickness of the silica layer. It is found by measuring in two different ambient media (air and pure buffer solution), as described by Landgren and Jönsson [37].

Determination of the thickness and refractive index of the adsorbed layer

The thickness of the adsorbed film, d_f , and the refractive index of the adsorbed film, n_f , can be determined from Equation (8.6). This is done using an iterative procedure. The value obtained for d_f is a complex value. However, this is not correct since the thickness of the layer is a real quantity. The iterative procedure continues until the imaginary part of d_f has been minimised. As can be seen from Equation (8.6), this gives a strong covariance between d_f and n_f . For a fixed value of β_f , if the value of d_f is found to be small, the value of n_f becomes large instead.

When the thickness of the adsorbed layer is small, it is difficult to resolve both d_f and n_f , and unphysical values are often found. Therefore, we did not use the procedure described above for this study, but instead the refractive index of the protein layer was fixed to 1.5, which should be a reasonable value for adsorbed protein layers [66].

Determination of the adsorbed mass

The adsorbed amount (mass per surface area), Γ , can be obtained in different manners. This is the formula from Cuypers *et al.* [67]:[§]

$$\Gamma = \frac{3d_f f(n_f)}{\frac{A}{M} - v \frac{n_0^2 - 1}{n_0^2 + 2}} (n_f - n_0), \quad (8.9)$$

where A is the molar refractivity of the compound, M is the molar weight, v is the specific volume and

$$f(n_f) = \frac{n_f + n_0}{(n_f^2 + 2)(n_0^2 + 2)}. \quad (8.10)$$

This more simple expression has been devised by de Feijter *et al.* [68]:

$$\Gamma = \frac{d_f (n_f - n_0)}{\left(\frac{dn}{dc}\right)} \quad (8.11)$$

[‡]In the reference, the λ has mistakenly been replaced by a 1.

[§]In the original version of the formula, Cuypers *et al.* used a prefactor of 0.3 instead of 3. This is only a matter of units – they wanted to make a unit conversion.

Here, the refractive index of the adsorbed film is assumed to increase linearly with the concentration and dn/dc is the refractive index increment of the adsorbed compound.

Due to a cancellation of errors, the adsorbed amount can be determined to a much higher degree of accuracy than the thickness and refractive index of the adsorbed layer. The de Feijter formula (8.11) contains the product of the layer thickness and the refractive index, which means that the uncertainties introduced in the iterative procedure described above disappear in this product. In the formula by Cuypers *et al.* a similar cancellation of errors occurs.

In this work, we have used the formula by Cuypers *et al.* to determine the adsorbed amount of histatin 5 from ellipsometry measurements. The value used for the specific volume was 0.70 ml/g, as calculated from the specific volumes of the amino acids of histatin 5 [69]. M/A was similarly determined to 3.95 g/ml [70]. It should be noted that the calculated adsorbed amounts depend directly on these values.

RESULTS

“ I was taught that the way of progress was neither swift nor easy. ”

Marie Curie, letter to her brother (1894)

In this chapter, I summarise the most important results from Papers I–IV, starting with histatin 5 and continuing with fibrinogen.

9.1 Histatin 5

9.1.1 Ellipsometry

In order to be able to develop and test the coarse-grained model for histatin 5 adsorption, we needed experimental data. Therefore, I measured the adsorbed amount of histatin 5 on hydrophilic silica at different pH and ionic strength using ellipsometry. The main results are shown in Figure 9.1. As the figure shows, the effect of increasing ionic strength is different depending on the pH of the buffer. Could our model explain this?

9.1.2 Single-protein coarse-grained Monte Carlo

We started out with a coarse-grained model of a single protein, very similar to the one used by Kurut *et al.* [51]. The surface was treated as completely flat with a smeared charge and the surface charge density was taken from the values of Samoshina *et al.* [36]. Salt and water were treated implicitly.

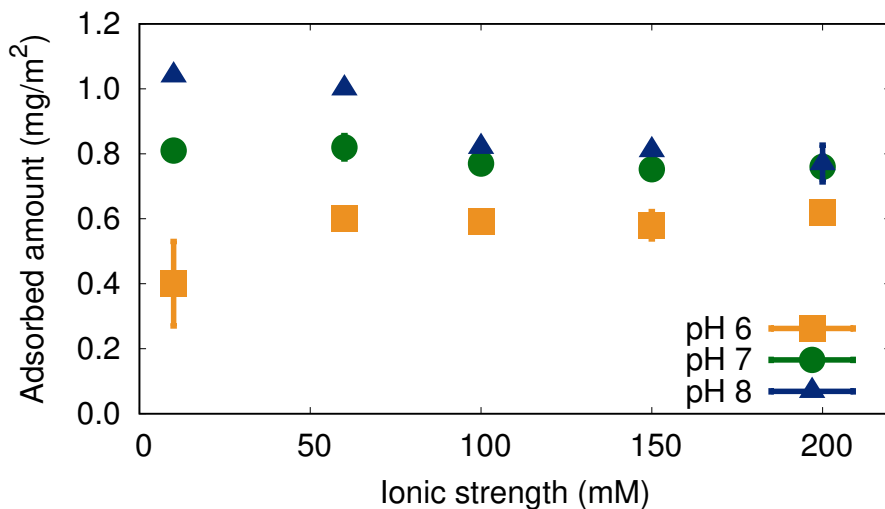


Figure 9.1: The adsorbed amount of histatin 5 to a silica surface after 60 minutes. The error bars show the standard deviation for the cases where more than one measurement was made (for pH 7, 10 mM and 100 mM the error bars are covered by the symbols). The concentration of histatin 5 in solution was 0.05 mg/ml.

This first study highlighted the importance of the increase in the negative surface charge of silica with pH. While the protein decreased its net positive charge with pH, the increase in surface charge made the protein adsorb more the higher the pH, see Figure 9.2. This was in agreement with the experimental results. However, the depth of the adsorption free energy well always decreased with increasing ionic strength, in contrast with the experiments at pH 6.

Using the Langmuir isotherm, we found that we needed a short-ranged attraction (Equation (7.1)) with $\varepsilon = 2.9 k_B T$ to get free energies in reasonable agreement with experimental data. This Lennard-Jones potential accounted for attractive interactions that were missing from our model.

Another (obviously) missing parameter was the presence of multiple proteins. We thought that the presence of multiple proteins at the surface could change the behaviour of the adsorption with ionic strength and therefore proceeded to the next study.

9.1.3 Multi-protein coarse-grained Monte Carlo

Our hypothesis was that the different dependencies of adsorbed amount on ionic strength depending on pH (see Figure 9.1) could be explained in terms of the difference in charge of the protein and the surface, see Figure 9.3. The argument was as follows: at low pH, the negative surface charge is low, while the positive charge of the protein is high. Adding salt will mainly lead to a screening of the

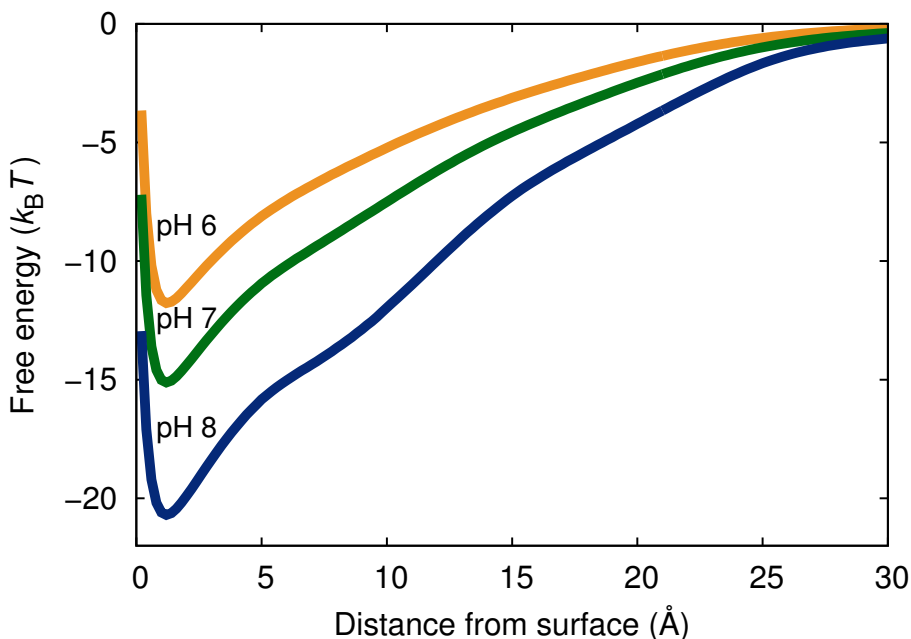


Figure 9.2: The adsorption free energies for a single histatin 5 molecule from simulations with 100 mM ionic strength and a short-ranged attraction (Equation (7.1)) with $\varepsilon = 2.9 k_B T$.

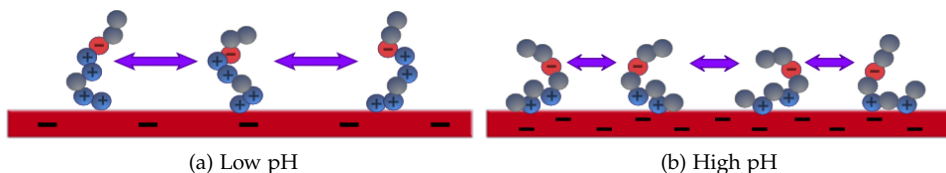


Figure 9.3: A schematic illustration of how the protein net charge and the surface charge density change depending on pH. At high pH, the adsorbed amount is higher than at low pH.

repulsion between adsorbed proteins, and thus more proteins will adsorb. At high pH, there is less repulsion between the proteins due to their lower charge. The salt will then mainly screen the attraction between the highly charged surface and the proteins, leading to a decrease in the adsorbed amount.

This hypothesis was *not* confirmed by our model. By tuning the value of ε we did find a value that showed a change in ionic strength dependence depending on pH, but the trends were opposite to the experimental ones, cf. Figures 9.1 and 9.4. Then, there was also the issue that in order to approach experimentally observed

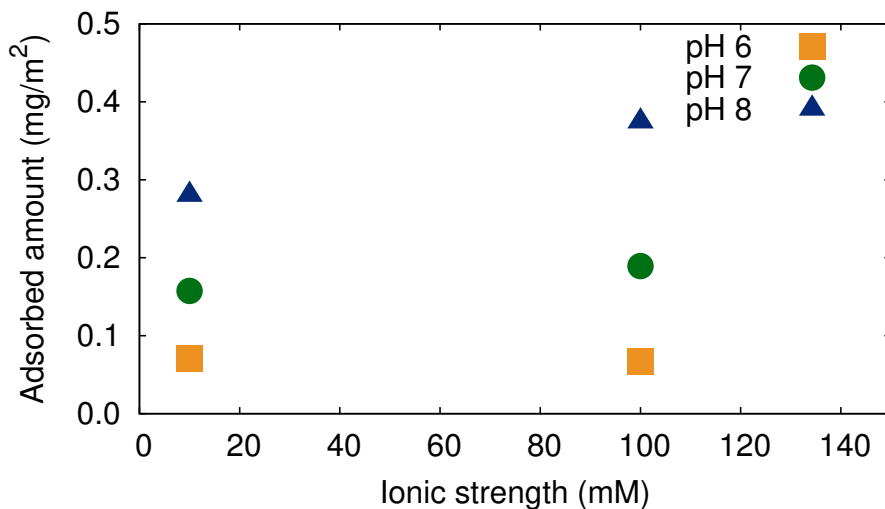


Figure 9.4: Adsorbed amount of histatin 5 from simulations as a function of ionic strength at three different pH-values when ϵ in Equation (7.1) is $2.0 k_B T$.

adsorbed amounts we needed an even greater value of ϵ than before – even though our bulk concentration was considerably higher than the experimental one.

9.1.4 Conformational swap Monte Carlo

We speculated in Paper I that a significant part of ϵ was needed because histatin 5, in our flexible bead model, had too high chain entropy in solution. Thus, the penalty for approaching the surface was higher in the model than for the real molecule. We decided to test this hypothesis by applying a method devised by Prytkova *et al.* [71], where conformations from all-atom molecular dynamics simulations in bulk were used in coarse-grained Monte Carlo simulations under different conditions (in our case with a charged surface). Instead of moving the various parts of the histatin 5 chain, all conformational changes were handled by a conformational swap move – swapping the current conformation for another one from a library. This would give a more realistic representation of the conformational entropy of histatin 5 since restraints on dihedral angles etc. were taken into account.

However, the results showed almost identical results for the adsorption free energies for the flexible bead model (CGMC (fully flexible)) and the conforma-

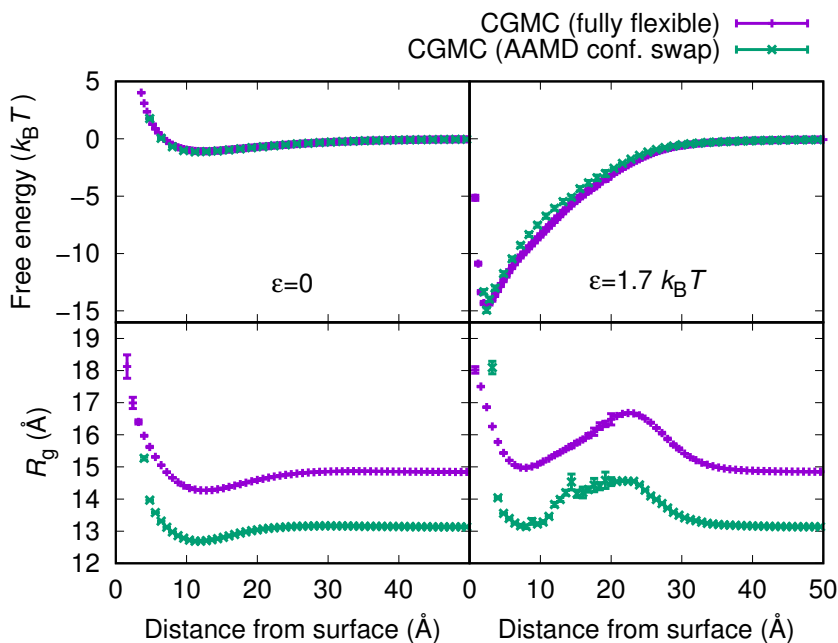


Figure 9.5: Comparison between the free energies of adsorption (top) and the radius of gyration (bottom) as a function of distance from the surface for the CGMC (fully flexible) model and the CGMC (AAMD conf. swap) model. The pH is 7, the ionic strength is 100 mM, the surface charge density is $-2.0 \mu\text{C}/\text{cm}^2$, and salt and surface charges are modelled implicitly. Error bars are typically smaller than the symbol size.

tional swap model (CGMC (AAMD conf. swap)), see Figure 9.5. The shape of the radius of gyration (R_g) curves are also very similar.*

We also used the conformational swap model to study the secondary structure of adsorbed histatin 5. It turned out that our model shows a slight increase in secondary structure motifs for adsorbed histatin 5 compared to histatin 5 in bulk.

9.1.5 The effect of urea on adsorption – an unsolved question

Urea is known for denaturing proteins. The exact mechanisms are not known but it seems that it disrupts hydrogen bonding and hydrophobic interactions.

We used buffers with 1 M urea to study the effect on protein adsorption. The idea was that if urea reduces the adsorbed amount, there is a hydrophobic

*Note that we used a 9-3 short-ranged potential (Equation (7.2)) instead of the 12-6 potential used in the previous studies (Equation (7.1)), thus a lower value of ϵ ($1.7 k_B T$) was most consistent with experiments.

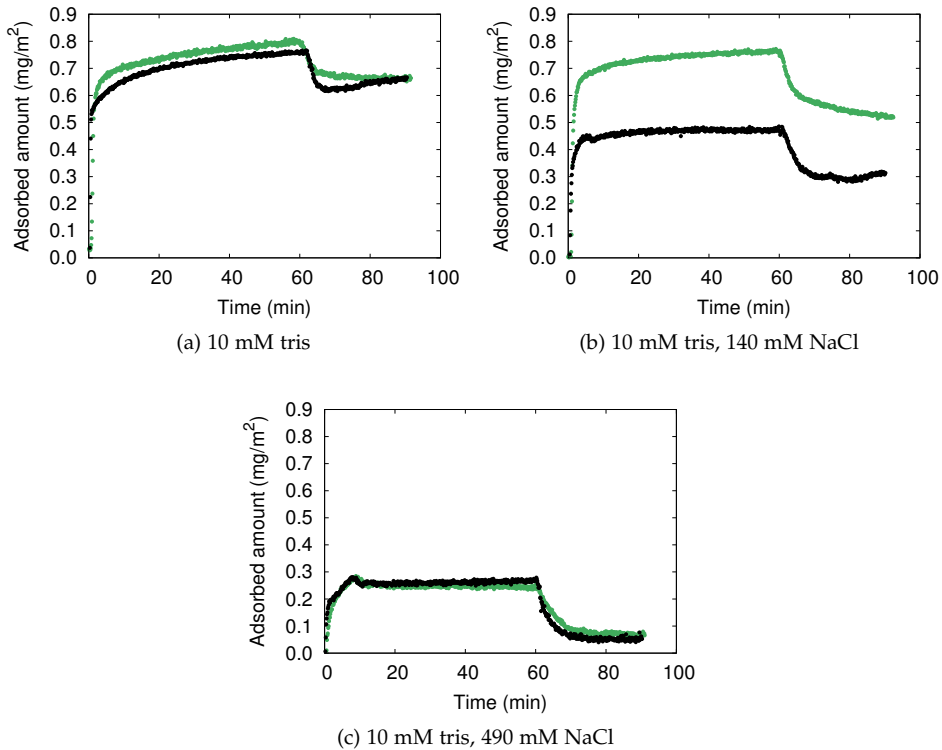


Figure 9.6: A comparison between the adsorption isotherms of histatin 5 on silica with 1 M urea (black curves) and without urea (green curves) at pH 7.0 and different ionic strengths.

attraction between the histatin 5 and the surface. The results of the measurements are presented in Figure 9.6. While urea has no effect on the adsorption at low ionic strength (10 mM) and high ionic strength (500 mM), it decreases the adsorbed amount significantly at 150 mM ionic strength. Since our simulation model is unable to describe effects of urea, we did not explore this further, and the results are not published.

9.2 Fibrinogen

9.2.1 Experimental background

It has been observed that the bacterium *S. epidermidis* attaches more to a flat silica surface that has been pre-coated with fibrinogen than to a clean silica surface. For a nanostructured surface (with attached nanospheres), it is the opposite [33]. We

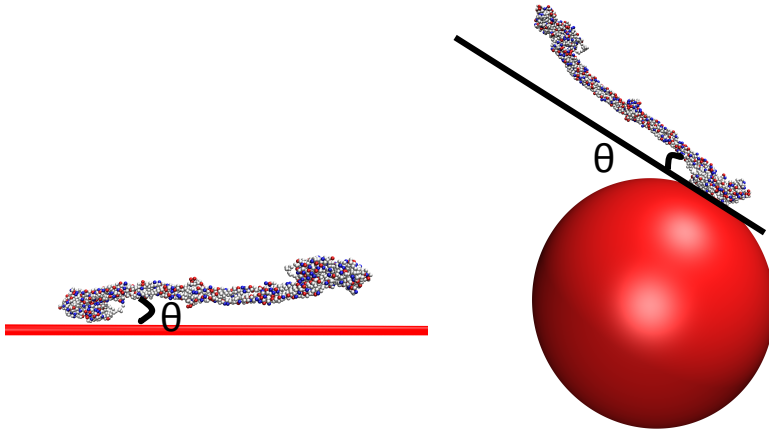


Figure 9.7: Two typical snapshots of fibrinogen adsorbed on a flat surface and a nanoparticle, respectively. The angle θ is the same in both cases but leads to different protrusion into the solvent.

wanted to investigate this with simulations in order to try to find an explanation for this behaviour.

9.2.2 Simulations of the main body of fibrinogen

The simulations of the main body of fibrinogen (in our model completely rigid) showed that fibrinogen attached similarly to the surface regardless of the surface curvature. However, the higher the surface curvature, the further the protein protrudes into solution, see Figure 9.7

9.2.3 Simulations of the disordered part of fibrinogen

The disordered fragments (α C-chains) of fibrinogen were simulated with almost the same model as for histatin 5. The results showed that there was a larger attraction between an α C-chain and the surface than between the fibrinogen main body and the surface. Thus, the disordered regions are important for the adsorption of fibrinogen.

DISCUSSION

“ We live in this world in order always to learn industriously and to enlighten each other by means of discussion and to strive vigorously to promote the progress of science and the fine arts. ”

Wolfgang Amadeus Mozart

In this chapter, I will discuss the results as summarised in the previous chapter.

10.1 Too little adsorption of histatin 5 – what are we missing?

There is always dispersion interactions between molecules and, since nothing says that the dispersion interactions between the protein and the surrounding water and the protein and the surface are equal, it is not strange if we need to add some kind of interaction representing dispersion attraction between the protein and the surface. Other possibilities are that the local water structure is important and/or that charge regulation of the surface is important. Even though the silica surface is hydrophilic, there could also be some hydrophobic interaction with the protein since most materials are more hydrophobic than water.

Likely, there are several effects that contribute to the need for a short-ranged attraction in addition to the electrostatic one. We also confirmed in Paper III that explicit surface charges and explicit grand canonical salt give somewhat stronger adsorption than implicit salt and a smeared surface charge for the system with histatin 5. The reason could be that entropic attraction is important. There is also a possibility that the distances between the negative charges at the surface

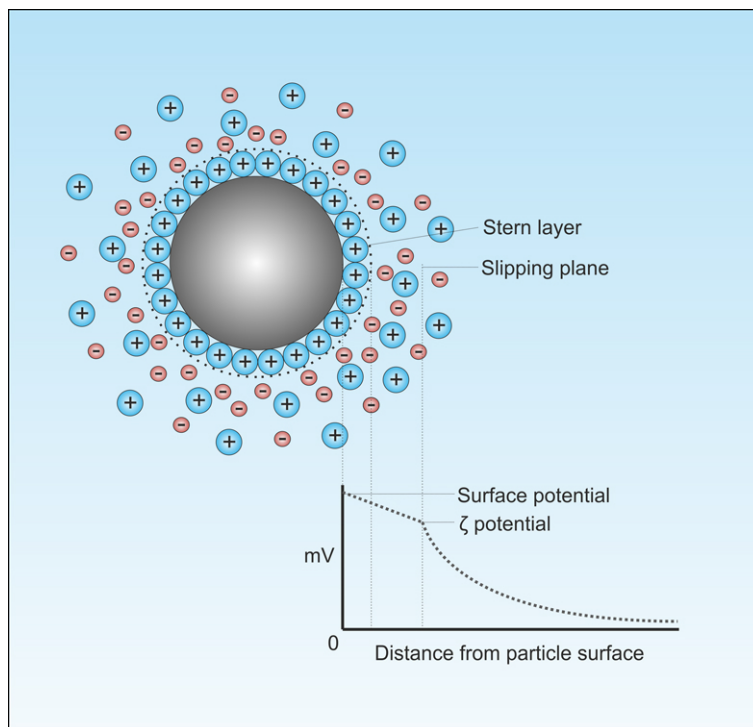


Figure 10.1: An illustration of the Stern layer and the slipping plane outside a negatively charged particle. (Creative Commons Attribution-Share Alike 3.0 Unported license, https://commons.wikimedia.org/wiki/File:Zeta_Potential_for_a_particle_in_dispersion_medium.png.)

and the positive charges in the histatin 5 chain match sometimes – leading to increased adsorption.

There is also a certain degree of insecurity as to whether the experimentally determined charge densities are truly the charges exactly at the surface, which is what we need to use the Gouy–Chapman theory. I have performed simulations with different sets of parameters for the silica (pK_a and silanol group density), see Paper IV, supplementary. When these surfaces are allowed to titrate, they give a surface charge density that is approximately five times higher than the experimentally measured values. Perhaps the theoretical values are more realistic, which would increase adsorption. Kubiak *et al.* used Gouy–Chapman theory to convert ζ -potential to charge density at pH 7.4 and 0.01 M ionic strength [72] and arrived at similar magnitude as Bolt and Samoshina *et al.* [35, 36], even though the ζ -potential is measured at the slipping plane and not at the surface, see Figure 10.1.

Even though the silica surfaces used for ellipsometry are smooth, they still

have some degree of roughness. If a positively charged amino acid explores a cavity, the attraction to the surface should increase compared to a completely smooth surface.

Our hypothesis that histatin 5 had too high chain entropy in solution with the flexible bead model seems to be incorrect in view of the results with the conformational swap model (Paper III).

10.2 The histatin 5 chain entropy and the conformational swap model

The adsorption free energy of the conformational swap model (with structures from all-atom simulations) coincides with the one from the fully flexible model (Figure 9.5), indicating that histatin 5 is too small for the chain entropy to be important for adsorption. However, for longer proteins, it is likely that the conformational swap model gives more realistic results than the flexible bead model. However, the disadvantage is that the longer the protein, the more computationally demanding the all-atom molecular dynamics simulations will be.

10.3 Opposite change in salt-dependence with pH – why?

The balance between repulsion between adsorbed proteins and attraction to the surface could be changed if including also charge regulation of the surface. The pK_a for the silanol groups is approximately 8, and if the charge regulation has more effect when the ionic strength is low, that could lead to the opposite trend to the one shown in Figure 9.4.

10.4 The effect of urea on adsorption – an unsolved question

Israelachvili writes: “Such molecules [as urea] are commonly referred to as *chaotropic agents* or *chaotropes*, a term that was coined to convey the idea that their disruption of the local water structure leads to chaos (not the least of which being produced in the minds of those trying to understand this phenomenon).” [49, p. 165].

I will not attempt to discuss the effect of urea in detail, however there is a study showing that the addition of salt to a 7 M aqueous urea solution made a protein go from unfolded to folded [73]. Thus, the salt counteracted the effect of the urea, similarly to what is seen when comparing Figures 9.6(b) and (c). However, this does not explain why urea had no effect at 10 mM ionic strength. My guess is that the almost unscreened electrostatic interactions between the surface and the proteins dominate in this system, and urea has only a minor effect on them (by increasing the relative permittivity).

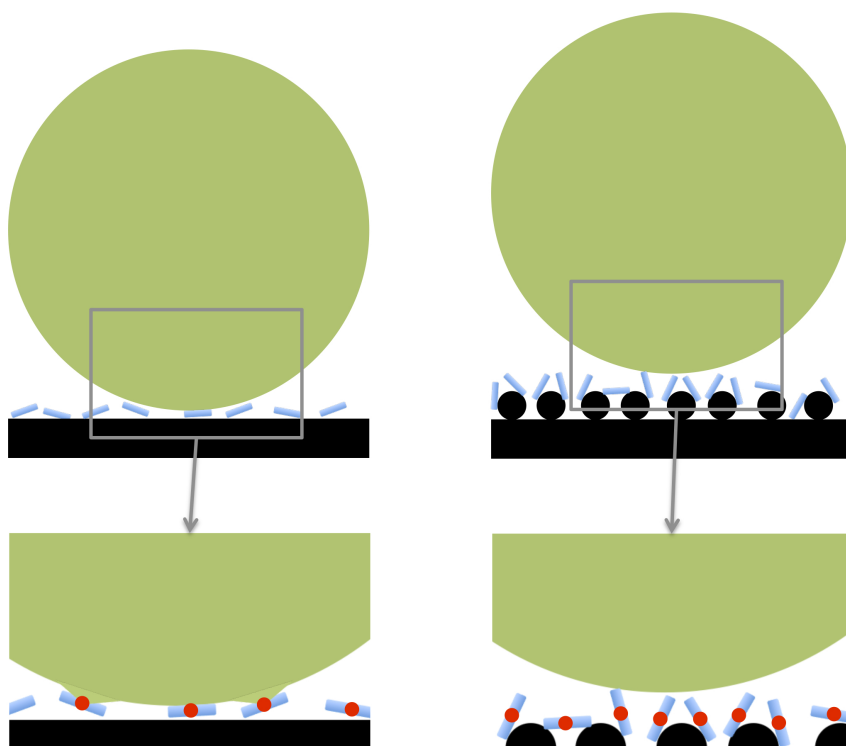


Figure 10.2: An illustration of how the difference in orientation of adsorbed fibrinogen (blue) makes it easier for *S. epidermidis* (green) to adhere to fibrinogen-coated smooth surfaces than fibrinogen-coated nanostructured surfaces. The red circles mark the epitope on fibrinogen that the bacteria bind to. The illustration is to scale when the bacterial diameter is 500 nm.

10.5 Fibrinogen and *S. epidermidis* adhesion

We hypothesise that the difference in *S. epidermidis* adhesion depends on the different orientations of the proteins relative to the flat surface, see Figure 10.2. When the surface is covered with nanoparticles, many of the fibrinogen molecules stand up, and the *S. epidermidis* is hindered from reaching the epitope that it binds to on fibrinogen, which is located in the middle of the protein.

OUTLOOK

“ The greatest enemy of progress is the illusion of knowledge. ”

John Young

Future studies on adsorption with the methods used in our study could involve:

- Using a titrating surface in coarse-grained simulations with explicit salt.
- Investigating histatin 5 adhesion to a hydrophobic surface.
- Investigating the effect of surface roughness using simulations.
- Extending the conformational swap model to other (longer) disordered proteins.
- Run simulations where the main body of fibrinogen is connected to its disordered fragments.
- Continuing to explore experimentally how the presence of urea changes protein adsorption.

Regarding the research field as a whole, better force fields for simulations with surfaces need to be developed. More comparisons with experiments are also needed. Preferably, experiments could be made with a surface that is not as complex as silica, which changes its charge significantly with pH and salt concentration.

REFERENCES

1. Baker, M. 1,500 scientists lift the lid on reproducibility. *Archives of biochemistry and biophysics* **2016**, 533, 452–454.
2. Collins, H.; Pinch, T. *The Golem: What Everyone Should Know About Science*, 2nd ed.; Cambridge University Press: New York, U.S.A., 1998; Chapter 2. Two experiments that ‘proved’ the theory of relativity, pp 27–55.
3. Haraway, D. Situated knowledges: The science question in feminism and the privilege of partial perspective. *Feminist studies* **1988**, 14, 575–599.
4. Berg, J. M.; Tymoczko, J. L.; Stryer, L. *Biochemistry*, 6th ed.; W. H. Freeman and Company: New York, U.S.A., 2007.
5. Oppenheim, F. G.; Xu, T.; McMillian, F. M.; Levitz, S. M.; Diamond, R. D.; Offner, G. D.; Troxler, R. F. Histatins, a novel family of histidine-rich proteins in human parotid secretion. Isolation, characterization, primary structure, and fungistatic effects on *Candida albicans*. *J. Biol. Chem.* **1988**, 263, 7472–7477.
6. Baum, B. J.; Bird, J. L.; Millar, D. B.; Longton, R. W. Studies on histidine-rich polypeptides from human parotid saliva. *Arch. Biochem. Biophys.* **1976**, 177, 427–436.
7. Baum, B. J.; Bird, J. L.; Longton, R. W. Polyacrylamide gel electrophoresis of human salivary histidine-rich-polypeptides. *J. Dent. Res.* **1977**, 56, 1115–1118.
8. Dill, K. A. Dominant forces in protein folding. *Biochemistry* **1990**, 29, 7133–7155.
9. Wright, P. E.; Dyson, H. J. Intrinsically unstructured proteins: re-assessing the protein structure-function paradigm. *J. Mol. Biol.* **1999**, 293, 321–331.
10. Dunker, A. K. et al. Intrinsically disordered protein. *J. Mol. Graphics Modell.* **2001**, 19, 26–59.
11. Dyson, H. J.; Wright, P. E. Intrinsically unstructured proteins and their functions. *Nat. Rev. Mol. Cell Biol.* **2005**, 6, 197–208.
12. Uversky, V. N.; Dunker, A. K. Understanding protein non-folding. *Biochim. Biophys. Acta, Proteins Proteomics* **2010**, 1804, 1231–1264.
13. Tompa, P. Intrinsically disordered proteins: a 10-year recap. *Trends Biochem. Sci.* **2012**, 37, 509–516.
14. Swaisgood, H. E. Chemistry of milk protein. *Developments in dairy chemistry* **1982**, 1, 1–59.
15. Raj, P. A.; Edgerton, M.; Levine, M. J. Salivary histatin 5: dependence of sequence, chain length, and helical conformation for candidacidal activity. *J. Biol. Chem.* **1990**, 265, 3898–3905.

16. Raj, P. A.; Marcus, E.; Sukumaran, D. K. Structure of human salivary histatin 5 in aqueous and nonaqueous solutions. *Biopolymers* **1998**, *45*, 51–67.
17. Stewart, A. F.; Bonsing, J.; Beattie, C. W.; Shah, F.; Willis, I. M.; Mackinlay, A. G. Complete nucleotide sequences of bovine alpha S2- and beta-casein cDNAs: comparisons with related sequences in other species. *Mol. Biol. Evol.* **1987**, *4*, 231–241.
18. MacKay, B. J.; Denepitiya, L.; Iacono, V. J.; Krost, S. B.; Pollock, J. J. Growth-inhibitory and bactericidal effects of human parotid salivary histidine-rich polypeptides on *Streptococcus mutans*. *Infect. Immun.* **1984**, *44*, 695–701.
19. Edgar, M.; Dawes, C., O'Mullane, D., Eds. *Saliva and Oral Health*, 3rd ed.; British Dental Association: London, U.K., 2004.
20. Arnebrant, T. In *Biopolymers at Interfaces*, 2nd ed.; Malmsten, M., Ed.; Marcel Dekker: New York, U.S.A., 2003; Chapter 29. Protein Adsorption in the Oral Environment, pp 811–855.
21. Castagnola, M.; Cabras, T.; Denotti, G.; Fadda, M.; Gambarini, G.; Lupi, A.; Manca, I.; Onnis, G.; Piras, V.; Soro, V.; Tambaro, S.; Messana, I. Circadian Rhythms of Histatin 1, Histatin 3, Histatin 5, Statherin and Uric Acid in Whole Human Saliva Secretion. *Biol. Rhythm Res.* **2002**, *33*, 213–222.
22. Campese, M.; Sun, X.; Bosch, J. A.; Oppenheim, F. G.; Helmerhorst, E. J. Concentration and fate of histatins and acidic proline-rich proteins in the oral environment. *Arch. Oral Biol.* **2009**, *54*, 345–353.
23. Levine, M. J. Development of artificial salivas. *Crit. Rev. Oral Biol. M.* **1993**, *4*, 279–286.
24. Lendenmann, U.; Grogan, J.; Oppenheim, F. Saliva and dental pellicle – a review. *Advances in dental research* **2000**, *14*, 22–28.
25. Jensen, J. L.; Lamkin, M. S.; Oppenheim, F. G. Adsorption of human salivary proteins to hydroxyapatite: a comparison between whole saliva and glandular salivary secretions. *J. Dent. Res.* **1992**, *71*, 1569–1576.
26. Siqueira, W.; Margolis, H.; Helmerhorst, E.; Mendes, F.; Oppenheim, F. Evidence of Intact Histatins in the in vivo Acquired Enamel Pellicle. *J. Dent. Res.* **2010**, *89*, 626–630.
27. Arendorf, T.; Walker, D. The prevalence and intra-oral distribution of *Candida albicans* in man. *Arch. Oral Biol.* **1980**, *25*, 1–10.
28. Akpan, A.; Morgan, R. Oral candidiasis. *Postgrad. Med. J.* **2002**, *78*, 455–459.
29. Tati, S.; Li, R.; Puri, S.; Kumar, R.; Davidow, P.; Edgerton, M. Histatin 5-Spermidine Conjugates Have Enhanced Fungicidal Activity and Efficacy as a Topical Therapeutic for Oral Candidiasis. *Antimicrob. Agents Chemother.* **2014**, *58*, 756–766.
30. McDonald, E. E.; Goldberg, H. A.; Tabbara, N.; Mendes, F. M.; Siqueira, W. L. Histatin 1 resists proteolytic degradation when adsorbed to hydroxyapatite. *J. Dent. Res.* **2011**, *90*, 268–272.
31. Vukosavljevic, D.; Hutter, J. L.; Helmerhorst, E. J.; Xiao, Y.; Custodio, W.; Zaidan, F. C.; Oppenheim, F. G.; Siqueira, W. L. Nanoscale adhesion forces between enamel pellicle proteins and hydroxyapatite. *J. Dent. Res.* **2014**, *93*, 514–519.
32. Kollman, J. M.; Pandi, L.; Sawaya, M. R.; Riley, M.; Doolittle, R. F. Crystal Structure of Human Fibrinogen. *Biochemistry* **2009**, *48*, 3877–3886.
33. Hulander, M.; Valen-Rukke, H.; Sundell, G.; Andersson, M. Influence of Fibrinogen on *Staphylococcus epidermidis* Adhesion Can Be Reversed by Tuning Surface Nanotopography. *ACS Biomater. Sci. Eng.* **2019**, *5*, 4323–4330.

34. Iler, R. K. *The chemistry of silica*, 1st ed.; John Wiley & Sons: New York, NY, U.S.A., 1979.
35. Bolt, G. H. Determination of the charge density of silica sols. *J. Phys. Chem.* **1957**, *61*, 1166–1169.
36. Samoshina, Y.; Nylander, T.; Shubin, V.; Bauer, R.; Eskilsson, K. Equilibrium Aspects of Polycation Adsorption on Silica Surface: How the Adsorbed Layer Responds to Changes in Bulk Solution. *Langmuir* **2005**, *21*, 5872–5881.
37. Landgren, M.; Jönsson, B. Determination of the optical properties of silicon/silica surfaces by means of ellipsometry, using different ambient media. *J. Phys. Chem.* **1993**, *97*, 1656–1660.
38. Hosoya, N.; Honda, K.; Iino, F.; Arai, T. Changes in enamel surface roughness and adhesion of *Streptococcus mutans* to enamel after vital bleaching. *J. Dent.* **2003**, *31*, 543–548.
39. Arends, J.; Jongebloed, W. L. The enamel substrate—characteristics of the enamel surface. *Swed. Dent. J.* **1976**, *1*, 215–224.
40. Arends, J. Studies on histidine-rich polypeptides from human parotid saliva. *J. Dent.* **1979**, *7*, 246–253.
41. Cai, K.; Bossert, J.; Jandt, K. D. Does the nanometre scale topography of titanium influence protein adsorption and cell proliferation? *Colloid Surface B* **2006**, *49*, 136–144.
42. Rechendorff, K.; Hovgaard, M. B.; Foss, M.; Zhdanov, V. P.; Besenbacher, F. Enhancement of Protein Adsorption Induced by Surface Roughness. *Langmuir* **2006**, *22*, 10885–10888.
43. Deligianni, D.; Katsala, N.; Ladas, S.; Sotiropoulou, D.; Amedee, J.; Missirlis, Y. Effect of surface roughness of the titanium alloy Ti–6Al–4V on human bone marrow cell response and on protein adsorption. *Biomaterials* **2001**, *22*, 1241–1251.
44. Horbett, T. A.; Brash, J. L., Eds. *Proteins at Interfaces II*; ACS Publications: Washington DC, U.S.A., 1995; Vol. 602.
45. Nakanishi, K.; Sakiyama, T.; Imamura, K. On the adsorption of proteins on solid surfaces, a common but very complicated phenomenon. *J. Biosci. Bioeng.* **2001**, *91*, 233–244.
46. Zhang, L.; Sun, Y. Molecular simulation of adsorption and its implications to protein chromatography: A review. *Biochem. Eng. J.* **2010**, *48*, 408–415, Invited Review Issue 2010.
47. Ozboyaci, M.; Kokh, D. B.; Corni, S.; Wade, R. C. Modeling and simulation of protein–surface interactions: achievements and challenges. *Q. Rev. Biophys.* **2016**, *49*.
48. Gray, J. J. The interaction of proteins with solid surfaces. *Curr. Opin. Struct. Biol.* **2004**, *14*, 110–115.
49. Israelachvili, J. N. *Intermolecular and Surface Forces*, 3rd ed.; Academic Press, Elsevier: Oxford, U.K., 2011.
50. Lund, M.; Jönsson, B. Charge regulation in biomolecular solution. *Q. Rev. Biophys.* **2013**, *46*, 265–281.
51. Kurut, A.; Henriques, J.; Forsman, J.; Skepö, M.; Lund, M. Role of histidine for charge regulation of unstructured peptides at interfaces and in bulk. *Proteins: Struct. Funct. Bioinf.* **2014**, *82*, 657–667.
52. Evans, D. F.; Wennerström, H. *The colloidal domain: where physics, chemistry, biology, and technology meet*, 2nd ed.; Wiley-VCH: Hoboken, NJ, U.S.A., 1999.
53. Hill, T. L. *An Introduction to Statistical Thermodynamics*, 2nd ed.; Addison-Wesley Publishing Company: Reading, MA, U.S.A., 1962.
54. McQuarrie, D. A. *Statistical Mechanics*, 1st ed.; Harper Collins Publishers: New York, U.S.A., 1976.

55. Frenkel, D.; Smit, B. *Understanding Molecular Simulation: From Algorithms to Applications*, 2nd ed.; Academic Press: San Diego, CA, U.S.A., 2002.
56. Henriques, J.; Skepö, M. Molecular Dynamics Simulations of Intrinsically Disordered Proteins: On the Accuracy of the TIP4P-D Water Model and the Representativeness of Protein Disorder Models. *J. Chem. Theory Comput.* **2016**, *12*, 3407–3415.
57. Best, R. B.; Zheng, W.; Mittal, J. Balanced Protein–Water Interactions Improve Properties of Disordered Proteins and Non-Specific Protein Association. *J. Chem. Theory Comput.* **2014**, *10*, 5113–5124.
58. Piana, S.; Donchev, A. G.; Robustelli, P.; Shaw, D. E. Water Dispersion Interactions Strongly Influence Simulated Structural Properties of Disordered Protein States. *J. Phys. Chem. B* **2015**, *119*, 5113–5123.
59. Metropolis, N.; Rosenbluth, A. W.; Rosenbluth, M. N.; Teller, A. H.; Teller, E. Equation of State Calculations by Fast Computing Machines. *J. Chem. Phys.* **1953**, *21*, 1087–1092.
60. Malmsten, M. In *Biopolymers at Interfaces*, 2nd ed.; Malmsten, M., Ed.; Marcel Dekker: New York, U.S.A., 2003; Chapter 21. Ellipsometry and Reflectometry for Studying Protein Adsorption, pp 539–582.
61. Skoog, D. A.; West, D. M.; Holler, F. J. *Fundamentals of Analytical Chemistry*, 6th ed.; Saunders College Publishing: Orlando, FL, U.S.A., 1992.
62. Kern, W.; Puotinen, D. A. Cleaning Solutions Based on Hydrogen Peroxide for use in Silicon Semiconductor Technology. *RCA Rev.* **1970**, *31*, 187–206.
63. Liu, X.; Dedinaite, A.; Nylander, T.; Dabkowska, A. P.; Skoda, M.; Makuska, R.; Claesson, P. M. Association of anionic surfactant and physisorbed branched brush layers probed by neutron and optical reflectometry. *J. Colloid Interface Sci.* **2015**, *440*, 245–252.
64. Azzam, R. M. A.; Bashara, N. M. *Ellipsometry and polarized light*, 1st ed.; North-Holland Publishing Company: Amsterdam/New York/Oxford, 1977.
65. Tibergh, F.; Landgren, M. Characterization of thin nonionic surfactant films at the silica/water interface by means of ellipsometry. *Langmuir* **1993**, *9*, 927–932.
66. Vörös, J. The Density and Refractive Index of Adsorbing Protein Layers. *Biophys. J.* **2004**, *87*, 553–561.
67. Cuypers, P. A.; Corsel, J. W.; Janssen, M. P.; Kop, J. M. M.; Hermens, W. T.; Hemker, H. C. The adsorption of prothrombin to phosphatidylserine multilayers quantitated by ellipsometry. *J. Biol. Chem.* **1983**, *258*, 2426–2431.
68. de Feijter, J. A.; Benjamins, J.; Veer, F. A. Ellipsometry as a tool to study the adsorption behavior of synthetic and biopolymers at the air–water interface. *Biopolymers* **1978**, *17*, 1759–1772.
69. Cohn, E. J.; Edsall, J. T. In *Proteins, Amino Acids and Peptides as Ions and Dipolar Ions*, 1st ed.; Cohn, E. J., Edsall, J. T., Eds.; Reinhold Publishing Corporation: New York, U.S.A., 1934; Chapter 16. Density and Apparent Specific Volume of Proteins, pp 370–381.
70. McMeekin, T. L.; Wilensky, M.; Groves, M. L. Refractive indices of proteins in relation to amino acid composition and specific volume. *Biochem. Biophys. Res. Commun.* **1962**, *7*, 151–156.
71. Prytkova, V.; Heyden, M.; Khago, D.; Freitas, J. A.; Butts, C. T.; Martin, R. W.; Tobias, D. J. Multi-Conformation Monte Carlo: A Method for Introducing Flexibility in Efficient Simulations of Many-Protein Systems. *J. Phys. Chem. B* **2016**, *120*, 8115–8126.

72. Kubiak, K.; Adamczyk, Z.; Wasilewska, M. Mechanisms of fibrinogen adsorption at the silica substrate determined by QCM-D measurements. *J. Colloid Interface Sci.* **2015**, *457*, 378–387.
73. Dötsch, V.; Wider, G.; Siegal, G.; Wüthrich, K. Salt-stabilized globular protein structure in 7 M aqueous urea solution. *{FEBS} Lett.* **1995**, *372*, 288–290.

ACKNOWLEDGEMENTS

Of course, this work would not have become something that I will be proud of without the help and inspiration from lots of people. Here I will mention the people who I believe have given the most important contributions to this thesis and to my life as a PhD student in Lund.

Marie Skepö, the principal supervisor for this project, thank you for offering me to do this project under your guidance. Thank you for balancing my negative thinking with your positive thinking, and for being so helpful and understanding when it comes to personal matters/problems.

Per-Olof Widmark, co-supervisor for this project, thank you for your support.

Johan Reimer, former co-supervisor for this project, thanks for supporting me in my decisions.

Torbjörn Åkesson, co-supervisor for this project during its first months. I remember the positive comments you gave me on a draft I sent you – they meant a lot to me. I am sad that I didn't get to know you more.

Jan Forsman, former co-supervisor for this project, thanks for answering my questions and for helping me with some chapters in my licentiate thesis.

Mikael Lund, thank you for all the help with Faunus and with Paper III. You have been like an extra supervisor for me and for that I am very grateful.

Tommy Nylander, thank you for all the help with ellipsometry and for introducing me to lots of interesting people at different conferences.

Marco Polimeni, **Mats Hulander**, and **Martin Andersson**, thanks for the nice research collaborations.

Anil Kurut Şabanoğlu, thank you for teaching me how to do ellipsometry and size exclusion chromatography, and for being such a nice colleague.

João Henriques, thank you for introducing me to Faunus and for sharing useful scripts with me.

My Hyltegren, thank you for helping me with the introduction to this thesis!

Nils Lenngren, thank you for sending me the Latex-template I used for both of my theses.

Ellen Rieloff, thanks for helping me with my Latex-related problems.

Paula Leckius, thank you for sharing your expertise on printing and for advising me on how to adapt the Latex-template.

Magnus Ullner, thank you for reading most of the manuscript for the thesis and for taking the time to discuss all of your suggested changes with me. That kind of discussions is what I appreciate the most in science.

Thank you to **all of my past and present colleagues at the divisions of theoretical and physical chemistry in Lund!** It has been great to experience the friendly environment at our divisions. Thanks for the Christmas parties, the Friday after works/drinking days and all of the great PhD parties that I've had the privilege to be invited to.

A special thank you to my office mates: **Carolina Cragnell**, it has always been fun to travel with you, to have morning chats and lunches, and to join you in the stable. **Linda Månsson, Mona Koder Hamid, and Amanda Eriksson Skog**, thank you for making the big room a lot less empty and for lunch company and small walks.

A special thank you also to all the members of the **Skepö research group**. Thanks for the group "fikas", the discussions, and the after works.

A great thank you to **ALL who participated in the Teokem Thursday evenings**. I felt really welcome here in Lund when I was introduced to the concept and I have so many fun memories to look back on – Game of Thrones, Dungeons and Dragons, Dixit and Once upon a time – it has been great! Of course it is **you**, the people rather than the games themselves, that I remember.

Lennart Piculell and Karin Schillén, thank you for introducing me to a woodwind quintet and a choir here in Lund!

Thank you to my fellow wind instrument players in the woodwind quintet **Ad libitum**. It has been good to get to know some people in Lund from outside of Lund university and to pick up the French horn again. I hope to be able to play with you for several more years to come.

A special thank you to **Aliza Wechsler** for reading the preface and suggesting changes in the language.

Alla min bekanta i Fältbiologerna och särskilt **redaktionen för Fältbiologen**, tack för alla aktiviteter och lärdomar! Utan er hade jag inte varit den jag är idag och utan de lärdomar jag fick i redaktionen hade denna avhandling aldrig blivit såhär bra. Att kunna ta emot kritik med glädje och tacksamhet är en enorm styrka som jag nu har med mig genom livet.

Malmö amatörteaterforum, Elin Fredrikson och alla mina kurskamrater i improvisationsteater – tack för alla roliga stunder vi haft och all övning i att släppa kontrollbehov och nervositet på scen och låta inspirationen flöda. Det var tack vare dig, **Elin**, som jag insåg att jag måste bli bättre på att säga ja till idéer – både mina och andras – även på jobbet.

Mamma, pappa och Jenny, tack för att ni alltid funnits med och stöttat mig även sedan jag flyttade till Lund och för alla trevliga stunder vi haft när ni hälsat på!

Jenny Hyllén-Cavallius, I am so grateful for having a friend like you since so many years. Thank you for supporting me in all of my life-changing decisions. You make me understand what to do without saying it.

Annika and **Bengt Dovrinder**, thank you for warmly welcoming me into your family!

Carl Dovrinder, thank you for bringing lots of music into my life, and for being more than I had dreamt of. No one can ever replace you!

And last but not least – thank you **Alve Hyltegren Dovrinder** for making this thesis writing seem less serious and more manageable. You have always been more important.

Adsorption of the intrinsically disordered saliva protein histatin 5 to silica surfaces. A Monte Carlo simulation and ellipsometry study

K. Hyltegren, T. Nylander, M. Lund, M. Skepö.

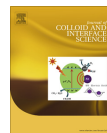
Journal of Colloid and Interface Science, 467, **2016**, pp. 280–290.

Reprinted with permission from Elsevier.



Contents lists available at ScienceDirect

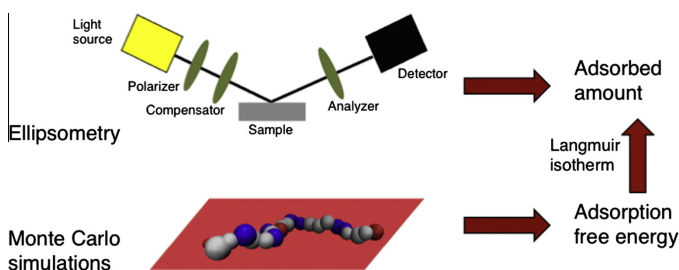
Journal of Colloid and Interface Science

journal homepage: www.elsevier.com/locate/jcis

Adsorption of the intrinsically disordered saliva protein histatin 5 to silica surfaces. A Monte Carlo simulation and ellipsometry study

Kristin Hyltegren^{a,*}, Tommy Nylander^b, Mikael Lund^a, Marie Skepö^a^a Division of Theoretical Chemistry, Lund University, P.O.B. 124, SE-221 00 Lund, Sweden^b Division of Physical Chemistry, Lund University, P.O.B. 124, SE-221 00 Lund, Sweden

GRAPHICAL ABSTRACT



ARTICLE INFO

Article history:
 Received 22 October 2015
 Revised 11 January 2016
 Accepted 13 January 2016
 Available online 14 January 2016

2010 MSC:
 00-01
 99-00

Keywords:
 Intrinsically disordered proteins
 Histatin 5
 Ellipsometry
 Monte Carlo simulations
 Coarse graining
 Charge regulation
 Adsorption

ABSTRACT

Hypothesis: The adsorption of histatin 5 to hydrophilic silica surfaces is governed by electrostatic attractive forces between the positive protein and the negative surface. Hence pH and ionic strength control the adsorbed amount, which can be described by coarse-grained Monte Carlo simulations accounting for electrostatic forces and charge regulation of the protein.

Experiments: The amount of histatin 5 adsorbed to hydrophilic silica surfaces at different pH and ionic strengths was measured using null ellipsometry. The results were compared with coarse-grained Monte Carlo simulations of a single histatin 5 molecule and a surface with a fixed, smeared charge set according to experimental values for silica. The Langmuir isotherm was used to calculate the surface coverage from the simulation results. The effect of charge regulation of the protein was investigated.

Findings: Even though electrostatic attractive forces are important for the investigated system, a non-electrostatic short-ranged attraction with a strength of about $2.9 k_B T$ per amino acid was needed in the simulations to get surface coverages close to experimental values. The importance of electrostatics increases with increasing pH. Charge regulation of the protein affected the results from the simulations only at high surface charge and low ionic strength.

© 2016 Elsevier Inc. All rights reserved.

* Corresponding author.

E-mail address: kristin.hyltegren@teokem.lu.se (K. Hyltegren).

1. Introduction

Histatin 5 is a short, basic protein containing 24 amino acid residues, of which seven are histidines (sequence: Asp-Ser-His-Ala-Lys-Arg-His-His-Gly-Tyr-Lys-Arg-Lys-Phe-His-Glu-Lys-His-Ser-His-Arg-Gly-Tyr [1]). It is present in human saliva and belongs to the family of intrinsically disordered proteins [2], as shown by CD spectroscopy [3] and NMR [4]. It has both antifungal [5] and antibacterial [6] properties, primarily against the fungus *Candida albicans*. Histatin 5 adsorbs to the cell wall/membrane of *Candida albicans* and enters and kills the cells. The mechanism by which the protein is transported into the cell may be a combination of transporter-mediated uptake across the cell wall, direct transfer across the membrane, and endocytosis [7]. Direct transfer across a liposome membrane has been observed [8]. The anticandidal activity has received much attention [1,3,7,9–12] and it has been shown that a conjugate of histatin 5 with spermidine is a potential drug against oral candidiasis [13]. Histatin 5 is also a constituent of the protective film called the enamel pellicle and offers some defence against acid-induced degradation of enamel [14].

Adsorption to negatively charged surfaces is crucial for the function of histatin 5 both as a part of the pellicle and as an antimicrobial agent. We have investigated the surface adsorption of histatin 5 to hydrophilic silica surfaces using ellipsometry and coarse-grained Monte Carlo simulations with the aim to answer three questions. The questions and the motivations behind them follow here:

Question 1: How does the adsorbed amount of histatin 5 depend on pH and ionic strength?

Motivation: In human whole saliva, the pH varies between approximately 5.7 and 7.8 [15], while the ionic strength of saliva from the parotid glands varies between 30 and 100 mM [16]. This natural variation makes it interesting to study how the adsorption of histatin 5 is affected by pH and ionic strength. Furthermore, the killing activity of histatin 5 has been shown to be dependent on these conditions. The ability of histatin 5 to kill *Candida albicans* decreases with increasing ionic strength [9,12], and while Xu et al. found no significant pH-dependence [9], Kacprzyk et al. found that histatin 5 killed *Candida albicans* more effectively at pH 7.4 than at pH 5.5 [17].

Question 2: Can we describe the adsorption of histatin 5 with a coarse-grained model with a single protein molecule?

Motivation: Coarse-grained models provide a way of investigating properties of large molecules at a reduced computational cost. The surface adsorption of histatin 5 has been studied previously using coarse-grained Monte Carlo simulations, where one coarse-grained histatin 5 molecule was adsorbed to a flat surface with a smeared charge [18]. The results were compared with atomistic simulations and density functional theory calculations. We want to extend previous work on the coarse-grained model by performing a corresponding experimental study to verify the simulation parameters and gain further insight into the adsorption mechanism by comparing experiments and simulations. By using the Langmuir adsorption isotherm to convert the adsorption free energies found from simulations into surface coverages, the results from simulations and experiments can be directly compared.

Question 3: Is charge regulation important for the adsorption of histatin 5 in a physiologically relevant system?

Motivation: The high content of histidines, which have a pK_a of ~ 6 , makes it possible for histatin 5 to regulate its charge depending on the environment at physiological pH. The positive net charge of histatin 5 increases when the protein approaches a negatively charged surface. Earlier coarse-grained Monte Carlo simulations have shown that this mechanism increases the surface adsorption under some conditions [18]. In order to gain further knowledge on

the importance of charge regulation, we use simulations to investigate whether this is the case also for the conditions studied here.

2. Materials and methods

2.1. Experimental

2.1.1. Materials

Chemicals. Synthetic histatin 5 was bought from American Peptide Company, Inc., U.S.A. (lots no V11131T1, 1312047T, and 1303040T). The peptide content was 59.7% and the purity of the peptide 95.8%. In order to remove excess salt and other impurities, the protein was purified using size exclusion chromatography, according to the procedure described in the Methods section below.

All buffer solutions were prepared using MilliQ water. Buffers containing 10 mM tris (Saveen Werner AB, Sweden, lot no. 22007904) were used at pH 7, 8 and 9. The pH was adjusted using 1 M hydrochloric acid. When a higher ionic strength was needed, sodium chloride (Scharlau, Spain, Prod. no. S002271000) was added to the buffer. For the measurements at pH 6, a 10 mM bis-tris (Merck Millipore, U.S.A., lot no. XA27K) buffer was prepared in the same way. At pH 4 and 5, a 10 mM buffer made from acetic acid (Scharlau, Spain, batch 34335) and sodium acetate (Sigma-Aldrich, U.S.A., lot no. BCBH6230V) was used.

Substrates. Silicon wafers which were oxidized to give an approximately 300 Å thick silica (silicon dioxide) layer were purchased from Semiconductor Wafer, Inc., Taiwan. The wafers were cut into pieces and cleaned in an alkaline solution with hydrogen peroxide, followed by cleaning in an acidic solution with hydrogen peroxide, according to the procedure described by Landgren and Jönsson [20]. This procedure has been shown to effectively remove organic contaminants and metal ions [21]. The slides were then stored in ethanol (Solveco AB, Sweden). Before the measurements, the surfaces were rinsed in three steps with water, ethanol and water, dried with nitrogen and put in a plasma cleaner (model PDC-3XG, Harrick, U.S.A.) for 5 min at a pressure of approximately 0.06 mbar. The plasma cleaning was done to remove any remaining organic contaminants.

Approximate surface charge densities of silica under different conditions can be found in Table 1. Note that the surface charge varies substantially with pH and ionic strength.

2.1.2. Methods

Size exclusion chromatography. Surface chemistry experiments are very sensitive to surface active impurities, and to ensure the purity of the histatin 5, size exclusion chromatography was used. The separation range of the column (Superdex 75 10/300 GL, GE Healthcare, Sweden) was 3–70 kDa. The column was filled with a 10 mM tris buffer with 140 mM NaCl at pH 7. NaCl was included in the buffer to reduce undesired electrostatic interactions between the column material and the protein.

Table 1
Approximate surface charge densities of silica particles at different pH-values and ionic strengths (I) adjusted with KCl, taken from Samoshina et al. [19].

| pH | Approximate surface charge density ($\mu\text{C}/\text{cm}^2$) | |
|----|--|----------------------|
| | $I = 10 \text{ mM}$ | $I = 100 \text{ mM}$ |
| 6 | −0.25 | −0.50 |
| 7 | −1.00 | −2.00 |
| 8 | −2.75 | −5.75 |
| 9 | −7.00 | −12.50 |

The freeze-dried peptide was dissolved in the running buffer at a concentration of approximately 10 mg/ml. After equilibrating the column with the buffer, 0.1 ml of the protein solution was injected. The sample corresponding to the middle of the UV absorption peak was collected; see [supplementary material](#).

Concentration measurements. All histatin 5 concentrations were measured with a NanoDrop 2000 spectrophotometer (Thermo Fisher Scientific, Inc., U.S.A.) at 280 nm. The extinction coefficient used was $2560 \text{ M}^{-1} \text{ cm}^{-1}$, calculated from the tyrosine content of the peptide [22,23].

Refractive index measurements. The refractive indices of the buffers were measured using an Abbe 60 refractometer (Bellingham & Stanley Ltd., UK) at wavelengths of 579.1, 546.1 and 435.8 nm. The refractive indices at the wavelength of the ellipsometer (401.5 nm) were extrapolated from these measurements using the two-term form of the Cauchy equation.

Null ellipsometry – theory. The experimental data on the adsorption of histatin 5 have been obtained using the technique of null ellipsometry. Ellipsometry is based on the use of elliptically polarized light and the fact that when light is reflected at a surface, the polarization changes. This change is different depending on the characteristics of the surface and the thickness and refractive index of the adsorbed layer. By using an appropriate angle of the polarizer before the reflection at the surface, linearly polarized light is obtained after reflection. This linearly polarized light can be cancelled by another polarizer, the analyzer. The raw data from null ellipsometry are the polarizer and analyzer angles that can be converted into the relative phase shift, Δ , and amplitude change, Ψ . From these angles, the refractive index and the thickness of the adsorbed layer are determined. However, at low surface coverage and/or thin layers, the refractive index and the thickness are interdependent, meaning that both the thickness and refractive index cannot be resolved. Therefore, a fixed refractive index of 1.5 was used for the adsorbed layer of histatin 5. This value is reasonable for an adsorbed protein layer [24]. The effect of choosing other refractive indices is shown in the [supplementary material](#). From the refractive index and the measured thickness of the layer, the adsorbed amount (dry mass) per surface area was calculated using the two-component model from Cuyper et al. [25]:

$$\Gamma = \frac{3df(n_f)}{A - \nu \frac{n_f^2 - 1}{n_0^2 + 2}} (n_f - n_0), \quad (1)$$

where d_f is the thickness of the adsorbed film, n_f is the refractive index of the film, n_0 is the refractive index of the buffer, A is the molar refractivity of the compound, M is the molar weight, ν is the specific volume and

$$f(n_f) = \frac{n_f + n_0}{(n_f^2 + 2)(n_0^2 + 2)}. \quad (2)$$

Due to the interdependence between the refractive index and the layer thickness, and to cancellation of errors, the value of the adsorbed amount is less prone to errors than the refractive index and the thickness of the layer [26]. The calculated value of the adsorbed amount is also less dependent on the optical model and can therefore be used for inhomogeneous layers as verified elsewhere [25,27].

The values used for the specific volume and M/A were 0.70 ml/g and 3.95 g/ml, respectively. These values were calculated from the amino acid composition of histatin 5 according to Cohn and Edsall [28] (specific volume) and McMeekin et al. [29] (M/A). The calculated adsorbed amount depends directly on these values.

Ellipsometry setup and procedure. The instrument used for this study was a Rudolph thin film ellipsometer (type 43603-200E, Rudolph Research Corp., U.S.A.). The measurements were performed using light at a wavelength of 401.5 nm emitted from a

xenon arc lamp. The angle of incidence was 67.9° . The surface was mounted in a holder inside a trapezoid cuvette where the light passed through perpendicular to the cuvette walls. The temperature in the cuvette was maintained at 25°C using a thermostat.

In order to determine the thickness of the oxide layer on the silicon surface, measurements were conducted both in air and in 5 ml buffer, while stirring with a magnetic stirrer. When all initial parameters had been determined, 100–300 μl of concentrated histatin 5 solution was added to the cuvette to give a final concentration of 0.05 mg/ml.

Since the purified protein was dissolved in a solution with an ionic strength of 150 mM, the buffer was exchanged before addition to the cuvette for the measurements at low ionic strength (10 and 60 mM) to make sure that extra salt from the buffer used for purification would not influence the total ionic strength in the cuvette. The exchange was made by adding the protein solution (approximately 200 μl) and the new buffer (approximately 1.5 ml) to a centrifugal concentrator (Vivaspin 2, MWCO 2 kDa, Sartorius Stedim Biotech GmbH, Germany) and then centrifuging (at $\sim 2500g$, 18°C , in a laboratory centrifuge of model MPW-260R, MPW Med. Instruments, Poland) until a volume close to the original volume of the protein solution was reached. This procedure was then repeated a second time.

The protein was allowed to adsorb for 60 min under agitation with a magnetic stirrer. Then, buffer solution was pumped through the cuvette at a speed of $\sim 16 \text{ ml/min}$. The rinsing with buffer was performed during 30 min.

2.2. Computational

Coarse-grained Monte Carlo simulations were performed using Faunus, a C++ framework for Metropolis Monte Carlo simulations [30].

2.2.1. Model

Table 2 shows all the terms contributing to the system energy Hamiltonian and the parameters of these terms are given in Table 3. All interactions were assumed to be pairwise additive. Other aspects of the model are described below.

The protein. The protein was coarse-grained using a bead model, where each amino acid and the N- and C-terminals are represented by soft spheres connected by harmonic bonds [31], see Fig. 1 for snapshots. This gives 26 beads for histatin 5. The equilibrium distance between the centres of the spheres was set to 4.0 Å,

Table 2
The terms of the system energy Hamiltonian.

| Type of energy | Expression (equation number) |
|-------------------------------------|--|
| Inter-bead interactions | |
| Debye–Hückel electrostatics | $\sum_{i=1}^{n-1} \sum_{j=i+1}^n \frac{q_i q_j}{4\pi\epsilon_0 \epsilon_r r_{ij}} e^{-kr_{ij}} \quad (3)$ |
| Harmonic bonds | $\sum_{i=1}^{n-1} k_b (R_i - R_{eq})^2 \quad (4)$ |
| Lennard-Jones (non-bonded beads) | $\sum_{i=1}^{n-2} \sum_{j=i+2}^n 4\epsilon_{ab} \left[\left(\frac{a_{ij}}{r_{ij}}\right)^{12} - \left(\frac{a_{ij}}{r_{ij}}\right)^6 \right] \quad (5)$ |
| Titration | |
| Intrinsic titration energy | $\sum_{i=1}^{n_i} k_b T (\text{pH} - \text{pK}_{a,i}) \ln 10, \text{ for } i \text{ protonated} \quad (6)$ |
| Protein–surface interactions | |
| Gouy–Chapman electrostatics | $\sum_{i=1}^n 2\epsilon_i k_b T \ln \left(\frac{1 + f_i e^{-\psi(r_i)/k_b T}}{1 - f_i e^{-\psi(r_i)/k_b T}} \right), \quad (7)$ |
| | where $f_i = \tanh \left[\frac{1}{2} \sinh^{-1} \left(\sqrt{\frac{q_i}{8\epsilon_0 \epsilon_r r_{ij} \rho_0}} \right) \right]$ |
| Shifted Lennard-Jones | $\sum_{i=1}^n \epsilon \left[\left(\frac{a_i/2}{(r_i/r_0)^{1/2}} \right)^{12} - 2 \left(\frac{a_i/2}{(r_i/r_0)^{1/2}} \right)^6 \right] \quad (8)$ |

Table 3

The parameters of the expressions in Table 2. All distances are measured from the centres of the beads.

| Parameter = value | Description |
|---|---|
| $n = 26$ | Number of beads |
| q_i | Charge of bead i |
| ϵ_0 | Permittivity of free space |
| $\epsilon_r = 78.54$ | Relative permittivity |
| r_{ij} | Distance between beads i and j |
| $\kappa^{-1} = \sqrt{\frac{\epsilon_0 \epsilon_r k_B T}{2N_A e^2}}$ | Debye screening length |
| k_B | Boltzmann's constant |
| $T = 298.15$ K | Temperature |
| N_A | Avogadro's constant |
| e | Elementary charge |
| $l = 10$ or 100 mM | Ionic strength |
| $n_b = n - 1$ | Number of bonds |
| $k_b = 0.76 k_B T / \text{\AA}^2$ [31] | Harmonic bond spring constant |
| R_i | Bond length of bond i |
| $R_{eq} = 4.0$ \AA | Equilibrium bond length |
| $\epsilon_{nb} = 0.05 k_B T$ | Interaction strength between non-bonded beads |
| $\sigma_{ij} = \frac{\sigma_i \sigma_j}{2}$ | Lennard-Jones diameter |
| σ_i | Diameter of bead i |
| n_p | Number of protonated beads |
| $pK_{a,i}$ | Acid dissociation constant of bead i |
| z_i | Charge number of bead i |
| $r_{s,i}$ | Distance between bead i and the surface |
| ρ | Surface charge density |
| $c_0 = 10$ or 100 mM | Concentration of 1:1 salt |
| $\epsilon = 2.9 k_B T$ | Bead-surface interaction strength |

corresponding to the contour length of one amino acid [32]. The diameters of the beads were calculated from the masses of the individual amino acids under the assumption that they are spherical, using a protein density of 1.525 g/ml calculated according to Fischer et al. [33].

The amino acid beads are titrating, meaning that they will acquire different charges depending on the electrostatics of the neighbouring amino acid residues, the external potential, the pH of the solution and the intrinsic pK_a of the amino acid residue. The intrinsic pK_a values were taken from Nozaki and Tanford [34].

The buffer. Solvent and salt were modelled implicitly, entering the model as a relative permittivity and a Debye screening length κ^{-1} , respectively.

The surface. The substrate was assumed to be a smooth Gouy-Chapman surface with a smeared charge. The charge densities under the different conditions used in the simulations were taken from the experimentally determined values in Table 1. In addition to electrostatics, there was also a Lennard-Jones potential with $\epsilon = 2.9 k_B T$ between the amino acid beads and the surface (Eq.

(8) in Table 2). The value of ϵ was determined by a comparison with experimental values using the Langmuir adsorption isotherm, see Section 3.3.

Each amino acid bead may approach the surface until there is zero distance between the centre of the bead and the surface. A hard wall repulsive potential prevents the bead from penetrating further into the surface. The Lennard-Jones potential between the surface and a bead is shifted so that it has its minimum at zero distance between the centre of the bead and the surface. If a normal Lennard-Jones potential is introduced, the repulsion sets in too early and the adsorption decreases instead of increasing.

2.2.2. Method

A single protein molecule was simulated using the Metropolis Monte Carlo scheme [35] in the canonical (NVT) ensemble. The simulation box was cubic with side lengths of 300 \AA, corresponding to three times the contour length of histatin 5 and 20 times the radius of gyration. In bulk, the boundary conditions were periodic in all directions. For surface simulations, hard boundaries were applied in the z -direction.

The following Monte Carlo moves were used:

1. Protein translation
2. Protein rotation
3. Single bead translation
4. Crankshaft (picks two beads randomly and defines the vector connecting them as the rotation axis, then rotates the beads between the picked ones by 180° around the axis)
5. Pivot rotations (defines a rotation axis in the same manner as with the crankshaft move, then rotates the beads at one end of the protein 180° around the axis)
6. Titration move (protonating or deprotonating a bead)

To improve sampling of the space far from the surface, an algorithm was used to restrict the mass centre of the histatin 5 molecule to different, but overlapping, parts of the simulation box. The simulations were run during $1\text{--}50 \times 10^8$ Monte Carlo steps depending on the system.

3. Results and discussion

3.1. Histatin 5 in bulk solution

Before discussing the surface adsorption of histatin 5, some relevant properties of histatin 5 in bulk solution will be presented.

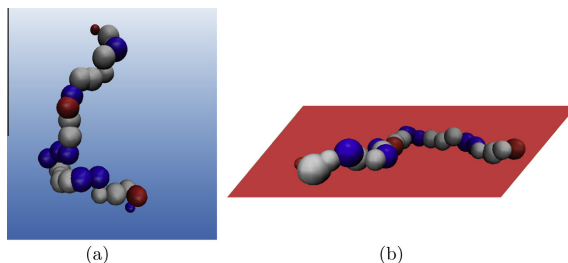


Fig. 1. Snapshots from simulations showing histatin 5 (a) in bulk solution and (b) adsorbed to a negatively charged surface. The blue beads are positively charged, the red ones are negatively charged and the grey ones are neutral. (For interpretation of the references to colour in this figure legend, the reader is referred to the web version of this article.)

3.1.1. Monte Carlo simulations

Conformational properties. The root mean square end-to-end distance of histatin 5 was found from simulations to be 39.3 Å at pH 7 and ionic strength 100 mM. This corresponds to 38% of the contour length of the protein. The radius of gyration was determined to be 14.9 Å under the same conditions, which is close to the experimental radius of gyration of 13.3–13.8 Å determined by SAXS (beamline BM29 at ESRF, Grenoble) [36]. The radius of gyration determined by simulations was found to slightly depend on pH and for the conditions used for the adsorption studies it varies between 14.6 Å (pH 9, ionic strength 100 mM) and 17.6 Å (pH 4, ionic strength 10 mM) according to simulations. The increase with lower pH is due to the increase in net charge of the protein. In a previous adsorption study of histatin 5, the radius of gyration was estimated to be 7 Å assuming a random coil conformation in a theta solvent [37], which is apparently unrealistic.

Net charge and capacitance. The average net charge of histatin 5 found from simulations at different pH values and two different ionic strengths is shown in Table 4. The ionic strengths match available experimental conditions for the charge density of silica surfaces [19].

Electrostatic screening makes the net charge slightly higher at high ionic strength (100 mM) than at low ionic strength (10 mM). The difference in charge is largest at pH 5–6, i.e. close to the pK_a of histidine (~6), where charge regulation of the protein is expected to have the largest effect [18]. The ability of the protein to charge regulate can be described in terms of a protein charge capacitance, $C = \langle Z^2 \rangle - \langle Z \rangle^2$, where Z is the net charge of the protein [38], which in this case is given by simulations. Fig. 2 shows that histatin 5 has a capacitance maximum at pH 5–6 and a minimum at pH 7–8.

In Fig. 3, the average charges of the different amino acid side chains and the N- and C-terminals at pH 6–8 are given. The charges are relatively evenly distributed throughout the protein, thus resembling a polyelectrolyte. Fig. 3(a) shows that at pH 6 the charges of the histidines are important for the overall protein charge, which is not the case at pH 7 and 8, see Fig. 3(b) and (c).

3.2. Surface adsorption of histatin 5

3.2.1. Ellipsometry

Effect of ionic strength. In Fig. 4 the plateau values of the total adsorbed amounts together with the irreversibly adsorbed amounts are shown for different ionic strengths at pH 7. The plateau values are recorded after 60 min of adsorption and the fraction remaining after 30 min of rinsing with buffer is considered as the irreversibly adsorbed amount. Note that the term irreversible here only concerns this aspect of reversibility.

Between ionic strengths of 10 mM and 200 mM (Debye screening lengths 30.4–6.8 Å) there is no clear effect of ionic strength on the total adsorbed amount. However, the fraction of protein that desorbs from the surface upon rinsing increases with ionic strength. This is reasonable considering the screening of the electrostatic attractive forces between histatin 5 and the surface. Thus,

Table 4
The average net charge of histatin 5 at different pH-values and ionic strengths (I) found from simulations.

| pH | Average net charge of histatin 5 | |
|----|----------------------------------|--------------|
| | $I = 10$ mM | $I = 100$ mM |
| 4 | 11.0 | 12.1 |
| 5 | 8.9 | 10.4 |
| 6 | 6.4 | 7.6 |
| 7 | 5.0 | 5.4 |
| 8 | 3.9 | 4.2 |
| 9 | 2.6 | 3.0 |

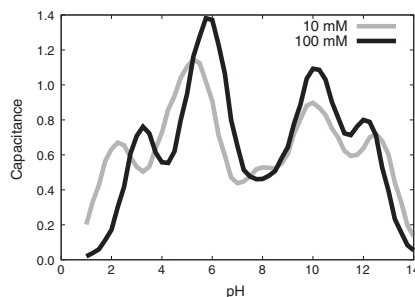


Fig. 2. The dimensionless capacitance, $C = \langle Z^2 \rangle - \langle Z \rangle^2$, of histatin 5 as a function of pH at ionic strengths 10 and 100 mM from simulations.

it is more likely that a histatin molecule will detach from the surface at a higher ionic strength. Since the electrostatic attraction is short-ranged when the ionic strength is high, it is less likely that the chain will re-attach to the surface before being removed due to the exchange of the protein solution with neat buffer.

Interestingly, there is essentially no effect on the total adsorbed amount when increasing the ionic strength from 10 mM to 200 mM. A rough estimate (assuming spherical molecules with a radius of gyration of 13.8 Å [36] covering a surface area corresponding to the area of a circle with the same radius) gives that the adsorbed amount corresponding to a monolayer of histatin 5 is 0.84 mg/m². Thus, there could be an energy barrier to increasing the adsorption beyond ~0.8 mg/m² since it requires more than monolayer coverage. Another possibility is that the decreased repulsion between the adsorbed histatin molecules compensates for the decrease in attraction between histatin 5 and the surface.

At an ionic strength of 500 mM, the calculated Debye screening length is 4.3 Å, meaning that any electrostatic (attractive) force between the protein and the surface is very short-ranged and not expected to be able to drive the adsorption.

Effect of pH. Table 5 shows the plateau values of the adsorbed amounts of histatin 5 at ionic strengths 10 and 150 mM for pH-values ranging from 4 to 9. The adsorbed amount increases with pH, with the possible exception of pH 6, ionic strength 10 mM, where four out of five measurements showed an adsorbed amount lower than at pH 5, ionic strength 10 mM. However, this particular system showed large fluctuations in the measured adsorbed amount leading to a high uncertainty in the reported value.

The effect of ionic strength on the adsorption depends on pH. For most pH-values, the adsorbed amount decreases with increasing ionic strength. However, at pH 5 and 7 the decrease is minor and at pH 6 there appears to be an increase. Fig. 5 shows a comparison of the dependence of the adsorbed amount on ionic strength at pH 7 and 8. Contrary to what was observed at pH 7, the adsorbed amount decreases considerably when the ionic strength increases at pH 8. Thus, at pH 8, the electrostatic attraction between the surface and the protein is strong enough for the electrostatic screening to make a difference.

3.2.2. Monte Carlo simulations

Effect of ionic strength. Fig. 6 shows the effect of changing the ionic strength from 10 mM to 100 mM on the free energy of adsorption at pH 7. Here, the screening of the electrostatic attraction between the protein and the surface that takes place at higher salt concentrations is not compensated for by the increased surface charge at higher ionic strength, i.e. the free energy minimum is

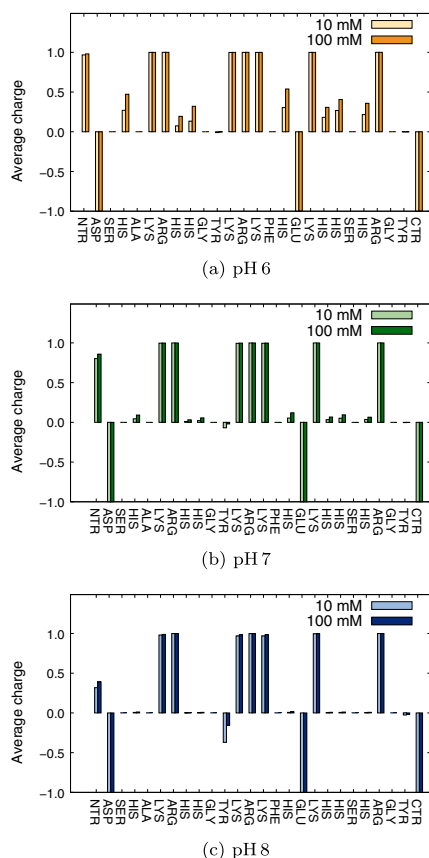


Fig. 3. Average charge for each amino acid in histatin 5 from simulations at 10 mM and 100 mM ionic strength.

lower for 10 mM than for 100 mM. At 10 mM, the free energy minimum is $-18 k_B T$ and at 100 mM it is $-15 k_B T$. However, this does not necessarily mean that the adsorbed amount should be lower at 100 mM than at 10 mM, since the repulsion between adsorbed proteins, that is ignored here, might have an impact. This repulsion decreases at high ionic strength and may explain the weak dependence on ionic strength in the experimentally observed adsorbed amounts.

The experimental results showed that more proteins are desorbed at high ionic strength than at low ionic strength. The fraction of protein that desorbs can be viewed as a measure of the strength of interaction with the surface, and since the coverage at pH 7 is not above monolayer coverage (0.84 mg/m^2) the proteins are all likely to interact with the surface in a similar manner. Thus, both simulations and experiments show that the attractive interaction strength is reduced at higher ionic strength.

Effect of pH. Fig. 7(a) shows the free energies of adsorption at pH 6–8 and an ionic strength of 100 mM. Here, two different processes

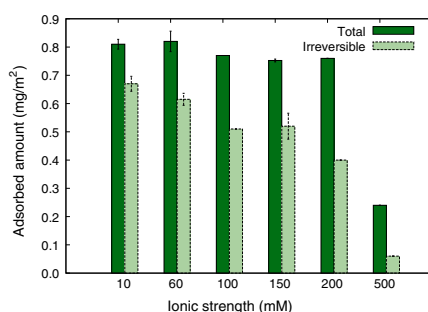


Fig. 4. Total adsorbed amount of histatin 5 recorded after 60 min and the irreversibly adsorbed amount (the amount that did not desorb after 30 min of rinsing with buffer). The buffer was 10 mM tris at pH 7, supplemented with the amount of NaCl needed to reach the desired ionic strength. The error bars show the standard deviations for the systems on which more than one measurement was made.

Table 5

The plateau adsorbed amount at different pH-values and two different ionic strengths (I). For the measurements that have been reproduced, the standard deviation is included.

| pH | Adsorbed amount (mg/m^2) | |
|----|-------------------------------------|----------------------|
| | $I = 10 \text{ mM}$ | $I = 150 \text{ mM}$ |
| 4 | 0.08 | 0.00 |
| 5 | 0.48 | 0.44 |
| 6 | 0.40 ± 0.13 | 0.58 ± 0.042 |
| 7 | 0.81 ± 0.017 | 0.75 ± 0.005 |
| 8 | 1.04 | 0.81 |
| 9 | 1.23 | 0.94 |

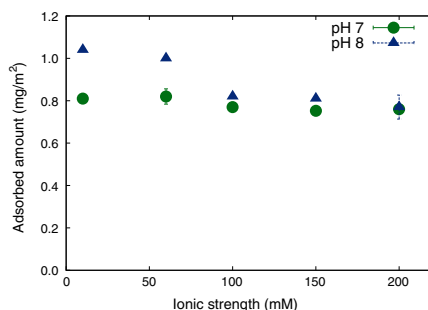


Fig. 5. The adsorbed amount recorded after 60 min as a function of ionic strength (10 mM tris + NaCl) for pH 7 and 8. The error bars show the standard deviations for the cases where more than one measurement was made (for the measurements at pH 7, ionic strength 10 mM and 150 mM, the error bars are covered by the symbols).

with opposing effects on the adsorption free energy are important. Firstly, there is the decrease of the positive protein charge with increasing pH, which decreases the attraction between the protein and the surface. Secondly, the negative surface charge increases with pH, which increases the attraction between the protein and the surface. Since the adsorption free energy minimum decreases

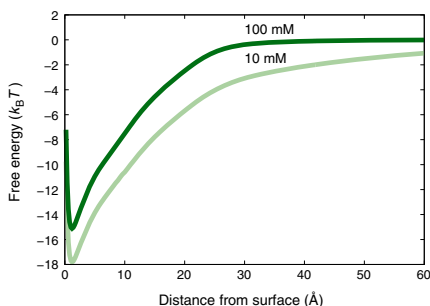


Fig. 6. Free energies of adsorption for histatin 5 at pH 7, ionic strength 10 mM and 100 mM, as a function of the distance between the surface and the protein centre-of-mass.

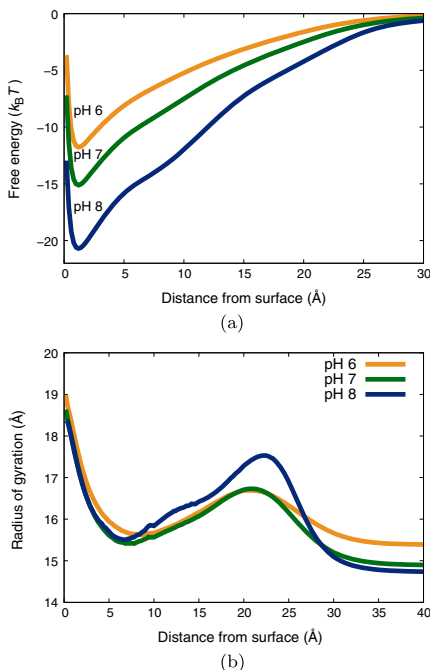


Fig. 7. (a) Free energies of adsorption, and (b) radius of gyration as a function of the mass centre distance from the surface for histatin 5 at pH 6–8, ionic strength 100 mM. Notice the different scales on the x-axis.

with pH, the change in surface charge is more important for the adsorption than the change in protein charge under the investigated conditions. This also agrees with the experimental results that showed an increase in adsorbed amount with increasing pH, reflecting the importance of the increasing surface charge. How-

ever, it should be noted that the decreased repulsion between adsorbed proteins at higher pH could also be of importance in a system with many molecules.

Regarding the dependence of the free energy on ionic strength, all simulated pH-values from 6 to 9 gave similar results compared to the ones showed for pH 7 in Fig. 6 (results not shown). This means that the differences in behaviour between different pH-values that was observed experimentally are not captured by the model.

Fig. 7(b) shows the radius of gyration (R_g) as a function of the protein mass centre distance from the surface for pH 6, 7 and 8 at an ionic strength of 100 mM. At a distance of approximately 20 Å, the histatin molecule is affected by the potential from the surface and stretches towards it, giving rise to an increase in R_g . This effect is most pronounced at pH 8, where the surface charge is higher. Closer to the surface, R_g decreases at first but as the protein comes even closer it is forced to stretch.

Fig. 8 displays the effective free energy per amino acid residue as a function of the distance from the surface and representative snapshots. As can be seen, no part of histatin 5 is repelled by the negatively charged surface, even though there are three negatively charged residues. This is due to the Lennard-Jones potential between the beads and the surface and to the fact that the negatively charged residues are evenly distributed along the molecule, see Fig. 3. It can be seen that beads 6–7 and 12–14 are more tightly bound to the surface than the other residues at pH 7 and 8. These residues are all positively charged lysines and arginines. The protein ends are more loosely bound since they contain negative residues – the C-terminal and the aspartic acid at the N-terminal.

Effect of charge regulation. Fig. 9(a) and (b) show the variation in net charge as the protein approaches the surface at 100 and 10 mM ionic strength. The change is approximately the same for both ionic strengths. It should be noted that even though histatin 5 has a capacitance maximum at pH 6 it only changes its charge by +0.5 when it approaches the surface while at pH 7 and 8, where there is a minimum in the capacitance, the change is larger. It turns out that the surface charge at pH 6 is too low to induce charge regulation of the protein in this system. Despite the fact that the capacitance is at a minimum, charge regulation is more important at pH 7 and 8 since the surface charge is substantially higher.

Fig. 9(c) shows free energies at 100 mM ionic strength compared to a system where titration of the amino acid residues is turned off and the residues instead have average charges found from bulk simulations. Charge regulation of the protein here seems unimportant for the adsorption even though the net charge is affected.

Fig. 9(d) shows the free energies at an ionic strength of 10 mM. Here, charge regulation of the protein affects the adsorption free energy at pH 8. Thus, charge regulation may be of importance even at the capacitance minimum of histatin 5 if the surface charge is high enough and the ionic strength is low.

However, in a biologically relevant system, charge regulation of histatin 5 at pH 6 may still be important. It was shown in the study by Kurut et al. [18] that charge regulation of histatin 5 may contribute to the adsorption at pH 6, ionic strength 80–150 mM, when the charge of the surface is $-5.3 \mu\text{C}/\text{cm}^2$ ($-300 \text{ Å}^2/e$) and there is no Lennard-Jones potential between the amino acids and the surface. This surface charge is comparable to that of a microbial membrane.

3.3. Comparison using the Langmuir isotherm

We want to directly compare the surface coverage from experiments and single-protein simulations. This can be done by using the Langmuir adsorption isotherm, which states that

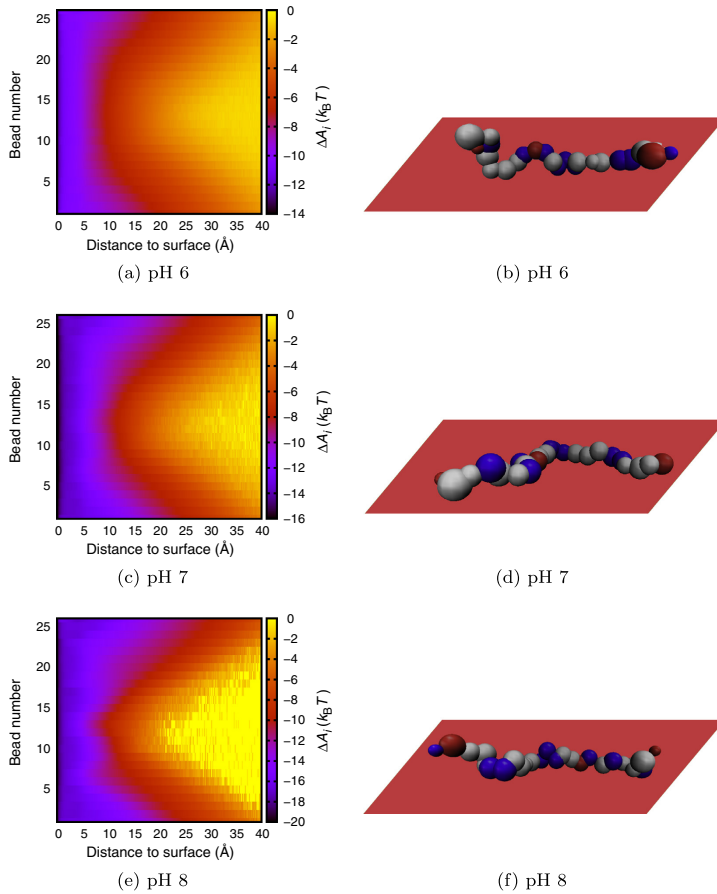


Fig. 8. (a, c, e) Free energies of adsorption per bead (ΔA_i) as a function of distance from the surface at ionic strength 100 mM. Note that the free energy scales are different! (b, d, f) Typical snapshots of adsorbed histatin 5 molecules for the different conditions.

$$\theta = \frac{KC}{1+KC}, \quad (9)$$

where θ is the fractional coverage of the surface, K is the protein-surface binding constant and C is the concentration of the protein in solution. The constant K can be found from

$$K \approx a \int_0^\infty (e^{-w(r_s)/k_B T} - 1) dr_s, \quad (10)$$

where $w(r_s)$ is the potential of mean force (free energy) between a protein centre-of-mass and the surface, and a is the maximum coverage expressed as the surface area per molecule. Since monolayer coverage was approximated to 0.84 mg/m^2 , $a \approx 600 \text{ \AA}^2$.

The basic conditions that must be fulfilled for the Langmuir isotherm model to be applicable are:

1. All adsorption sites are equivalent.
2. Each adsorption site can bind at most one solute molecule (maximum monolayer coverage).
3. The adsorbed molecules do not interact with each other.
4. The adsorption process is thermodynamically reversible.

For the system studied here, all of these conditions are not fulfilled, for example it appears that histatin 5 can adsorb in more than monolayer coverage (experimental coverage $> 0.84 \text{ mg/m}^2$ in some cases). Even though all conditions are generally not fulfilled in an experimental system, the model can still serve as a tool for comparing simulations with experiments.

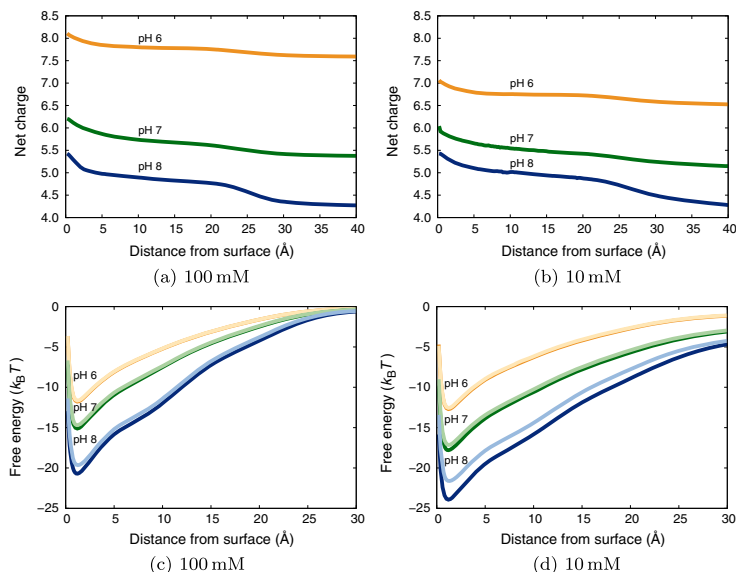


Fig. 9. (a and b) Net charge of histatin 5 as a function of the mass centre distance from the surface at pH 6–8, ionic strengths 100 and 10 mM. (c and d) Free energies of adsorption for histatin 5 at pH 6–8, ionic strengths 100 and 10 mM, modelled with (dark lines) and without (bright lines) protein charge regulation. Notice the different scales on the x-axis.

It has been shown previously for the intrinsically disordered protein β -casein that in order to observe adsorption in simulations under the same conditions as observed experimentally, a short-ranged non-electrostatic potential must be included [39]. The same observation was made here for histatin 5 at pH 6 and lower, even though the protein and the surface are oppositely charged in contrast to the case of β -casein. In the study of β -casein a Lennard-Jones potential was included in the simulations and ϵ was chosen as the smallest possible value that gave rise to adsorption under the studied conditions. Here, we take the comparison with experiments one step further by choosing the value of ϵ from the comparison using the Langmuir adsorption isotherm.

The surface coverage given by experiments and simulations with different values of ϵ are shown in Table 6. At pH 4 and 5, experimentally determined surface charges were not available since they are too low. The surface charge at pH 4 was set to 0 and the charge density at pH 5 was set to 1/5 of the charge density at pH 6 with the same ionic strength.

The lowest possible value of ϵ that still gives adsorption at pH 4, ionic strength 10 mM, is $2.0 k_B T$. The value that seems most reasonable from a comparison with experiments is $2.9 k_B T$, since it gives values closest to experiments for pH 5–7. However, it overestimates the adsorption at pH 4. In three cases (pH 8 and 9), the experimentally found adsorbed amount was above monolayer coverage, which cannot be reproduced by the Langmuir model. Another problem that occurs regardless of the value of ϵ is that the behaviour when the ionic strength is increased cannot, in general, be reproduced. At pH 7, the small difference seen experimentally can be reproduced, but at lower pH the change in adsorbed amount is larger than observed experimentally and for the case of pH 6 of the wrong sign. One reason for this could be that repul-

sion between adsorbed proteins is important. Another possibility is that the experiments measuring the surface charges used for the simulations were made on a slightly different type of surface (silica particles), which may not correspond exactly to the ones used in the adsorption experiments. The estimated charges at pH 4 and 5 may also not be completely accurate. At lower surface coverage, the calculated surface coverage from simulations is very sensitive to small changes in surface charge and ϵ due to the exponential in Eq. (10). For example, an increase in ϵ with $0.1 k_B T$ may increase the calculated adsorbed amount by a factor of three.

Fig. 10 shows a correlation plot using $\epsilon = 2.0 k_B T$ and $\epsilon = 2.9 k_B T$. Since $2.9 k_B T$ gives the closest correspondence with experiments it was chosen as the value of ϵ for the simulations presented above. The main reason for the need of such a large ϵ is that our model of the protein overestimates the entropy of the chain by ignoring most effects of side chains and steric hindrances.

4. Conclusions

We have investigated the adsorption of histatin 5 to negatively charged surfaces using ellipsometry and coarse-grained Monte Carlo simulations of a single protein. The experimental surface was hydrophilic silica while the simulated surface was completely flat with a smeared charge corresponding to experimentally measured charge densities [19]. While previous ellipsometry measurements have been made on the effect of concentration and hydrophobicity on the adsorption to this type of surface [37], this is the first such study on the effect of pH and ionic strength. In the present study, the bulk concentration of histatin 5 was 0.05 mg/ml.

Table 6

Fractional surface coverage (θ) from experiments and simulations with different values of ϵ for the Lennard-Jones potential between the amino acid beads and the surface. The data from simulations were calculated using the Langmuir adsorption isotherm and the assumption of a maximum (monolayer) surface coverage of 0.84 mg/m².

| pH, ionic strength | Experimental | $\epsilon = 2.0 k_B T$ | $\epsilon = 2.8 k_B T$ | $\epsilon = 2.9 k_B T$ | $\epsilon = 3.0 k_B T$ |
|--|--------------|------------------------|------------------------|------------------------|------------------------|
| 4, 10 mM | 0.095 | 1.4×10^{-4} | 0.094 | 0.28 | 0.56 |
| 4, 150 ^a /100 ^b mM | 0.00 | 3.9×10^{-5} | 0.082 | 0.20 | 0.45 |
| 5, 10 mM | 0.57 | 4.5×10^{-4} | 0.18 | 0.54 | 0.76 |
| 5, 150 ^a /100 ^b mM | 0.52 | 1.9×10^{-4} | 0.095 | 0.28 | 0.53 |
| 6, 10 mM | 0.48 | 0.0023 | 0.52 | 0.76 | 0.93 |
| 6, 150 ^a /100 ^b mM | 0.69 | 6.0×10^{-4} | 0.27 | 0.53 | 0.72 |
| 7, 10 mM | 0.96 | 0.19 | 0.99 | 1.00 | 1.00 |
| 7, 100 mM | 0.92 | 0.0091 | 0.85 | 0.97 | 0.99 |
| 8, 10 mM | 1.2 | 0.98 | 1.00 | 1.00 | 1.00 |
| 8, 100 mM | 0.98 | 0.55 | 1.00 | 1.00 | 1.00 |
| 9, 10 mM | 1.5 | 1.00 | 1.00 | 1.00 | 1.00 |
| 9, 150 ^a /100 ^b mM | 1.1 | 0.98 | 1.00 | 1.00 | 1.00 |

^a Experiments.

^b Simulations.

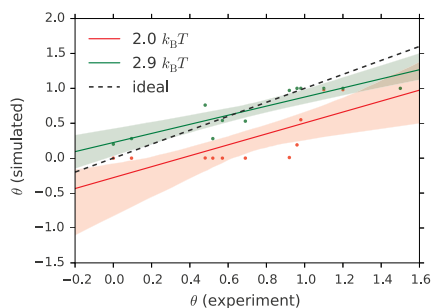


Fig. 10. The correlation between experimental and simulated data for the fractional surface coverage (θ). The coloured areas show the 95% confidence interval. (For interpretation of the references to colour in this figure legend, the reader is referred to the web version of this article.)

We have shown that the adsorbed amount increases with pH. In a previous simulation study of histatin 5, where the surface charge was kept constant, the adsorption was instead observed to be stronger at pH 6 than at pH 7 and 8 [18]. This difference highlights the importance of the change in surface charge depending on pH and ionic strength.

When increasing the ionic strength, our experiments show that the effect on the adsorbed amount depends on the pH of the solution. This cannot be explained by our single-protein simulations. Introducing several protein molecules is the next step to develop and evaluate our coarse-grained model.

We find that at pH 7, 0.8 mg/m² of histatin 5 adsorbs at ionic strengths 10–200 mM. This corresponds approximately to a monolayer (~0.84 mg/m²). For the highest bulk concentrations used in the aforementioned earlier ellipsometry study (5–10 µg/ml) the same adsorbed amount was observed [37]. The concentration range of 5 µg/ml to 0.05 mg/ml overlaps with the concentrations of histatin 5 found in saliva [40,41].

Our hypothesis at the beginning of the study was that electrostatic interactions govern the adsorption of histatin 5. However, by using the Langmuir adsorption isotherm we find that a non-electrostatic Lennard-Jones attraction with $\epsilon = 2.9 k_B T$ between each amino acid and the surface is needed in the simulations in order to observe similar adsorption as in the experiments. The main reason for the need of such a high short-ranged attraction

is to compensate for the overestimated entropy of the chain in the Monte Carlo simulations. The rest of the Lennard-Jones potential represents van der Waals interactions, hydrogen bonding and possibly charge regulation of the surface. Hydrophobic interactions are expected to be unimportant [37]. Work is ongoing to determine the influence of charge regulation of the surface.

Despite the histidine richness of histatin 5, charge regulation of the protein did not affect the adsorption under most conditions studied using simulations. The increase in surface charge with pH led to the counterintuitive result that charge regulation was more important at pH 8 than at pH 6 even though the protein has its highest capacity to charge regulate at pH 6.

Acknowledgements

We acknowledge financial support from: Organizing Molecular Matter (OMM); Vinnova, the Vinnmer programme; The Royal Physiographic Society in Lund; Per-Eric and Ulla Schyberg's Foundation; and the Crafoord Foundation. The simulations were performed on resources provided by the Swedish National Infrastructure for Computing (SNIC) at the center for scientific and technical computing at Lund University (LUNARC).

Appendix A. Supplementary material

Supplementary data associated with this article can be found, in the online version, at <http://dx.doi.org/10.1016/j.jcis.2016.01.025>.

References

- [1] F.G. Oppenheim, T. Xu, F.M. McMillan, S.M. Levitz, R.D. Diamond, G.D. Offner, R.F. Troxler, Histatins, a novel family of histidine-rich proteins in human parotid secretion. Isolation, characterization, primary structure, and fungistatic effects on *Candida albicans*, *J. Biol. Chem.* 263 (1988) 7472–7477.
- [2] A. Dunker, J. Lawson, C.J. Brown, R.M. Williams, P. Romero, J.S. Oh, C.J. Oldfield, A.M. Campen, C.M. Ratliff, K.W. Higgs, J. Ausio, M.S. Nissen, R. Reeves, C. Kang, C.R. Kissinger, R.W. Bailey, M.D. Griswold, W. Chiu, E.C. Garner, Z. Obradovic, Intrinsically disordered protein, *J. Mol. Graph. Modell.* 19 (2001) 26–59.
- [3] P.A. Raj, M. Edgerton, M.J. Levine, Salivary histatin 5: dependence of sequence, chain length, and helical conformation for candidacidal activity, *J. Biol. Chem.* 265 (1990) 3898–3905.
- [4] P.A. Raj, E. Marcus, D.K. Sukumaran, Structure of human salivary histatin 5 in aqueous and nonaqueous solutions, *Biopolymers* 45 (1998) 51–67.
- [5] J.J. Pollock, L. Denepitiya, B.J. MacKay, V.J. Iacono, Fungistatic and fungicidal activity of human parotid salivary histidine-rich polypeptides on *Candida albicans*, *Infect. Immun.* 44 (1984) 702–707.
- [6] B.J. MacKay, L. Denepitiya, V.J. Iacono, S.B. Krost, J.J. Pollock, Growth-inhibitory and bactericidal effects of human parotid salivary histidine-rich polypeptides on *Streptococcus mutans*, *Infect. Immun.* 44 (1984) 695–701.
- [7] S. Puri, M. Edgerton, How does it kill? – Understanding the candidacidal mechanism of salivary histatin 5, *Eukaryot. Cell* 13 (2014) 958–964.

- [8] A.L. den Hertog, H.W. Wong Fong Sang, R. Kraayenhof, J.G.M. Bolscher, W. Van't Hof, E.C.I. Veerman, A.V. Nieuw Amerongen, Interactions of histatin 5 and histatin 5-derived peptides with liposome membranes: surface effects, translocation and permeabilization, *Biochem. J.* 379 (2004) 665–672.
- [9] T. Xu, S.M. Levitz, R.D. Diamond, F.G. Oppenheim, Anticandidal activity of major human salivary histatins, *Infect. Immun.* 59 (1991) 2549–2554.
- [10] M. Edgerton, S.E. Koshlukova, T.E. Lo, B.G. Chrzan, R.M. Straubinger, P.A. Raj, Candidacidal activity of salivary histatins. Identification of a histatin 5-binding protein on *Candida albicans*, *J. Biol. Chem.* 273 (1998) 20438–20447.
- [11] E.J. Helmerhorst, P. Breeuwer, W. van't Hof, E. Walgreen-Weterings, L.C.J.M. Oomen, E.C.I. Veerman, A.V.N. Amerongen, T. Abée, The cellular target of histatin 5 on *Candida albicans* is the energized mitochondrion, *J. Biol. Chem.* 274 (1999) 7286–7291.
- [12] E.J. Helmerhorst, W. van't Hof, P. Breeuwer, E.C.I. Veerman, T. Abée, R.F. Troxler, A.V.N. Amerongen, F.G. Oppenheim, Characterization of histatin 5 with respect to amphipathicity, hydrophobicity, and effects on cell and mitochondrial membrane integrity excludes a candidacidal mechanism of pore formation, *J. Biol. Chem.* 276 (2001) 5643–5649.
- [13] S. Tati, R. Li, S. Puri, R. Kumar, P. Davidow, M. Edgerton, Histatin 5-spermidine conjugates have enhanced fungicidal activity and efficacy as a topical therapeutic for oral candidiasis, *Antimicrob. Agents Chemother.* 58 (2014) 756–766.
- [14] W. Siqueira, H. Margolis, E. Helmerhorst, F. Mendes, F. Oppenheim, Evidence of intact histatins in the in vivo acquired enamel pellicle, *J. Dent. Res.* 89 (2010) 626–630.
- [15] M. Edgar, C. Dawes, D. O'Mullane (Eds.), *Saliva and Oral Health*, third ed., British Dental Association, London, 2004.
- [16] W. Kreusser, A. Heidland, H. Hennemann, M.E. Wigand, H. Knauf, Mono- and divalent electrolyte patterns, pCO₂ and pH in relation to flow rate in normal human parotid saliva, *Eur. J. Clin. Invest.* 2 (1972) 398–406.
- [17] L. Kacprzyk, V. Rydengård, M. Mörgelin, M. Davoudi, M. Pasupuleti, M. Malmsten, A. Schmidtchen, Antimicrobial activity of histidine-rich peptides is dependent on acidic conditions, *Biochim. Biophys. Acta, Biomembr.* 1768 (2007) 2667–2680.
- [18] A. Kurut, J. Henriques, J. Forsman, M. Skepö, M. Lund, Role of histidine for charge regulation of unstructured peptides at interfaces and in bulk, *Proteins: Struct., Funct., Bioinf.* 82 (2014) 657–667.
- [19] Y. Samoshina, T. Nylander, V. Shubin, R. Bauer, K. Eskilsson, Equilibrium aspects of polycation adsorption on silica surface: how the adsorbed layer responds to changes in bulk solution, *Langmuir* 21 (2005) 5872–5881. PMID: 15952836.
- [20] M. Landgren, B. Jönsson, Determination of the optical properties of silicon/silica surfaces by means of ellipsometry, using different ambient media, *J. Phys. Chem.* 97 (1993) 1656–1660.
- [21] W. Kern, D.A. Puotinen, Cleaning solutions based on hydrogen peroxide for use in silicon semiconductor technology, *RCA Rev.* 31 (1970) 187–206.
- [22] H. Edelhoch, Spectroscopic determination of tryptophan and tyrosine in proteins, *Biochemistry* 6 (1967) 1948–1954.
- [23] S.C. Gill, P.H. von Hippel, Calculation of protein extinction coefficients from amino acid sequence data, *Anal. Biochem.* 182 (1989) 319–326.
- [24] J. Vörös, The density and refractive index of adsorbing protein layers, *Biophys. J.* 87 (2004) 553–561.
- [25] P.A. Cuyper, J.W. Corssel, M.P. Janssen, J.M.M. Kop, W.T. Hermens, H.C. Hemker, The adsorption of prothrombin to phosphatidylserine multilayers quantitated by ellipsometry, *J. Biol. Chem.* 258 (1983) 2426–2431.
- [26] M. Malmsten, *Biopolymers at Interfaces*, second ed., Marcel Dekker, New York, U.S.A., 2003. pp. 539–582.
- [27] M.-L. Ainalan, R.A. Campbell, T. Nylander, Interactions between DNA and poly (amido amine) dendrimers on silica surfaces, *Langmuir* 26 (2010) 8625–8635.
- [28] E.J. Cohn, J.T. Edsall, *Proteins, Amino Acids and Peptides as Ions and Dipolar Ions*, first ed., Reinhold Publishing Corporation, New York, U.S.A., 1934. pp. 370–381.
- [29] T.L. McMeekin, M. Wilensky, M.L. Groves, Refractive indices of proteins in relation to amino acid composition and specific volume, *Biochem. Biophys. Res. Commun.* 7 (1962) 151–156.
- [30] B. Stenqvist, A. Thuresson, A. Kurut, R. Vácha, M. Lund, Faunus – a flexible framework for Monte Carlo simulation, *Mol. Simul.* 39 (2013) 1233–1239.
- [31] C.H. Evers, T. Andersson, M. Lund, M. Skepö, Adsorption of unstructured protein β -casein to hydrophobic and charged surfaces, *Langmuir* 28 (2012) 11843–11849. PMID: 22783871.
- [32] S.R.K. Ainavarapu, J. Bruijic, H.H. Huang, A.P. Wiita, H. Lu, L. Li, K.A. Walther, M. Carrion-Vazquez, H. Li, J.M. Fernandez, Contour length and refolding rate of a small protein controlled by engineered disulfide bonds, *Biophys. J.* 92 (2007) 225–233.
- [33] H. Fischer, I. Polikarpov, A.F. Craievich, Average protein density is a molecular-weight-dependent function, *Protein Sci.* 13 (2004) 2825–2828.
- [34] Y. Nozaki, C. Tanford, Examination of titration behavior, in: *Enzyme Structure, Methods in Enzymology*, vol. 11, Academic Press, 1967, pp. 715–734.
- [35] N. Metropolis, A.W. Rosenbluth, M.N. Rosenbluth, A.H. Teller, E. Teller, Equation of state calculations by fast computing machines, *J. Chem. Phys.* 21 (1953) 1087–1092.
- [36] C. Craggell, D. Durand, B. Cabane, M. Skepö, Coarse-grained Modelling of the Intrinsically Disordered Protein Histatin 5 in Solution, Monte Carlo Simulations in Combination with SAXS, *Proteins*, 2015 (submitted for publication).
- [37] I.E. Svendsen, L. Lindh, T. Arnebrant, Adsorption behaviour and surfactant elution of cationic salivary proteins at solid/liquid interfaces, studied by in situ ellipsometry, *Colloids Surf., B* 53 (2006) 157–166.
- [38] M. Lund, B. Jönsson, Charge regulation in biomolecular solution, *Quart. Rev. Biophys.* 46 (2013) 265–281.
- [39] J. Henriques, M. Skepö, A coarse-grained model for flexible (phospho)proteins: adsorption and bulk properties, *Food Hydrocolloids* 43 (2015) 473–480.
- [40] M. Castagnola, T. Cabras, G. Denotti, M. Fadda, G. Gambarini, A. Lupi, I. Manca, G. Onnis, V. Piras, V. Soro, S. Tambaro, I. Messina, Circadian rhythms of histatin 1, histatin 3, histatin 5, statherin and uric acid in whole human saliva secretion, *Biol. Rhythm Res.* 33 (2002) 213–222.
- [41] M. Campese, X. Sun, J.A. Bosch, F.G. Oppenheim, E.J. Helmerhorst, Concentration and fate of histatins and acidic proline-rich proteins in the oral environment, *Arch. Oral Biol.* 54 (2009) 345–353.

Supplementary material

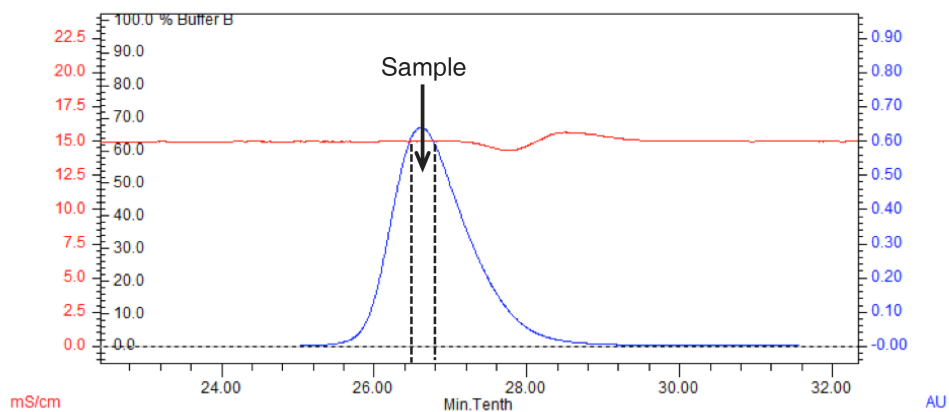


Figure 1: A chromatogram from size exclusion chromatography of histatin 5. The red curve shows the conductivity of the solution and the blue curve shows the absorbance at a wavelength of 280 nm. The sample was collected between the dotted lines as indicated in the chromatogram.

1. Purification using size exclusion chromatography

The chromatogram from one of the size exclusion chromatography runs is shown in Fig. 1. The dotted lines indicate where the sample was collected. The change in conductivity of the solution after the sample was collected indicates that counterions that were present in the freeze-dried histatin 5 were removed during the purification.

2. Reproducibility of ellipsometry measurements

The reproducibility of the ellipsometry measurements was checked by conducting four measurements on the reference system (pH 7, ionic strength 150 mM),

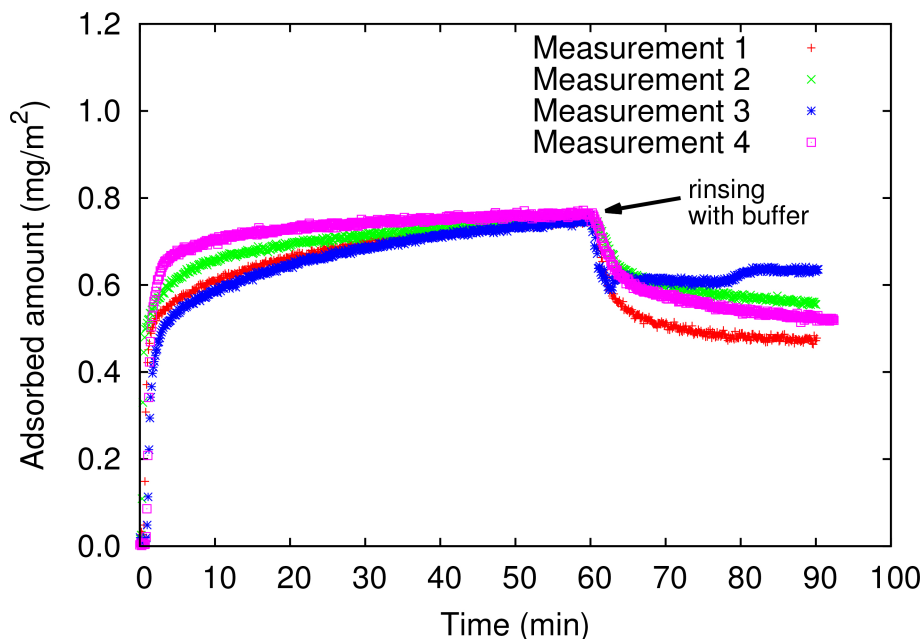


Figure 2: Results from the four ellipsometry measurements on the reference system with pH 7 and ionic strength 150 mM. Note that measurement 3 failed after the start of the rinsing with buffer.

see Fig. 2. The kinetics of the adsorption differ somewhat between the different measurements but the plateau value of the adsorbed amount after 60 minutes of adsorption is reproducible. This value is 0.75 mg/m^2 and the standard deviation is 0.005 mg/m^2 . After 60 minutes of adsorption, buffer solution was pumped through the cuvette during 30 minutes. Measurement 3 failed during the rinsing. The other three measurements gave an average adsorbed amount of 0.52 mg/m^2 after rinsing. The standard deviation was 0.045 mg/m^2 .

3. Effect of changing the refractive index of the adsorbed layer

Figure 3 shows how changing the value of the refractive index of the adsorbed protein layer affects the calculated adsorbed amount. As the refractive index is increased, the calculated adsorbed amount increases slightly. When the refrac-

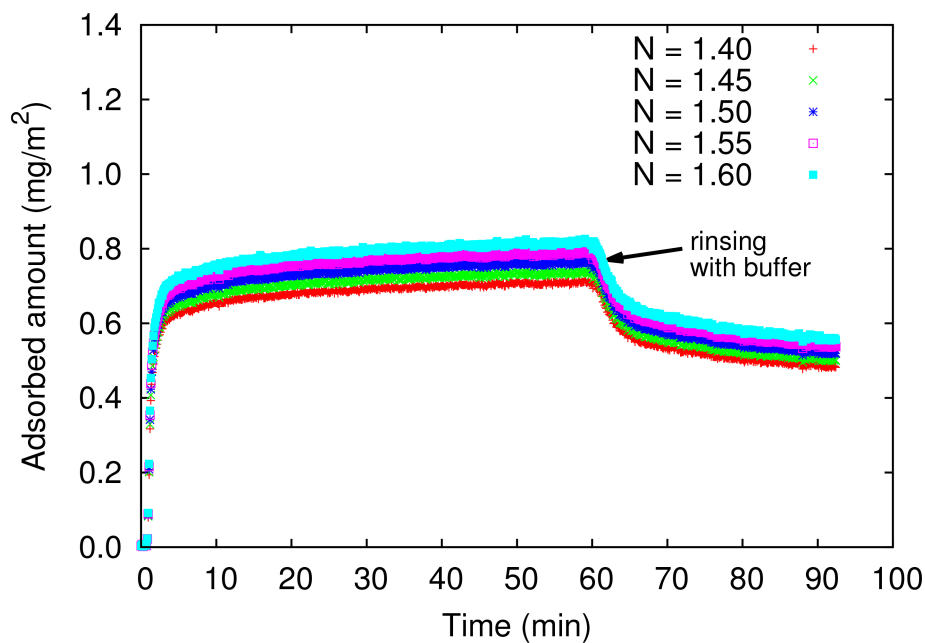


Figure 3: The adsorption isotherm from measurement 4 at pH 7, 150 mM ionic strength using different refractive indices (N) for the adsorbed protein layer.

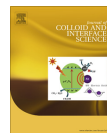
tive index is decreased, the calculated adsorbed amount instead decreases. This is not expected to affect the comparison between different pH values and ionic strengths that is made in our study.

Adsorption of polyelectrolyte-like proteins to silica surfaces and the impact of pH on the response to ionic strength. A Monte Carlo simulation and ellipsometry study

K. Hyltegren, M. Skepö.

Journal of Colloid and Interface Science, 494, 2017, pp. 266–273.

Reprinted with permission from Elsevier.



Regular Article

Adsorption of polyelectrolyte-like proteins to silica surfaces and the impact of pH on the response to ionic strength. A Monte Carlo simulation and ellipsometry study

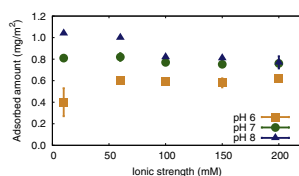


Kristin Hyltegren*, Marie Skepö

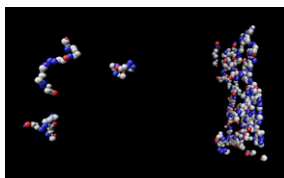
Division of Theoretical Chemistry, Lund University, P.O.B. 124, SE-221 00 Lund, Sweden

GRAPHICAL ABSTRACT

Ellipsometry measurements



Coarse-grained simulations



ARTICLE INFO

Article history:

Received 7 October 2016
 Revised 18 January 2017
 Accepted 19 January 2017
 Available online 24 January 2017

2010 MSC:
 00–01
 99–00

Keywords:

Polyelectrolytes
 Intrinsically disordered proteins
 Histatin 5
 Ellipsometry
 Monte Carlo simulations
 Coarse graining
 Charge regulation
 Adsorption

ABSTRACT

Hypothesis: The adsorbed amount of the polyelectrolyte-like protein histatin 5 on a silica surface depends on the pH and the ionic strength of the solution. Interestingly, an increase in ionic strength affects the adsorbed amount differently depending on the pH of the solution, as shown by ellipsometry measurements (Hyltegren, 2016). We have tested the hypothesis that the same (qualitative) trends can be found also from a coarse-grained model that takes all charge–charge interactions into account within the frameworks of Gouy–Chapman and Debye–Hückel theories.

Experiments: Using the same coarse-grained model as in our previous Monte Carlo study of single protein adsorption (Hyltegren, 2016), simulations of systems with many histatin 5 molecules were performed and then compared with ellipsometry measurements. The strength of the short-ranged attractive interaction between the protein and the surface was varied.

Findings: The coarse-grained model does not qualitatively reproduce the pH-dependence of the experimentally observed trends in adsorbed amount as a function of ionic strength. However, the simulations cast light on the balance between electrostatic attraction between protein and surface and electrostatic repulsion between adsorbed proteins, the deficiencies of the Langmuir isotherm, and the implications of protein charge regulation in concentrated systems.

© 2017 Elsevier Inc. All rights reserved.

1. Introduction

Histatin 5 is a small protein (24 amino acid residues long) present in human saliva [2]. It does not have a well-defined

* Corresponding author.

E-mail address: kristin.hyltegren@teokem.lu.se (K. Hyltegren).

three-dimensional structure under physiological conditions [3,4] and is thus considered to be an intrinsically disordered protein [5].

At neutral pH, histatin 5 has eight positive charges and three negative charges, which are rather evenly distributed over the protein [1]. This, in combination with the lack of a substantial amount of hydrophobic amino acid residues (histatin 5 only contains one phenylalanine and one alanine), makes histatin 5 resemble a polyelectrolyte [6].

Histatin 5 has attracted significant interest, mainly because of its capacity to kill the fungus *Candida albicans* [2,3,7–12] and the possibility of using it as the active substance in new peptide-based antifungal drugs [13,14].

Interestingly, histatin 5 is still effective against *Candida albicans* when adsorbed to hard surfaces present in the mouth [15]. It has been suggested that developing antimicrobial peptides that selectively stick to hydroxyapatite (the main material of the tooth enamel) could be a way to increase their therapeutic activity by reducing the proteolytic degradation that is otherwise a problem [16]. The rationale behind this idea is the observation that histatin 1 is able to resist proteolytic degradation by binding to hydroxyapatite [17], and the same is expected for histatin 5.

The present study is focused on investigating the pH- and ionic strength-dependence of the adsorption of histatin 5. Hopefully, a fundamental understanding of the adsorption of histatin 5 will contribute both to the understanding of polyelectrolyte adsorption in general and to the development of new antifungal peptides.

Earlier studies of adsorption of polyelectrolytes show no consensus regarding how the adsorption changes upon the addition of salt [18–26]. One reason could be that in many systems that have been studied, the charge density of the polyelectrolyte and/or the surface is too low for interactions between charged groups of the polyelectrolyte and the surface to be the dominant factor behind adsorption [27].

Our previous combined ellipsometry and Monte Carlo simulation study indicates that this is the case for the adsorption of histatin 5 to hydrophilic silica surfaces [1]. Therefore, a short-ranged potential was introduced between the surface and the amino acids in the simulations. It represents interactions such as van der Waals forces, hydrophobic interactions and hydrogen bonding, and corrects for possible overestimation of the entropy of the free histatin 5 chain.

We have observed experimentally (using ellipsometry) that the adsorbed amount of histatin 5 is generally dependent on ionic strength – but the trend is different depending on pH [1]. Our hypothesis was that this could be explained by the differences in the charges of the protein and the surface depending on pH (see Fig. 1 for an illustration). The argument was as follows:

When pH is lowered, the positive charge of the protein increases while the magnitude of the negative surface charge decreases. This would lead to an increase in the electrostatic repulsion between adsorbed protein molecules and probably to a decrease in electrostatic attraction between the protein molecules and the surface. When salt is added to the system, the primary effect would be the screening of the repulsion between the adsorbed proteins, inducing a higher adsorbed amount. At high pH, the protein is only weakly positively charged while the surface

has a high negative charge. The addition of salt will then mainly screen the attraction between the proteins and the surface, and thus, the adsorbed amount will decrease.

In previous coarse-grained Monte Carlo simulation studies of the adsorption of histatin 5, only a single protein molecule was included [1,28]. In this infinitely diluted system, adsorption is always disfavoured when the ionic strength is increased. In the present study, we tested the hypothesis that by including several histatin 5 molecules (taking multi-protein effects into account) Monte Carlo simulations using the same coarse-grained model would give the trends observed experimentally.

2. Materials and methods

2.1. Simulations

Coarse-grained Monte Carlo simulations were performed using Faunus, a C++ framework for Metropolis Monte Carlo simulations [29].

2.1.1. Model

In this coarse-grained model, each amino acid and the N- and C-terminals of the protein are represented as spheres (beads). Table 1 shows all the terms contributing to the system energy Hamiltonian, and the parameters of these terms are given and explained in Table 2. All interactions were assumed to be pairwise additive. The model has been described in detail elsewhere [1].

The protein–protein interactions were limited to those of the minimum image convention.

2.1.2. Method

The protein molecules were simulated using the Metropolis Monte Carlo scheme [31] in the canonical (NVT) ensemble. The simulation box had periodic boundaries in the *xy*-directions and hard boundaries in the *z*-direction (normal to the surface). The side lengths were 150 Å in the *xy*-directions and 300 Å in the *z*-direction. A length of 300 Å corresponds to three times the contour length of histatin 5 and twenty times the radius of gyration [6]. An increase in the *xy* side lengths does not change the simulation results when the total concentration of histatin 5 in the box is kept constant.

Most simulations were performed with 20 protein molecules in the box ($N_{\text{His}} = 20$). When needed, more molecules were included. The constant number of histatin 5 molecules meant that the bulk concentration at equilibrium varied depending on the number of adsorbed molecules. This is not expected to affect the qualitative comparison with experimental results. The only effect will be that the observed changes in adsorbed amounts with increased ionic strength will be less pronounced than in a system with constant concentration.

When choosing a constant N_{His} it is important that the number is high enough to obtain a bulk concentration, while still low enough not to give rise to unrealistic adsorption due to repulsion between the molecules in the bulk. The latter could lead to significant adsorption also to the surface constituting the uncharged boundary of the box in the *z*-direction. $N_{\text{His}} = 20$ was found to be

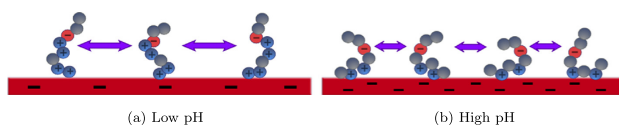


Fig. 1. A schematic illustration of how the protein net charge and the surface charge density depend on pH. At high pH, the adsorbed amount is higher than at low pH.

Table 1

The terms of the system energy Hamiltonian.

| Type of energy | Expression (equation number) |
|--|--|
| Inter-bead interactions | |
| Debye–Hückel electrostatics (screened Coulomb) | $\sum_{i,j=1}^{n-1} \sum_{k=i+1}^n \frac{q_i q_j}{4\pi\epsilon_0\epsilon_r r_{ij}} e^{-k r_{ij}} \quad (1)$ |
| Harmonic bonds | $\sum_{i,j=1}^{n_b} k_b (R_{ij} - R_{eq})^2 \quad (2)$ |
| Lennard-Jones (non-bonded beads) | $\sum_{i,j=1}^{n-2} \sum_{k=j+2}^n 4\epsilon_{ab} \left[\left(\frac{\sigma_{ij}}{r_{ij}}\right)^{12} - \left(\frac{\sigma_{ij}}{r_{ij}}\right)^6 \right] \quad (3)$ |
| Titration | |
| Intrinsic titration energy | $\sum_{i=1}^{n_b} k_b T (\text{pH} - \text{pK}_{a,i}) \ln 10, \quad \text{for } i \text{ protonated} \quad (4)$ |
| Protein–surface interactions | |
| Gouy–Chapman electrostatics | $\sum_{i=1}^n 12z_i k_b T \ln \left(\frac{1 + f_{\text{Gouy}}^{-1} \rho}{1 - f_{\text{Gouy}}^{-1} \rho} \right), \quad \text{where} \quad (5)$ |
| | $f_0 = \tanh \left[\frac{1}{2} \sinh^{-1} \left(\frac{\rho}{\sqrt{8k_b T \epsilon_0 \epsilon_r n_b}} \right) \right]$ |
| Short-ranged potential | $\sum_{i,j=1}^n e^{-\left[\left(\frac{a_i/2}{r_{ij} + a_i/2}\right)^{12} - 2 \left(\frac{a_i/2}{r_{ij} + a_i/2}\right)^6 \right]} \quad (6)$ |

Table 2

The parameters of the expressions in Table 1. All distances are measured from the centres of the beads.

| Parameter = value | Description |
|---|---|
| $n = 26$ | Number of beads |
| q_i | Charge of bead i |
| ϵ_0 | Permittivity of free space |
| $\epsilon_r = 78.54$ | Relative permittivity of water |
| r_{ij} | Distance between beads i and j |
| $\kappa^{-1} = \sqrt{\frac{\epsilon_0 \epsilon_r k_b T}{2N_A e^2}}$ | Debye screening length |
| k_b | Boltzmann's constant |
| $T = 298.15 \text{ K}$ | Temperature |
| N_A | Avogadro's constant |
| e | Elementary charge |
| $l = 10 \text{ or } 100 \text{ mM}$ | Ionic strength |
| $n_b = n - 1$ | Number of bonds |
| $k_b = 0.76 k_b T / \text{\AA}^2$ [30] | Harmonic bond spring constant |
| R_i | Bond length of bond i |
| $R_{eq} = 4.0 \text{ \AA}$ | Equilibrium bond length |
| $\epsilon_{ab} = 0.05 k_b T$ | Interaction strength between non-bonded beads |
| $\sigma_{ij} = \frac{a_i + a_j}{2}$ | Lennard-Jones diameter |
| a_i | Diameter of bead i |
| n_p | Number of protonated beads |
| $\text{pK}_{a,i}$ | Acid dissociation constant of bead i |
| z_i | Charge number of bead i |
| $r_{s,i}$ | Distance between bead i and the surface |
| ρ | Surface charge density |
| $c_0 = 10 \text{ or } 100 \text{ mM}$ | Concentration of 1:1 salt |
| ϵ | Bead–surface interaction strength |

a good choice for most cases based on the balance between these two criteria.

The following Monte Carlo moves were used:

1. Protein translation.
2. Protein rotation.
3. Single bead translation.
4. Crankshaft (picks two beads randomly and defines the vector connecting them as the rotation axis, then rotates the beads between the picked ones around the axis).
5. Pivot rotations (defines a rotation axis in the same manner as with the crankshaft move, then rotates the beads at one end of the protein around the axis).
6. Reptation move (moves the first or last bead of a protein molecule to a random position within the bond distance and then moves the neighbouring bead to the former position of the bead that was moved first etc. until the whole molecule has been moved).

7. Titration move (changes the charge of a bead to mimic protonation/deprotonation).

The adsorbed amount can be calculated using:

$$\Gamma = \int_0^\infty (\rho(z) - \rho_{\text{bulk}}) dz, \quad (7)$$

where $\rho(z)$ is the local concentration of histatin 5 at a distance z from the surface and ρ_{bulk} is the concentration of histatin 5 in the bulk. However, since the simulation box is not infinitely long, it is not possible to use an integration limit of infinity as above. Hence, an upper limit of approximately 2/3 of the box length was used, in order to avoid any effects of the boundary of the box. Denoting the highest value of z used for the integration as z_{max} , Eq. (7) becomes:

$$\Gamma = \int_0^{z_{\text{max}}} (\rho(z) - \rho_{\text{bulk}}) dz. \quad (8)$$

2.2. Experiments

2.2.1. Method

The adsorption experiments that have been used for qualitative comparison with the simulations were performed using ellipsometry. A silica surface was immersed into a buffer with a specified ionic strength and pH, and the adsorption of histatin 5 was followed for 60 min after which a plateau value of the adsorbed amount was generally well established. The bulk concentration of histatin 5 was 0.05 mg/ml. The experimental details, as well as most of the results, are described in our previous article on the adsorption of histatin 5 [1]. However, in the present study additional measurements were made at pH 6.

2.2.2. The silica surfaces

To the authors' knowledge, the exact surface charge densities of the silica surfaces used for ellipsometry have not been determined. In Table 3 experimental values for silica particles with a diameter of 0.3 μm are given. The charge density of a flat silica surface may be slightly smaller than that of a curved surface. However, Behrens and Grier calculated surface charge densities for flat silica surfaces and for silica particles with a diameter of 1 μm and found that the difference was small even at a salt concentration as low as 10^{-6} M [33]. Thus, the values presented in Table 3 are expected to be valid also for a flat surface. Any difference in the charge density between the used silica surfaces and the silica particles is, in our opinion, more likely due to differences in fabrication and cleaning than to the difference in curvature. It has been shown that cleaning with an alkaline solution gives a higher surface charge density than cleaning with an acidic solution [34]. The surfaces used for ellipsometry were cleaned with an alkaline solution followed by cleaning with an acidic solution as described by Landgren and Jönsson [35], while the silica particles referred to in Table 3 were treated only with an acidic solution [32].

Table 3Approximate surface charge densities of silica particles at different pH-values and ionic strengths (I) adjusted with KCl, taken from Samoshina et al. [32].

| pH | Approximate surface charge density ($\mu\text{C}/\text{cm}^2$) | |
|----|--|----------------------|
| | $I = 10 \text{ mM}$ | $I = 100 \text{ mM}$ |
| 6 | −0.25 | −0.50 |
| 7 | −1.00 | −2.00 |
| 8 | −2.75 | −5.75 |
| 9 | −7.00 | −12.50 |

3. Results and discussion

3.1. Experimental results

In Fig. 2, ellipsometry results for the adsorbed amount of histatin 5 on hydrophilic silica are presented. Here, it is shown that both the pH and the ionic strength affect the adsorption, and that different trends are captured; i.e. for pH 6 the adsorption seems to increase when the ionic strength is increased from 10 to 60 mM, for pH 7 it is approximately constant for ionic strengths between 10 and 200 mM, whereas for pH 8 it decreases with ionic strength.

3.2. Simulation results

Due to the fact that 7 out of 24 amino acids are histidines ($pK_a \approx 6$), histatin 5 has a tendency to charge regulate near physiological conditions. The capacitance curve for a single protein can be found in our previous study [1]. Histatin 5 has capacitance maxims at pH 6 and pH 10, and a minimum at pH 7–8.

The system of interest is rather complex due to the fact that both the surface charge density and the protein net charge are affected by pH and ionic strength. The average protein net charge determined from simulations can be found in Table 4.

In the following, a systematic study will be performed with the aim to capture experimental results and to elucidate the importance of the different electrostatic mechanisms governing the adsorbed amount of histatin 5. Therefore, results of some simplified versions of the system will be studied before progressing to more complex systems.

3.2.1. Constant surface charge and only charge–charge interactions between the surface and the proteins

In the simulations presented in this section, a constant surface charge density was used for all conditions. The reason was to determine the effect of the variation in protein charge with pH without having to account for how pH affects the surface charge. The chosen surface charge density corresponds to silica at pH 7 and 100 mM ionic strength, i.e. approximately $-2.0 \mu\text{C}/\text{cm}^2$ ($-1.2 \times 10^{-3} \text{ e}/\text{\AA}^2$) [32].

The only forces present between the protein molecules and the surface are the electrostatic forces between the charged amino acid residues and the surface, and an excluded-volume effect due to the fact that the protein cannot penetrate the surface.

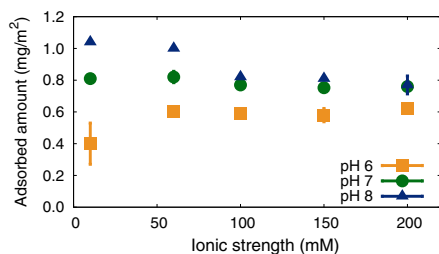


Fig. 2. The plateau value of the adsorbed amount of histatin 5 as a function of ionic strength at different pH-values displays different trends depending on the pH. Ellipsometry results from our earlier study [1] complemented with a few additional measurements. The error bars show the standard deviation for the cases where more than one measurement has been made (for the measurements at pH 7, ionic strengths 10 mM and 150 mM, the error bars are covered by the symbols).

Table 4

The average net charge of histatin 5 in bulk solution at different pH-values and ionic strengths (I) found from simulations [1].

| pH | Average net charge of histatin 5 | |
|----|----------------------------------|----------------------|
| | $I = 10 \text{ mM}$ | $I = 100 \text{ mM}$ |
| 6 | 6.4 | 7.6 |
| 7 | 5.0 | 5.4 |
| 8 | 3.9 | 4.2 |

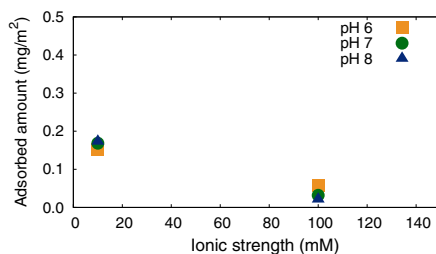


Fig. 3. The adsorbed amount of histatin 5 as a function of ionic strength at different pH-values and a constant surface charge of $-1.2 \times 10^{-3} \text{ e}/\text{\AA}^2$. Results from simulations.

In Fig. 3, the adsorbed amounts found from these simulations (and Eq. (8)) can be viewed. Despite the fact that the protein molecules differ in charge depending on the pH, the adsorbed amount is approximately the same regardless of pH. This could be explained as follows:

The effect of ionic strength is a sum of the effects on (1) the repulsion between adsorbed proteins (decreases with ionic strength leading to more adsorption) and (2) the attraction between the surface and the proteins (decreases with ionic strength leading to less adsorption). Here, the sum of the two effects seems to be almost the same regardless of pH, i.e. pH 6 or pH 8, but the balance between repulsion and attraction is most probably different depending on pH.

3.2.2. Constant surface charge and a short-ranged attraction between the surface and the proteins

In our previous study, a short-ranged attractive potential (Eq. (6) in Table 1) was included in the Hamiltonian in order to achieve quantitative correspondence between the binding constants from single-protein simulations and the results from ellipsometry measurements. The interaction strength of the potential, ϵ , was determined to be $2.9 k_B T$. Hence, the next step is to utilise that potential, see results in Fig. 4.

The inclusion of the short-ranged attraction increases the adsorbed amount. This makes electrostatic protein–protein repulsion more important, leading to an increase in the adsorbed amount with ionic strength since the electrostatic repulsion decreases. Similarly, our simulations show that if the surface charge is increased for the case when there is no short-ranged attraction, the adsorbed amount will increase as the ionic strength is increased from 10 mM to 100 mM (results not shown).

A theoretical study of the adsorption of polyelectrolytes on an oppositely charged surface by van de Steeg et al. gave similar results – when only electrostatic interactions between the polyelectrolytes and the surface were taken into account, the adsorbed amount decreased as a function of ionic strength while the introduction of a sufficiently large short-ranged attractive interaction

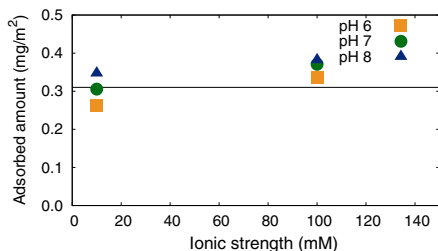


Fig. 4. The adsorbed amount of histatin 5 from simulations as a function of ionic strength at different pH-values and a constant surface charge of $-1.2 \times 10^{-3} \text{ e}/\text{\AA}^2$, including a short-ranged attractive potential with ϵ equal to $2.9 k_B T$. The black line shows the adsorbed amount of the same protein without charges.

lead to an increase with ionic strength [36]. The van de Steeg study was made using numerical calculations based on the self-consistent field theory that was developed by Scheutjens and Fleer for adsorption of polymers [37,38] and extended to polyelectrolytes by Böhmer et al. [39]. One of the differences between their results and ours is that they found that the adsorbed amount always decreases with ionic strength when there is no short-ranged attraction, while we found that for high enough surface charges it is possible to observe an increase. It has been argued that mean-field approaches, such as the one used by van de Steeg et al., tend to erroneously predict monotonous desorption when the ionic strength increases, and that this is due to the lack of ion correlations. A more suitable approach could be correlation-corrected classical polymer density functional theory, which for pure electrosorption of polyelectrolytes in a highly charged system predicts an increase in adsorbed amount when increasing the ionic strength at low salt concentrations, until a maximum is reached after which the adsorbed amount decreases with ionic strength [27].

There is a possibility that the uneven charge distribution over the histatin 5 molecule leads to different adsorption than for an equivalent polyelectrolyte with an evenly distributed charge. Therefore, simulations were performed where the net charge of histatin 5 was evenly divided among the 26 beads. The adsorbed amounts are somewhat lower when the net charge is evenly distributed, especially for low ionic strength, but the qualitative behaviour when increasing ionic strength is the same (results not shown).

The black line in Fig. 4 represents the adsorbed amount given by simulations with uncharged protein molecules. Thus, it can be seen whether the net effect of the protein charge is to increase the attractive interactions with the surface or to increase the repulsive interactions between adsorbed proteins. For example, at pH 6 and ionic strength 10 mM, the charged protein adsorbs in a lower amount than the uncharged protein, i.e. the charges introduced more repulsion than attraction into the system.

3.2.3. Surface charge varying depending on pH and salt content, and short-ranged attractive interactions of different strengths between the surface and the proteins

In this section, the system resembles the real experimental system, with respect to how the surface charge density is affected by pH and ionic strength, according to Table 3. Also, different values of the strength of the short-ranged attractive interaction (ϵ) will be investigated.

Figure 5 shows how the adsorbed amount of histatin 5 is varying with ionic strength at different pH-values, utilising different

values of ϵ . Figure 5(a) and (b) shows that for low values of ϵ (corresponding to low adsorbed amounts), the adsorbed amount decreases with increasing ionic strength. At $\epsilon = 2.0 k_B T$, the trend differs depending on pH, although in conflict with the experimental results given in Fig. 2.

When ϵ is increased further, the increase in adsorbed amount with ionic strength becomes even more pronounced, until all of the histatin 5 molecules present in the simulation box have adsorbed to the surface. This corresponds to an adsorbed amount of $0.45 \text{ mg}/\text{m}^2$. Notice that the surface is not saturated with proteins.

An interpretation of the results is the following: For a low value of ϵ (giving rise to a low adsorbed amount), the repulsion between adsorbed proteins is small and thus it is the screening of the attraction between the proteins and the surface that determines how the adsorbed amount changes with addition of salt i.e. the adsorbed amount decreases when salt is added, see Fig. 5(a) and (b).

As the adsorbed amount increases, the electrostatic repulsion between the adsorbed proteins also increases, and there will be a transition when it becomes important. Thereafter, the adsorbed amount increases upon the addition of salt due to electrostatic screening, see Fig. 5(c) and (d). However, the initial increase may be followed by a decrease with ionic strength at high salt concentrations in case the adsorbed amount for a corresponding uncharged or fully screened system is lower than the maximum adsorbed amount for the charged system.

Even higher values of ϵ can be studied if the number of histatin 5 molecules in the box is increased. Values up to $5.0 k_B T$ have been evaluated and the same qualitative behaviour as in Fig. 5(d) was found (results not shown).

3.2.4. Implicit/explicit counterions

The model used is very simple in several respects, for example both the counterions and the solvent are treated implicitly. The inclusion of the protein molecules' counterions in the model could in principle affect the adsorption in case the distribution of counterions around the adsorbed protein molecules is not properly described by the screened Coulomb potential (Eq. (1) in Table 1). However, the inclusion of explicit counterions in the simulations had no significant effect on the adsorbed amounts (data not shown).

3.3. Comparisons between multi-protein and single-protein simulations

Here, comparisons will be made between adsorbed amounts determined by single- versus multi-protein simulation studies. Furthermore, the effect of protein charge regulation will be considered.

3.3.1. Langmuir isotherm

In our previous single-protein simulations, the value of ϵ was determined by comparing the adsorbed amount obtained from experiments with the adsorbed amounts calculated using the Langmuir isotherm and the potentials of mean force from single-protein simulations [1]. The question is if this is a feasible approach.

The Langmuir adsorption isotherm relates the adsorbed amount of an adsorbate to its binding constant to the surface and its bulk concentration as follows:

$$\theta = \frac{KC}{1 + KC} \quad (9)$$

where θ is the fractional coverage of the surface, K is the adsorbate-surface binding constant and C is the concentration of the adsorbate

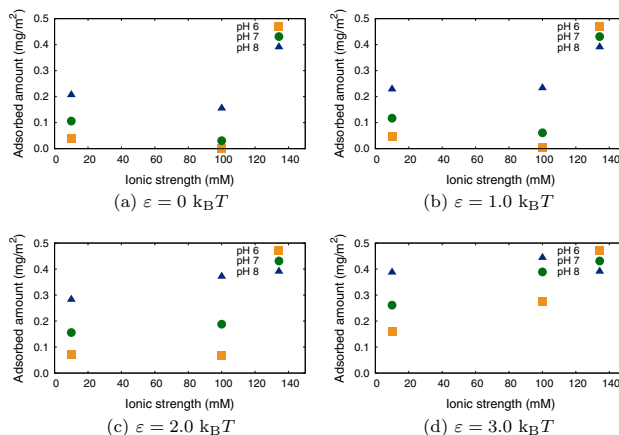


Fig. 5. Adsorbed amount of histatin 5 from simulations as a function of ionic strength at three different pH-values. Whether the adsorbed amount increases or decreases with ionic strength depends on the strength (ϵ) of the short-ranged attractive potential between the amino acid beads and the surface.

in solution. The binding constant for histatin 5 was calculated from single-protein simulations using

$$K \approx a \int_0^\infty (e^{-w(r_s)/k_B T} - 1) dr_s, \quad (10)$$

where $w(r_s)$ is the potential of mean force (free energy) between a protein and the surface, r_s is the distance between the protein centre-of-mass and the surface, and a is the maximum coverage (monolayer) expressed as the surface area per molecule [1].

A comparison between the multi-protein and single-protein simulations was performed as follows: Firstly, the potentials of mean force determined by single-protein simulations with $\epsilon = 2.9 k_B T$ were used to determine K in Eq. (10). Then the resulting K was used in Eq. (9) together with the bulk concentration resulting from the corresponding simulation with $N_{\text{His}} = 20$ (ranging from 0.09 to 9.6 mg/ml). This gave a θ in Eq. (9) equal to one for all simulated conditions (pH 6–8, ionic strengths 10 or 100 mM). Thus, the adsorbed amounts should be equal to a monolayer (approximated to 0.84 mg/ml [1]) if the Langmuir approach can correctly describe the simulated systems.

The maximum adsorbed amount that was found when $N_{\text{His}} = 20$ and $\epsilon = 2.9 k_B T$ was 0.44 mg/ml (pH 8, ionic strength 100 mM). This corresponds to almost full adsorption of the molecules in the box. By increasing N_{His} from 20 to 40 it becomes possible to reach an adsorbed amount of 0.84 mg/ml. However, this change increases the adsorbed amount only from 0.44 mg/ml to 0.57 mg/ml while the bulk concentration increases by more than a factor of 100 (from 0.09 to 11 mg/ml). The disagreement with the result expected from the Langmuir isotherm illustrates that the repulsion between adsorbed protein molecules, which is ignored by the Langmuir isotherm, is of great importance in the multi-protein simulations.

3.3.2. Charge regulation

Previously, it has been shown that charge regulation of histatin 5 is of importance when the system is infinitely diluted, i.e. the charging of the histidines may give important contributions to the free energy of adsorption, in case the surface charge is high

enough [28,1]. For example, charge regulation effects are visible when the surface charge density is $-5.3 \mu\text{C}/\text{cm}^2$ ($-1/300 e/\text{\AA}^2$) at pH 6 (capacitance maximum of histatin 5) and ionic strength 100 mM.

The corresponding simulation for a concentrated system ($N_{\text{His}} = 20$) shows that charge regulation is significantly less pronounced, however still apparent. Figure 6 shows the changes in net charge as functions of the distance of the mass centre of the protein from the surface. The shapes of the curves are similar but for the single-protein case, charge regulation is more long-ranged and the protein gains approximately three more positive elementary charges when approaching the surface, compared to two elementary charges for the multi-protein case. Due to the presence of other positively charged protein molecules in the adsorbed layer, it is less favourable for the protein to increase its charge close to the surface in the concentrated system. Hence, we do not expect the effect of charge regulation of the protein to be as important in a

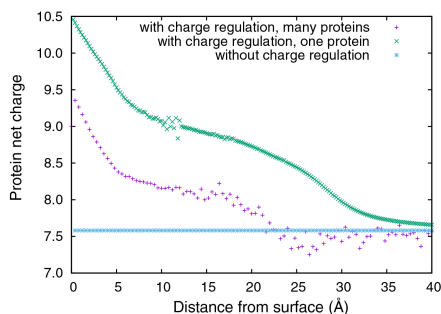


Fig. 6. Net charge of histatin 5 as a function of the distance of its mass centre from the surface at pH 6, ionic strength 100 mM and a surface charge density of $-5.3 \mu\text{C}/\text{cm}^2$ ($-1/300 e/\text{\AA}^2$). Results from simulations.

concentrated/multi-protein system as in a very dilute/single-protein system.

Considering the results in Fig. 6, it seems that single-protein simulations are too simplified to be able to describe charge regulation in real systems where protein adsorption occurs, unless the protein concentration is extremely low. However, if the surface also contains titrating groups, which are not accounted for in this model, that could possibly increase the effect of charge regulation of the protein since the surface might significantly increase its charge when an oppositely charged polyelectrolyte adsorbs, see Samoshina et al. [32] and Xie et al. [40].

4. Conclusions

The adsorbed amount of histatin 5 on a silica surface depends on the pH and the ionic strength of the solution [1]. The objective of this study was to test the hypothesis that the same (qualitative) behaviour could be found with Monte Carlo simulations using a previously developed coarse-grained model for flexible proteins [1,28,41,30]. While previous simulations included only a single protein (infinitely dilute system), the simulations in this study included several proteins (concentrated system) – capturing therefore also the electrostatic repulsion between adsorbed proteins.

By tuning the strength of the short-ranged attractive interaction (Eq. (6) in Table 1) between the protein's amino acid residues and the surface, different trends were observed regarding the ionic strength dependence of the adsorbed amount. This observation is in agreement with previous model results in the literature [36]. However, there was a mismatch between the experimental trends and the simulated trends. In spite of this, we believe that the simulations have cast light on some of the aspects of the adsorption of flexible polyelectrolytes/proteins, e.g. the balance between electrostatic attraction between protein and surface and electrostatic repulsion between adsorbed proteins, the deficiencies of the Langmuir isotherm and protein charge regulation in concentrated systems.

Future studies could involve, for example, an in-depth study of how the conformational entropy of histatin 5 is treated in the model, as well as a study of titrating surfaces.

Acknowledgements

We acknowledge financial support from: Organizing Molecular Matter (OMM) and Swedish Foundation for Laryngectomees. The simulations were performed on resources provided by the Swedish National Infrastructure for Computing (SNIC) at the centre for scientific and technical computing at Lund University (LUNARC).

Carl Dovrinder (Lund, Sweden) is acknowledged for making Fig. 1.

References

- [1] K. Hyltegren, T. Nylander, M. Lund, M. Skepö, Adsorption of the intrinsically disordered saliva protein histatin 5 to silica surfaces. A Monte Carlo simulation and ellipsometry study, *J. Colloid Interface Sci.* 467 (2016) 280–290.
- [2] F.G. Oppenheim, T. Xu, F.M. McMillan, S.M. Levitz, R.D. Diamond, G.D. Offner, R.F. Troxler, Histatins, a novel family of histidine-rich proteins in human parotid secretion. Isolation, characterization, primary structure, and fungistatic effects on *Candida albicans*, *J. Biol. Chem.* 263 (1988) 7472–7477.
- [3] P.A. Raj, M.J. Levine, Salivary histatin 5: dependence of sequence, chain length, and helical conformation for candidacidal activity, *J. Biol. Chem.* 265 (1990) 3898–3905.
- [4] P.A. Raj, E. Marcus, D.K. Sukumaran, Structure of human salivary histatin 5 in aqueous and nonaqueous solutions, *Biopolymers* 45 (1998) 51–67.
- [5] A.K. Dunker, J.D. Lawson, C.J. Brown, R.M. Williams, P. Romero, J.S. Oh, C.J. Oldfield, A.M. Campen, C.M. Ratliff, K.W. Hippis, J. Ausio, M.S. Nissen, R. Reeves, C. Kang, C.R. Kissinger, R.W. Bailey, M.D. Griswold, W. Chiu, E.C. Garner, Z. Obradovic, Intrinsically disordered protein, *J. Mol. Graphics Modell.* 19 (2001) 26–59.
- [6] C. Craggell, D. Durand, B. Cabane, M. Skepö, Coarse-grained modelling of the intrinsically disordered protein Histatin 5 in solution. Monte Carlo simulations in combination with SAXS, *Proteins: Struct. Funct. Bioinf.* 84 (2016) 777–791.
- [7] J.J. Pollock, L. Denepitiya, B.J. MacKay, V.J. Iacono, Fungistatic and fungicidal activity of human parotid salivary histidine-rich polypeptides on *Candida albicans*, *Infect. Immun.* 44 (1984) 702–707.
- [8] S. Puri, M. Edgerton, How does it kill? – understanding the candidacidal mechanism of salivary Histatin 5, *Eukaryot. Cell* 13 (2014) 958–964.
- [9] T. Xu, S.M. Levitz, R.D. Diamond, F.G. Oppenheim, Anticandidal activity of major human salivary histatins, *Infect. Immun.* 59 (1991) 2549–2554.
- [10] M. Edgerton, S.E. Koshlukova, T.E. Lo, B.G. Chrzan, R.M. Straubinger, P.A. Raj, Candidacidal activity of salivary histatins. Identification of a histatin 5-binding protein on *Candida albicans*, *J. Biol. Chem.* 273 (1998) 20438–20447.
- [11] E.J. Helmerhorst, P. Breeuwer, W. van't Hof, E. Walgreen-Weterings, L.C.J.M. Oomen, E.C.I. Veerman, A.V.N. Amerongen, T. Abée, The cellular target of histatin 5 on *Candida albicans* is the energized mitochondrion, *J. Biol. Chem.* 274 (1999) 7286–7291.
- [12] E.J. Helmerhorst, W. van't Hof, P. Breeuwer, E.C.I. Veerman, T. Abée, R.F. Troxler, A.V.N. Amerongen, F.G. Oppenheim, Characterization of histatin 5 with respect to amphiphaticity, hydrophobicity, and effects on cell and mitochondrial membrane integrity excludes a candidacidal mechanism of pore formation, *J. Biol. Chem.* 276 (2001) 5643–5649.
- [13] K. Kavanagh, S. Dowd, Histatins: antimicrobial peptides with therapeutic potential, *J. Pharmacy Pharmacol.* 56 (2004) 285–289.
- [14] S. Tati, R. Li, S. Puri, R. Kumar, P. Davidow, M. Edgerton, Histatin 5-spermidine conjugates have enhanced fungicidal activity and efficacy as a topical therapeutic for oral candidiasis, *Antimicrob. Agents Chemother.* 58 (2014) 756–766.
- [15] D. Vukosavljevic, W. Custodio, A. Del Bel Cury, W. Siqueira, The effect of histatin 5, adsorbed on PMMA and hydroxyapatite, on *Candida albicans* colonization, *Yeast* 29 (2012) 459–466.
- [16] D. Vukosavljevic, J.L. Hutter, E.J. Helmerhorst, Y. Xiao, W. Custodio, F.C. Zaidan, F.G. Oppenheim, W.L. Siqueira, Nanoscale adhesion forces between enamel pellicle proteins and hydroxyapatite, *J. Dent. Res.* 93 (2014) 514–519.
- [17] E.E. McDonald, H.A. Goldberg, N. Tabbara, F.M. Mendes, W.L. Siqueira, Histatin 1 resists proteolytic degradation when adsorbed to hydroxyapatite, *J. Dent. Res.* 90 (2011) 268–272.
- [18] O.J. Rojas, P.M. Claesson, D. Muller, R.D. Neuman, The effect of salt concentration on adsorption of low-charge-density polyelectrolytes and interactions between polyelectrolyte-coated surfaces, *J. Colloid Interface Sci.* 205 (1998) 77–88.
- [19] R. Mészáros, L. Thompson, M. Bos, P. de Groot, Adsorption and electrokinetic properties of polyethylenimine on silica surfaces, *Langmuir* 18 (2002) 6164–6169.
- [20] N. Hansupalak, M.M. Santore, Sharp polyelectrolyte adsorption cutoff induced by a monovalent salt, *Langmuir* 19 (2003) 7423–7426.
- [21] R. Mészáros, I. Varga, T. Gilányi, Adsorption of poly(ethyleneimine) on silica surfaces: effect of pH on the reversibility of adsorption, *Langmuir* 20 (2004) 5026–5029.
- [22] S.-C. Liufu, H.-N. Xiao, Y.-P. Li, Adsorption of cationic polyelectrolyte at the solid/liquid interface and dispersion of nanosized silica in water, *J. Colloid Interface Sci.* 285 (2005) 33–40.
- [23] L.-E. Enarsson, L. Wågberg, Polyelectrolyte adsorption on thin cellulose films studied with reflectometry and quartz crystal microgravimetry with dissipation, *Biomacromolecules* 10 (2009) 134–141.
- [24] T. Saarinen, M. Österberg, J. Laine, Properties of cationic polyelectrolyte layers adsorbed on silica and cellulose surfaces studied by QCM-D—effect of polyelectrolyte charge density and molecular weight, *J. Dispersion Sci. Technol.* 30 (2009) 969–979.
- [25] J. Hierrezuelo, I. Szilagyi, A. Vaccaro, M. Borkovec, Probing nanometer-thick polyelectrolyte layers adsorbed on oppositely charged particles by dynamic light scattering, *Macromolecules* 43 (2010) 9108–9116.
- [26] E. Seyrek, J. Hierrezuelo, A. Sadeghpour, I. Szilagyi, M. Borkovec, Molecular mass dependence of adsorbed amount and hydrodynamic thickness of polyelectrolyte layers, *Phys. Chem. Chem. Phys.* 13 (2011) 12716–12719.
- [27] F. Xie, T. Nylander, L. Piculell, S. Utsei, L. Wågberg, T. Åkesson, J. Forsman, Polyelectrolyte adsorption on solid surfaces: theoretical predictions and experimental measurements, *Langmuir* 29 (2013) 12421–12431.
- [28] A. Kurut, J. Henriques, J. Forsman, M. Skepö, M. Lund, Role of histidine for charge regulation of unstructured peptides at interfaces and in bulk, *Proteins: Struct. Funct. Bioinf.* 82 (2014) 657–667.
- [29] B. Stenqvist, A. Thuresson, A. Kurut, R. Vácha, M. Lund, Faunus – a flexible framework for Monte Carlo simulation, *Mol. Simul.* 39 (2013) 1233–1239.
- [30] C.H. Evers, T. Andersson, M. Lund, M. Skepö, Adsorption of unstructured protein β -casein to hydrophobic and charged surfaces, *Langmuir* 28 (2012) 11843–11849.
- [31] N. Metropolis, A.W. Rosenbluth, M.N. Rosenbluth, A.H. Teller, E. Teller, Equation of state calculations by fast computing machines, *J. Chem. Phys.* 21 (1953) 1087–1092.
- [32] Y. Samoshina, T. Nylander, V. Shubin, R. Bauer, K. Eskilsson, Equilibrium aspects of polycation adsorption on silica surface: how the adsorbed layer responds to changes in bulk solution, *Langmuir* 21 (2005) 5872–5881.
- [33] S.H. Behrens, D.G. Grier, The charge of glass and silica surfaces, *J. Chem. Phys.* 115 (2001) 6716–6721.
- [34] X. Liu, A. Dedinaite, T. Nylander, A.P. Dabkowska, M. Skoda, R. Makuska, P.M. Claesson, Association of anionic surfactant and physisorbed branched brush

- layers probed by neutron and optical reflectometry, *J. Colloid Interface Sci.* 440 (2015) 245–252.
- [35] M. Landgren, B. Jönsson, Determination of the optical properties of silicon/silica surfaces by means of ellipsometry, using different ambient media, *J. Phys. Chem.* 97 (1993) 1656–1660.
- [36] H.G.M. van de Steeg, M.A. Cohen Stuart, A. de Keizer, B.H. Bijsterbosch, Polyelectrolyte adsorption: a subtle balance of forces, *Langmuir* 8 (1992) 2538–2546.
- [37] J.M.H.M. Scheutjens, G.J. Fleer, Statistical theory of the adsorption of interacting chain molecules. 1. Partition function, segment density distribution, and adsorption isotherms, *J. Phys. Chem.* 83 (1979) 1619–1635.
- [38] J.M.H.M. Scheutjens, G.J. Fleer, Statistical theory of the adsorption of interacting chain molecules. 2. Train, loop, and tail size distribution, *J. Phys. Chem.* 84 (1980) 178–190.
- [39] M.R. Böhrer, O.A. Evers, J.M.H.M. Scheutjens, Weak polyelectrolytes between two surfaces: adsorption and stabilization, *Macromolecules* 23 (1990) 2288–2301.
- [40] F. Xie, H. Lu, T. Nylander, L. Wågberg, J. Forsman, Theoretical and experimental investigations of polyelectrolyte adsorption dependence on molecular weight, *Langmuir* 32 (2016) 5721–5730.
- [41] J. Henriques, M. Skepö, A coarse-grained model for flexible (phospho)proteins: adsorption and bulk properties, *Food Hydrocolloids* 43 (2015) 473–480.

PAPER III

Integrating All-Atom and Coarse-Grained Simulations—Toward Understanding of IDPs at Surfaces

K. Hyltegren, M. Polimeni, M. Skepö, M. Lund.

Journal of Chemical Theory and Computation, 16, 2020, pp. 1843–1853.

Reprinted with permission from *Journal of Chemical Theory and Computation*.
Copyright © 2020 American Chemical Society.

Integrating All-Atom and Coarse-Grained Simulations—Toward Understanding of IDPs at Surfaces

Kristin Hyltegren,* Marco Polimeni,* Marie Skepö,* and Mikael Lund*

Cite This: *J. Chem. Theory Comput.* 2020, 16, 1843–1853

Read Online

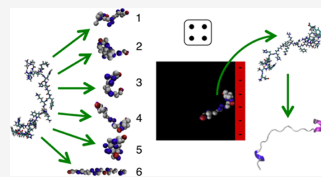
ACCESS |

Metrics & More

Article Recommendations

Supporting Information

ABSTRACT: We present a scheme for transferring conformational degrees of freedom from all-atom (AA) simulations of an intrinsically disordered protein (IDP) to coarse-grained (CG) Monte Carlo (MC) simulations using conformational swap moves. AA simulations of a single histatin 5 peptide in water were used to obtain a structural ensemble, which is reweighted in a CGMC simulation in the presence of a negatively charged surface. For efficient sampling, the AA trajectory was condensed using two approaches: RMSD clustering (based on the root-mean-square difference in atom positions) and a “naïve” truncation, where only every 100th frame of the trajectory was included in the library. The results show that even libraries with few structures well reproduce the radius of gyration and interaction free energy as functions of the distance from the surface. We further observe that the surface slightly promotes the secondary structure of histatin 5 and more so if using explicit surface charges rather than smeared charges.



1. INTRODUCTION

Approximately 30% of the proteins in eukaryotes have disordered regions composed of 50 amino acid residues or more.¹ Despite the abundance of such intrinsically disordered proteins (IDPs), or intrinsically disordered protein regions, the structure–function paradigm stated for a long time that a well-defined three-dimensional (3D) structure was required for protein function. However, after it was realized that IDPs are important and functional, they have become a popular research area.^{1–6} Many IDPs gain secondary structure when adsorbing onto surfaces, for example, to a membrane.⁷ It is therefore important to study the change in structure upon adsorption and its relationship to protein function. While this is challenging with all-atom (AA) molecular dynamics (MD) simulations, due to the lack of suitable force fields for adsorption, this work represents a first step toward studying the secondary structure of IDPs at interfaces using a method integrating AAMD and coarse-grained (CG) Monte Carlo (MC) simulations. In this study, our model protein is the IDP histatin 5.

Histatin 5 consists of 24 amino acid residues and is present in human saliva.⁸ While it is considered to be disordered, there is experimental evidence of a polyproline II structure in bulk solution.⁹ Histatin 5 has antifungal properties, and it has been suggested that this protein, or conjugates between a fragment of histatin 5 and spermidine, could work as drugs against oral candidiasis.^{10,11} However, one of the problems is that histatin 5 is quickly degraded in the oral environment.¹² Since adsorption might reduce the proteolytic degradation of histatin 5,¹³ designing an antifungal peptide that adsorbs more strongly to the tooth enamel could be a way of limiting the problem of proteolytic degradation.¹⁴ Thus, if the understanding of the mechanisms behind the adsorption of histatin 5 to negatively

charged surfaces is enhanced, we could gain insights of relevance for the design of new peptide-based antifungal drugs.

The time scale for reaching equilibrium adsorption of histatin 5 to a negatively charged surface in experiments is on the order of an hour while AAMD simulations are on the order of microseconds. Thus, performing normal AAMD simulations to investigate the adsorption of proteins is often infeasible. One way of reducing the computational cost of the simulations is by coarse-graining the system.

In coarse-grained simulations of proteins, two extreme methods can be used to represent the conformations of the proteins. In the case of relatively rigid proteins, it is possible to use a single conformation, obtained, for example, from the crystal structure of the protein.¹⁵ In contrast, a disordered protein can be modeled with each amino acid residue represented as a bead on a completely flexible necklace. In the former case, the model suffers from too little flexibility, while in the latter case, the protein is instead too flexible—considering that the angular distribution is not limited by anything other than the requirement that beads cannot overlap with each other.

Prytkova et al. reduced the problems associated with the use of only a single structure by employing a small library of structures obtained from AAMD simulations of a single protein in the solvent.¹⁶ The structures from the MD simulations were clustered together to form a small set of representative structures. In the following CGMC simulations, they added a

Received: October 18, 2019

Published: February 9, 2020

trial move where one protein conformation was swapped for another one from the library. The new conformations were picked from the library with a probability corresponding to their occurrence in the trajectory from the MD simulations. The presence of the other proteins in the solution introduces a bias to the distribution of conformations generated by the MD simulations. Thus, the final probability that a certain conformation is accepted is different from the probability that it is picked as a trial conformation from the library, and the ensemble of accepted structures represents the concentrated system rather than the single-protein system.

Using the method proposed by Prytkova et al.,¹⁶ the impact of the number of protein structures in the library, when simulating many-protein systems, was investigated by Majumdar et al.¹⁹ The method has also been applied to the flexible polymer poly(ethylene glycol) to study crowding effects.¹⁸ As these studies have shown, the described method can be applied, for example, to simulate biological systems such as the crowded environment inside cells or in the extracellular matrix. However, the described methodology could also be applied to systems biased in other ways—not necessarily by increasing the concentration of the protein/polymer. For example, the conditions under which the original distribution was sampled could be changed with respect to geometry, e.g., by introducing a charged surface as in this work. An important benefit of the method is that it is generally computationally inexpensive. The cost is equivalent to rigid-body approaches, however incorporating a much larger degree of realism.^{16,17}

To simulate histatin 5 in bulk solution and at a planar interface, we use both a similar approach to that used by Prytkova et al.¹⁶ and the so-called bead–necklace model that has been used previously for histatin 5.^{19–21} The same bead–necklace model has also been used for β -casein.^{22,23} In the bead–necklace model, each amino acid residue and the two terminals are represented as spheres (beads) and the following approximations are made:

1. The surface charge is smeared and the interaction between the amino acid charges and the surface is represented by a Gouy–Chapman potential.
2. The interaction/distance between two bonded amino acid residues is described by a harmonic potential. (Neighboring residues can overlap.)
3. Non-neighboring amino acid residues interact via a soft sphere potential. The sphere sizes are calculated using the masses of the individual amino acids under the assumption that they are spherical, using a protein density of 1.525 g/mL calculated according to Fischer et al.²⁴
4. The charge of each amino acid residue is in the center of the sphere representing the residue.
5. The solvent is treated implicitly, represented by the dielectric constant.
6. The salt ions are treated implicitly using the Debye screening length.

It was determined that in order to match experimental adsorption data from ellipsometry measurements, a short-ranged attraction of relatively large magnitude needs to be included in addition to the electrostatic attraction between the protein and the oppositely charged surface.²⁰ Part of this additional attraction could possibly be explained if there is artificially high flexibility of our bead–necklace model. Since there are no restrictions on the angles between the amino acid residues (except that non-neighboring beads cannot overlap),

the chain entropy may be overestimated causing too large entropic repulsion between the protein and the surface. This will be investigated in the present study, where information on the conformational entropy from AAMD simulations is transferred to CGMC simulations.

Other factors that may increase the attraction between the protein and the surface, which are not accounted for in the previous model, are counterion release and matching of the distances between positive charges in the protein and negative charges on the surface. To determine the importance of these two aspects, we performed simulations with grand canonical salt (including explicit counterions) and explicit surface charges, in addition to the simulations with implicit salt and surface charge.

If the bias introduced to the ensemble of structures constituting the library is too large, the method with swap moves might fail to accurately represent the conditions of the MC simulations. For example, if no or very few elongated protein structures are present in the library, a system where the amino acids are highly attracted to a surface will not be accurately described by the simulation with swap moves since structures corresponding to a protein lying flat on the surface cannot be found in the library. Therefore, we tested the method before applying it to the library of structures from MD simulations. We compared the surface adsorption obtained from MC simulations using the original flexible bead model (CGMC (fully flexible) model from now on) with the surface adsorption obtained from MC simulations with swap moves using a library of structures generated by the flexible bead model in bulk (CGMC (conf. swap)). The surface biases the distribution of conformations from the bulk trajectory, and if this perturbation approach gives equal results as the flexible model with internal degrees of freedom, it shows that the perturbation approach works.

After the validation, we applied the method to a trajectory coarse-grained from an AAMD simulation with the hypothesis that this gives a more realistic representation of the structure of histatin 5, and its conformational entropy.

Finally, we analyze the secondary structure of the conformations found in the adsorbed layer. The result is compared to bulk secondary structure to find surface-induced conformational changes.

As mentioned, we have performed both simulations with implicit (smeared) surface charge and implicit salt in the solution (represented by the Debye screening length) and simulations with explicit surface charges and explicit grand canonical salt. The simulations with explicit charges were performed both to investigate whether they would give a larger attraction to the surface and to determine if the change in the secondary structure of the adsorbed proteins would be larger. It has previously been shown that if the spacing between negative charges at the surface matches the spacing between positive charges in an α -helix, the presence of the surface may induce folding of an otherwise disordered protein.²⁵ Thus, it is likely that surface charges need to be modeled explicitly when the secondary structure of adsorbed proteins is to be investigated.

2. METHODOLOGY

For the simulations with conformational swap moves (CGMC (conf. swap) and CGMC (AAMD conf. swap); see Table 1), the structure libraries/trajectories were generated from two different types of simulations: CGMC (fully flexible) model^{19–23} described in Introduction, and AAMD simulations. The CGMC (conf. swap) simulations were made to validate the approach

Table 1. Different Models for Histatin 5 Referred to in This Study

| model | conformation change by |
|------------------------|--|
| AAMD | internal degrees of freedom |
| CGMC (fully flexible) | internal degrees of freedom |
| CGMC (AAMD conf. swap) | swap moves (library from AAMD) |
| CGMC (conf. swap) | swap moves (library from CGMC, fully flexible) |

with swap moves. All MC simulations were performed using Faunus, a framework for Monte Carlo simulations.²⁶ The results are averages of eight different simulation runs with slightly different displacement parameters, and the error bars represent the standard deviation of these simulations.

2.1. Monte Carlo (Fully Flexible) Details. The MC moves employed for the CGMC (fully flexible) simulations were: translation of the entire protein, rotation of the entire protein, translation of a single bead, crankshaft,⁴ and pivot rotations.⁶ In earlier studies, a titration move was also included, but here the amino acid residues had constant charges to make the CGMC (fully flexible) simulations comparable to the CGMC (AAMD conf. swap) simulations that had constant charge.

The system energy was

$$U = \sum_{i=1}^{n-1} \sum_{j=i+1}^n \frac{q_i q_j}{4\pi\epsilon_0\epsilon_r r_{ij}} e^{-\kappa r_{ij}} + \sum_{i=1}^{n_b} k_b (R_i - R_{eq})^2 + \sum_{i=1}^{n-2} \sum_{j=i+2}^n 4\epsilon_{nb} \left[\left(\frac{\sigma_{ij}}{r_{ij}} \right)^{12} - \left(\frac{\sigma_{ij}}{r_{ij}} \right)^6 \right] \quad (1)$$

where $n = 26$ is the number of beads, q_i is the charge of bead i , ϵ_0 is the permittivity of free space, $\epsilon_r = 78.5$ is the relative permittivity of water, r_{ij} is the distance between the centers of beads i and j , $\kappa^{-1} = 9.62$ Å is the Debye screening length (corresponding to an ionic strength of 100 mM), $n_b = n - 1$ is the number of bonds, k_b is the spring constant of the harmonic bond, R_i is the bond length of bond i , $R_{eq} = 4.0$ Å is the equilibrium bond length, $\epsilon_{nb} = 0.05 k_B T$ is the interaction strength between nonbonded bead pairs, k_B is the Boltzmann constant, $T = 298$ K is the temperature, and σ_{ij} is the sum of the radii of beads i and j .^c

The charges of the amino acid residues were set to the most probable charges at the simulated pH (pH 7), meaning that the C-terminal, as well as the aspartic and glutamic acid residues, each got a charge of -1 , while the N-terminal, as well as the lysine and arginine residues, each got a charge of $+1$ —resulting in a net charge of $+5$ for the entire protein.

The bulk simulation, which was used to generate the library for CGMC (conf. swap) simulations, was run in 10^7 Monte Carlo steps in a cubic box with side length 150 Å and with periodic boundary conditions. The structures were saved with a probability of 0.001, resulting in a library of 10 207 conformations that was used directly in the simulations with swap moves. The results of the simulations using the CGMC (conf. swap) method were compared to the results of the simulations with a surface using the CGMC (fully flexible) method to ensure that the two approaches are equivalent.

In the surface simulations, the simulation box had periodic boundaries in the xy -directions but not in the z -direction (direction perpendicular to the surface). The box was 300 Å long in the z -direction and 150 Å long in the xy -directions.

In the simulations with a charged surface, the surface charge density was $-2.0 \mu\text{C}/\text{cm}^2$ ($-1.25 \times 10^{-3} e/\text{\AA}^2$), corresponding to the surface charge density of silica under the simulated conditions.²⁷

The surface was treated as completely smooth with a uniform charge distribution. The electrostatic potential energy between the charges on the protein and the surface was calculated using the Gouy–Chapman theory, according to the following equations

$$V_{GC} = \sum_{i=1}^n 2z_i k_B T \ln \left(\frac{1 + \Gamma_0 e^{-\kappa r_{i,s}}}{1 - \Gamma_0 e^{-\kappa r_{i,s}}} \right) \quad (2)$$

where

$$\Gamma_0 = \tanh \left[\frac{1}{2} \sinh^{-1} \left(\frac{\rho}{\sqrt{8k_B T c_0 \epsilon_0 \epsilon_r}} \right) \right] \quad (3)$$

ρ is the surface charge density, c_0 is the concentration of 1:1 salt, z_i is the charge number of protein bead i , and $r_{i,s}$ is the distance between the surface and the center of bead i .

For several simulations, a short-ranged Lennard-Jones-type interaction between the surface and the amino acid beads was used in addition to the electrostatic potential. The short-ranged attraction was

$$V_{LJ} = \sum_{i=1}^n \frac{3\sqrt{3}}{2} \epsilon \left[\left(\frac{\sigma_i}{r_i + \sigma_i} \right)^9 - \left(\frac{\sigma_i}{r_i + \sigma_i} \right)^3 \right] \quad (4)$$

where ϵ represents the interaction strength ($-\epsilon$ is the minimum value of the potential between each amino acid bead and the surface) and σ_i is the radius of the amino acid bead. The potential is shifted so that it is zero when the distance between the surface and the center of the bead is zero. This is the closest possible distance in the model, and if the normal form of the Lennard-Jones potential is kept, the repulsion may “win” over the attraction so that the adsorption decreases when the Lennard-Jones attraction is turned on, thus counteracting the purpose.

By comparison with ellipsometry data for histatin 5 adsorbing to a hydrophilic silica surface,²⁰ we here find that a reasonable value for ϵ is $1.7 k_B T$.

2.2. All-Atom MD. In production simulations using the CGMC (AAMD conf. swap) approach, the coarse-grained structure libraries were based on trajectories from AAMD simulations of a single histatin 5 molecule in bulk solution using GROMACS 4.6.7.^{28–31} Henriques et al. evaluated different force fields and water models and compared to small-angle X-ray scattering (SAXS) data for histatin 5, showing that the approaches by Best et al. (increasing the protein–water interactions)³² and Piana et al. (creating a new water model with increased dispersion interactions)³³ produce results in good agreement with experimental data, while traditional force fields and water models give too collapsed protein structures.^{34,35} In this work, we used a trajectory from previous simulations by Henriques and Skeps³⁵ using the water model TIP4P-D devised by Piana et al.³³ and the force field AMBER99SB-ILDN.³⁶ The simulation was run in a triplicate of 500 ns each. This is enough for properties describing the shape and size of the protein, such as the radius of gyration, to converge.³⁵ However, the secondary structure may require simulation times on the order of 10–100 μs to converge.³³ Thus, the secondary structure analysis performed in the Results section

is meant as a comparison between bulk and adsorbed histatin 5 and should not be interpreted as giving exact numbers.

2.2.1. Trajectory Reduction. We used two different approaches to reduce the MD trajectory to a feasible number of structures. In the “naïve” approach, every 100th structure from the trajectory was chosen and then coarse-grained to amino acid level. This resulted in a library of 1500 structures, where each amino acid and the terminals are represented as spheres centered on the center of mass of the amino acid or terminal. The charges were placed in the middle of the spheres, and the radii of the spheres were calculated from the masses of the individual amino acids/terminals and a common density, as in previous studies using the CGMC (fully flexible) model.^{20,21}

In a more sophisticated approach, the MD trajectory was clustered into a number of representative structures using the GROMOS algorithm described by Daura et al.³⁷ For different cutoffs in RMSD (the root-mean-square difference in atom positions), the trajectory composed of the central structure of each cluster was coarse-grained in the same manner as with the “naïve” approach. Further, according to the number of structures composing the cluster, a weight was assigned to each frame in the trajectory. To find a good compromise between the number of structures in the library and the reproducibility of the average properties of the protein, we first monitored the number of clusters generated as a function of the RMSD cutoff, then we compared the radius of gyration (R_g) distribution obtained from the full coarse-grained MD trajectory to those obtained from libraries derived with different cutoffs in RMSD. In Figure 1, the gray bars represent the R_g distribution of

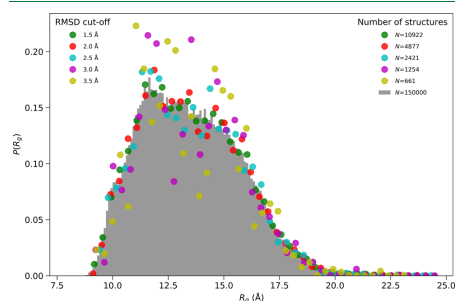


Figure 1. R_g distribution of the full coarse-grained MD trajectory (gray) and the clustered trajectories (colored dots) obtained through GROMOS algorithm³⁷ exploring different RMSD cutoffs.

the full coarse-grained MD trajectory, while the colored dots represent the clustered trajectories for different RMSD cutoffs. As expected, shorter cutoffs involve more structures and the related trajectories better fit the gray distribution. However, a good compromise is represented by the cyan curve (cutoff = 2.5 Å), which involves only 2421 structures (~1/60 of the structures composing the full trajectory) but still fits well to the shape of the full distribution. Higher cutoffs lead to smaller libraries, but those do not represent the original distribution anymore.

2.3. Monte Carlo (Conformational Swap) Details. The MC simulations with swap moves have three types of possible moves: translation and rotation of the entire protein and the swap move where the protein conformation is swapped for a new

one that is randomly chosen from the library. In the swap move, the mass center is fixed but the rotational orientation of the new conformation is randomized. The change in the internal energy of the protein is not evaluated.

Simulations were made using both implicit and explicit surface charges and salt. For all simulations with implicit surface charges and salt, Faunus git revision aa6f933 was used. For the simulations with explicit surface charges and salt, git revision d87e8bb was used.

2.3.1. Implicit Surface Charge. The simulations with implicit surface charge were made with the same parameters as described in Monte Carlo (Fully Flexible) Details. However, the internal energy of the protein was not evaluated since this was already done by the simulations that yielded the conformations in the library. Thus, the energy evaluated was

$$H = V_{GC} + V_{IJ} \quad (5)$$

2.3.2. Explicit Surface Charges. Finally, simulations with grand canonical salt (including counterions) and explicit surface charges were performed. These simulations included an insertion/deletion move where a salt ion pair is inserted or removed—preserving the electrostatic neutrality of the system. The activities of the ions in solution were set to 78 mM, giving an ionic strength of 100 mM in bulk solution, corresponding to an activity coefficient of 0.78. The ion radius was 1.9 Å. The surface charge density was $-2.0 \mu\text{C}/\text{cm}^2$ as above. The charges were placed hexagonally on one xy box side, and periodic boundary conditions were used in the xy -directions. The box was 300 Å long in the z -direction, and the surface was $182 \text{ Å} \times 158 \text{ Å}$ to accommodate the hexagonal lattice. The system energy in the grand canonical simulations was

$$U = \sum_{i=1}^{N-1} \sum_{j=i+1}^N \left(\frac{q_i q_j}{4\pi\epsilon_0 \epsilon_r r_{ij}} + V_{HS} \right) \quad (6)$$

where the sum should be taken only over particles/beads that are not connected with bonds; thus, the internal energy of the protein is not evaluated. N is the number of particles in the system (beads + ions + surface charges) and

$$V_{HS} = \begin{cases} 0, & r_{ij} \geq \sigma_{ij} \\ \infty, & r_{ij} < \sigma_{ij} \end{cases} \quad (7)$$

3. RESULTS

The different types of simulations that were performed are summarized in Table 2.

3.1. Validation of Method. Here, the method with conformational swap moves is validated by comparing CGMC (fully flexible) and CGMC (conf. swap) simulations (case nos. 1 and 2 in Table 2) as outlined in Methodology.

Table 2. Different Types of Simulations Performed

| case no | CGMC type | charge model | trajectory reduction |
|---------|-----------------|--------------|----------------------|
| 1 | fully flexible | implicit | none |
| 2 | conf. swap | implicit | naïve |
| 3 | AAMD conf. swap | implicit | naïve |
| 4 | AAMD conf. swap | implicit | RMSD clustering |
| 5 | AAMD conf. swap | explicit | naïve |
| 6 | AAMD conf. swap | explicit | RMSD clustering |

Figure 2 shows the free energy of adsorption for case 1 and case 2 for two systems: one with only electrostatic attraction

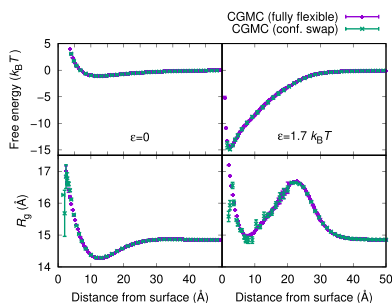


Figure 2. Comparison of the free energy of adsorption (top) and the radius of gyration (bottom) as a function of mass center distance from the surface for histatin 5 in CGMC (fully flexible) and CGMC (conf. swap) simulations. The pH is 7, the ionic strength is 100 mM, the surface charge density is $-2.0 \mu\text{C}/\text{cm}^2$, and salt ions and surface charges are modeled implicitly. The error bars are typically smaller than the symbol size.

between the protein and the surface and one with a short-ranged attraction included as well. Clearly, the perturbation approach is applicable even when the perturbation due to the surface is large, i.e., the attraction between the protein and the surface is high. However, when there is a short-ranged attraction, the protein's mass center can get as close as 0.8 Å from the surface in CGMC (fully flexible) simulations, while in CGMC (conf. swap) simulations, no proteins closer than 1.6 Å from the surface are found; see Figure 2 (top).

Figure 2 shows how the radius of gyration is affected when the protein approaches the surface for case 1 and case 2. The two methods give the same result except at very short distances to the surface.

In Figure 3, the distributions of R_g ($P(R_g)$) for the adsorbed layer for case 1 and case 2 are compared. The protein is considered to be adsorbed when the distance between the mass center and the surface is less than 30 Å —the distance where the free-energy well starts to form. With no short-ranged attraction between the surface and the protein, the two methods give the same $P(R_g)$. However, as the short-ranged attraction is increased, the results differ more significantly. When $\epsilon = 1.0 k_B T$, a conformation with $R_g = 14 \text{ Å}$ has started to become preferred relative to the other conformations. This is even more clear when $\epsilon = 1.7 k_B T$ (see the inset of Figure 3), where it seems that the protein gets stuck in two different conformations for large parts of the simulation. Indeed, there is only 0.025% acceptance of the swap moves. For comparison, 90.6% of the swap moves are accepted when there is no short-ranged attraction. Snapshots of the two preferred conformations are shown in Figure 4.

3.2. Application of Method—"Naïve" Approach. Here we apply the method to distribution of structures from all-atom simulations.³⁵ The library of structures was constructed with the "naïve" method: using every 100th conformation from the all-atom trajectory (1500 conformations in total). These simulations were labeled "case 3" in Table 2.

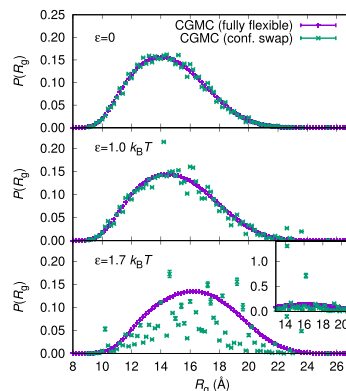


Figure 3. $P(R_g)$ for the adsorbed layer using the two methods. The inset shows $P(R_g)$ for $\epsilon = 1.7 k_B T$ on a different scale. The pH is 7, the ionic strength is 100 mM, the surface charge density is $-2.0 \mu\text{C}/\text{cm}^2$, and salt and surface charges are modeled implicitly. The error bars are typically smaller than the symbol size.

3.2.1. Radius of Gyration Distributions. Figure 5 shows the histatin 5 radius of gyration distributions, $P(R_g)$, from the complete coarse-grained trajectory from AAMD simulations, from the trajectory that was reduced by the naïve method described above, and from a trajectory from CGMC (fully flexible) bulk simulations. CGMC (fully flexible) simulations give essentially a Gaussian distribution of the radius of gyration, while AAMD gives an R_g distribution with a steeper slope on shorter length scales, representing more compact conformations. Furthermore, the peak in $P(R_g)$ from the AAMD simulations is shifted toward lower R_g compared to the peak from the CGMC (fully flexible) simulations. The coarse-grained trajectory from the all-atom simulations has a root-mean-square (rms) R_g of 13.1 Å , and the bead model gives an rms R_g of $14.84 \pm 0.009 \text{ Å}$. These values can be compared to the experimental values from SAXS, where the rms R_g of histatin 5 has been found from $P(r)$ to be $13.8 \pm 0.04 \text{ Å}$.³⁸ The Guinier approximation gives a value of 13.3 Å . However, the value from $P(r)$ is likely to be more accurate since it is calculated from the complete scattering curve, in contrast to the Guinier approximation.³⁹ Thus, the experimental rms R_g lies between the rms R_g 's of the two different models, though somewhat closer to that of the coarse-grained MD trajectory. However, the R_g calculated from the positions of the atoms/beads in the simulations is not directly comparable to the R_g calculated from SAXS experiments, since the SAXS data also include a contribution from the hydration layer around the protein. However, it has been shown that when the water model TIP4P-D is used, as in this MD trajectory, the contribution to R_g from the hydration layer is negligible for histatin 5 (and possibly for other IDPs).⁴⁰

The force field and the water model used for these MD simulations managed to well reproduce the Kratky plot and $P(r)$ from SAXS.³⁵ This is also possible to achieve with a coarse-grained flexible bead model,³⁸ but the ensemble of conformations from AAMD simulations is likely to be more realistic since these simulations include restraints on, for example, dihedral angles.

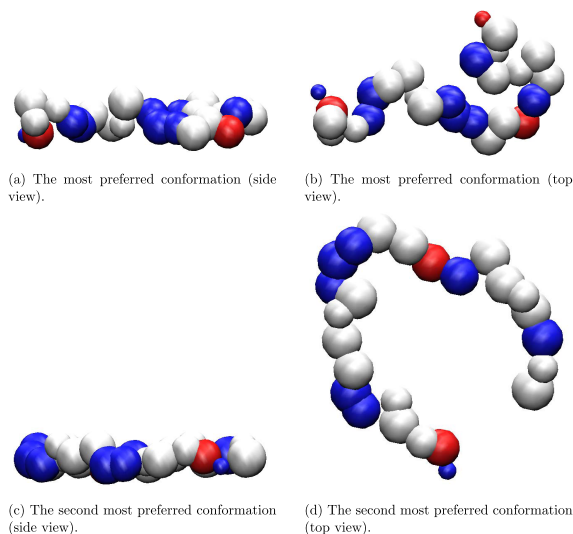


Figure 4. Snapshots of the two most preferred conformations in CGMC (conf. swap) simulations with a short-ranged attraction with $e = 1.7 k_B T$ between the surface and each amino acid. The pH is 7, the ionic strength is 100 mM, the surface charge density is $-2.0 \mu\text{C}/\text{cm}^2$, and salt and surface charges are modeled implicitly. Blue represents positively charged amino acid residues, red negatively charged residues, and gray neutral residues.

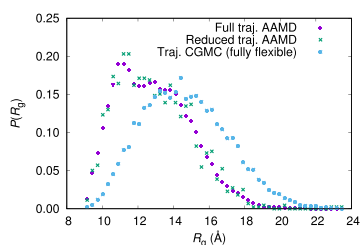


Figure 5. Comparison of $P(R_g)$ of the coarse-grained version of the trajectory from AAMD simulations (full and reduced to every 100th frame) to that of CGMC (fully flexible) simulations.

Figure 6 shows how the distribution of the radius of gyration of histatin 5 is perturbed by the introduction of the charged surface (with and without the short-ranged attraction). With only electrostatic attraction, the distribution is unshifted compared to the bulk trajectory. However, with short-ranged attraction, the stretched histatin 5 structures are strongly favored. The $P(R_g)$'s for the adsorbed layers are not significantly different from those of the entire simulations (data not shown).

3.2.2. Interfacial Free Energy and Radius of Gyration. In Figure 7 (top), the free energies of adsorption from case 3 and case 1 simulations are compared. The two models give very similar results both with and without short-ranged attraction. However, as before, the simulation with swap moves does not sample proteins as close to the surface as the method with internal degrees of freedom.

Figure 7 (bottom) displays the rms radius of gyration as a function of the distance from the surface for the two different

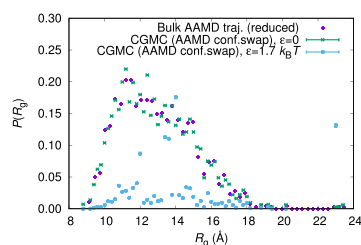


Figure 6. Perturbation of $P(R_g)$ (from the MD trajectory) by the presence of the negatively charged surface with and without short-ranged attraction. The pH is 7, the ionic strength is 100 mM, the surface charge density is $-2.0 \mu\text{C}/\text{cm}^2$, and salt and surface charges are modeled implicitly. The simulation with $e = 1.7 k_B T$ strongly prefers conformations with the highest R_g . These data points are outside the plot area. The error bars are typically smaller than the symbol size.

models. As expected from Figure 5, the radius of gyration is generally larger for CGMC (fully flexible) than for CGMC (AAMD conf. swap). However, the shapes of the curves are similar for the two models, although with the R_g increasing more steeply close to the surface for the CGMC (AAMD conf. swap) simulation—a difference that was not observed in the comparison made in Figure 2. Thus, this difference is caused not by the swap move approach itself, but rather by the difference in the protein conformations available within the two models.

3.3. Application of Method—RMSD Clustering. Simulations have been made with four different clustered trajectories obtained with different RMSD cutoffs: 1.0, 2.5, 3.0, and 5.0 Å.

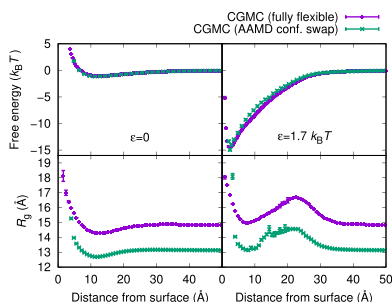


Figure 7. Comparison of free energies of adsorption (top) and R_g (bottom) as a function of distance from the surface for case 3 (CGMC (AAMD conf. swap)) and case 1 (CGMC (fully flexible)) simulations, with and without short-ranged attraction. The pH is 7, the ionic strength is 100 mM, the surface charge density is $-2.0 \mu\text{C}/\text{cm}^2$, and salt and surface charges are modeled implicitly. The error bars are typically smaller than the symbol size.

These simulations are labeled case 4 in Table 2. The trajectory with an RMSD cutoff of 1.0 Å is expected to closely resemble the original trajectory, while 2.5 Å, as mentioned earlier, gives a good compromise between having a reduced number of structures, yet still representing the original trajectory. At 3.0 Å, the R_g distribution has started to deviate significantly from that of the original trajectory (see Figure 1) and a cutoff of 5.0 Å is expected to give only a crude description of the original MD trajectory.

Figure 8 shows that the results (free energy and radius of gyration) from simulations with the RMSD clustered

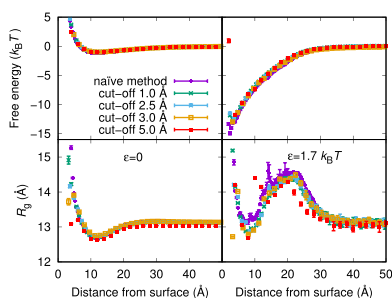


Figure 8. Free energy of adsorption (top) and rms radius of gyration (bottom) as a function of the distance between the mass center and the surface from simulations with structure libraries generated using the “naïve” approach (case 3) and different RMSD cutoffs (case 4). The pH is 7, the ionic strength is 100 mM, the surface charge density is $-2.0 \mu\text{C}/\text{cm}^2$, and salt and surface charges are modeled implicitly.

trajectories are very similar, while the naïve approach (case 3) gives a somewhat deeper free-energy minimum.

Figure 9 shows the R_g distributions from simulations with different cutoffs in RMSD, with and without a short-ranged attraction between the amino acids and the surface. When $\epsilon = 0$, the “naïve” approach and the clustered trajectory with a cutoff of 1.0 Å gave similar results, while $P(R_g)$ is somewhat smoother for the simulations using the clustered trajectory. With a short-

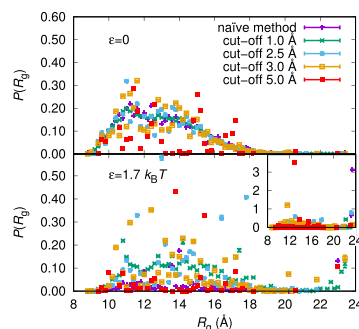


Figure 9. Distributions of the radius of gyration of adsorbed proteins from simulations using the “naïve” approach (case 3) and different RMSD cutoffs (case 4), with and without a short-ranged attraction between the amino acids and the surface. The inset shows the distribution of R_g when $\epsilon = 1.7 k_B T$ on a different scale. The pH is 7, the ionic strength is 100 mM, the surface charge density is $-2.0 \mu\text{C}/\text{cm}^2$, and salt and surface charges are modeled implicitly. The error bars are typically smaller than the symbol size.

range attraction ($\epsilon = 1.7 k_B T$) between the surface and the amino acids, a small number of conformations are preferred, especially when using the “naïve” approach or an RMSD cutoff of 5.0 Å. However, while the simulation using the “naïve” approach favors the conformation with the largest R_g , the simulation with the RMSD cutoff of 5.0 Å favors a conformation with $R_g = 12.8 \text{ Å}$.

3.4. Simulations with Grand Canonical Salt and Explicit Surface Charges. Simulations were performed with grand canonical salt and hexagonally packed explicit surface charges to analyze whether this approach would increase adsorption and/or induce secondary structure. These simulations are labeled “case 5” in Table 2. Figure 10 shows a

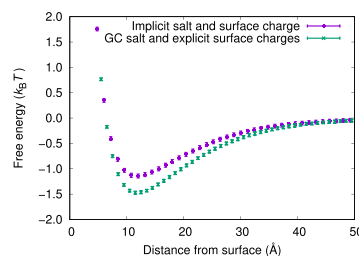


Figure 10. Free energies of adsorption using implicit surface charges and salt compared to explicit surface charges and grand canonical (GC) salt using the “naïve” approach. The pH is 7, the ionic strength is 100 mM, and the surface charge density is $-2.0 \mu\text{C}/\text{cm}^2$.

comparison of the free energy of adsorption using implicit surface charges and ions (case 3) and explicit surface charges and ions (case 5) when there is only electrostatic attraction between the protein and the surface ($\epsilon = 0$). The comparison shows that the free-energy minimum is deeper for case 5 than for case 3 and that the area of the free energy well is also larger.

3.5. Secondary Structure Analysis. The secondary structure of histatin 5 in the all-atom trajectory³⁵ was analyzed using DSSP and GROMACS. The results are a rough estimate of the bulk secondary structure since the conformational space is enormous and not fully sampled by the MD simulations.³⁵

Figure 11 and Table 3 strongly suggest that histatin 5 is disordered in aqueous bulk solution. The secondary structure

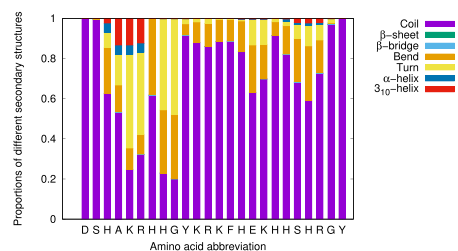


Figure 11. Secondary structures of histatin 5 from the “naive” trajectory from all-atom simulations in bulk per amino acid residue.

Table 3. Percentages of the Different Types of Secondary Structures for the Amino Acids of Histatin 5 in Bulk and Adsorbed to a Negatively Charged Surface for the Trajectories Reduced Using the “Naive” Approach and RMSD Clustering Using Cutoffs of 2.5 and 5.0 Å^a

| structure | naive (%) | 2.5 Å (%) | 5.0 Å (%) |
|---|------------------|------------------|------------------|
| (a) From Structural Ensemble in the Absence of Charged Surface | | | |
| coil | 71.05 | 70.85 | 66.73 |
| β -bridge | 0.12 | 0.08 | 0.00 |
| bend | 14.51 | 14.65 | 11.50 |
| turn | 11.28 | 11.34 | 14.73 |
| α -helix | 0.91 | 1.12 | 1.04 |
| 3_{10} -helix | 2.14 | 1.96 | 6.00 |
| (b) From Structural Ensemble in the Presence of a Surface with Implicit Charges and Implicit Salt Ions (Cases 3 and 4) | | | |
| coil | 70.70 \pm 0.16 | 70.36 \pm 0.09 | 66.31 \pm 0.07 |
| β -bridge | 0.12 \pm 0.01 | 0.10 \pm 0.01 | 0.00 \pm 0.00 |
| bend | 14.77 \pm 0.03 | 14.94 \pm 0.09 | 11.56 \pm 0.06 |
| turn | 11.34 \pm 0.09 | 11.39 \pm 0.11 | 14.96 \pm 0.14 |
| α -helix | 0.91 \pm 0.05 | 1.20 \pm 0.03 | 0.96 \pm 0.05 |
| 3_{10} -helix | 2.16 \pm 0.09 | 2.01 \pm 0.06 | 6.20 \pm 0.06 |
| (c) From Structural Ensemble in the Presence of a Surface with Explicit Charges and Explicit Grand Canonical Salt (Cases 5 and 6) | | | |
| coil | 70.13 \pm 0.04 | 70.17 \pm 0.04 | 66.27 \pm 0.03 |
| β -bridge | 0.14 \pm 0.00 | 0.10 \pm 0.01 | 0.00 \pm 0.00 |
| bend | 15.13 \pm 0.06 | 15.02 \pm 0.03 | 11.87 \pm 0.03 |
| turn | 11.42 \pm 0.03 | 11.61 \pm 0.04 | 14.55 \pm 0.05 |
| α -helix | 0.92 \pm 0.02 | 1.11 \pm 0.02 | 0.96 \pm 0.02 |
| 3_{10} -helix | 2.26 \pm 0.02 | 2.00 \pm 0.02 | 6.36 \pm 0.03 |

^aBetween the surface and the protein, there is only electrostatic interaction. The pH is 7, the ionic strength is 100 mM, and the surface charge density is $-2.0 \mu\text{C}/\text{cm}^2$.

motifs are mainly short bends and turns. The table gives the percentages of all amino acid residues that are part of different secondary structures, while the figure displays the proportions of secondary structures for each amino acid residue in the MD trajectory reduced by the “naive” approach.

Simulations of surface adsorption were performed using RMSD clustered trajectories as well as the naive approach. The trajectories of structures found in the coarse-grained simulations were saved, and then the secondary structures of the corresponding all-atom conformations were analyzed to determine if the surface induces a change in the secondary structure of the protein.

To determine whether local or nonlocal electrostatic interactions between the protein and the charges on the surface would induce secondary structure, we performed simulations with explicit surface charges and grand canonical salt as well as implicit surface charge and implicit salt. In these secondary structure simulations, no short-ranged attraction between the surface and the protein was added. A comparison of the results is displayed in Table 3.

Figure 12 shows the same analysis as Figure 11 for adsorbed proteins with grand canonical salt and explicit surface charges.

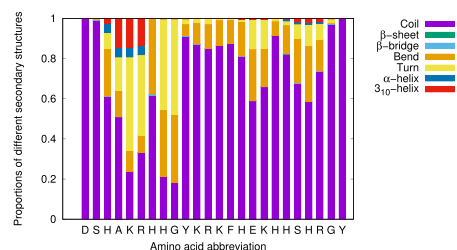


Figure 12. Secondary structures per amino acid residue of adsorbed histatin 5 from the simulations with grand canonical salt and explicit surface charges using the “naive” trajectory. The pH is 7, the ionic strength is 100 mM, and the surface charge density is $-2.0 \mu\text{C}/\text{cm}^2$.

The reason that the secondary structure analysis was not performed for the case with a short-ranged attraction to the surface was that there were too few structures that fit close to the surface to accurately represent the adsorbed layer.

4. DISCUSSION

4.1. Validation of Method. The simulations using conformational swap moves gave free energies and R_g 's as a function of distance from the surface in agreement with the method using a flexible protein (Figure 2). When a strong bias is introduced to the trajectory used for the conformational swap simulations, very few conformations from the trajectory dominate. This was, for example, noted in Figure 3 when there was a short-ranged attraction between the amino acids and the surface of $\epsilon = 1.7 k_B T$. It is clear from the snapshots in Figure 4 that the two most preferred conformations are very flat, and therefore, all amino acid residues can come close to the interface and interact favorably with the short-ranged potential. Here, the requirement that all structures present in the surface simulations are also present in the bulk simulations generating the library of conformations is not fulfilled. Thus, an analysis of the adsorbed structures will give an unrealistic result since too few conformations in the trajectory from simulations in bulk match the condition that all amino acids should be closely adsorbed to the surface.

Poor sampling due to a too high barrier for swapping may be solved by introducing penalty functions or by using parallel

tempering. However, here, simulations with slightly different displacement parameters gave the same results in terms of $P(R_g)$ (results not shown). Thus, it seems that the result presented here is not due to poor sampling.

4.2. Application of Method—"Naive" Approach. The similarity between the free-energy curves from CGMC (AAMD conf. swap) and CGMC (fully flexible) simulations (Figure 7) suggests that the hypothesis that the CGMC (fully flexible) model has unrealistically high conformational entropy in solution is false. Indeed, the entropic repulsion between a neutral surface and a histatin 5 molecule is the same for the CGMC (AAMD conf. swap) and CGMC (fully flexible) approach (results not shown).

4.3. Application of Method—RMSD Clustering. The simulations with different cutoffs in RMSD give very similar results for the free energy of adsorption (Figure 8) and R_g as a function of the distance from the surface. However, using a cutoff of 5.0 Å, R_g as a function of the distance from the surface deviates significantly from the results using smaller cutoffs. Thus, the trajectory made using the cutoff of 5.0 Å is too small to give accurate R_g .

The somewhat deeper free-energy minimum for the "naïve" approach when $\epsilon = 1.7 k_B T$ (Figure 8) can be attributed to the fact that the "naïve" trajectory includes the very stretched conformation that is dominant in simulations including a short-ranged attraction to the surface (Figure 6).

For simulations with a surface and $\epsilon = 0$, $P(R_g)$ becomes less and less smooth with increasing cutoff (Figure 9). When $\epsilon = 1.7 k_B T$, the pattern is less clear. Any flat structure in the library will be favored by the strongly attractive surface. The bulk simulation has not sampled enough of these flat structures to give a reliable $P(R_g)$ when there is such a high short-ranged attraction to the surface. When choosing the number of structures to use in the library of conformations, one must consider what kind of data is needed from the simulations. While the free energy of adsorption is relatively insensitive to the choice of the number of structures, it is impossible to get a reliable $P(R_g)$ with only a few structures in the library.

Another possible method for clustering is the combinatorial averaged transient structure (CATS) clustering method.⁴¹ It is developed for proteins that rapidly sample many conformations and is sometimes more suitable for IDPs than RMSD clustering. The CATS method is better at finding unique structures and representing local minima in the energy landscape than RMSD clustering.

4.4. Simulations with Grand Canonical Salt and Explicit Surface Charges. The simulations with explicit grand canonical salt (including counterions) and explicit surface charges gave more adsorption than the simulations with implicit charges and salt. The higher adsorption is more realistic compared to experimental results.²⁰ Thus, it seems that explicit charges on the surface and in solution are important when modeling the adsorption of histatin 5. However, an additional short-ranged attraction is still needed to approach the experimental results.

4.5. Secondary Structure Analysis. The results in Table 3 show that for all cases, there is a slight reduction in coil content when the protein is adsorbed. The coil content is further reduced in the simulations with explicit surface charges compared to the simulations with implicit charge, indicating that the explicit surface charges induce secondary structure to a somewhat higher extent. Thus, local electrostatic interactions are likely to be important. The amount of secondary structure

could possibly be controlled by adjusting the distance between the surface charges to match the spacing in α -helical histatin 5. Figure 13 shows a helical wheel of histatin 5. In particular, if the

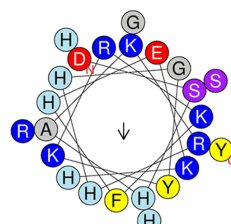


Figure 13. Helical wheel (α -helix) of histatin 5. Blue represents positively charged amino acid residues, red represents negatively charged residues, purple represents polar residues, and yellow represents aromatic residues.

pH is low (histidine positively charged), many positive charges would be present on one side of the α -helix, possibly inducing α -helix formation in the same manner as described by Lundqvist et al. for a designed peptide.²⁵

The content of bends and 3_{10} -helices increases somewhat when the protein is adsorbed, while the change in the content of other secondary structure motifs varies between the different trajectories and simulation methods.

A comparison of Figures 11 and 12 shows that the small change in the secondary structure is hardly visible for any of the individual amino acids.

However, when the bias to the original distribution of structures is too large, a couple of structures may dominate throughout the simulation, as in Figure 3 (inset) and Figure 9 (inset), where $\epsilon = 1.7 k_B T$. These structures cannot be taken to accurately represent the new distribution of structures. Thus, some caution should be taken when analyzing (in this case) adsorbed structures since the library of structures generated in bulk is not always large enough to represent the ensemble of adsorbed conformations.

5. CONCLUSIONS

Extending a recently developed structural swap move,¹⁶ we show that conformational degrees of freedom from all-atom simulations of a disordered protein in water can be effectively transferred to coarse-grained Monte Carlo simulations of a more complex system containing a charged, planar interface. This gives a significantly more realistic picture of the system of interest than using, for example, a coarse-grained model with beads connected by harmonic springs used in earlier studies.^{19–23,38,42–45} In the present study, the original distribution of conformations from all-atom simulations of histatin 5 in bulk was biased by the introduction of a coarse-grained, charged surface. The results for the free energy of adsorption as well as the shape of the radius of gyration as a function of distance from the surface were close to those of previous models using harmonically connected amino acid beads.²⁰ We further find that the entropic repulsion between the surface and the protein is similar for the two models.

By back-mapping the CGMC histatin 5 trajectory to all-atom resolution, we show that the secondary structure of surface-adsorbed conformations slightly increases compared to bulk

solution. Using explicit surface charges further increases the secondary structure content compared to smeared out charges, suggesting that local electrostatic interactions promote the formation of internal structure. This possibility to directly connect the adsorbed ensemble to all-atom resolution at modest computational cost is a valuable step toward the understanding of IDPs at surfaces and in more complex environments.

■ ASSOCIATED CONTENT

Supporting Information

The Supporting Information is available free of charge at <https://pubs.acs.org/doi/10.1021/acs.jctc.9b01041>.

Example input for running conformational swap moves in the Faunus software (ZIP)

■ AUTHOR INFORMATION

Corresponding Authors

Kristin Hyltegren – Division of Theoretical Chemistry, Lund University, SE-221 00 Lund, Sweden; Email: kristin.hyltegren@teokem.lu.se

Marco Polimeni – Division of Theoretical Chemistry, Lund University, SE-221 00 Lund, Sweden; Email: marco.polimeni@teokem.lu.se

Marie Skepö – Division of Theoretical Chemistry, Lund University, SE-221 00 Lund, Sweden; LINXS—Lund Institute of Advanced Neutron and X-ray Science, SE-223 70 Lund, Sweden; orcid.org/0000-0002-8639-9993; Email: marie.skepö@teokem.lu.se

Mikael Lund – Division of Theoretical Chemistry, Lund University, SE-221 00 Lund, Sweden; LINXS—Lund Institute of Advanced Neutron and X-ray Science, SE-223 70 Lund, Sweden; orcid.org/0000-0001-8178-8175; Email: mikael.lund@teokem.lu.se

Complete contact information is available at: <https://pubs.acs.org/doi/10.1021/acs.jctc.9b01041>

Notes

The authors declare no competing financial interest.

■ ACKNOWLEDGMENTS

The authors acknowledge financial support from the Crafoord Foundation; the Science Faculty, Lund University; The Swedish Resource Foundation; and the European Union through the Innovative Training Network, PIPPI. The simulations were performed on resources provided by the Swedish National Infrastructure for Computing (SNIC) at the center for scientific and technical computing at Lund University (LUNARC).

■ ADDITIONAL NOTES

^aPicks two beads randomly and defines the vector connecting them as the rotation axis, then rotates the beads between the picked ones around this axis.

^bDefines a rotation axis in the same manner as with the crankshaft move, then rotates the beads at one end of the protein around this axis.

^cTo prevent complete overlap between neighboring oppositely charged beads, neighboring beads also have small cores given by 0.0001 times the Lennard-Jones potential (term three) in eq 1.

■ REFERENCES

- (1) Dunker, A.; Lawson, J.; Brown, C. J.; Williams, R. M.; Romero, P.; Oh, J. S.; Oldfield, C. J.; Campen, A. M.; Ratliff, C. M.; Hipps, K. W.; Ausio, J.; Nissen, M. S.; Reeves, R.; Kang, C.; Kissinger, C. R.; Bailey, R. W.; Griswold, M. D.; Chiu, W.; Garner, E. C.; Obradovic, Z. Intrinsically disordered protein. *J. Mol. Graphics Modell.* **2001**, *19*, 26–59.
- (2) Wright, P. E.; Dyson, H. Intrinsically unstructured proteins: re-assessing the protein structure-function paradigm. *J. Mol. Biol.* **1999**, *293*, 321–331.
- (3) Dyson, H. J.; Wright, P. E. Intrinsically unstructured proteins and their functions. *Nat. Rev. Mol. Cell Biol.* **2005**, *6*, No. 197.
- (4) Uversky, V. N.; Dunker, A. K. Understanding protein non-folding. *Biochim. Biophys. Acta, Proteins Proteomics* **2010**, *1804*, 1231–1264.
- (5) Tompa, P. Intrinsically disordered proteins: a 10-year recap. *Trends Biochem. Sci.* **2012**, *37*, 509–516.
- (6) Oldfield, C. J.; Dunker, A. K. Intrinsically disordered proteins and intrinsically disordered protein regions. *Annu. Rev. Biochem.* **2014**, *83*, 553–584.
- (7) Uversky, V. N. Intrinsically Disordered Proteins and Their Environment: Effects of Strong Denaturants, Temperature, pH, Counter Ions, Membranes, Binding Partners, Osmolytes, and Macromolecular Crowding. *Protein J.* **2009**, *28*, 305–325.
- (8) Oppenheim, F. G.; Xu, T.; McMillan, F. M.; Levitz, S. M.; Diamond, R. D.; Offner, G. D.; Troxler, R. F. Histatins, a novel family of histidine-rich proteins in human parotid secretion. Isolation, characterization, primary structure, and fungistatic effects on *Candida albicans*. *J. Biol. Chem.* **1988**, *263*, 7472–7477.
- (9) Jephthah, S.; Staby, L.; Kragelund, B. B.; Skepö, M. Temperature Dependence of Intrinsically Disordered Proteins in Simulations: What are We Missing. *J. Chem. Theory Comput.* **2019**, *15*, 2672–2683.
- (10) Kavanagh, K.; Dowd, S. Histatins: antimicrobial peptides with therapeutic potential. *J. Pharm. Pharmacol.* **2004**, *56*, 285–289.
- (11) Tati, S.; Li, R.; Puri, S.; Kumar, R.; Davidow, P.; Edgerton, M. Histatin 5-Spermidine Conjugates Have Enhanced Fungicidal Activity and Efficacy as a Topical Therapeutic for Oral Candidiasis. *Antimicrob. Agents Chemother.* **2014**, *58*, 756–766.
- (12) Helmerhorst, E.; Alagü, A.; Siqueira, W.; Oppenheim, F. Oral fluid proteolytic effects on histatin 5 structure and function. *Arch. Oral Biol.* **2006**, *51*, 1061–1070.
- (13) McDonald, E.; Goldberg, H.; Tabbara, N.; Mendes, F.; Siqueira, W. Histatin 1 Resists Proteolytic Degradation when Adsorbed to Hydroxyapatite. *J. Dent. Res.* **2011**, *90*, 268–272.
- (14) Vukosavljevic, D.; Hutter, J.; Helmerhorst, E.; Xiao, Y.; Custodio, W.; Zaidan, F.; Oppenheim, F.; Siqueira, W. Nanoscale Adhesion Forces between Enamel Pellicle Proteins and Hydroxyapatite. *J. Dent. Res.* **2014**, *93*, 514–519.
- (15) Lund, M.; Jönsson, B. A Mesoscopic Model for Protein-Protein Interactions in Solution. *Biophys. J.* **2003**, *85*, 2940–2947.
- (16) Prytkova, V.; Heyden, M.; Khago, D.; Freitas, J. A.; Butts, C. T.; Martin, R. W.; Tobias, D. J. Multi-Conformation Monte Carlo: A Method for Introducing Flexibility in Efficient Simulations of Many-Protein Systems. *J. Phys. Chem. B* **2016**, *120*, 8115–8126.
- (17) Majumdar, B. B.; Prytkova, V.; Wong, E. K.; Freitas, J. A.; Tobias, D. J.; Heyden, M. Role of Conformational Flexibility in Monte Carlo Simulations of Many-Protein Systems. *J. Chem. Theory Comput.* **2019**, *15*, 1399–1408.
- (18) Majumdar, B. B.; Ebbinghaus, S.; Heyden, M. Macromolecular crowding effects in flexible polymer solutions. *J. Theor. Comput. Chem.* **2018**, *17*, No. 1840006.
- (19) Kurat, A.; Henriques, J.; Forsman, J.; Skepö, M.; Lund, M. Role of histidine for charge regulation of unstructured peptides at interfaces and in bulk. *Proteins* **2014**, *82*, 657–667.
- (20) Hyltegren, K.; Nylander, T.; Lund, M.; Skepö, M. Adsorption of the intrinsically disordered saliva protein histatin 5 to silica surfaces. A Monte Carlo simulation and ellipsometry study. *J. Colloid Interface Sci.* **2016**, *467*, 280–290.
- (21) Hyltegren, K.; Skepö, M. Adsorption of polyelectrolyte-like proteins to silica surfaces and the impact of pH on the response to ionic

- strength. A Monte Carlo simulation and ellipsometry study. *J. Colloid Interface Sci.* **2017**, *494*, 266–273.
- (22) Evers, C. H.; Andersson, T.; Lund, M.; Skepö, M. Adsorption of Unstructured Protein -Casein to Hydrophobic and Charged Surfaces. *Langmuir* **2012**, *28*, 11843–11849.
- (23) Henriques, J.; Skepö, M. A coarse-grained model for flexible (phospho)proteins: Adsorption and bulk properties. *Food Hydrocolloids* **2015**, *43*, 473–480.
- (24) Fischer, H.; Polikarpov, I.; Craievich, A. F. Average protein density is a molecular-weight-dependent function. *Protein Sci.* **2004**, *13*, 2825–2828.
- (25) Lundqvist, M.; Nygren, P.; Jonsson, B.-H.; Broo, K. Induction of Structure and Function in a Designed Peptide upon Adsorption on a Silica Nanoparticle. *Angew. Chem., Int. Ed.* **2006**, *45*, 8169–8173.
- (26) Stenqvist, B.; Thuresson, A.; Kurut, A.; Vácha, R.; Lund, M. Faunus - a flexible framework for Monte Carlo simulation. *Mol. Simul.* **2013**, *39*, 1233–1239.
- (27) Samoshina, Y.; Nylander, T.; Shubin, V.; Bauer, R.; Eskilsson, K. Equilibrium Aspects of Polycation Adsorption on Silica Surface: How the Adsorbed Layer Responds to Changes in Bulk Solution. *Langmuir* **2005**, *21*, 5872–5881.
- (28) Berendsen, H.; van der Spoel, D.; van Drunen, R. GROMACS: A message-passing parallel molecular dynamics implementation. *Comput. Phys. Commun.* **1995**, *91*, 43–56.
- (29) Lindahl, E.; Hess, B.; van der Spoel, D. GROMACS 3.0: a package for molecular simulation and trajectory analysis. *J. Mol. Model.* **2001**, *7*, 306–317.
- (30) Van der Spoel, D.; Lindahl, E.; Hess, B.; Groenhof, G.; Mark, A. E.; Berendsen, H. J. C. GROMACS: Fast, flexible, and free. *J. Comput. Chem.* **2005**, *26*, 1701–1718.
- (31) Hess, B.; Kutzner, C.; van der Spoel, D.; Lindahl, E. GROMACS 4: Algorithms for Highly Efficient, Load-Balanced, and Scalable Molecular Simulation. *J. Chem. Theory Comput.* **2008**, *4*, 435–447.
- (32) Best, R. B.; Zheng, W.; Mittal, J. Balanced Protein-Water Interactions Improve Properties of Disordered Proteins and Non-Specific Protein Association. *J. Chem. Theory Comput.* **2014**, *10*, 5113–5124.
- (33) Piana, S.; Donchev, A. G.; Robustelli, P.; Shaw, D. E. Water Dispersion Interactions Strongly Influence Simulated Structural Properties of Disordered Protein States. *J. Phys. Chem. B* **2015**, *119*, 5113–5123.
- (34) Henriques, J.; Cragnell, C.; Skepö, M. Molecular Dynamics Simulations of Intrinsically Disordered Proteins: Force Field Evaluation and Comparison with Experiment. *J. Chem. Theory Comput.* **2015**, *11*, 3420–3431.
- (35) Henriques, J.; Skepö, M. Molecular Dynamics Simulations of Intrinsically Disordered Proteins: On the Accuracy of the TIP4P-D Water Model and the Representativeness of Protein Disorder Models. *J. Chem. Theory Comput.* **2016**, *12*, 3407–3415.
- (36) Lindorff-Larsen, K.; Piana, S.; Palmo, K.; Maragakis, P.; Klepeis, J. L.; Dror, R. O.; Shaw, D. E. Improved side-chain torsion potentials for the Amber ff99SB protein force field. *Proteins* **2010**, *78*, 1950–1958.
- (37) Daura, X.; Gademann, K.; Jaun, B.; Seebach, D.; Gunsteren, W.; Mark, A. Peptide folding: When simulation meets experiment. *Angew. Chem., Int. Ed.* **1999**, *38*, 236–240.
- (38) Cragnell, C.; Durand, D.; Cabane, B.; Skepö, M. Coarse-grained modelling of the intrinsically disordered protein Histatin 5 in solution. Monte Carlo simulations in combination with SAXS. *Proteins* **2016**, *84*, 777–791.
- (39) Glatter, O. A new method for the evaluation of small-angle scattering data. *J. Appl. Crystallogr.* **1977**, *10*, 415–421.
- (40) Henriques, J.; Arleth, L.; Lindorff-Larsen, K.; Skepö, M. On the Calculation of SAXS Profiles of Folded and Intrinsically Disordered Proteins from Computer Simulations. *J. Mol. Biol.* **2018**, *430*, 2521–2539.
- (41) Ezerski, J. C.; Cheung, M. S. CATS: A Tool for Clustering the Ensemble of Intrinsically Disordered Peptides on a Flat Energy Landscape. *J. Phys. Chem. B* **2018**, *122*, 11807–11816.
- (42) Skepö, M.; Linse, P.; Arnebrant, T. Coarse-Grained Modeling of Proline Rich Protein 1 (PRP-1) in Bulk Solution and Adsorbed to a Negatively Charged Surface. *J. Phys. Chem. B* **2006**, *110*, 12141–12148.
- (43) Skepö, M. Model simulations of the adsorption of statherin to solid surfaces: Effects of surface charge and hydrophobicity. *J. Chem. Phys.* **2008**, *129*, No. 185101.
- (44) Cragnell, C.; Rieloff, E.; Skepö, M. Utilizing Coarse-Grained Modeling and Monte Carlo Simulations to Evaluate the Conformational Ensemble of Intrinsically Disordered Proteins and Regions. *J. Mol. Biol.* **2018**, *430*, 2478–2492.
- (45) Rieloff, E.; Tully, M. D.; Skepö, M. Assessing the Intricate Balance of Intermolecular Interactions upon Self-Association of Intrinsically Disordered Proteins. *J. Mol. Biol.* **2019**, *431*, 511–523.

PAPER IV

Adsorption of Fibrinogen on Silica Surfaces—The Effect of Attached Nanoparticles

K. Hyltegren, M. Hulander, M. Andersson, M. Skepö.

Biomolecules, 10, 2020, 413.

© This is an open access article distributed under the Creative Commons Attribution License which permits unrestricted use, distribution, and reproduction in any medium, provided the original work is properly cited.

Article

Adsorption of Fibrinogen on Silica Surfaces—The Effect of Attached Nanoparticles

Kristin Hyltegren ^{1,*}, Mats Hulander ², Martin Andersson ² and Marie Skepö ^{1,3,*}

¹ Division of Theoretical Chemistry, Lund University, POB 124, SE-221 00 Lund, Sweden

² Applied Chemistry, Chemistry and Chemical Engineering, Chalmers University of Technology, Chalmersplatsen 4, SE-412 96 Göteborg, Sweden; mats.hulander@chalmers.se (M.H.); martin.andersson@chalmers.se (M.A.)

³ LINXS—Lund Institute of Advanced Neutron and X-ray Science, Scheelevägen 19, SE-223 70 Lund, Sweden

* Correspondence: kristin.hyltegren@teokem.lu.se (K.H.); marie.skepo@teokem.lu.se (M.S.)

Received: 14 February 2020; Accepted: 3 March 2020; Published: 6 March 2020



Abstract: When a biomaterial is inserted into the body, proteins rapidly adsorb onto its surface, creating a conditioning protein film that functions as a link between the implant and adhering cells. Depending on the nano-roughness of the surface, proteins will adsorb in different amounts, with different conformations and orientations, possibly affecting the subsequent attachment of cells to the surface. Thus, modifications of the surface nanotopography of an implant may prevent biomaterial-associated infections. Fibrinogen is of particular importance since it contains adhesion epitopes that are recognized by both eukaryotic and prokaryotic cells, and can therefore influence the adhesion of bacteria. The aim of this study was to model adsorption of fibrinogen to smooth or nanostructured silica surfaces in an attempt to further understand how surface nanotopography may affect the orientation of the adsorbed fibrinogen molecule. We used a coarse-grained model, where the main body of fibrinogen (visible in the crystal structure) was modeled as rigid and the flexible α C-chains (not visible in the crystal structure) were modeled as completely disordered. We found that the elongated fibrinogen molecule preferably adsorbs in such a way that it protrudes further into solution on a nanostructured surface compared to a flat one. This implicates that the orientation on the flat surface increases its bio-availability.

Keywords: protein adsorption; coarse-grained modeling; fibrinogen; nanoparticles; nanotopography

1. Introduction

When a biomaterial is inserted into the body, a protein film consisting of plasma proteins from the blood is immediately formed on the implant surface. The 340 kDa glycoprotein fibrinogen is an abundant protein in the blood of vertebrates and is primarily involved in blood clotting and readily adsorbs to biomaterial surfaces upon implantation. In a wound, thrombin polymerizes fibrinogen into fibrin that, together with platelets, form a clot over the wound. When adsorbed to the surface of a biomaterial, fibrinogen can trigger inflammatory responses and subsequent formation of a fibrous capsule that can lead to failure or loss of function of the biomaterial. The fibrinogen molecule harbors epitopes that are recognized by both human and bacterial cells through specific integrins [1–4]. An infection on an implant can have severe consequences and is one of the most common causes of implant failure and need for revision surgery. Surface modifications at the nanoscale have previously been suggested as a promising approach to prevent adhesion of bacteria and development of biomaterial-associated infections on implants [5]. A leading cause for biomaterial-associated infections is the bacterium *Staphylococcus epidermidis* [6], which is normally present on human skin. A recent study found that the ability of *S. epidermidis* to adhere on adsorbed fibrinogen is highly dependent on

the nanostructure of the underlying substrate, possibly by affecting the orientation or conformation of the adsorbed fibrinogen molecule [7].

In the present study, we used coarse-grained Monte Carlo simulations to investigate how fibrinogen adsorbs to smooth and nanostructured surfaces (with attached nanoparticles). This enabled us to analyze in more detail how fibrinogen adsorbs and explain the experimental findings described above. We investigated the effect of surface charge, the effect of nanoparticle size, the angles between bound fibrinogen and the surface, and the effect of the disordered fragments (the α C-chains) of fibrinogen.

Human fibrinogen consists of two symmetrical halves that each contain three polypeptide chains called $A\alpha$ (610 amino acid residues), $B\beta$ (461 amino acid residues), and γ (411 amino acid residues). The chains are connected to each other by several disulfide bonds. Fibrinogen folds into a 45-nm-long rod with two thicker nodules (the D domains) at the ends, and one nodule in the middle of the rod (the E domain). The C-terminal 410 amino acid residues of the $A\alpha$ -chains are not visible in the crystal structure [8] and are here counted as the disordered α C-chains, which extend out from the two D domains (sometimes only the C-terminal 400 residues are included). NMR studies have shown that the α C-regions of bovine fibrinogen each contain a structured domain of approximately 60 amino acid residues [9]. However, the stability of this structure is low. Human fibrinogen seems to have α C-domains with similar structure but even less stable than the bovine ones [10].

In one of the simplest models that has been used for simulations of fibrinogen, the protein is approximated as an elongated ellipsoid [11] (see Figure 1a). In another study of fibrinogen adsorption, the protein was described as three connected squares [12] (see Figure 1b). Zhdanov et al. described fibrinogen as a linear pentamer with a monomer diameter of 7.5 nm [13] (see Figure 1c). A somewhat more detailed model that has been used to describe fibrinogen in simulations is a linear chain consisting of 23 touching spheres of different diameters, mimicking the differences in thickness at different parts of the fibrinogen rod [14,15] (see Figure 1d). The spheres at the ends had a diameter of 6.7 nm, the one in the middle 5.3 nm, and the remaining ones 1.5 nm. This model was later extended by adding two side arms representing the α C-chains [16] (see Figure 1f). The side arms were also linear but the angle ϕ between the side arms and the body of the protein was varied.

Atomistic molecular dynamics simulations of the main body of fibrinogen (excluding the α C-chains and other flexible parts not visible in the crystal structure) in solution have also been performed, revealing bending motions of the protein [17]. An atomistic representation of the fibrinogen crystal structure is shown in Figure 1h. The simulations showed that two hinges are responsible for the flexibility of the protein while the rest of the fibrinogen main body does not undergo large conformational changes. Based on these results, a simplified coarse-grained model of fibrinogen was developed (see Figure 1e). In that model, fibrinogen is represented by a stiff central rod connected to two other rods that can pivot around the hinges. The ends of the protein and the central domain are represented as spheres.

The atomistic simulations of fibrinogen in solution were followed by a study of fibrinogen adsorption on mica and graphite, where one half of the symmetric fibrinogen rod was modeled atomistically [18]. The binding of fibrinogen to gold nanoparticles has been studied using a coarse-grained model where fibrinogen was modeled from the crystal structure determined by Kollman et al. [8] and each amino acid residue was represented as a sphere (see Figure 1g). The amino acids interacted via a bonded potential (a sum of potentials for bonds, angles and dihedrals) and a nonbonded potential (two Lennard-Jones-type potentials – one local and one nonlocal) [19].

We used the model depicted in Figure 1g, where each amino acid of the crystal structure is coarse-grained into a sphere. However, we considered the molecule as completely rigid and thus the spheres did not move relative to each other. Such a model was also used by Lopez and Lobaskin [20]. This model has an intermediate level of detail and takes the charge distribution over the molecule into account. This enables us to study the electrostatic effects behind the adsorption of fibrinogen.

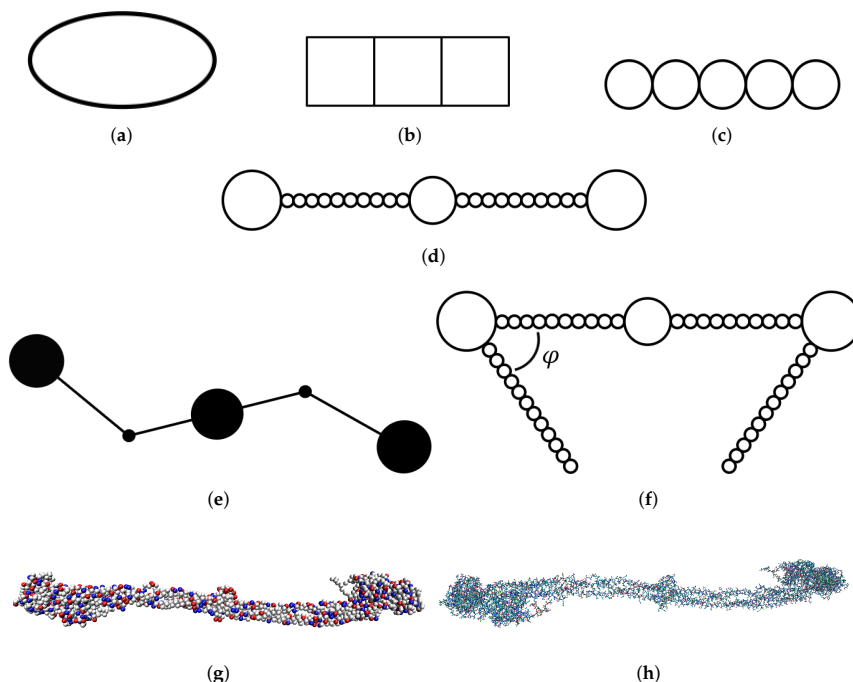


Figure 1. Depiction of models that have been used for simulations of fibrinogen with increasing level of detail: (a) ellipsoid model [11]; (b) rigid connected squares model [12]; (c) rigid linear pentamer model [13]; (d) rigid linear chain model [14,15]; (e) coarse-grained model with two hinges [17]; (f) rigid linear chain model with two side arms and different ϕ angles [16]; (g) coarse-grained model from crystal structure, either completely rigid (this work [20]) or somewhat flexible [19]; and (h) atomistic model from crystal structure [17].

We found that the main body of fibrinogen protrudes more into solution the larger the curvature of the surface. The fibrinogen main body is anchored to the surface by one of its D domains in the same way regardless of the curvature, thus the effect on the protein orientation seems to be solely a function of the curvature. Our model included only electrostatic interactions (and excluded volume), but the results are still similar to those of Lopez and Lobaskin, who studied fibrinogen adsorption onto hydrophobic surfaces [20].

It has been suggested that fibrinogen may adsorb to negatively charged surfaces by means of electrostatic interactions between the net positively charged α C-domains and the surface [22–25]. However, in our present study, the α C-chain was found to have a net negative charge. This difference is likely to be due to the treatment of the histidines. While we treated them as having zero charge, Doolittle et al., for example, used a histidine pK_a of 6.7 to calculate the charge of the A α -chain at pH 7.3, giving a non-negligible charge on the histidines [21].) Our comparison of the free energies of adsorption of the main body and the disordered fragments reveals that there is a stronger attraction between one disordered fragment and the surface than between the fibrinogen main body and the surface.

2. Materials and Methods

2.1. Coarse-Grained Model

The main body of fibrinogen was modeled as a rigid molecule with a structure equal to the crystal structure of human fibrinogen [8]. There is a slight difference between the two molecules that form the asymmetric unit of the structure, and in this study biological assembly 1 was chosen. Each amino acid was modeled as a sphere with a radius of 2.5 Å. This radius gives the sphere a smaller volume than that of most amino acid residues but a more realistic contact separation between charges, which were modeled as point charges located in the centers of the spheres. The pH was set to 7.4. Therefore, the aspartic acid and glutamic acid residues were fully deprotonated (charge -1) while the lysine and arginine residues were fully protonated (charge $+1$). The crystal structure also contained four bound calcium ions with a charge of $+2$ each. The N- and C-terminals were modeled as separate spheres with charges of $+1$ and -1 , respectively. The number of charged histidine residues was estimated to be negligible. All of the positions of the spheres were fixed relative to each other. The synthetic peptides that were present when growing the crystals to determine the crystal structure were not included in our protein model. Since the C-terminal parts of the α -chains were not included in the crystal structure, the charges of the C-terminals of the parts of the α -chains present in the crystal structure were set to zero.

Since some parts of fibrinogen are flexible, most notably the α C-chains, 35 % of the amino acid residues were not visible in the electron density maps, and thus they are not part of the crystal structure determined by Kollman et al. [8]. To determine the role of the α C-chains for adsorption we studied an α C-chain (residues 201–610 of the A α -chain were here counted as the α C-chain since they were not part of the crystal structure) separately using a coarse-grained model that has been used previously for flexible proteins [26–30], with the exception that here the spheres representing amino acids are hard instead of soft. In the present study, the electrostatic interactions were described using Debye–Hückel theory, taking particle size into account using the following expression for the potential energy:

$$w_{ij} = \begin{cases} \frac{e^2}{4\pi\epsilon_0\epsilon_r} \frac{z_i z_j}{r_{ij}(1+\kappa\sigma_{ij})} e^{-\kappa(r_{ij}-\sigma_{ij})}, & r_{ij} \geq \sigma_{ij} \\ \infty, & r_{ij} < \sigma_{ij} \end{cases} \quad (1)$$

where e is the elementary charge, ϵ_0 is the vacuum permittivity, $\epsilon_r = 78.5$ is the relative permittivity of the solvent, r_{ij} is the distance between the centers of particles i and j , z_i is the charge number of i , and σ_{ij} is the distance between the centers of particles i and j at contact. The Debye screening length (κ^{-1}) is calculated from the following equation:

$$\kappa^{-1} = \sqrt{\frac{\epsilon_0\epsilon_r k_B T}{2 \times 10^3 N_A e^2 I}} \quad (2)$$

where k_B is Boltzmann's constant, T is the temperature, N_A is Avogadro's constant and I is the ionic strength of the solution.

The radius of the amino acid spheres was set to 2.0 Å to allow for realistic distances between bonded residues. Bonded amino acids are connected with a harmonic potential:

$$w_b = k_h (R_b - R_{eq})^2 \quad (3)$$

where $k_h = 0.76k_B T / \text{\AA}^2$ is the spring constant, R_b is the bond length between the centers of the spheres, and $R_{eq} = 4.1 \text{\AA}$ is the equilibrium distance of the harmonic potential measured between the centers of the spheres. Non-bonded spheres also interact via a Lennard-Jones potential:

$$w_{LJ} = 4\epsilon_{nb} \left[\left(\frac{\sigma_{ij}}{r_{ij}} \right)^{12} - \left(\frac{\sigma_{ij}}{r_{ij}} \right)^6 \right] \quad (4)$$

where $\epsilon_{nb} = 0.05k_B T$ is the interaction strength. The smooth surface was modeled as completely flat with a smeared charge distribution. The electrostatic interactions between the charged amino acids and the surface were modeled using Gouy–Chapman theory for a 1:1 salt:

$$w_{GC} = 2z_i k_B T \ln \left(\frac{1 + \Gamma_0 e^{-\kappa r_{s,i}}}{1 - \Gamma_0 e^{-\kappa r_{s,i}}} \right), \quad (5)$$

$$\Gamma_0 = \tanh \left[\frac{1}{2} \sinh^{-1} \left(\frac{\rho}{\sqrt{8k_B T c_0 \epsilon_0 \epsilon_r}} \right) \right] \quad (6)$$

where $r_{s,i}$ is the distance between the surface and the center of amino acid i , ρ is the surface charge density, and c_0 is the concentration of 1:1 salt. The concentration of 1:1 salt was set to 0.025 M.

The idea was to compare with the silica surfaces used in the experiments made by Hulander et al. [7], both with and without adsorbed silica nanoparticles. The surfaces were hydrophilic and therefore no hydrophobic attraction between the protein and the surface was included. The charges of the adsorbed nanoparticles were calculated to give the same surface charge density as that of the flat surface and the charges were placed in the centers of the spheres. Adsorption to free nanoparticles was also studied. The nanoparticles interacted with the amino acid beads according to Equation (1). The z -axis constituted the normal to the surface and the boundaries of the simulation box were periodic in the xy -directions. The side lengths of the simulation box varied between 150 and 420 nm depending on the system.

2.2. Method

The simulations were performed using the Metropolis Monte Carlo algorithm [31] in the NVT ensemble. The software used for the simulations was Faunus, a framework for Metropolis Monte Carlo simulations [32]. For the simulations of the main body of fibrinogen, two types of moves were used: translation and rotation of the fibrinogen entity. For the simulations of the α C-chains crankshaft moves (pick two beads randomly and define the vector connecting them as the rotation axis, and then rotate the beads between the picked ones around this axis), pivot moves (define a rotation axis in the same manner as with the crankshaft move, and then rotate the beads at one end of the protein around this axis) and single bead translation were also included.

2.3. Analysis

The angle between the protein main body and the surface of a nanoparticle was found in the following way: a line was drawn between the middle of the protein main body and the middle of the nanoparticle. Then, the cosine of the angle between this line and the protein was recorded.

The radius of gyration (R_g) of the α C-chain was found using the following equation:

$$R_g^2 = \frac{1}{M_w} \sum_{i=1}^N m_i \times (\mathbf{r}_i - \mathbf{r}_{cm})^2, \quad (7)$$

where M_w is the molecular weight of the α C-chain, m_i is the mass of amino acid bead i , N is the number of beads, \mathbf{r}_i is the coordinates of bead i , and \mathbf{r}_{cm} is the coordinates of the chain center-of-mass.

3. Results and Discussion

3.1. Characterization of Fibrinogen

The net charge of the main body of fibrinogen present in the crystal structure is -8 (counting also the bound calcium ions). When including the flexible parts of the $A\alpha$ -chains that are not visible in the crystal structure, the net charge becomes -12 . Figure 2b shows how the charges are distributed over twenty bins in the longitudinal direction of the fibrinogen crystal structure. While the ends and the middle of the protein are net negatively charged, there are also parts of the protein that are net positively charged. These are potentially important for the ability of fibrinogen to adsorb to negatively charged surfaces.

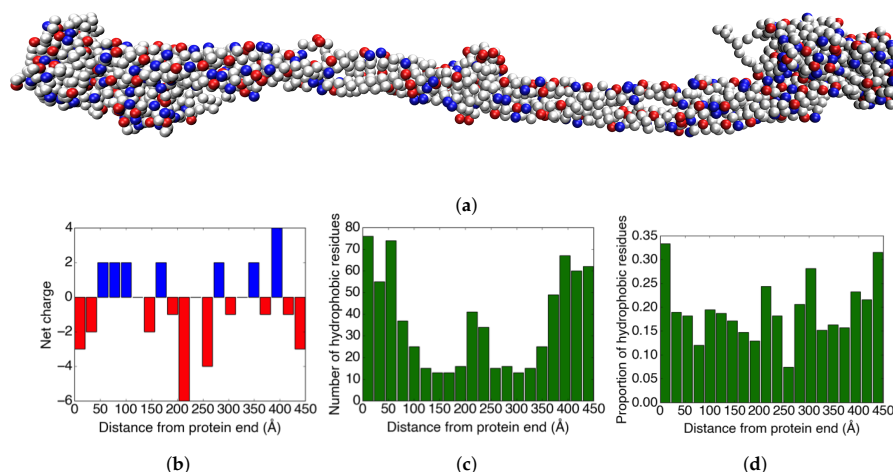


Figure 2. (a) An image of the coarse-grained fibrinogen body from the crystal structure. The red amino acid residues are negatively charged, the blue residues are positively charged, and grey represents neutral residues. (b) The charge distribution in the longitudinal direction of the fibrinogen crystal structure. (c) The distribution of hydrophobic amino acid residues in the longitudinal direction of the fibrinogen crystal structure. (d) The proportion of the $\geq 20\%$ solvent-accessible amino acid residues that are hydrophobic for each bin.

In addition to the charge distribution, the distribution of hydrophobic amino acids on the surface of the protein could also be important for adsorption. Therefore, we studied how the hydrophobic amino acid residues (Ala, Gly, Ile, Leu, Met, Phe, Pro, and Val) are distributed over the protein. Figure 2c shows how the hydrophobic amino acid residues are distributed over the crystal structure of fibrinogen. As expected, there is a clear correlation between the thickness of the protein and the number of hydrophobic amino acid residues (cf. Figure 2a).

Figure 2d displays the proportion of the surface-accessible residues that are hydrophobic for 20 bins in the longitudinal direction of the fibrinogen crystal structure. The solvent-accessible residues were found using Swiss PDB viewer [33], and the threshold for counting the residue as solvent-accessible was set to $\geq 20\%$ solvent accessibility. The results show that the ends of the protein have a surface that is somewhat more hydrophobic than the rest of the protein.

3.2. Adsorption Simulations of the Main Body of Fibrinogen

In the simulations, we studied how different surface charges (density and sign), as well as the presence of charged spherical nanoparticles on the flat surface, affect adsorption of fibrinogen. We

also compared adsorption onto nanoparticles with different size and different spacing on the flat surface. The aim was mainly to explain the finding that adsorbed fibrinogen increases the amount of *S. epidermidis* that adheres to a flat surface, while the presence of adsorbed fibrinogen has the opposite effect when nanoparticles are attached to the flat surface [7].

3.2.1. Adsorption onto a Flat Surface

The surface charge densities used were $\pm 0.001 e/\text{\AA}^2$, $\pm 0.005 e/\text{\AA}^2$, and $\pm 0.01 e/\text{\AA}^2$. Mainly the negatively charged surfaces were investigated. A realistic surface charge density for silica at pH 7.4 and ionic strength 0.025 M would be approximately $-0.001 e/\text{\AA}^2$ according to experimental measurements [34,35]. However, according to simulation results, a realistic surface charge density is $-0.005 e/\text{\AA}^2$ (see the Supplementary Materials).

Figure 3a shows that, for both positive and negative surface charges, the fibrinogen body adsorbs solely due to electrostatic forces if the surface charge is high enough. It seems that different orientations of the protein are preferred depending on the sign of the surface charge, with the protein being more inclined to stand up at the surface if the charge is positive (the mass center of the protein is approximately half of a fibrinogen length away from the surface at one of the two free energy minima). This is also illustrated in Figure 3b, showing the distribution of the cosine of the angles between the adsorbed proteins and the surface normal for the highest surface charge densities. A value of 0 corresponds to the protein lying flat on the surface and a value of 1 to the protein standing up with its axis completely parallel to the normal of the surface. When the surface charge is positive, it is strongly favored that an adsorbed protein lies flat against the surface, although there is also a small maximum at a cosine of ~ 0.9 , which is completely absent when the surface charge is negative.

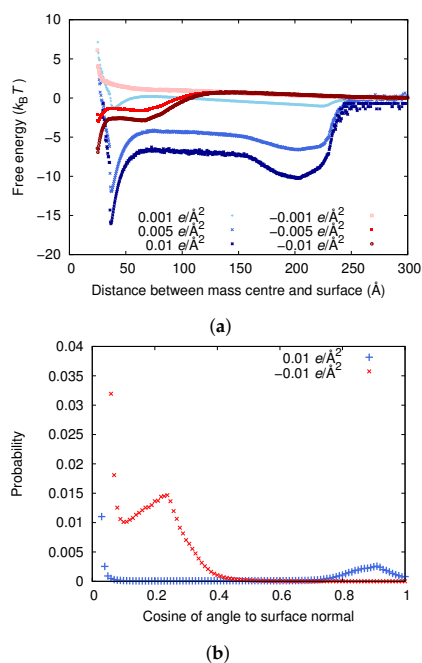


Figure 3. Cont.

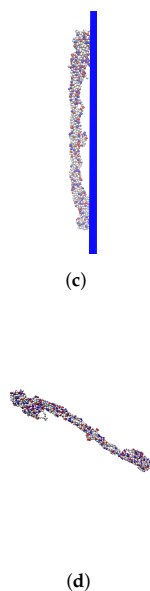


Figure 3. (a) The adsorption free energies for the fibrinogen main body to surfaces with different surface charge densities. (b) Distribution of cosine of the angle between the surface normal and an adsorbed protein for the higher surface charge densities. (The upper limit of the y -axis has been set so that it is possible to view peaks other than the ones for small cosine.) (c) A configuration with cosine close to 0, corresponding to the deepest free energy well when the surface charge is $0.01e/\text{\AA}^2$. (d) A configuration with high cosine, corresponding to the second free energy well when the surface charge is $0.01e/\text{\AA}^2$.

The fact that the fibrinogen main body adsorbs to both positively and negatively charged surfaces, if they are charged enough, emphasizes the importance of local electrostatic interactions between different charged groups in the protein and at the surface. However, since no adsorption is observed at the experimentally determined surface charge of approximately $-0.001e/\text{\AA}^2$ (see Figure 3), something is clearly missing in the model. It is probable that the experimental methods do not yield the surface charge exactly at the surface. Kubiak et al. calculated a surface charge density by using Gouy–Chapman theory to convert ζ -potential to charge density [25]. Even though the charge of the slipping plane (where the ζ -potential is measured) should probably be considerably lower than the surface charge, they found the same charge magnitude as those measured by Bolt [34] and Samoshina et al. [35]. Therefore, the surface charge of $-0.005e/\text{\AA}^2$ determined by simulations (see the Supplementary Materials) may be more reliable.

It might also be the case that other attractive forces need to be included in the simulations in order for them to match experiments. These could represent van der Waals forces or hydrogen bonding between the surface and the protein. In addition, electrostatic attraction tends to increase when having explicit surface charges and explicit ions in the solvent, which we did not have. Another possibility is that the repulsion is overestimated since the amino acids are treated as hard spheres.

3.2.2. Adsorption Onto a Surface with Attached Nanoparticles

Table 1 shows a comparison between the adsorbed fractions of fibrinogen on the flat surfaces and the surfaces with attached nanoparticles. The nanoparticles had a radius of 20 nm and the surface coverage was 40 %. The nanoparticles were hexagonally packed. The simulations show that fibrinogen adsorbs more often on the nanostructured surfaces than on the flat surfaces in the simulations, in agreement with previous QCM-D measurements [7].

Table 1. The proportions of the fibrinogen main body that are adsorbed in simulations with flat and nanostructured surfaces.

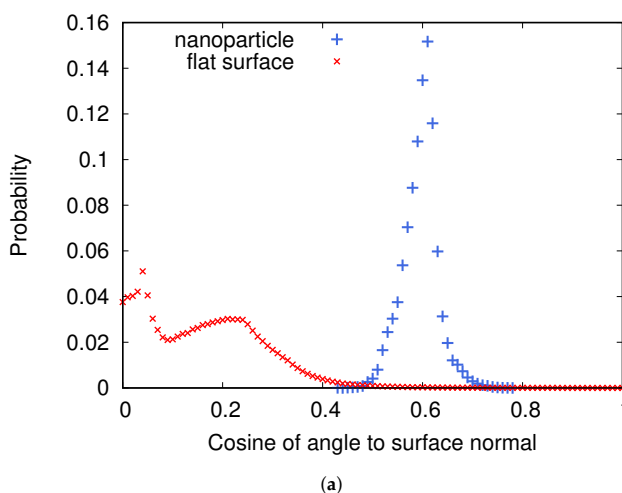
| Surface Type | Charge Density ($e/\text{\AA}^2$) | Adsorbed Proportion (%) |
|----------------|-------------------------------------|-------------------------|
| Flat | −0.001 | 0.503 |
| Nanostructured | −0.001 | 2.17 |
| Flat | −0.005 | 7.88 |
| Nanostructured | −0.005 | 100 |
| Flat | −0.01 | 39.2 |
| Nanostructured | −0.01 | 100 |

The fact that adsorption is higher on nanostructured surfaces is partly due to the fact that they have a larger available surface area due to the added nanoparticles. However, Rechendorff et al., who studied adsorption of fibrinogen onto surfaces with different degrees of roughness, found that the adsorbed amount of fibrinogen increased more with roughness than the available surface area did [36]. Using Monte Carlo simulations, they found that fibrinogen is likely to adsorb to a higher degree with an end-on orientation on the rough surfaces, increasing the number of fibrinogen molecules that can bind.

Another reason for the increase in adsorption could be that the total charge of the nanoparticles and the flat surface is larger than that of the flat surface alone, which should increase the adsorption according to Figure 3a.

Figure 4a shows the distributions of cosine of the angle between a nanoparticle and an adsorbed fibrinogen and between the flat surface and an adsorbed fibrinogen when the surface charge density is $-0.005e/\text{\AA}^2$. On the flat surface, fibrinogen prefers to adsorb with the whole main body close to the surface, while on the nanoparticles it protrudes further out in the solution. Figure 4b–c shows two preferred orientations of fibrinogen adsorbed on the two types of surfaces.

It appears that one of the D domains adsorbs close to the surface, and that the angle between the D domain and the rest of the fibrinogen rod, combined with the surface curvature, determines the angle between the entire fibrinogen main body and the surface.

**Figure 4.** Cont.

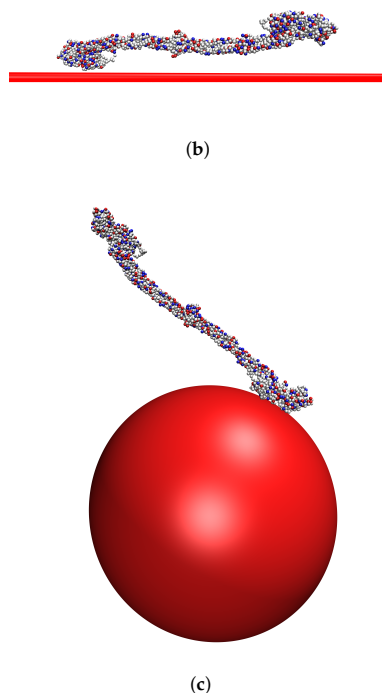


Figure 4. (a) The distributions of cosine of the angle between fibrinogen and the normal to the surface it is adsorbed to for two cases: when adsorbed to a nanoparticle attached to a flat surface and when adsorbed to a flat surface without nanoparticles. The surface charge density is $-0.005e/\text{\AA}^2$. (b) A typical orientation of fibrinogen adsorbed on the flat surface. (c) A typical orientation of fibrinogen adsorbed on a nanoparticle.

3.2.3. Adsorption Onto Nanoparticles with Different Size

The results show that fibrinogen adsorbs more strongly to small nanoparticles (see Figure 5), and more fibrinogen adsorbs to smaller nanoparticles per surface area (see Table 2). (Since essentially all protein adsorbs for the higher surface charges, only results from the lowest charge are shown here and in corresponding tables). However, while more fibrinogen adsorbs to small nanoparticles than larger ones per surface area, less fibrinogen adsorbs to the small nanoparticles than the larger ones if comparing adsorbed amount per nanoparticle (see Table 2).

The fact that less fibrinogen adsorbs to the small nanoparticles than the larger ones, if comparing the adsorbed amount per nanoparticle, is of course due to the larger surface area of the larger nanoparticles. This result is in agreement with the results of Lundqvist et al., showing a larger protein adsorption on larger nanoparticles for a constant nanoparticle concentration [37]. However, Lundqvist et al. could not determine whether this was due to the difference in curvature of the particles or the difference in available surface area between the samples.

The explanation for the observation that fibrinogen binds more strongly to smaller nanoparticles may lie in the fact that the ends of the rigid part of the fibrinogen molecule are approximately neutral (see Figure 2b), with several positive charges available for favorable interaction with the surface, while the middle of the molecule is negatively charged. Thus, if the positive charges at one end of the protein bind to the negative surface in the same way regardless of the surface curvature, the adsorption is more

favorable the further away from the surface that the negatively charged middle part of the protein ends up.

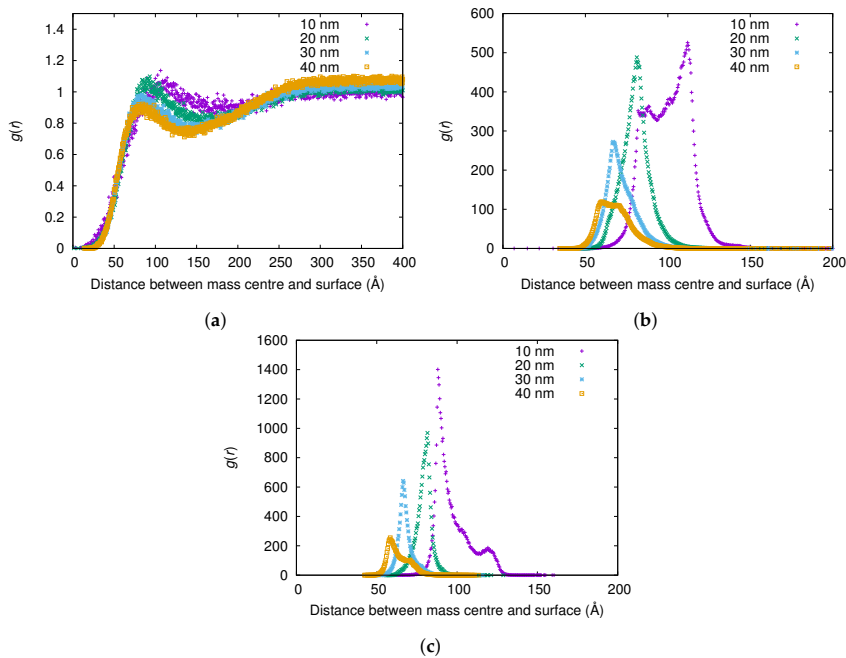


Figure 5. The radial distribution function $g(r)$ between the surface of the nanoparticle and the mass center of the main body of fibrinogen for different nanoparticle radii and surface charge densities: (a) $-0.001e/\text{\AA}^2$; (b) $-0.005e/\text{\AA}^2$; and (c) $-0.01e/\text{\AA}^2$. The $g(r)$ are normalized using the (constant) concentration of fibrinogen in the simulation box instead of a bulk concentration for each simulation, since reliable bulk concentrations could not be determined from the simulations with highest attraction to the surface.

Table 2. The adsorbed proportion of the fibrinogen main body per surface area in simulations with a single nanoparticle with different radii when the surface charge density is $-0.001e/\text{\AA}^2$.

| Nanoparticle Radius (nm) | Adsorbed Proportion (%) | Adsorbed Proportion/Surface Area (10^{-6} nm^{-2}) |
|--------------------------|-------------------------|--|
| 10 | 0.179 | 3.78 |
| 20 | 0.474 | 1.64 |
| 30 | 0.825 | 0.729 |
| 40 | 1.27 | 0.628 |

The angle between the adsorbed fibrinogen molecule and the surface of the nanoparticle increases as the size of the nanoparticle decreases (see Figure 6). This is due to the fact that fibrinogen adsorbs with one of its ends on the surface of the particle in a similar way regardless of the nanoparticle size, and the higher is the curvature of the particle, the larger is the angle. Similar results were obtained by Lopez and Lobaskin for fibrinogen adsorption onto hydrophobic nanoparticles [20].

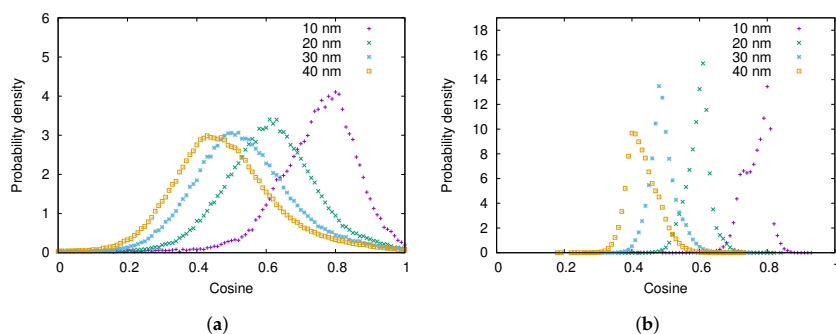


Figure 6. The distribution of cosine of the angle between the surface normal and the adsorbed fibrinogen main body for different nanoparticle radii when the surface charge density is: (a) $-0.001e/\text{\AA}^2$; and (b) $-0.005e/\text{\AA}^2$.

3.2.4. Adsorption Onto Nanostructured Surfaces with Different Nanoparticle Size

Here, adsorption of the fibrinogen main body onto surfaces with attached nanoparticles of different sizes are compared. Firstly, the number density of nanoparticles on the surface is held constant (distance between centers of nearest neighbors = 60 nm) and, secondly, the surface coverage of the nanoparticles is constant (40 %). The nanoparticle radii are 10, 20, and 30 nm. On all surfaces studied here, the nanoparticles were packed hexagonally. When the nanoparticle number density is constant, the adsorbed fraction of fibrinogen is highest for a nanoparticle radius of 20 nm (see the second column of Table 3). When the nanoparticle radius is increased from 10 to 20 nm, the available surface area increases since the nanoparticles become larger and thus contribute with more surface area. However, when the nanoparticle radius is further increased to 30 nm, the spheres are in contact with each other and thus the available surface area decreases. Thus, in this case, the nanoparticles with 20 nm radius give maximum adsorption since they give the largest available surface area.

Table 3. The adsorbed proportion of the fibrinogen main body in simulations with flat surfaces with attached nanoparticles with different radii for a fixed distance between centers of nearest neighbors (nn) and a fixed surface coverage of nanoparticles (sc). The surface charge density for the flat surface and the nanoparticles is $-0.001e/\text{\AA}^2$.

| Nanoparticle Radius (nm) | Adsorbed Proportion (%), nn = 60 nm | Adsorbed Proportion (%), sc = 40 % |
|--------------------------|-------------------------------------|------------------------------------|
| 10 | 1.05 | 1.50 |
| 20 | 2.17 | 2.17 |
| 30 | 1.46 | 2.73 |

When the nanoparticle surface coverage is constant at 40 %, the adsorbed fraction increases with nanoparticle size for all sizes used, see the third column of Table 3. Here, the total surface area of the spheres is the same for all three nanoparticle radii. Thus, it could be expected from the results of the simulations with single nanoparticles that more fibrinogen would adsorb onto the surface with small nanoparticles. However, when the small nanoparticles are attached to a flat surface, a larger proportion of the surface area of each sphere is blocked by the flat surface than for the larger spheres. This makes the surface area that is available for fibrinogen adsorption smaller for surfaces with smaller attached nanoparticles.

3.2.5. Adsorption Onto Nanostructured Surfaces with Different Nanoparticle Spacing

Simulations with nanostructured surfaces with nanoparticles of 20 nm radius were performed for different spacings between the nanoparticles. The center-to-center distance between nearest neighbors was varied between 40 and 90 nm in steps of 10 nm. The adsorbed fractions are shown in Figure 7.

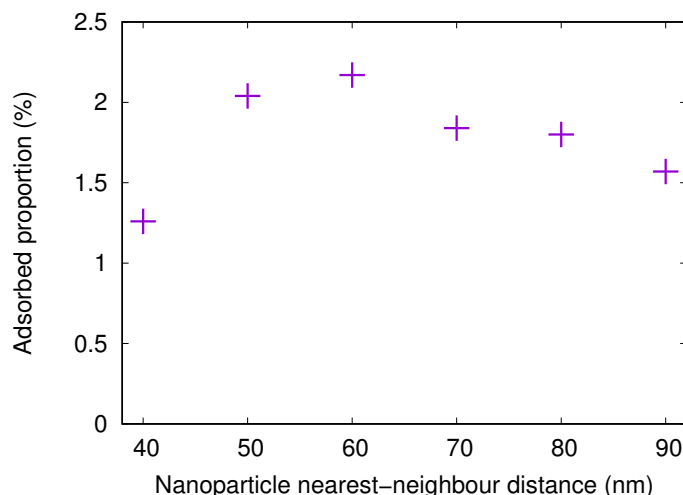


Figure 7. The adsorbed proportion of the fibrinogen main body in simulations with flat surfaces with attached nanoparticles (20 nm radius) with different distances between centers of nearest neighbors. The surface charge density for the flat surface and the nanoparticles is $-0.001e/\text{\AA}^2$.

The adsorbed amount onto a surface with attached nanoparticles with a radius of 20 nm increases when the nearest neighbor center-to-center distance increases from 40 to 60 nm. This is due to the fact that, when the nanoparticles are close to each other, it is difficult or impossible for the protein to adsorb between the nanoparticles. However, for 60 nm spacing, the available surface area is large. As the spacing increases even more, the nanoparticles become fewer, thus reducing the available surface area and the adsorbed amount.

3.3. Simulations of the α C-Chain of Fibrinogen

3.3.1. Simulations in Bulk and with a Flat Surface

The charges of the α C-chain are relatively evenly distributed over the molecule (see Figure 8a). However, some parts of the chain are net positively charged, possibly contributing to the adsorption of the chain on a negatively charged surface. Figure 8d shows that the α C-chain adsorbs electrostatically to surfaces with charge densities of $-0.005 e/\text{\AA}^2$ and $-0.01 e/\text{\AA}^2$, as the main body of fibrinogen did. However, the free energy minima for the α C-chain is lower than for the fibrinogen main body (Figure 3a). Figure 8b shows the distribution of the radius of gyration of the α C-chain in bulk and Figure 8c shows the distribution of the shape factor, R_{ee}^2/R_g^2 , where R_{ee} is the end-to-end distance and R_g is the radius of gyration. A shape factor of 6 is characteristic of a Gaussian chain and a shape factor of 12 corresponds to a rigid rod. Thus, the α C-chain behaves as a Gaussian chain in the simulations.

A comparison between the free energies in Figures 3 and 8 shows that the α C-chains are important for the adsorption of the complete fibrinogen since the free energy minimum is lower than for the fibrinogen main body.

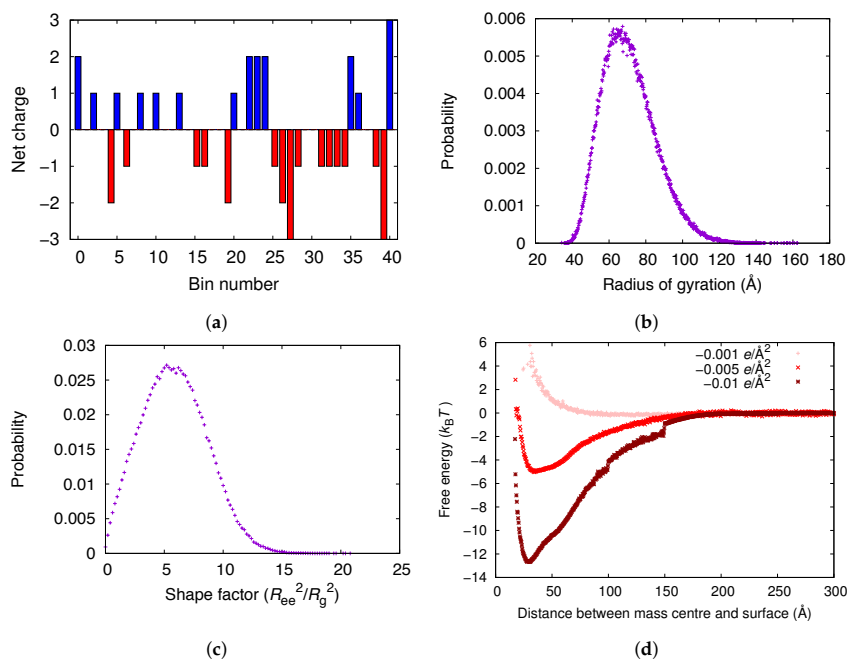


Figure 8. (a) The distribution of charges of the α C-chain divided into 41 bins (10 amino acid residues per bin) starting from the N-terminal. The negative charge of the C-terminal is included. (b) The distribution of the radius of gyration of the α C-chain in bulk. (c) The distribution of the shape factor of the α C-chain in bulk. (d) The adsorption free energies for the α C-chain to surfaces with different negative surface charge densities.

3.3.2. Adsorption onto different types of surfaces

Table 4 shows the proportions of the α C-chain that adsorbs to a flat and a nanostructured surface, respectively, in the simulations. The nanostructured surface is the same as in Section 3.2.2. The trends are the same as for the main body of fibrinogen (Table 1) but the adsorbed amounts of the α C-chain are higher, again showing the importance of the α C-chains for the overall adsorption.

Table 4. The proportions of the fibrinogen α C-chain that are adsorbed in simulations with flat and nanostructured surfaces.

| Surface Type | Charge Density ($e/\text{\AA}^2$) | Adsorbed Proportion (%) |
|----------------|-------------------------------------|-------------------------|
| Flat | -0.001 | 1.23 |
| Nanostructured | -0.001 | 3.14 |
| Flat | -0.005 | 60.1 |
| Nanostructured | -0.005 | 100 |
| Flat | -0.01 | 100 |
| Nanostructured | -0.01 | 100 |

3.3.3. Adsorption Onto Nanoparticles with Different Size

From $g(r)$ in Figure 9a, no significant difference can be observed between the adsorption of the α C-chain of fibrinogen onto nanoparticles with radii of 10, 20, 30, and 40 nm when the surface charge density is $-0.001 e/\text{\AA}^2$. However, when the surface charge density is $-0.01 e/\text{\AA}^2$, the α C-chain adsorbs more strongly to the smallest nanoparticle (radius 10 nm) (see Figure 9b).

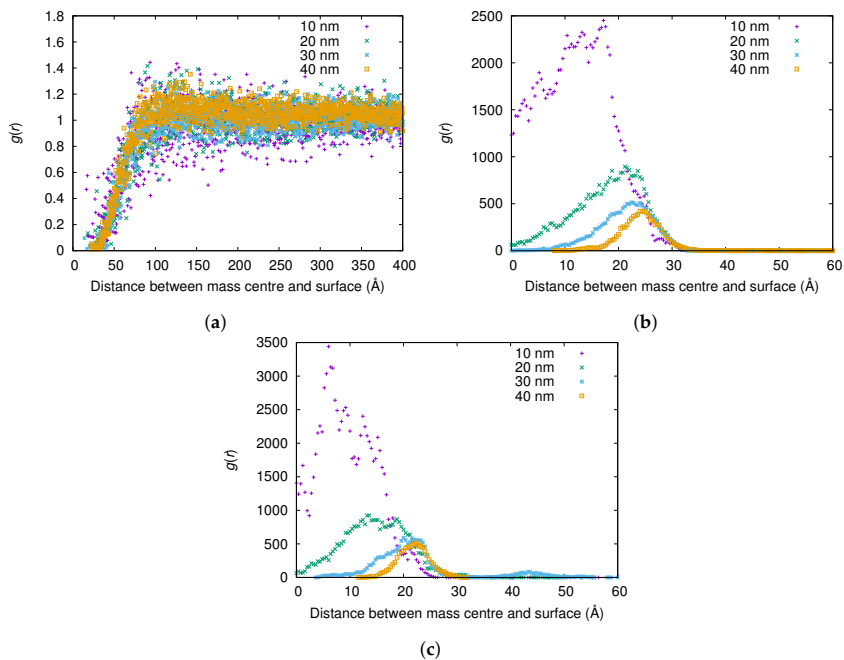


Figure 9. The radial distribution function $g(r)$ between the surface of the nanoparticle and the mass center of the α C-chain for different nanoparticle radii and surface charge densities: (a) $-0.001e/\text{\AA}^2$; (b) $-0.005e/\text{\AA}^2$; and (c) $-0.01e/\text{\AA}^2$. The $g(r)$ are normalized using the (constant) concentration of the α C-chain in the simulation box instead of a bulk concentration for each simulation, since reliable bulk concentrations could not be determined from the simulations with highest attraction to the surface.

Table 5, however, shows that more of the α C-chain adsorbs on the smaller nanoparticles (radii 10 and 20 nm) per surface area also for the lower surface charge density of $-0.001e/\text{\AA}^2$.

Table 5. The adsorbed proportion of the α C-chain of fibrinogen per surface area in simulations with a single nanoparticle with different radii when the surface charge density is $-0.001e/\text{\AA}^2$.

| Nanoparticle Radius (nm) | Adsorbed Proportion (%) | Adsorbed Proportion/Surface Area (10^{-6} nm^{-2}) |
|--------------------------|-------------------------|--|
| 10 | 0.128 | 1.02 |
| 20 | 0.392 | 0.781 |
| 30 | 0.774 | 0.684 |
| 40 | 1.38 | 0.687 |

The trends here are the same as for the main body of fibrinogen. The reason could be that, due to the smaller surface area of the 10-nm nanoparticles, negative amino acid residues on an adsorbed protein that are further away from the surface do not feel as much repulsion as they would in the same conformation adsorbed on a larger nanoparticle.

3.3.4. Adsorption Onto Nanostructured Surfaces with Different Nanoparticle Size

Here, the results from adsorption simulations of the α C-chain onto the same nanostructured surfaces as studied for the fibrinogen main body (Section 3.2.4) is presented. The trends for the adsorbed fractions are the same as for the fibrinogen main body (cf. Tables 3 and 6). The reason is the same as described previously—the trends follow the available surface area.

Table 6. The adsorbed proportion of the fibrinogen α C-chain in simulations with flat surfaces with attached nanoparticles with different radii for a fixed distance between centers of nearest neighbors (nn) and a fixed surface coverage of nanoparticles (sc). The surface charge density for the flat surface and the nanoparticles is $-0.001e/\text{\AA}^2$.

| Nanoparticle Radius (nm) | Adsorbed Proportion (%), nn = 60 nm | Adsorbed Proportion (%), sc = 40 % |
|--------------------------|-------------------------------------|------------------------------------|
| 10 | 1.54 | 1.69 |
| 20 | 3.15 | 3.15 |
| 30 | 1.95 | 3.34 |

3.3.5. Adsorption Onto Nanostructured Surfaces with Different Nanoparticle Spacing

Here, results from simulations with nanostructured surfaces with nanoparticles of 20 nm radius and different spacings are presented. The adsorbed fractions are shown in Figure 10. The trends are the same as for the fibrinogen main body, with the highest adsorbed amount when the distance between the centers of neighboring particles is 60 nm. Here, the optimal combination of available surface area *between* the particles and available surface area *on* the particles is found.

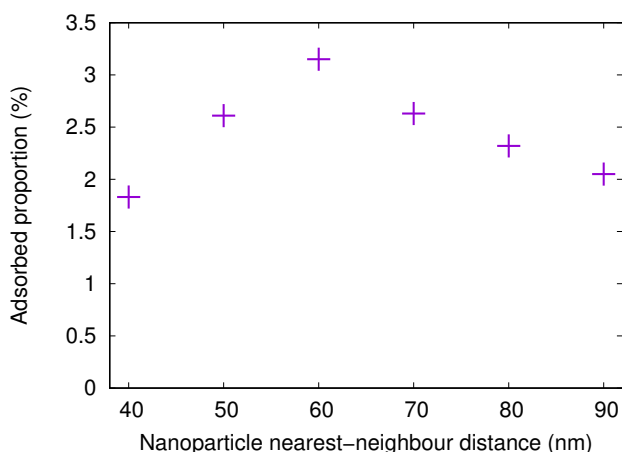


Figure 10. The adsorbed proportion of the fibrinogen α C-chain in simulations with flat surfaces with attached nanoparticles (20 nm radius) with different distances between centers of nearest neighbors. The surface charge density for the flat surface and the nanoparticles is $-0.001e/\text{\AA}^2$.

4. Conclusions

We used coarse-grained simulations to study the adsorption of the fibrinogen main body, as well as the fibrinogen α C-chain, on negatively charged smooth surfaces, nanospheres, and flat surfaces with attached nanospheres.

Our study confirms that the disordered α C-chains of fibrinogen are important for adsorption on negatively charged surfaces. A single α C-chain attaches more firmly than the fibrinogen main body.

When fibrinogen adsorbs to surfaces with attached nanospheres, the available surface area is generally what determines the proportion of fibrinogen that is adsorbed. However, when the different parts of the fibrinogen molecule are adsorbed to spherical nanoparticles in solution, the adsorbed amount per surface area increases as the size of the nanoparticle decreases. The reason could be that that negatively charged amino acid residues feel less repulsion from the negatively charged nanoparticle the smaller it is, since the surface area is smaller.

We found that the main body of fibrinogen protrudes more into solution as the curvature of the surface increases, and that the main body of fibrinogen is anchored to the surface through one of is

D-domains. This was found true regardless of the surface curvature and the orientation therefore seems to be solely a function of the surface curvature. Thus, we hypothesize that fibrinogen adsorbed on surfaces with attached nanoparticles makes cell-binding epitopes less available to attaching cells. This could explain previous findings where the adhesion of *S. epidermidis* was hampered on fibrinogen adsorbed to nanostructured compared to smooth substrates.

Supplementary Materials: The following are available online at

<http://www.mdpi.com/2218-273X/10/3/413/s1>, Figure S1: title, Table S1: title, Video S1: title.

Author Contributions: Conceptualization, K.H., M.H., M.A., and M.S.; Data curation, K.H.; Formal analysis, K.H.; Funding acquisition, M.S.; Investigation, K.H.; Methodology, K.H. and M.S.; Project administration, M.H. and M.S.; Resources, M.S.; Software, K.H.; Supervision, M.H., M.A., and M.S.; Validation, K.H.; Visualization, K.H.; Writing—original draft, K.H.; and Writing—review and editing, K.H., M.H., M.A., and M.S. All authors have read and agreed to the published version of the manuscript.

Funding: This research received no external funding.

Acknowledgments: The simulations were performed on resources provided by the Swedish National Infrastructure for Computing (SNIC) at the center for scientific and technical computing at Lund University (LUNARC).

Conflicts of Interest: The authors declare no conflict of interest. The funders had no role in the design of the study; in the collection, analyses, or interpretation of data; in the writing of the manuscript, or in the decision to publish the results.

References

1. Pei, L.; Palma, M.; Nilsson, M.; Guss, B.; Flock, J.I. Functional Studies of a Fibrinogen Binding Protein from *Staphylococcus epidermidis*. *Infect. Immun.* **1999**, *67*, 4525–4530, Available online: <https://iai.asm.org/content/67/9/4525.full.pdf>
2. Davis, S.L.; Gurusiddappa, S.; McCrea, K.W.; Perkins, S.; Höök, M. SdrG, a Fibrinogen-binding Bacterial Adhesin of the Microbial Surface Components Recognizing Adhesive Matrix Molecules Subfamily from *Staphylococcus epidermidis*, Targets the Thrombin Cleavage Site in the B β Chain. *J. Biol. Chem.* **2001**, *276*, 27799–27805, doi:10.1074/jbc.M103873200.
3. Arciola, C.R.; Campoccia, D.; Gamberini, S.; Donati, M.; Montanaro, L. Presence of fibrinogen-binding adhesin gene in *Staphylococcus epidermidis* isolates from central venous catheters-associated and orthopaedic implant-associated infections. *Biomaterials* **2004**, *25*, 4825–4829, doi:10.1016/j.biomaterials.2003.11.056.
4. Hu, W.J.; Eaton, J.W.; Ugarova, T.P.; Tang, L. Molecular basis of biomaterial-mediated foreign body reactions. *Blood* **2001**, *98*, 1231–1238.
5. Ramasamy, M.; Lee, J. Recent nanotechnology approaches for prevention and treatment of biofilm-associated infections on medical devices. *BioMed Res. Int.* **2016**, *2016*, doi:10.1155/2016/1851242.
6. McCann, M.T.; Gilmore, B.F.; Gorman, S.P. *Staphylococcus epidermidis* device-related infections: Pathogenesis and clinical management. *J. Pharm. Pharmacol.* **2008**, *60*, 1551–1571.
7. Hulander, M.; Valen-Rukke, H.; Sundell, G.; Andersson, M. Influence of Fibrinogen on *Staphylococcus epidermidis* Adhesion Can Be Reversed by Tuning Surface Nanotopography. *ACS Biomater. Sci. Eng.* **2019**, *5*, 4323–4330, doi:10.1021/acsbomaterials.9b00450.
8. Kollman, J.M.; Pandi, L.; Sawaya, M.R.; Riley, M.; Doolittle, R.F. Crystal Structure of Human Fibrinogen. *Biochemistry* **2009**, *48*, 3877–3886, doi:10.1021/bi802205g, PMID: 19296670.
9. Burton, R.A.; Tsurupa, G.; Medved, L.; Tjandra, N. Identification of an Ordered Compact Structure within the Recombinant Bovine Fibrinogen α C-Domain Fragment by NMR. *Biochemistry* **2006**, *45*, 2257–2266, doi:10.1021/bi052380c, PMID: 16475814.
10. Tsurupa, G.; Hantgan, R.R.; Burton, R.A.; Pechik, I.; Tjandra, N.; Medved, L. Structure, Stability, and Interaction of the Fibrin(ogen) α C-Domains. *Biochemistry* **2009**, *48*, 12191–12201, doi:10.1021/bi901640e, PMID: 19928926.
11. Vilaseca, P.; Dawson, K.A.; Franzese, G. Understanding and modulating the competitive surface-adsorption of proteins through coarse-grained molecular dynamics simulations. *Soft Matter* **2013**, *9*, 6978–6985.

12. Siegismund, D.; Keller, T.F.; Jandt, K.D.; Rettenmayr, M. Fibrinogen Adsorption on Biomaterials—A Numerical Study. *Macromol. Biosci.* **2010**, *10*, 1216–1223, doi:10.1002/mabi.201000120.
13. Zhdanov, V.P.; Rechendorff, K.; Hovgaard, M.B.; Besenbacher, F. Deposition at Glancing Angle, Surface Roughness, and Protein Adsorption: Monte Carlo Simulations. *J. Phys. Chem. B* **2008**, *112*, 7267–7272, doi:10.1021/jp709806k, PMID: 18503271.
14. Adamczyk, Z.; Barbasz, J.; Cieřla, M. Kinetics of Fibrinogen Adsorption on Hydrophilic Substrates. *Langmuir* **2010**, *26*, 11934–11945, doi:10.1021/la101261f, PMID: 20575543.
15. Adamczyk, Z.; Barbasz, J.; Cieřla, M. Mechanisms of Fibrinogen Adsorption at Solid Substrates. *Langmuir* **2011**, *27*, 6868–6878, doi:10.1021/la200798d, PMID: 21545097.
16. Adamczyk, Z.; Cichocki, B.; Ekiel-Jeřewska, M.L.; Słowicka, A.; Wajnryb, E.; Wasilewska, M. Fibrinogen conformations and charge in electrolyte solutions derived from DLS and dynamic viscosit measurements. *J. Colloid Interface Sci.* **2012**, *385*, 244–257, doi:10.1016/j.jcis.2012.07.010.
17. Köhler, S.; Schmid, F.; Settanni, G. The Internal Dynamics of Fibrinogen and Its Implications for Coagulation and Adsorption. *PLOS Comput. Biol.* **2015**, *11*, e1004346, doi:10.1371/journal.pcbi.1004346.
18. Köhler, S.; Schmid, F.; Settanni, G. Molecular Dynamics Simulations of the Initial Adsorption Stages of Fibrinogen on Mica and Graphite Surfaces. *Langmuir* **2015**, *31*, 13180–13190, doi:10.1021/acs.langmuir.5b03371, PMID: 26569042.
19. Tavanti, F.; Pedone, A.; Menziani, M.C. Competitive Binding of Proteins to Gold Nanoparticles Disclosed by Molecular Dynamics Simulations. *J. Phys. Chem. C* **2015**, *119*, 22172–22180, doi:10.1021/acs.jpcc.5b05796.
20. Lopez, H.; Lobaskin, V. Coarse-grained model of adsorption of blood plasma proteins onto nanoparticles. *J. Chem. Phys.* **2015**, *143*, 243138, doi:10.1063/1.4936908.
21. Doolittle, R.; Watt, K.; Cottrell, B.; Strong, D.; Riley, M. The amino acid sequence of the α -chain of human fibrinogen. *Nature* **1979**, *280*, 464.
22. Jung, S.Y.; Lim, S.M.; Albertorio, F.; Kim, G.; Gurau, M.C.; Yang, R.D.; Holden, M.A.; Cremer, P.S. The Vroman Effect: A Molecular Level Description of Fibrinogen Displacement. *J. Am. Chem. Soc.* **2003**, *125*, 12782–12786, doi:10.1021/ja037263o, PMID: 14558825.
23. Marchin, K.L.; Berrie, C.L. Conformational Changes in the Plasma Protein Fibrinogen upon Adsorption to Graphite and Mica Investigated by Atomic Force Microscopy. *Langmuir* **2003**, *19*, 9883–9888, doi:10.1021/la035127r.
24. Lin, Y.; Wang, J.; Wan, L.J.; Fang, X.H. Study of fibrinogen adsorption on self-assembled monolayers on Au(111) by atomic force microscopy. *Ultramicroscopy* **2005**, *105*, 129–136, doi:10.1016/j.ultramic.2005.06.028.
25. Kubiak, K.; Adamczyk, Z.; Wasilewska, M. Mechanisms of fibrinogen adsorption at the silica substrate determined by QCM-D measurements. *J. Colloid Interface Sci.* **2015**, *457*, 378–387, doi:10.1016/j.jcis.2015.07.009.
26. Evers, C.H.; Andersson, T.; Lund, M.; Skepö, M. Adsorption of Unstructured Protein β -Casein to Hydrophobic and Charged Surfaces. *Langmuir* **2012**, *28*, 11843–11849, doi:10.1021/la300892p, PMID: 22783871.
27. Kurut, A.; Henriques, J.; Forsman, J.; Skepö, M.; Lund, M. Role of histidine for charge regulation of unstructured peptides at interfaces and in bulk. *Proteins Struct. Funct. Bioinf.* **2014**, *82*, 657–667, doi:10.1002/prot.24445.
28. Henriques, J.; Skepö, M. A coarse-grained model for flexible (phospho)proteins: Adsorption and bulk properties. *Food Hydrocoll.* **2015**, *43*, 473–480, doi:10.1016/j.foodhyd.2014.07.002.
29. Hyltegren, K.; Nylander, T.; Lund, M.; Skepö, M. Adsorption of the intrinsically disordered saliva protein histatin 5 to silica surfaces. A Monte Carlo simulation and ellipsometry study. *J. Colloid Interface Sci.* **2016**, *467*, 280 – 290, doi:10.1016/j.jcis.2016.01.025.
30. Hyltegren, K.; Skepö, M. Adsorption of polyelectrolyte-like proteins to silica surfaces and the impact of pH on the response to ionic strength. A Monte Carlo simulation and ellipsometry study. *J. Colloid Interface Sci.* **2017**, *494*, 266–273.
31. Metropolis, N.; Rosenbluth, A.W.; Rosenbluth, M.N.; Teller, A.H.; Teller, E. Equation of State Calculations by Fast Computing Machines. *J. Chem. Phys.* **1953**, *21*, 1087–1092, doi:10.1063/1.1699114.
32. Stenqvist, B.; Thuresson, A.; Kurut, A.; Vácha, R.; Lund, M. Faunus—A flexible framework for Monte Carlo simulation. *Mol. Simul.* **2013**, *39*, 1233–1239, doi:10.1080/08927022.2013.828207.
33. Guex, N.; Peitsch, M.C. SWISS-MODEL and the Swiss-Pdb Viewer: An environment for comparative protein modeling. *Electrophoresis* **1997**, *18*, 2714–2723.
34. Bolt, G.H. Determination of the Charge Density of Silica Sols. *J. Phys. Chem.* **1957**, *61*, 1166–1169, doi:10.1021/j150555a007.

35. Samoshina, Y.; Nylander, T.; Shubin, V.; Bauer, R.; Eskilsson, K. Equilibrium Aspects of Polycation Adsorption on Silica Surface: How the Adsorbed Layer Responds to Changes in Bulk Solution. *Langmuir* **2005**, *21*, 5872–5881, doi:10.1021/la050069q, PMID: 15952836.
36. Rechendorff, K.; Hovgaard, M.B.; Foss, M.; Zhdanov, V.P.; Besenbacher, F. Enhancement of Protein Adsorption Induced by Surface Roughness. *Langmuir* **2006**, *22*, 10885–10888, doi:10.1021/la0621923, PMID: 17154557.
37. Lundqvist, M.; Sethson, I.; Jonsson, B.H. Protein Adsorption onto Silica Nanoparticles: Conformational Changes Depend on the Particles' Curvature and the Protein Stability. *Langmuir* **2004**, *20*, 10639–10647, doi:10.1021/la0484725, PMID: 15544396.



© 2020 by the authors. Licensee MDPI, Basel, Switzerland. This article is an open access article distributed under the terms and conditions of the Creative Commons Attribution (CC BY) license (<http://creativecommons.org/licenses/by/4.0/>).

Supplementary Material

Kristin Hyltegren, Mats Hulander, Martin Andersson, Marie Skepö

Table 1 shows the different sets of parameters from different sources that were used for simulating titrating silica surfaces with Faunus [6]. Tables 2–3 show the simulation results for the surface charge density and the ratio between simulated charge and the experimentally reported charge by Samoshina et al. [5] for ionic strengths of 10 and 100 mM, respectively. The charges were placed on a square lattice in the simulations.

On average, the surface charge density from simulations was 5.0 times the experimentally determined charge.

| Parameter set | pK _a 1 | Percentage (%) | pK _a 2 | Percentage (%) | Silanol group density (Å ⁻²) |
|---------------|-------------------|----------------|-------------------|----------------|--|
| 1 [4] | 7.6 | 100 | - | - | 0.08 |
| 2 [3] | 4.5 | 19 | 8.5 | 81 | 0.049 |
| 3 [2] | 5.5 | 15 | 9.0 | 85 | 0.049 |
| 4 [1] | 7.1 | 100 | - | - | 0.049 |

Table 1: The four sets of parameters that were used for titrating surface simulations and the references for the parameter sets. Some find that there are two types of silanol groups with different pK_a values while others find only one type of group.

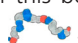


| Parameter set | Charge density (e/Å ²) | Simulated charge/experimental |
|---------------|------------------------------------|-------------------------------|
| 1 | -0.00198 | 3.17 |
| 2 | -0.00477 | 7.64 |
| 3 | -0.00318 | 5.09 |
| 4 | -0.00238 | 3.81 |

Table 2: Charge densities found from titrating silica surface simulations at pH 7 and ionic strength 10 mM and their relation to the experimentally determined surface charge.

| Parameter set | Charge density (e/Å ²) | Simulated charge/experimental |
|---------------|------------------------------------|-------------------------------|
| 1 | -0.00467 | 3.74 |
| 2 | -0.00877 | 7.03 |
| 3 | -0.00600 | 4.81 |
| 4 | -0.00595 | 4.76 |

References

- [1] Michael L Hair and William Hertl. “Acidity of surface hydroxyl groups”. In: *J. Phys. Chem.* 74.1 (1970), pp. 91–94.
- [2] Lawrence H Allen, Egon Matijevic, and Louis Meites. “Exchange of Na⁺ for the silanolic protons of silica”. In: *J. Inorg. Nucl. Chem.* 33.5 (1971), pp. 1293–1299.
- [3] Shaowei Ong, Xiaolin Zhao, and Kenneth B Eisenthal. “Polarization of water molecules at a charged interface: second harmonic studies of the silica/water interface”. In: *Chem. Phys. Lett.* 191.3-4 (1992), pp. 327–335.
- [4] Motoyoshi Kobayashi et al. “Aggregation and charging of colloidal silica particles: effect of particle size”. In: *Langmuir* 21.13 (2005), pp. 5761–5769.
- [5] Yulia Samoshina et al. “Equilibrium Aspects of Polycation Adsorption on Silica Surface: How the Adsorbed Layer Responds to Changes in Bulk Solution”. In: *Langmuir* 21.13 (2005), pp. 5872–5881.
- [6] Björn Stenqvist et al. “Faunus — a flexible framework for Monte Carlo simulation”. In: *Mol. Simul.* 39.14-15 (2013), pp. 1233–1239.

In this book you will meet three main characters: the saliva protein histatin 5 , the blood protein fibrinogen , and a negatively charged silicon dioxide surface . The book describes the interactions between the proteins and the surface, which have been studied mainly using coarse-grained modelling. In the coarse-grained models, every amino acid of the proteins has been represented as a sphere, and thus the details of an all-atom representation disappear. This decreases the computational cost of the simulations and makes the simulation results easier to explain, since there are less parameters involved. However, the coarse-graining also introduces limits to which properties that can be studied.



In this book, you can also follow a fourth character, Kristin Hyltegren, on her research journey, read about how the modelling worked out, and the conclusions.